

**RHEOLOGICAL CHARACTERISATION OF HIGHLY  
CONCENTRATED MINERAL SUSPENSIONS USING AN  
ULTRASONIC VELOCITY PROFILER**

**by**

**Reinhardt Kotzé**

**Thesis submitted in fulfilment of the requirements for the**

**MTech: Electrical Engineering Degree**

**in the Faculty of Engineering**

**at the**

**CAPE PENINSULA UNIVERSITY OF TECHNOLOGY**

**Supervisor: Dr Rainer Haldenwang**

**Co-supervisor: Prof. Jevon Davies**

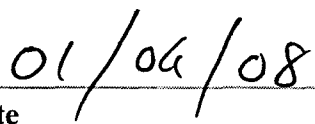
**Cape Town  
November 2007**

---

## DECLARATION

I, Reinhardt Kotzé, declare that the contents of this thesis represent my own unaided work, and that the thesis has not previously been submitted for academic examination towards any qualification. Furthermore, it represents my own opinions and not necessarily those of the Cape Peninsula University of Technology.

  
Signed

  
Date

---

# **RHEOLOGICAL CHARACTERISATION OF HIGHLY CONCENTRATED MINERAL SUSPENSIONS USING AN ULTRASONIC VELOCITY PROFILER**

**Reinhardt Kotzé**

## **ABSTRACT**

The rheological behaviour of non-Newtonian, highly concentrated and non-transparent fluids used in industry have so far been analysed using commercially available instruments, such as conventional rotational rheometers and tube viscometers. When dealing with the prediction of non-Newtonian flows in pipes, pipe fittings and open channels, most of the models used are empirical in nature. The fact that the fluids or slurries that are used normally are opaque, effectively narrows down the variety of applicable in-line rheometers even further, as these instruments are normally based on laser or visible light techniques, such as Laser Doppler Anemometry. Electrical Resistance Tomography is a non-invasive method used to look into opaque suspensions during pipe flow, but cannot be used to measure in-line rheometry.

In this research, an Ultrasound Pulsed Echo Doppler Velocity Profile technique (UVP), in combination with a pressure difference (PD) was tested to provide in-line measurement of rheological parameters. The main objective of this research was to evaluate the capabilities of the UVP-PD technique for rheological characterisation of different concentrations of non-transparent non-Newtonian slurries.

A unique pipe viscometer was designed and constructed. It consisted of four pipes, one of stainless steel and three of PVC, linked to an in-line mass-flow meter and equipped with two different ranges of pressure transducers on each pipe. The stainless steel pipe, with an inner diameter of 16 mm, was equipped with a specially designed flow adapter for in-line rheological characterisation using the UVP-PD method. The three PVC pipes with different diameters of 9 mm, 13 mm and 16 mm served as a tube viscometer for in-line rheological characterisation of mineral suspensions. The experimental investigation covered a wide range of solids concentrations (5 % to 12 %), slurry relative densities (1.03 to 1.198), flow rates (0.07 to 0.50 l/s) and yield stresses (0 to 50 Pa). This instrument and measurement technique was evaluated and tested with highly concentrated non-Newtonian CMC solutions as well as bentonite and kaolin mineral suspensions.

Results determined by the UVP-PD method were compared with results obtained by off-line rheometry and in-line tube viscometry. It was found that kaolin suspensions influenced velocity profile measurements due to ultrasound attenuation and absorption while bentonite suspensions influenced tube viscometer and off-line rheometric measurements due to high viscosities and flow limitations in the system. The agreement between the UVP-PD method, tube viscometry and conventional rheometry was found to be good (within 15 %) for all of the highly concentrated mineral suspensions investigated over a given range of shear rates.

The main advantage of the in-line UVP-PD rheometric method is its applicability for flow behaviour characterisation of non-transparent and highly concentrated suspensions while the process conditions (i.e. volumetric flow rate, absolute pressure and temperature) are kept constant. This method, if used in combination with a pressure difference technique (PD), has been found to have a significant potential in the development process of new in-line rheometers for process control within the mining industry.

---

## DEDICATION

To my father, my inspiration and my teacher

To my mother, always supportive and understanding

To my eldest brother, who always makes me laugh

To my only sister, the angel of our family

To my three youngest brothers, the joy of our family

With love to all of you

*Life is not difficult; we tend to make it difficult for ourselves. In the end it all revolves around self-discipline.*

*LEON KOTZÉ*

*Engineering is the art or science of making practical.*

*SAMUEL C. FLORMAN*

*Vertrou op die Here met alles wat jy het. Moenie staat maak op jou eie insigte nie. Vra na die wil van God in alles wat jy doen. Hy sal die regte pad vir jou wys.*

*SPREUKE 3:5-6*

---

## ACKNOWLEDGEMENTS

I wish to thank:

- **Dr Rainer Haldenwang and Prof. Jevon Davies, my supervisors, who guided me through the whole research process with much encouragement, wisdom and enthusiasm;**
- **Prof Paul Slatter, head of the Flow Process Research Centre (FPRC), whose valuable input is always appreciated;**
- **Richard du Toit, FPRC laboratory manager, is acknowledged for his support with all the laboratory equipment and setup needed for this research;**
- **Naziem George, for his support on rotary viscometry;**
- **Dr Johan Wiklund (SIK, Sweden) is acknowledged for his technical support on the UVP-PD rheometric method, as well as for reviewing my thesis;**
- **Jon-David Steffen, for the development of the pipe rig software, as well as his support with regard to programming;**
- **Dr Jean-Claude Willemetz, founder of Signal Processing SA; his technical support on UVP measurements with the DOP1000 UVP monitor was very helpful;**
- **Olivier Mariette at Met-Flow SA, Switzerland, for the demonstration of the UVP monitor at the FPRC and for his technical support;**
- **Prof. Erich J. Windhab for introducing the UVP-PD technique to Dr. Haldenwang and the FPRC;**
- **Dr Jeelani Shaik, Dr Peter Fischer and Beat Birkhoffer for their support during my stay at the Swiss Federal Institute of Technology in Zurich, Switzerland (ETHZ); the knowledge gained on curve fitting, programming, rheological and experimental aspects, was a very important part of this research;**
- **Joachim Macke is acknowledged for the design and construction of the ultrasound flow adapters and pressure adapters;**
- **Andrew Sutherland, for his support on data acquisition and noise reduction;**
- **Dr Verushca Fester, for her assistance with balanced beam tube viscometry;**
- **The Flow Process Research Centre (FPRC) at the Cape Peninsula University of Technology (CPUT) where I was given the opportunity to conduct the research;**
- **The Centre for Instrumentation Research (CIR), for their assistance with electronic instrumentation;**
- **My parents for their continuous support during all these years. Their love and belief in me helped me not to give up at the difficult moments.**
- **My girlfriend, for her love and support; and**
- **My colleagues and everybody who somehow contributed to this work are also acknowledged.**

The financial assistance of the National Research Foundation towards the research is acknowledged. Opinions expressed in this thesis and the conclusions arrived at are those of the author and are not necessarily to be attributed to the National Research Foundation.

## NOMENCLATURE

<i>Symbol</i>	<i>Description</i>	<i>Unit</i>
$A$	cross sectional area	$m^2$
$A_{MAX}$	wave amplitude	mm
$A$	US active beam diameter	mm
$a$	US transducer active diameter	m
$b$	US transducer housing diameter	mm
$C_V$	solids volumetric concentration	%
$c$	ratio between plug and outer pipe radius	
$c$	sound velocity	m/s
$c_L$	resistance coefficient for frontal correction in a cylinder-measuring system	
$c_{nm}$	elasticity modulus	Pa
$c_v$	specific heat capacity	J/g/K
$D$	internal pipe diameter	m
$d$	layer thickness	mm
$\Delta d$	moving distance along US beam or measuring line	mm
$E$	Young's modulus	Pa, N/m <sup>2</sup>
$e$	maximum error	
$F$	force	N
$F_{prf}$	pulse repetition frequency	Hz
$f$	fanning friction factor	
$f$	ultrasound wave frequency	Hz
$f_d$	Doppler shift frequency	Hz

---

$f_e, f_o$	frequency of emitted ultrasound wave	Hz
$f_r$	frequency of reflected ultrasound wave	Hz
$G$	pseudo shear rate	1/s
$g$	gravitational acceleration	m/s <sup>2</sup>
$H$	height	m
$h$	gap in plate measuring system	m
$h_f$	frictional head	m
$I$	US intensity	W/cm <sup>2</sup>
$K$	fluid consistency index	Pa.s
$K$	volumetric elasticity modulus	Pa
$K_{AD}$	bulk modulus	Pa, N/m <sup>2</sup>
$k$	(angular) wave number	
$k$	pipe roughness	m
$L$	pipe length, characteristic length	m
$M$	mass	kg
$N$	number of cycles per US pulse	
$N_c$	number of channels/measuring volumes	
$N_f$	near-field distance of US transducer	m
$n$	flow behaviour index	
$P, p$	pressure, acoustic pressure	Pa
$P_{max}$	maximum measurable depth	m
$Q$	volumetric flow rate	m <sup>3</sup> /s
$R$	pipe radius (outer)	m
$R_b$	radius of rotary viscometer bob	m
$R_c$	radius of rotary viscometer cup	m

---

---

$Re$	Reynolds number	
$r$	pipe radius (inner)	m
$r_1, r_2$	acoustic energy reflection coefficient	%
$S$	relative density	
$\Delta s$	moving distance along mainstream direction	mm
$T$	Temperature	°C
$T, t$	Time	sec
$T$	Torque	N.m
$T_{prf}$	time between two US emissions	sec
$t_d$	time delay	s
$u, v$	point velocity	m/s
$V$	average velocity	m/s
$V_{max}$	maximum measurable velocity	m/s
$V_{Tr}$	target velocity	mm/s
$V_t$	velocity in direction of US beam or measuring line	mm/s
$w$	channel width	m
$w$	mass flow rate	kg/s
$x$	distance	m
$z$	on-axis co-ordinate of US beam	m
$z$	specific acoustic impedance	gr/(cm <sup>2</sup> s)



***Greek Symbols***

$\alpha_0$	spatial attenuation coefficient	dB/cm
$\beta$	cone angle	degrees
$\dot{\gamma}$	shear rate	s <sup>-1</sup>
$\dot{\gamma}_w$	wall shear rate	s <sup>-1</sup>
$\dot{\gamma}_{wN}$	pseudo wall shear rate	s <sup>-1</sup>
$\gamma_0$	US beam divergence half-angle	degrees
$\Delta$	increment	
$\delta$	ratio between cup and bob radius	
$\delta_0$	temporal attenuation coefficient	1/sec
$\varepsilon$	deformation	
$\Theta$	volume compaction	1/Pa
$\theta$	incline, Doppler angle	degrees
$\kappa_1, \kappa_t$	acoustic energy transmission coefficient	%
$\lambda$	wavelength	m
$\lambda_{LM}, \mu_{LM}$	Lame constants	
$\lambda_0$	thermal conductivity	W.m <sup>-1</sup> .K <sup>-1</sup>
$\mu$	Newtonian or apparent viscosity	Pa.s
$\mu_s$	shear viscosity	Pa.s
$\nu$	kinematic viscosity	m <sup>2</sup> .s <sup>-1</sup>
$\nu_p$	Poisson's modulus	
$\rho$	material, fluid or slurry density	kg.m <sup>-3</sup>
$\rho_w$	density of water	kg.m <sup>-3</sup>
$p_0$	reference acoustic pressure of US sensor	Pa
$\tau$	shear stress	Pa

---

$\tau_w$	wall shear stress	Pa
$\tau_y$	yield stress	Pa
$\tau_0$	damping time coefficient	dB/sec
$\phi$	diameter	mm
$\omega$	velocity function, angular velocity, angular frequency	rad.s <sup>-1</sup>

### *Subscripts*

<i>MAX, max</i>	maximum
<i>m</i>	mixture (mineral suspension)
<i>x, y, z</i>	Cartesian coordinates
<i>yx, rz</i>	shear stress components
<i>w</i>	water
<i>0</i>	state of the medium at rest

---

## ABBREVIATIONS AND ACRONYMS

ADC:	Analog-to-Digital Converter
AToM:	Acoustic Time of Flight Measurement
CIR:	Centre for Instrumentation Research
CMC:	Carboxymethyl cellulose
DMEA:	Demodulated Echo Amplitude
DOP1000:	UVP monitor supplied by Signal Processing SA, Switzerland
ERT:	Electrical Resistance Tomography
ETHZ:	Swiss Federal Institute of Technology, Zurich
FPRC:	Flow Process Research Centre
ISUD:	<i>International Symposium on Ultrasonic Doppler Methods for Fluid Mechanics and Fluid Engineering</i>
LDA:	Laser Doppler Anemometry
LSB:	Least Significant Bit
MRI:	Magnetic Resonance Imaging
PC:	Personal Computer
PD:	Pressure Difference
PRF:	Pulse Repetition Frequency
PVC:	Polyvinyl chloride
SNR:	Signal-to-Noise Ratio
TGC:	Time Gain Control
UDV:	Ultrasonic Doppler Velocimetry
US:	Ultrasound
UVP:	Ultrasonic Velocity Profiling

---

## TERMS AND CONCEPTS CITED

- Laminar flow:** Nonturbulent streamline flow in parallel layers.
- Turbulent flow:** Flow in which the velocity at any point varies erratically.
- Transition:** The region or process acting between the laminar and turbulent flow regimes.
- Newtonian fluid:** Any fluid that has a directly proportional relationship between shear stress and shear rate. Water is an example of a Newtonian fluid.
- Reynolds number:** The ratio between viscous and inertial forces is proportional to the Reynolds number. The number is expressed in terms of the density, velocity, characteristic length and the viscosity of the fluid. This number is also used to define whether a fluid is laminar or turbulent.
- Viscosity:** A measure of the resistance to flow of a fluid under an applied force.
- Transducer:** A device that converts one type of energy to another, or responds to a physical parameter. A transducer is, in its fundamental form, a passive component. If the component is electrical, it generally has two electrical terminals.
- Friction factor:** There are two kinds of friction factors: The fanning friction factor is proportional to shear stress at pipe/conduit wall as number of velocity heads and is used in momentum transfer in general and turbulent flow calculations, in particular. It is equivalent to (1/4) the Darcy friction factor.
- Shear Stress:** Shear stress is a stress state where the shape of a material tends to change (usually by "sliding" forces – torque by transversely-acting forces) without particular volume change.

- 
- Dilatent fluid:** Any fluid which shows an increase in apparent viscosity with increasing shear rate; also known as a shear-thickening fluid.
- Acoustic impedance:** The ratio of acoustic excess pressure to the particle velocity. It is defined as  $z = \rho \cdot c$ .
- Spatial Resolution:** Distance between the center of adjacent measuring volumes or channels inside a measuring window.
- Time Resolution:** Sampling time of one velocity profile measurement. Directly influenced by the number of ultrasonic repetitions per profile.
- Aliasing:** Artefact that occurs when the Doppler-induced frequency shift exceeds one half of the UVP instrument's pulse repetition frequency (PRF).
- Doppler effect:** The apparent change in frequency and wavelength of a wave that is perceived by an observer moving relative to the source of the waves.
- Quantisation error:** Rounding error between the analogue input voltage to the ADC and the output digitized value.

## TABLE OF CONTENTS

DECLARATION .....	i
ABSTRACT.....	ii
DEDICATION.....	iii
ACKNOWLEDGEMENTS.....	iv
NOMENCLATURE .....	v
ABBREVIATIONS AND ACRONYMS.....	x
TERMS AND CONCEPTS CITED .....	xi
CONTENTS.....	xiii
LIST OF FIGURES .....	xviii
LIST OF TABLES.....	xxi
<b>CHAPTER 1.....</b>	<b>1.1</b>
<b>INTRODUCTION.....</b>	<b>1.1</b>
1.1 STATEMENT OF THE PROBLEM.....	1.1
1.2 OBJECTIVE.....	1.2
1.3 METHODOLOGY .....	1.2
1.3.1 Literature review (Chapter 2).....	1.4
1.3.2 Methods of investigation and apparatus (Chapter 3) .....	1.4
1.3.3 Results and discussion (Chapter 4) .....	1.4
1.3.4 Summary, conclusions and recommendations (Chapter 5).....	1.4
1.4 DELINEATION .....	1.5
1.5 SUMMARY .....	1.5
<b>CHAPTER 2.....</b>	<b>2.1</b>
<b>LITERATURE REVIEW .....</b>	<b>2.1</b>
2.1 INTRODUCTION.....	2.1
2.2 RHEOLOGY .....	2.1
2.2.1 Introduction.....	2.1
2.2.2 Flow regimes.....	2.2
2.2.2.1 Laminar flow.....	2.3
2.2.2.2 Turbulent flow .....	2.3
2.2.2.3 Transitional flow.....	2.4
2.2.3 Fluid behaviour .....	2.4
2.2.3.1 Newtonian fluid behaviour .....	2.4
2.2.3.2 Non-Newtonian fluid behaviour .....	2.5

2.2.4	Non-Newtonian models .....	2.7
2.2.4.1	Pseudoplastic or shear-thinning model .....	2.7
2.2.4.2	Bingham plastic model .....	2.7
2.2.4.3	Herschel-Bulkley or yield-pseudoplastic model .....	2.8
2.2.5	Rheometry for non-Newtonian models .....	2.9
2.2.5.1	Rotational viscometry .....	2.10
2.2.5.2	Tube viscometry .....	2.11
2.2.6	Pipe flow .....	2.15
2.2.6.1	Newtonian pipe flow.....	2.15
2.2.6.2	Non-Newtonian pipe flow.....	2.17
2.2.7	Conclusion .....	2.21
2.3	ULTRASOUND PHYSICS.....	2.22
2.3.1	Introduction.....	2.22
2.3.2	Ultrasound propagating in fluids.....	2.22
2.3.3	Ultrasound propagating at the boundary between two materials .....	2.24
2.3.4	Influences on ultrasound propagation .....	2.30
2.3.4.1	Influence of absolute pressure and density on ultrasound .....	2.30
2.3.4.2	Influence of fluid viscosity on ultrasound .....	2.32
2.3.4.3	Influence of solids concentration on ultrasound in fluid suspensions.....	2.33
2.3.4.4	Influence of temperature on ultrasound .....	2.34
2.3.5	Conclusion .....	2.35
2.4	ULTRASONIC DOPPLER VELOCIMETRY (UDV) .....	2.35
2.4.1	Introduction.....	2.35
2.4.2	The Doppler effect .....	2.36
2.4.3	Working principle of Ultrasonic Doppler Velocimetry .....	2.38
2.4.4	Doppler spectrum.....	2.40
2.4.5	Conclusion .....	2.42
2.5	THE UVP-PD RHEOMETRIC METHOD .....	2.42
2.5.1	Introduction.....	2.42
2.5.2	UVP-PD data acquisition and processing procedures.....	2.43
2.5.3	Research studies based on UVP-PD .....	2.45
2.5.4	Conclusion .....	2.50
<b>CHAPTER 3</b>	.....	<b>3.1</b>
<b>METHODS OF INVESTIGATION AND APPARATUS</b>	.....	<b>3.1</b>
3.1	INTRODUCTION.....	3.1
3.2	APPARATUS.....	3.2
3.2.1	Rheometers.....	3.2

3.2.2	Experimental flow loop (pilot study) .....	3.3
3.2.3	The Pipe rig .....	3.4
3.2.3.1	Pressure tappings and transducers .....	3.5
3.2.3.2	Pump .....	3.6
3.2.4	Ultrasound instrumentation .....	3.7
3.2.4.1	UVP monitor and parameters .....	3.7
3.2.4.2	Ultrasound transducers .....	3.14
3.2.4.3	Flow adapter geometry and sensor installation .....	3.18
3.3	CALIBRATION PROCEDURES .....	3.20
3.3.1	Pressure transducers .....	3.20
3.3.2	Mass-flow meter .....	3.21
3.3.3	Clear water test in tube viscometer .....	3.23
3.3.4	UVP monitor .....	3.26
3.4	MEASURED VARIABLES .....	3.26
3.4.1	Measurement of pipe diameters .....	3.26
3.4.2	Slurry density .....	3.27
3.4.3	Slurry temperature .....	3.28
3.4.4	Particle size distribution .....	3.29
3.4.5	Velocity of sound .....	3.31
3.5	COMBINED ERRORS .....	3.35
3.5.1	Pipe diameter .....	3.36
3.5.2	Wall shear stress .....	3.36
3.5.3	Pseudo shear rate .....	3.38
3.6	EXPERIMENTAL PROCEDURES AND INVESTIGATION .....	3.39
3.6.1	Tube viscometer rig .....	3.39
3.6.2	In-line rheometer .....	3.40
3.6.2.1	Velocity profile measurement optimisation .....	3.40
3.6.2.2	Velocity profile analysis .....	3.42
3.6.2.3	Calculation of rheological parameters .....	3.46
3.7	MINERAL SUSPENSIONS TESTED .....	3.51
3.7.1	Water .....	3.51
3.7.2	Carboxymethyl Cellulose (CMC) .....	3.51
3.7.3	Bentonite .....	3.52
3.7.4	Kaolin .....	3.52
3.8	GENERAL OBSERVATIONS .....	3.52
3.8.1	Pressure fluctuations in pulsating flow .....	3.52
3.8.2	Off-line vs in-line velocity of sound measurements .....	3.53
3.8.3	Temporal behaviour of sound velocity in mineral suspensions .....	3.56



3.8.4 Time frame aliasing.....	3.57
3.8.5 Reflected wave effect.....	3.59
3.9 CONCLUSION .....	3.60
3.9.1 Empirical behaviour.....	3.60
3.9.2 Experimental equipment and procedures .....	3.61
<b>CHAPTER 4.....</b>	<b>4.1</b>
<b>ANALYSIS OF RESULTS .....</b>	<b>4.1</b>
4.1 INTRODUCTION.....	4.1
4.2 CARBOXYMETHYL CELLULOSE (CMC).....	4.1
4.2.1 Carboxymethyl Cellulose 5.3% w/w.....	4.2
4.2.2 Carboxymethyl Cellulose 6% w/w.....	4.8
4.2.3 Carboxymethyl Cellulose 6.5% w/w.....	4.10
4.3 BENTONITE.....	4.12
4.3.1 Bentonite 5.7% w/w.....	4.12
4.3.2 Bentonite 6.5% w/w.....	4.17
4.3.3 Bentonite 7% w/w.....	4.20
4.3.4 Bentonite 7.5% w/w (pilot study) .....	4.22
4.4 KAOLIN.....	4.24
4.4.1 Kaolin 8.7% v/v .....	4.24
4.4.2 Kaolin 10% v/v .....	4.30
4.4.3 Kaolin 12% v/v .....	4.32
4.5 CONCLUSION .....	4.34
<b>CHAPTER 5.....</b>	<b>5.1</b>
<b>SUMMARY, CONTRIBUTIONS, RECOMMENDATIONS AND CONCLUSIONS .....</b>	<b>5.1</b>
5.1 INTRODUCTION.....	5.1
5.2 SUMMARY .....	5.1
5.3 CONTRIBUTIONS.....	5.5
5.4 LIMITATIONS .....	5.5
5.5 RECOMMENDATIONS FOR FUTURE RESEARCH .....	5.7
5.6 CONCLUSIONS .....	5.10
5.7 FUTURE OUTLOOK .....	5.11
REFERENCES .....	R1

---

<b>APPENDIX A</b> .....	
EXPERIMENTAL RESULTS .....	A.1
A.1 EXPERIMENTAL AND THEORETICAL PROFILES .....	A.2
A.2 OFF-LINE FLOW CURVES .....	A.12
A.3 PIPE VISCOMETER DATA .....	A.17
<b>APPENDIX B</b> .....	
DRAWING OF THE PIPE VISCOMETER RIG .....	B.1

## LIST OF FIGURES

Figure 1.1:	Flow chart of research approach .....	1.3
Figure 2.1:	Example of turbulent and laminar flow.....	2.3
Figure 2.2:	Schematic representation of unidirectional flow .....	2.4
Figure 2.3:	Relationship between shear stress and shear rate for Newtonian and non-Newtonian fluids (Chhabra & Richardson, 1999).....	2.6
Figure 2.4:	Measuring systems of rotational viscometers .....	2.10
Figure 2.5:	Air-driven pipe viscometer.....	2.12
Figure 2.6:	Flow through a circular pipe .....	2.16
Figure 2.7:	Velocity and shear stress distribution in a pipe.....	2.16
Figure 2.8:	Shear stress distribution in a pipe.....	2.17
Figure 2.9:	Laminar velocity profiles for power-law fluids.....	2.19
Figure 2.10:	Laminar velocity profiles for Bingham plastic fluids (Steffe, 1996) .....	2.21
Figure 2.11:	Attenuation of an ultrasound wave (Ouriev, 2000).....	2.23
Figure 2.12:	Ultrasound wave propagating between two materials (Ouriev, 2000).....	2.24
Figure 2.13:	Transducer installation setups and US wave propagation: a) which is in contact with the investigated fluid; b) without contact with the investigated fluid (Ouriev, 2000) .....	2.27
Figure 2.14:	Normal stresses acting on a material element (Ouriev, 2000).....	2.31
Figure 2.15:	Reflection from a moving particle.....	2.37
Figure 2.16:	Schematic of the ultrasound beam configuration where $a$ is the active beam diameter (Ouriev, 2000).....	2.38
Figure 2.17:	Illustration of a moving target particle within a channel or measuring volume (Ouriev, 2000) .....	2.39
Figure 2.18:	Principle illustration of Doppler ultrasound flow velocity measurement. The transducer positioned with Doppler angle $\theta$ to the flow direction (Ouriev, 2000).....	2.41
Figure 2.19:	General flowchart of the UVP-PD rheometric method (Wiklund, 2003).....	2.44
Figure 3.1:	Measuring systems used for off-line rheology .....	3.3
Figure 3.2:	Experimental flow loop at ETH .....	3.4
Figure 3.3:	Pipe rig layout .....	3.5
Figure 3.4:	Pressure adapter and configuration .....	3.5
Figure 3.5:	Pulsation damping unit.....	3.6
Figure 3.6:	Comparison between maximum measurable depth and velocity .....	3.10

Figure 3.7:	Variation of the velocity spread distance along the pipe diameter by Doppler angle modification: a) $\theta_1$ and b) $\theta_2$ .....	3.12
Figure 3.8:	Sound field generated by an US transducer (Met-Flow, 2002).....	3.15
Figure 3.9:	Lateral dimensions of measuring volumes versus position along US beam (Signal Processing SA, 2007).....	3.16
Figure 3.10:	Spectral characteristics of 4 MHz Met-Flow SA transducer.....	3.17
Figure 3.11:	US pulse emission with remaining ringing .....	3.18
Figure 3.12:	Schematic illustration of the flow adapter fitted with two transducers .....	3.19
Figure 3.13:	Low-range point pressure transducer calibration constants .....	3.21
Figure 3.14:	Mass-flow meter calibration for CMC 7 %.....	3.22
Figure 3.15:	Clear water test data against Colebrook-White equation in 9 mm pipe .....	3.24
Figure 3.16:	Clear water test data against Colebrook-White equation in 13 mm pipe .....	3.25
Figure 3.17:	Clear water test data against Colebrook-White equation in 16 mm pipe .....	3.25
Figure 3.18:	Particle size distribution of kaolin.....	3.29
Figure 3.19:	Particle size distribution of bentonite.....	3.30
Figure 3.20:	Principle scheme of off-line velocity of sound measurement (Ouriev, 2000).....	3.31
Figure 3.21:	Off-line sound velocity measurement in distilled water.....	3.33
Figure 3.22:	Schematic illustration of method used for in-line velocity of sound measurement .....	3.34
Figure 3.23:	Pipe wall shear stress combined errors.....	3.37
Figure 3.24:	Highest combined errors for calculating pseudo shear rate.....	3.38
Figure 3.25:	Region used for volume flow rate calculation.....	3.42
Figure 3.26:	Yield stress estimation using the plug radius .....	3.45
Figure 3.27:	Flow curves obtained from different estimated wall positions .....	3.48
Figure 3.28:	Experimental and power-law fitted velocity profiles for CMC 6 % w/w .....	3.49
Figure 3.29:	Flow curves obtained from different flow rates for CMC 6 % w/w.....	3.50
Figure 3.30:	Pressure fluctuations in pulsating flow .....	3.53
Figure 3.31:	The velocity of sound in air/water mixtures at 20°C (Povey, 1997) .....	3.55
Figure 3.32:	Sound velocity as function of temperature for some investigated fluids .....	3.56
Figure 3.33:	Schematic illustration of time frame aliasing.....	3.57
Figure 3.34:	Time frame aliasing example on oscilloscope.....	3.58
Figure 3.35:	Loss of data due to interference from stationary echo .....	3.58
Figure 3.36:	Influence of multiple reflections on measured profile for kaolin 8.7 % v/v .....	3.59
Figure 4.1:	Experimental and theoretical velocity profile for CMC 5.3 % w/w.....	4.2
Figure 4.2:	Flow curve measured by off-line rheometer for CMC 5.3 % w/w.....	4.4
Figure 4.3:	Pipe data measured by the tube viscometer for CMC 5.3 % w/w.....	4.5
Figure 4.4:	Flow curve measured by the tube viscometer for CMC 5.3 % w/w.....	4.5

Figure 4.5:	CMC 5.3 % w/w rheogram .....	4.6
Figure 4.6:	Variation with shear rate in viscosity for CMC 5.3 % w/w .....	4.7
Figure 4.7:	CMC 6 % w/w rheogram .....	4.9
Figure 4.8:	Variation with shear rate in viscosity for CMC 6 % w/w .....	4.9
Figure 4.9:	CMC 6.5 % w/w rheogram .....	4.10
Figure 4.10:	Variation with shear rate in viscosity for CMC 6.5 % w/w .....	4.11
Figure 4.11:	Experimental and theoretical velocity profile for bentonite 5.7 % w/w.....	4.12
Figure 4.12:	Flow curve measured by off-line rheometer for bentonite 5.7 % w/w.....	4.14
Figure 4.13:	Pipe data measured by the tube viscometer for bentonite 5.7 % w/w.....	4.14
Figure 4.14:	Flow curve measured by the tube viscometer for bentonite 5.7 % w/w.....	4.15
Figure 4.15:	Bentonite 5.7 % w/w rheogram.....	4.16
Figure 4.16:	Variation with shear rate in viscosity for bentonite 5.7 % w/w .....	4.16
Figure 4.17:	Bentonite 6.5 % w/w rheogram.....	4.18
Figure 4.18:	Variation with shear rate in viscosity for bentonite 6.5 % w/w .....	4.19
Figure 4.19:	Bentonite 7 % w/w rheogram.....	4.20
Figure 4.20:	Variation with shear rate in viscosity for bentonite 7 % w/w .....	4.21
Figure 4.21:	Bentonite 7.5 % w/w rheogram.....	4.22
Figure 4.22:	Variation with shear rate in viscosity for bentonite 7.5 % w/w .....	4.23
Figure 4.23:	Experimental and theoretical velocity profile for kaolin 8.7 % v/v .....	4.24
Figure 4.24:	Flow curve measured by off-line rheometer for kaolin 8.7 % v/v .....	4.26
Figure 4.25:	Pipe data measured by the tube viscometer for kaolin 8.7 % v/v.....	4.27
Figure 4.26:	Flow curve measured by the tube viscometer for kaolin 8.7 % v/v .....	4.27
Figure 4.27:	Kaolin 8.7 % v/v rheogram .....	4.28
Figure 4.28:	Variation with shear rate in viscosity for kaolin 8.7 % v/v .....	4.29
Figure 4.29:	Kaolin 10 % v/v rheogram .....	4.30
Figure 4.30:	Variation with shear rate in viscosity for kaolin 10 % v/v.....	4.31
Figure 4.31:	Kaolin 12 % v/v rheogram .....	4.32
Figure 4.32:	Variation with shear rate in viscosity for kaolin 12 % v/v.....	4.33

## LIST OF TABLES

Table 2.1:	Newtonian, Bingham plastic and Power-law Fluids as special cases of the Herschel-Bulkley model (Equation. 2.6).....	2.9
Table 2.2:	Sound velocity and ultrasound wave amplitude measurements in PVC .....	2.30
Table 3.1:	Ultrasound transducer beam geometry.....	3.14
Table 3.2:	Pipe roughness results for different pipe diameters .....	3.26
Table 3.3:	Actual pipe diameters of the tube viscometer .....	3.27
Table 3.4:	Summary of combined errors for different pipe diameters .....	3.36
Table 3.5:	Volumetric flow rate calculations for different wall positions.....	3.43
Table 3.6:	Comparison between volumetric flow rate calculations for the same wall positions at two different velocities .....	3.44
Table 3.7:	Yield stress measurements obtained from three different methods.....	3.46
Table 3.8:	Rheological parameters for different estimated wall positions .....	3.48
Table 3.9:	Power-law model parameters obtained from experimental velocity profiles.....	3.50
Table 3.10:	In-line and off-line velocity of sound results for different concentrations of CMC .....	3.54
Table 3.11:	In-line and off-line velocity of sound results for different concentrations of kaolin .....	3.54
Table 3.12:	In-line and off-line velocity of sound results for different concentrations of bentonite .....	3.54
Table 4.1:	UVP parameter settings for CMC 5.3 % w/w .....	4.3
Table 4.2:	Test conditions for CMC 5.3 % w/w.....	4.3
Table 4.3:	Rheological parameters obtained from three different methods for CMC 5.3 % w/w.....	4.7
Table 4.4:	Rheological parameters obtained from three different methods for CMC 6 % w/w.....	4.10
Table 4.5:	Rheological parameters obtained from three different methods for CMC 6.5 % w/w.....	4.11
Table 4.6:	UVP parameter settings for bentonite 5.7 % w/w.....	4.13
Table 4.7:	Test conditions for bentonite 5.7 % w/w.....	4.13
Table 4.8:	Rheological parameters obtained from three different methods for bentonite 5.7 % w/w.....	4.17
Table 4.9:	Rheological parameters obtained from three different methods for bentonite 6.5 % w/w.....	4.19

---

Table 4.10:	Rheological parameters obtained from three different methods for bentonite 7 % w/w.....	4.22
Table 4.11:	Rheological parameters obtained from three different methods for bentonite 7.5 % w/w.....	4.23
Table 4.12:	UVP parameter settings for kaolin 8.7 % v/v.....	4.25
Table 4.13:	Test conditions for kaolin 8.7 % v/v .....	4.25
Table 4.14:	Rheological parameters obtained from three different methods for kaolin 8.7 % v/v .....	4.29
Table 4.15:	Rheological parameters obtained from three different methods for kaolin 10 % v/v .....	4.31
Table 4.16:	Rheological parameters obtained from three different methods for kaolin 12 % v/v .....	4.33

# **CHAPTER ONE**

## **INTRODUCTION**



# CHAPTER ONE

## INTRODUCTION

The rheological behaviour of non-Newtonian, highly concentrated and non-transparent fluids used in industry have so far been analysed using commercially available instruments, such as conventional rotational rheometers and tube viscometers. When dealing with the prediction of non-Newtonian flows in pipes, pipe fittings and open channels, most of the models used are empirical in nature (Haldenwang, Slatter, Alderman, Kotzé, Sery & George, 2006).

The fact that the fluids or slurries that are used normally are opaque effectively narrows down the variety of applicable in-line rheometers even further, as these instruments are normally based on laser or visible light techniques, such as Laser Doppler Anemometry. Electrical Resistance Tomography (ERT) is a non-invasive method used to look into opaque suspensions during pipe flow, but cannot be used to measure in-line rheometry.

For mines and tailing facilities to control processes, knowledge of the rheological parameters of the slurries is essential. If one can instantaneously observe a change in the rheology of the slurries being transported, pipe blockages and other problematic situations can be prevented. However, obtaining the rheology of these mining tailings is complex and in-line rheometry would be of great assistance to the mining industry.

Ultrasound Velocity Profiling is a viable method available to accomplish in-line, non-invasive rheometry of complex non-Newtonian fluids. As far as can be ascertained, the Ultrasonic Velocity Profile with Pressure Difference (UVP-PD) method has not been used to measure velocity profiles and rheological parameters of mineral suspensions such as mining tailings.

### 1.1 STATEMENT OF THE PROBLEM

The fundamental problem is to predict the flow behaviour of non-Newtonian slurries in pipes for the mining industry. The rheological characterisation of the slurries is an important issue that has a direct effect on the effectiveness of the flow predictions (Haldenwang, 2003). If non-Newtonian fluid systems are considered commercial process rheometers are fairly unreliable.

This is due to the direct influence on the microstructure of measuring the geometries and the invasive methods on which they are based (Ouriev & Windhab, 2002). Certain authors believe that tube viscometers are best suited for this specific application as they are geometrically similar to a pipeline (Lazarus & Slatter, 1988). However, tube viscometry is time-consuming and design engineers do not have the luxury of unlimited time to entertain the diversities of experimental research (Haldenwang *et al.* 2006).

The UVP-PD technique is an alternative method for in-line, non-invasive rheological characterisation of highly concentrated mineral suspensions, but this method has limitations. The fluids or slurries under test need to have particles suspended in it for the ultrasound to reflect from it to generate echoes, which are needed for determining velocity profiles for each test condition. There are many parameters (which are explained in Chapter 3) to consider in order to achieve maximum accuracy in measuring velocity profiles. For each concentration and test situation, there are optimum settings for the different parameters. Incorrect settings or values of these parameters will cause the measurement of velocity profiles to be inaccurate. Also, thicker concentrations and different types of suspensions attenuate the ultrasound beam more, which influences measurements. Different pipe materials and pipe thicknesses absorb ultrasound energy and cause part of the ultrasound beam to reflect, thus minimizing the intensity of the beam entering the fluid. These are just some of the aspects involved in using the UVP-PD technique. Velocity profiles that are inaccurate will yield inaccurate rheological parameters.

## 1.2 OBJECTIVE

The main objective of this research was to investigate the UVP-PD measuring technique and to determine how effective the UVP-PD method is in measuring rheological parameters of different concentrations of model mineral suspensions. Further objectives were to compare the rheological results obtained from tube and rotational viscometry and the UVP-PD method.

## 1.3 METHODOLOGY

To reach the objectives, the following research methodology was followed. Viscous mineral suspensions to be tested were to cover a wide range of viscous characteristics and include materials that could be characterised by using the following rheological models, namely:

Power-law, Bingham plastic and Hershel–Bulkley.

The overall approach is displayed in flow-chart format in Figure 1.1.

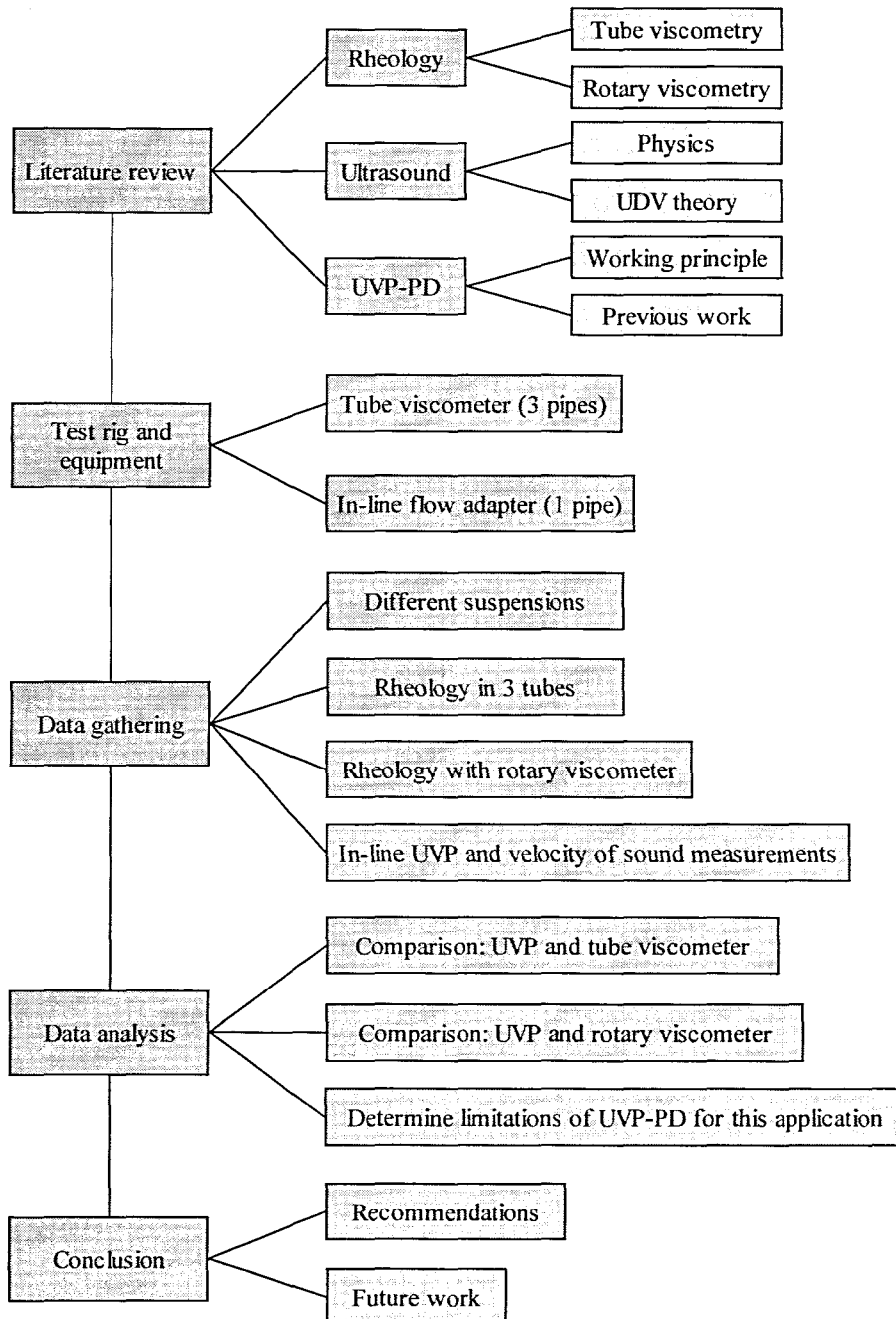


Figure 1.1: Flow chart of research approach

### **1.3.1 Literature review (Chapter 2)**

Due the multi-disciplinary nature of the research presented in this thesis, the literature review is divided into three parts, namely: rheology, ultrasound and previous research conducted in which the ultrasound (UVP-PD method) is used in order to rheologically characterise different types of fluids (rheology). Tube viscometry and the rotary viscometer, as well pipe flow (velocity profiles), are presented. The basic physics of ultrasound and concepts such as the Doppler effect are described. Previous work involving the UVP-PD method will be discussed.

### **1.3.2 Methods of investigation and apparatus (Chapter 3)**

A special pipe rig was designed and constructed to conduct all the tests. It consisted of three different diameter pipes which were linked to an in-line tube viscometer. Three pipes were used as a tube viscometer to rheologically characterise the materials in-line. A stainless steel pipe fitted with housing adapters for ultrasound transducers was used to measure rheological parameters of materials in-line. Three rheologically different non-Newtonian fluids were tested over a wide range of laminar flow rates.

### **1.3.3 Results and discussion (Chapter 4)**

The results obtained from experimental tests for the different materials are presented in this chapter. Results obtained with the use of ultrasound are compared with in-line tube viscometry as well as off-line conventional rheometry. These findings are also compared with previous research and conclusions that are reached are discussed.

### **1.3.4 Summary, conclusions and recommendations (Chapter 5)**

The significant contributions of this research are presented in this chapter, as well as conclusions drawn from experimental work. Limitations of the new UVP-PD method are discussed and recommendations are made for future research in this field.

## **1.4 DELINEATION**

This research was based on testing the capabilities of the UVP monitors supplied by Met-Flow SA only, and not on other commercially available UVP systems. A further focus concerned comparing the accurate measurement of the rheology of different concentrations of non-Newtonian fluids using only a tube viscometer and the UVP-PD method. Rotary viscometers and no other types of viscometers, such as capillary viscometers, were to be used for further comparison.

## **1.5 SUMMARY**

The introduction, problem statement and objective of the research and the layout of this thesis are presented in this chapter. In Chapter 2, a literature review and previous research will be presented.

# **CHAPTER TWO**

**THEORY**

**AND**

**LITERATURE REVIEW**

## CHAPTER TWO

### THEORY AND LITERATURE REVIEW

#### 2.1 INTRODUCTION

The theory and literature on rheology, ultrasound and previous work done with the UVP-PD method are presented in this chapter. The first section, on rheology, includes basic rheological terms and definitions, rheological models and parameters, as well as conventional off-line and in-line techniques for rheological analysis. Basic ultrasound physics is introduced in Section 2.3 and Ultrasonic Doppler Velocimetry (UDV) is presented in Section 2.4. This section explains the working principle of UDV and how it is used to obtain velocity profiles in pipe flow. The last section discusses previous work done with the UVP-PD method and shows how this method can be used to obtain rheological parameters of different types of fluids, including model and industrial suspensions.

#### 2.2 RHEOLOGY

This section on rheology is divided into five sub-sections, namely: flow regimes, fluid behaviour, non-Newtonian models, rheometry for non-Newtonian models and pipe flow.

##### 2.2.1 Introduction

Rheology is defined as the science of deformation and flow of matter. “The term ‘rheology’ originates from the Greek: ‘rheos’ meaning ‘the river’, ‘flowing’, ‘streaming’. Thus, rheology is literally ‘flow science’” (Mezger, 2002). Within the context of this work, rheology is defined as the viscous characteristics of a mineral suspension or slurry. The science of rheology as it is known today owes its origin to Sir Isaac Newton who postulated a direct relationship between the shear stress and shear rate in a fluid. This relationship is however only valid for Newtonian fluids and not for non-Newtonian slurries. Rheology can be defined generally as the viscous characteristics of slurry, and more precisely as the relationship between shear stress and shear rate, as measured in a viscometer and presented in a plot of shear stress versus shear rate, called

a rheogram (Slatter, 1997).

### 2.2.2 Flow regimes

There are three different flow regimes, namely laminar, turbulent and transitional flow. Osborne Reynolds was the first to investigate these flow regions and he developed the following relationship, which is now called the Reynolds number. The Reynolds number is proportional to the ratio between inertial and viscous forces and is defined as follows:

$$Re = \frac{\rho VD}{\mu} \quad (2.1)$$

By experiment, Reynolds determined that laminar flow occurs when the Reynolds number was less than approximately 2000, and that turbulent flow occurs with Reynolds numbers above 4000. The region between laminar and turbulent flow is an unstable region called the transition zone. When pipeline design is of concern the identification of the transition between laminar and turbulent flow is of great importance because the fluid flow behaviour changes fundamentally at the transition zone. Slatter and Lazarus (1993) formulated a new Reynolds number,  $Re_2$ , for non-Newtonian fluids:

$$Re_2 = \frac{8\rho V^2}{\tau_y + K\left(\frac{8V}{D}\right)^n} \quad (2.2)$$

The use of  $Re_2$  was proved to be a reliable predictor of the laminar/turbulent transition and is recommended for design purposes (Slatter & Lazarus, 1993).



### 2.2.2.1 Laminar flow

In laminar flow, the motion of the particles of fluid is very orderly, with all particles moving in straight lines parallel to the pipe walls. From this statement, it is understandable that laminar flow is often referred to as streamline flow (Mobley, 2000). It must be noted that laminar flow needs to be obtained for rheological characterisation of fluids using tube viscometry, which is explained in Section 2.2.5.2. This is also a requirement for the UVP measurements. The reason for this is that the theoretical formulas and models, which are discussed in the next sub-section, are only viable for laminar flow.

### 2.2.2.2 Turbulent flow

Turbulence is a natural form of fluid motion which is characterised by irregular, random movement of fluid both parallel and transverse to the direction of the main flow (Mobley, 2000). A typical example of both laminar and turbulent flow can be observed in the smoke from a cigarette, as in Figure 2.1.

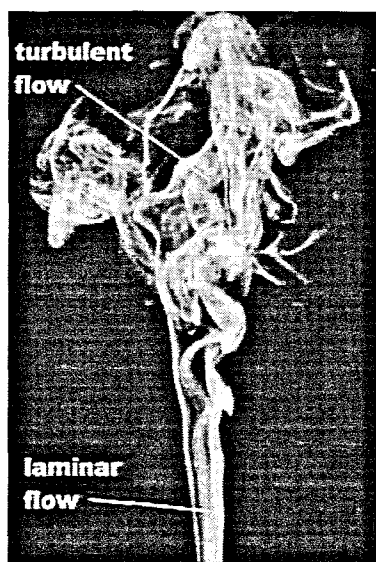


Figure 2.1: Example of turbulent and laminar flow (Bechtold, 2006)

### 2.2.2.3 Transitional flow

The transition between laminar and turbulent flow is very rapid and is often difficult to identify. It is known that laminar flow will exist below a particular velocity and turbulent flow exists above a particular velocity. The transition region can therefore be expressed as a region acting between these two critical velocities. It must be noted that this region is a function of the velocity as well as of the Reynolds number (Thorvaldsen, 1996). Due to the unstable nature of this region, detection of transitional flow becomes quite a difficult challenge.

## 2.2.3 Fluid behaviour

In this section, two types of flow behaviour are described, namely Newtonian and non-Newtonian fluid behaviour.

### 2.2.3.1 Newtonian fluid behaviour

Consider a very thin layer of fluid between two parallel planes a distance  $dy$  apart, as illustrated in Figure 2.2. If the fluid is subjected to a shear by the application of a force  $F$ , this will be balanced by an equal and opposite internal frictional force in the fluid. For a Newtonian fluid in laminar flow, the resulting shear stress is equal to the product of the shear rate and the viscosity of the fluid.

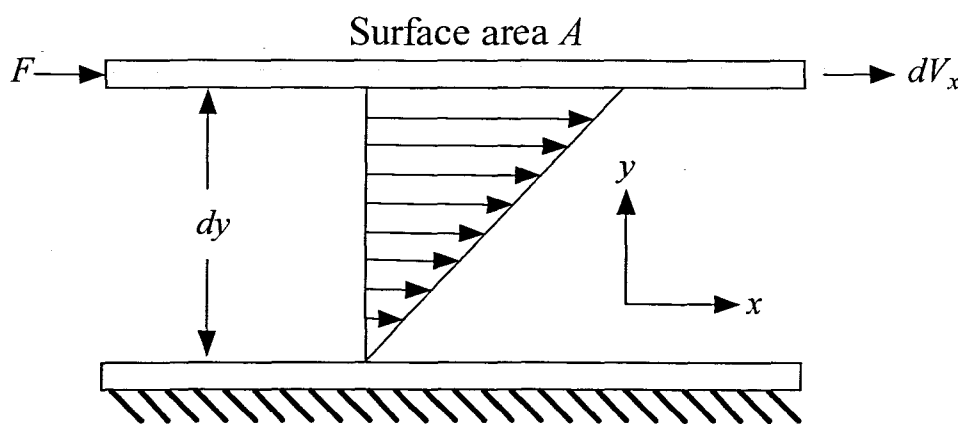


Figure 2.2: Schematic representation of unidirectional flow

In this case, the shear rate may be expressed as the velocity gradient in the direction perpendicular to that of the shear force:

$$\frac{F}{A} = \tau_{yx} = \mu \left( -\frac{dV_x}{dy} \right) = \mu \dot{\gamma}_{yx}. \quad (2.3)$$

Note that the first subscript on  $\tau$  and  $\dot{\gamma}$  indicates the direction normal to that of the shearing force, while the second subscript refers to the direction of the force and flow (Chhabra & Richardson, 1999).

The relationship between the shear stress and the shear rate of a fluid owes its original identification to Sir Isaac Newton (Barr, 1931). The ratio of shear stress to shear rate is defined as the Newtonian viscosity  $\mu$ , and is independent of shear rate ( $\dot{\gamma}_{yx}$ ) or shear stress ( $\tau_{yx}$ ), depending only on the material and its temperature and pressure. The plot of shear stress ( $\tau_{yx}$ ) against shear rate ( $\dot{\gamma}_{yx}$ ) is called a ‘flow curve’ or ‘rheogram’ and for a Newtonian fluid the flow curve will be a straight line of slope,  $\mu$ , and passing through the origin. The single constant of proportionality,  $\mu$ , thus completely describes the flow behaviour of a Newtonian fluid at a fixed temperature and pressure (Chhabra & Richardson, 1999).

The relationship between shear stress and shear rate for a Newtonian fluid is depicted in Figure 2.3.

### 2.2.3.2 Non-Newtonian fluid behaviour

A fluid is characterised as a non-Newtonian fluid when the relationship between the shear stress and shear rate of the fluid is not constant. That is, the flow curve of the fluid is non-linear or does not pass through the origin. The apparent viscosity of a non-Newtonian fluid at a given temperature and pressure depends on flow conditions such as shear rate or flow geometry (Chhabra & Richardson, 1999).

Non-Newtonian fluids can be classified into two types, the one known as ‘time-dependent fluid’ and the other one as ‘time-independent fluid’ (Mott, 2006). The model mining suspensions used

in this research are classified as time-independent fluids to a certain degree, because of the slow settling time of the particles in the slurries. Thus care should be taken while testing any non-Newtonian slurry.

Different non-Newtonian fluids can be described by different rheological models. Figure 2.3 depicts different relationships between shear stress and shear rate. The rheological models used to rheologically characterise the mineral suspensions in this work are described in the next section. It must be noted that the flow behaviour depicted in Figure 2.3 is only for time-independent fluids.

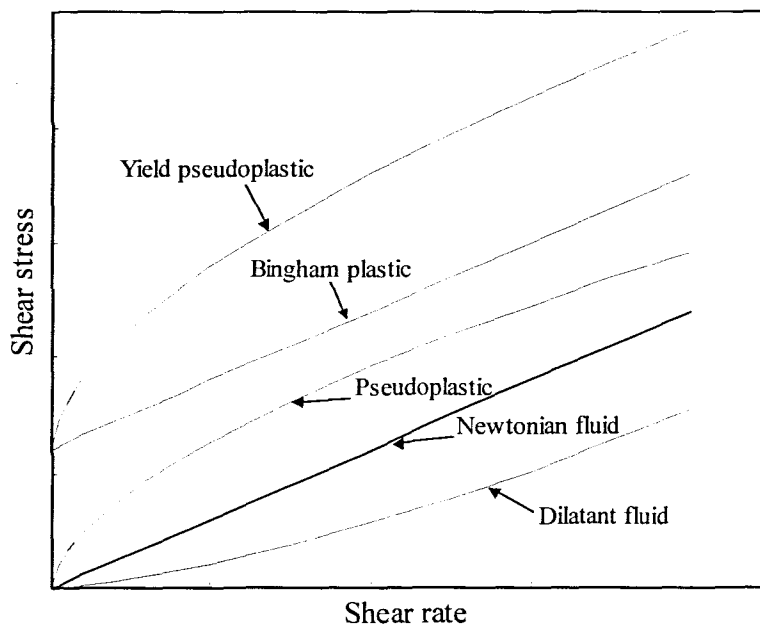


**Figure 2.3: Relationship between shear stress and shear rate for Newtonian and non-Newtonian fluids (Chhabra & Richardson, 1999)**

## 2.2.4 Non-Newtonian models

The models used to rheologically classify the model mining suspensions used in this thesis are the pseudoplastic, Bingham and yield-pseudoplastic models.

### 2.2.4.1 Pseudoplastic or shear-thinning model

This is the most common type of time-independent non-Newtonian fluids and is characterised by an apparent viscosity which decreases with increasing shear rate. The mathematical model for this kind of behaviour is as follows:

$$\tau = K(\dot{\gamma})^n . \quad (2.4)$$

This mathematical model is also known as the power-law model. In this equation,  $K$  and  $n$  are two empirical curve-fitting parameters and are known as the fluid consistency coefficient and the flow behaviour index respectively (Chhabra & Richardson, 1999). Depending on the value of the fluid behaviour index,  $n$ , the following rheological models can be described by the power-law model:

- Pseudoplastic or shear-thinning  $(n < 1)$
- Newtonian  $(n = 1)$
- Dilatant or shear-thickening  $(n > 1)$

### 2.2.4.2 Bingham plastic model

This is the simplest model describing the flow behaviour of a non-Newtonian fluid with a yield stress. The yield stress of a fluid can be defined as the force per unit area required to break down the rigid structure of the material and initiate laminar flow (Chhabra & Richardson, 1999). Slurries with a yield stress are widely found in the mining industry and represent a big challenge for pipeline and open channel designers, as these fluids are very viscous and require a much higher pumping pressure.

The equation for the Bingham plastic model is as follows:

$$\tau = \tau_y + K(\dot{\gamma}). \quad (2.5)$$

The Bingham plastic model is a linear equation and the shear stress intercept represents the yield stress of the fluid (Chhabra & Richardson, 1999).

#### 2.2.4.3 Herschel-Bulkley or yield-pseudoplastic model

To embrace the non-linear curve for the pseudoplastic flow behaviour, a simple generalisation of the Bingham plastic model is made. The flow curve can be described as follows:

$$\tau = \tau_y + K(\dot{\gamma})^n. \quad (2.6)$$

This is in fact a yield power-law model (see Equation 2.4) with  $\tau_y$  equal to zero. It will be noted that the Herschel-Bulkley model can easily be modified to describe the previously mentioned models. Table 2.1 shows how special cases of the Herschel-Bulkley model can be used to describe the flow behaviour of Newtonian, Bingham plastic or Power-law fluids (Steffe, 1996).

**Table 2.1: Newtonian, Bingham plastic and Power-law Fluids as special cases of the Herschel-Bulkley model (Equation. 2.6)**

Fluid	$K$	$n$	$\tau_y$	Typical Examples
Herschel-Bulkley	$> 0$	$0 < n < 1$	$> 0$	minced fish paste, raisin paste
Newtonian	$> 0$	1	0	water, fruit juice, milk, honey, vegetable oil
shear-thinning (pseudoplastic)	$> 0$	$0 < n < 1$	0	applesauce, banana puree, orange juice concentrate
shear-thickening (dilatant)	$> 0$	$1 < n < \infty$	0	some types of honey, 40% raw cornstarch solution
Bingham plastic	$> 0$	1	$> 0$	Toothpaste, tomato paste

### 2.2.5 Rheometry for non-Newtonian models

Rheometry or viscometry deals with the establishment of a relationship between the shear stress and shear rate of a specific fluid. This relationship is used to establish rheological parameters used in the relevant rheological model for the specific fluid or suspension. The rheological parameters are  $\tau_y$ ,  $K$  and  $n$  (Slatter, 1997). In order to establish these parameters, tube, capillary or rotational viscometers are used. The rheological characterisation of mineral suspensions are complex and both rotary and tube viscometers can be used, but have limitations (Haldenwang *et al.* 2006). Conventional rheometers, such as rotational and oscillation rheometers, are instruments that are freestanding and require samples to be taken and analysed in a laboratory. Analog programmers and on-line recorders for plotting flow curves have been on the market since around 1970. Around 1980, measuring data could be stored and many analysis methods were handled by digitally controlled instruments, including complex ones (Mezger, 2002).

In this research, only tube and rotary viscometers were used for the rheological characterisation of the model mining suspensions.

### 2.2.5.1 Rotational viscometry

Various configurations of rotational viscometers are used to rheologically characterise the flow behaviour of non-Newtonian fluids.

There are two main types of rotary viscometers, namely controlled shear rate instruments and controlled shear stress instruments (Chhabra & Richardson, 1999). Rotational viscometers can be fitted with various types of measuring geometries, such as parallel plate, cone and plate, and concentric cylinder systems (Steffe, 1996). Some of these measuring systems are illustrated in Figure 2.4 below (Haldenwang, 2003).

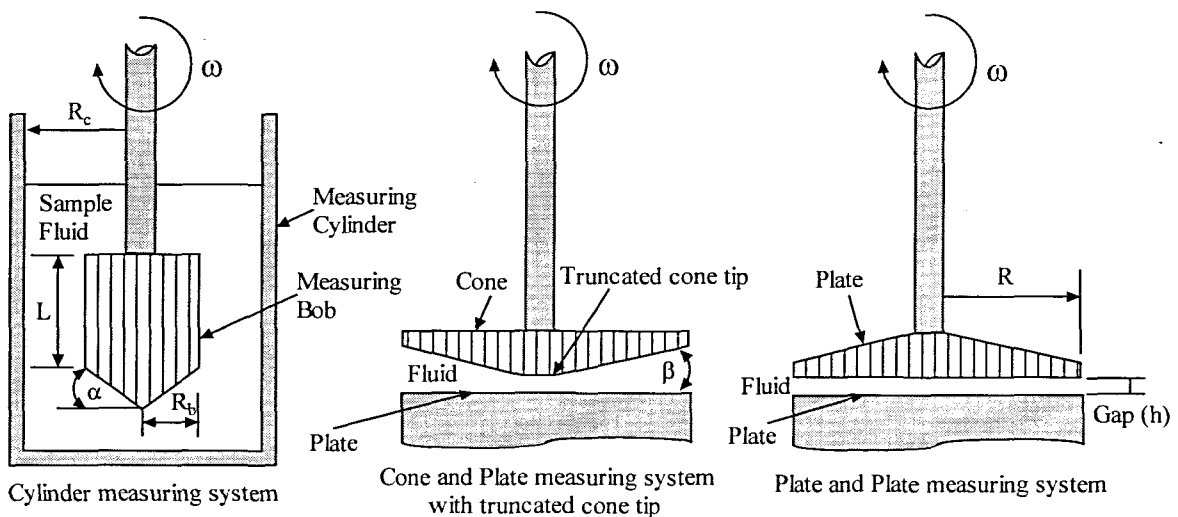


Figure 2.4: Measuring systems of rotational viscometers

It must be noted that the concentric cylinder geometry was used throughout this research and thus only this particular measuring system will be discussed.

- Concentric cylinder measuring system

The concentric cylinder viscometer operates in a moderate shear rate range, which makes it a good choice for collecting data used in many engineering calculations (Steffe, 1996). There are a variety of concentric cylinder measuring systems and the one depicted in Figure 2.4 is only one



type. This type of system has a truncated cone at the lower end of the inner cylinder to minimise end-effects (Chhabra & Richardson, 1999).

The shear stress and shear rate in the shearing gap are only valid for very thin gaps and most suppliers of instruments make assumptions when calculating the shear stress and shear rates.

The representative shear stress ( $\tau$ ) and shear rate ( $\dot{\gamma}$ ), according to Metzger (1998), are as follows:

$$\tau = \left( \frac{\delta^2}{2\delta^2} \right) \left( \frac{T}{2\pi L(R_b)^2 c_L} \right) \quad \text{and} \quad \dot{\gamma} = \omega \left( \frac{\delta^2}{(\beta^2 - 1)} \right), \quad (2.7)$$

where  $\delta = \frac{R_c}{R_b}$ , and  $c_L$  = the resistance coefficient for the frontal area correction. This is found empirically.

The main sources of error in the concentric cylinder type measuring system arise from end-effects, wall slip, inertia, secondary flows, viscous heating effects and misalignment of the geometry (Chhabra & Richardson, 1999).

### 2.2.5.2 Tube viscometry

Tube viscometers may be placed in three basic categories, namely: glass capillaries (often called U-tube viscometers), high pressure capillaries and pipe viscometers. All establish a pressure difference to create flow (Steffe, 1996).

If one uses pipe viscometers, the flow rate and pressure drop need to be measured at multiple different flow rates in laminar flow, usually in two pipes, and then flow curves need to be constructed and rheological parameters extracted. Figure 2.5 below shows how a pump or gas system can be used to create a driving force in pipe viscometers.

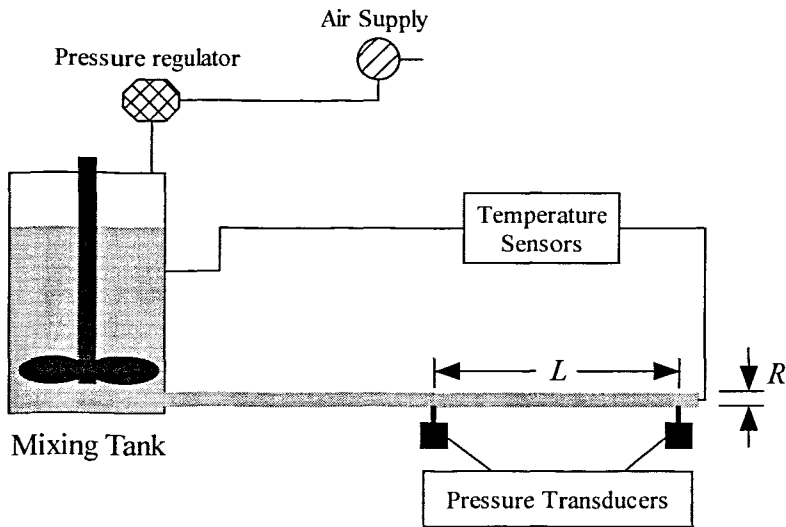


Figure 2.5: Air-driven pipe viscometer

The Balanced Beam Tube Viscometer, originally conceived and developed at the University of Cape Town, South Africa, in the 1980s, is a pipe viscometer which uses compressed air as a driving force in order to initiate laminar flow (Lazarus & Sive, 1984; Lazarus & Slatter, 1986; Neill, 1988; Hardy, 2002; Haldenwang *et al.*, 2006).

For fully developed flow, the relationship between the wall shear stress  $\tau_w$ , the volumetric flow rate  $Q$  and the shear stress  $\tau$ , are as follows:

$$\frac{Q}{\pi R^3} = \frac{1}{\tau_w^3} \int_0^{\tau_w} \tau^2 f(\tau) d\tau, \quad (2.8)$$

where  $\tau_w = \frac{R}{2} \left( \frac{-\Delta P}{L} \right)$  and  $\left( \frac{-\Delta P}{L} \right)$  are equal to the pressure drop per unit length of the pipe.

The shear stress  $\tau$  at any radius  $r$  in the pipe is:

$$\tau = \frac{r}{2} \left( \frac{-\Delta P}{L} \right). \quad (2.9)$$

For a given material, a graph of  $\frac{Q}{\pi R^3}$  vs.  $\tau_w$  gives a unique line for all values of  $R$  and  $\frac{-\Delta P}{L}$  (Chhabra & Richardson, 1999).

The shear rate at the pipe wall is given as  $\frac{4Q}{\pi R^3}$  or  $\left( \frac{8V}{D} \right)$ . The problem with tube viscometry is that the  $\left( \frac{8V}{D} \right)$  values obtained are not the true shear rate values but the wall shear rate values for a non-Newtonian fluid. Thus, this pseudo shear rate has to be transformed to the true shear rate,  $(\dot{\gamma})$ .

According to Chhabra & Richardson (1999), for flow curves of unknown form, Equation 2.8 (after some manipulation) yields:

$$f(\tau_w) = \left( \frac{8V}{D} \right) \left\{ \left( \frac{3}{4} \right) + \frac{d(\log 8V/D)}{4d(\log \tau_w)} \right\}. \quad (2.10)$$

Various forms of this equation are used, a common form being:

$$\dot{\gamma}_w = \dot{\gamma}_{wN} \left( \frac{3n' + 1}{4n'} \right), \quad (2.11)$$

where  $\dot{\gamma}_{wN} = \left( \frac{8V}{D} \right)$ .

The expression for  $n'$  is:

$$n' = \frac{d(\log \tau_w)}{d(\log \dot{\gamma}_{wN})} \quad (2.12)$$

From Equation 2.12 it can be seen that  $n'$  is obtained by plotting a log-log pseudo shear diagram with  $\tau_w$  versus  $\dot{\gamma}_{wN}$  for the laminar flow region, and then obtaining the slope of the tangent of the graph. The slope of this pseudo shear diagram will only be approximately constant if the fluid is a power-law fluid (Chhabra & Richardson, 1999).

**The Rabinowitsch-Mooney transformation procedure for pipe viscometer data can be summarised as follows (Haldenwang, 2003):**

- Plot the laminar flow data  $\left(\frac{D\Delta P}{4L}\right)$  and  $\left(\frac{8V}{D}\right)$  obtained from a tube viscometer on a log-log scale. Different diameter pipes will coincide in the laminar region, whereas the turbulent data will not.
- Fit a mathematical function to the laminar flow data and obtain the first derivative of the equation. This equation will be equal to  $n'$ .
- Calculate  $\dot{\gamma}_w$  using Equation 2.11.
- Plot  $\tau_w$  versus  $\dot{\gamma}_w$  on a logarithmic scale.
- Fit the appropriate equation (Herschel-Bulkley, power-law or Bingham plastic model) to suit the data.
- From these equations, the rheological parameters  $\tau_y$ ,  $K$  and  $n$  can be obtained.

The main sources of error in tube viscometry arise from wall slip and entrance or exit losses (Chhabra & Richardson, 1999).

- Wall slip

Chhabra & Richardson (1999) warn that serious errors may be incurred due to wall slip. In concentrated suspensions, wall slip occurs when the layer of particles near the pipe wall are more dilute than the bulk flow. As a result, apparent slip will occur due to the decrease in viscosity near the pipe wall.

It is important to use more than one pipe diameter in order to detect wall slip. If three pipe diameters are used, the data sets obtained from the laminar flow regions will coincide if there is no wall slip. If this is not the case, the slip velocity must be calculated for each pipe and deducted from the measured average velocity.

- Entrance and exit losses

To minimise entrance and exit losses, one must ensure that the flow is fully developed before differential pressure readings are taken. Slatter (1994) and Haldenwang (2003) used 50 pipe diameters unobstructed flow before and after test sections.

## 2.2.6 Pipe flow

In this section, the fundamentals of Newtonian and non-Newtonian pipe flow are presented.

### 2.2.6.1 Newtonian pipe flow

Consider the laminar, steady and fully-developed flow of a Newtonian fluid in a circular pipe of radius  $R$ , as shown in Figure 2.6. The force balance on a fluid element situated at distance  $r$  from the centre line can be written as:

$$p(\pi r^2) - (p + \Delta p)\pi r^2 = \tau_{rz} \cdot 2\pi rL \quad (2.13)$$

$$\tau_{rz} = \left( \frac{-\Delta P}{L} \right) \frac{r}{2}. \quad (2.14)$$

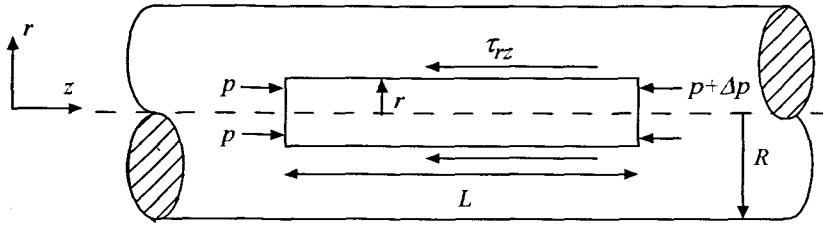


Figure 2.6: Flow through a circular pipe

Equation 2.14 and Figure 2.6 are applicable to laminar and turbulent flow of any fluid since it is based on a simple force balance and no assumption has been made concerning the type of flow or fluid behaviour (Chhabra & Richardson, 1999).

The shear stress at the pipe wall of radius  $R$  is:

$$\tau_w = \frac{D\Delta P}{4L} \quad (2.15)$$

Figure 2.7 depicts a representation of the shear stress and velocity distribution in fully developed laminar flow in a pipe.

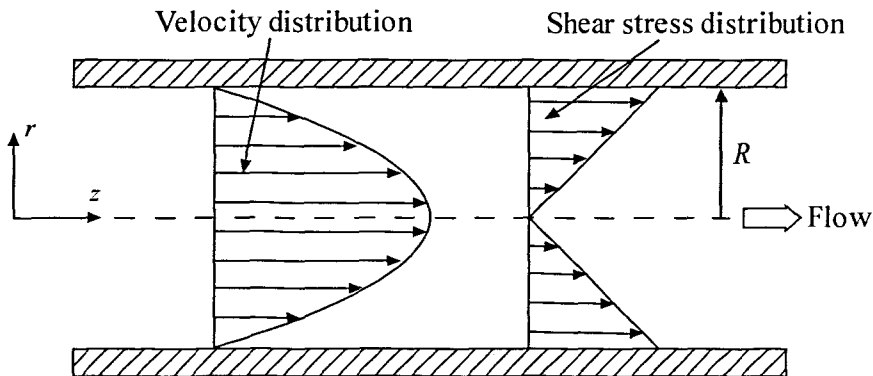


Figure 2.7: Velocity and shear stress distribution in a pipe

From Figure 2.7, it can be seen that the shear stress is at maximum at the pipe wall and zero at the centre of the pipe. The velocity distribution is parabolic and is at maximum at the centre of the pipe and at minimum at the pipe wall.

Figure 2.8 shows the shear stress distribution in a pipe. The flow in the pipe is a function of the wall shear stress, viscosity and diameter (Haldenwang, 2003).

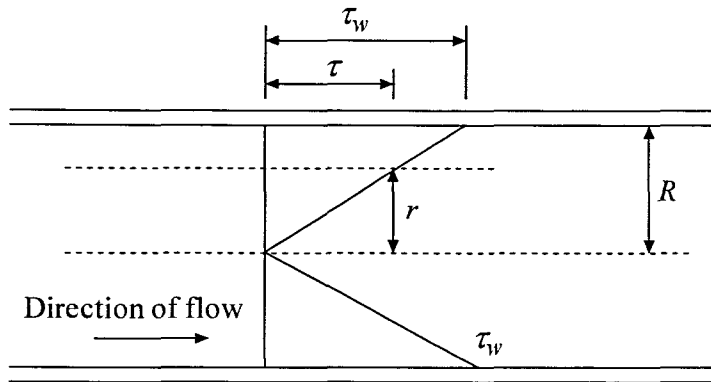


Figure 2.8: Shear stress distribution in a pipe

Integrating over the pipe radius yields:

$$V = \frac{\tau_w D}{8\mu}. \quad (2.16)$$

From Equation 2.16, the relationship between the wall shear stress and  $\left(\frac{8V}{D}\right)$  is derived:

$$\tau_w = \mu \cdot \left(\frac{8V}{D}\right). \quad (2.17)$$

### 2.2.6.2 Non-Newtonian pipe flow

Rheological properties have a strong influence on the shape of the velocity profiles in pipe flow, due to the strong shear rate dependence, which gives a non-linear distribution of shear rates. Understanding these profiles is important for developing a clear picture of instrument performance and in calculating the rheological parameters for a particular fluid. Since tube viscometers operate in the laminar flow regime, only laminar flow velocity profiles are presented here. Velocity profiles for power-law, Bingham plastic and Herschel-Bulkley fluids are discussed.

- Power-law fluids

Equations 2.4 and 2.15 can be combined and integrated (assuming zero velocity at the pipe wall) to give the radial velocity, shear rate and viscosity profiles:

$$v = \left( \frac{nR}{(1+n)} \right) \left( \frac{R\Delta P}{2LK} \right)^{\frac{1}{n}} \left( 1 - \left( \frac{r}{R} \right)^{1+\frac{1}{n}} \right) \quad (2.18)$$

$$\dot{\gamma} = \left( \frac{r\Delta P}{2LK} \right)^{\frac{1}{n}} \quad (2.19)$$

and 
$$\mu = \frac{\tau}{\dot{\gamma}} = K \left( \frac{r\Delta P}{2LK} \right)^{1-\frac{1}{n}}. \quad (2.20)$$

The wall shear rate and the viscosity at the pipe wall are given by:

$$\dot{\gamma}_w = \left( \frac{R\Delta P}{2LK} \right)^{\frac{1}{n}} \quad (2.21)$$

and 
$$\mu_w = \frac{\tau_w}{\dot{\gamma}_w} = K \left( \frac{R\Delta P}{2LK} \right)^{1-\frac{1}{n}}. \quad (2.22)$$

Although the power-law model predicts an unrealistic infinite shear viscosity at the centre of the pipe for shear-thinning fluids ( $n < 1$ ), it predicts a realistic finite viscosity at the pipe wall (Wiklund, Johansson, Shaik, Fischer, Windhab, Stading & Hermansson, 2002).

Equation 2.18 can be used to obtain the volumetric flow rate:

$$Q = 2\pi \int_0^R v r dr = \frac{\pi n R^3}{(3n+1)} \left( \frac{R\Delta P}{2LK} \right)^{\frac{1}{n}}. \quad (2.23)$$

Figure 2.9 shows different laminar velocity profiles for power-law fluids with different values for the flow behaviour index. Lower values of the flow behaviour index result in a flatter velocity profile. The curve for a Newtonian fluid is found at  $n = 1.0$  (Steffe, 1996).



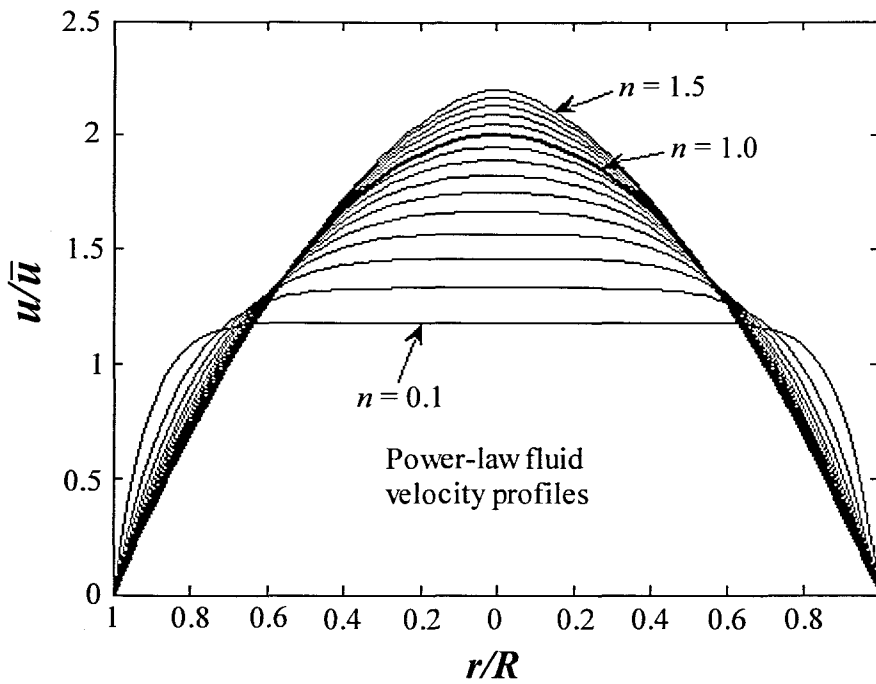


Figure 2.9: Laminar velocity profiles for power-law fluids

Clearly, the flow behaviour index has a very strong influence on the velocity profile of the fluid.

- Bingham plastic and Herschel-Bulkley fluids

Some non-Newtonian fluids do not flow until a critical yield stress  $\tau_y$  is exceeded. The application of a stress greater than the yield stress results in the formation of a moving plug in the centre of the pipe (see Figure 2.10).

Equations 2.15 and 2.6 can be combined and integrated (assuming zero velocity at the pipe wall) to give the radial velocity, shear rate and viscosity profiles:

$$v = \left( \frac{n}{(1+n)} \right) \left( \frac{\Delta P}{2LK} \right)^{\frac{1}{n}} \left( (R - R_{plug})^{1+\frac{1}{n}} - (r - R_{plug})^{1+\frac{1}{n}} \right) \quad (2.24)$$

$$\dot{\gamma} = \left( \frac{\Delta P}{2LK} \right)^{\frac{1}{n}} (r - R_{plug})^{\frac{1}{n}} \quad (2.25)$$

$$\mu = \frac{\tau}{\dot{\gamma}} = K \left( \frac{\Delta P}{2LK} \right)^{1-\frac{1}{n}} \left( \frac{r}{(r - R_{plug})^{\frac{1}{n}}} \right), \quad (2.26)$$

where  $R_{plug} = \frac{2L\tau_y}{\Delta P}$  is the plug radius. At the pipe wall, the shear rate and viscosity are given by:

$$\dot{\gamma}_w = \left( \frac{\Delta P}{2LK} \right)^{\frac{1}{n}} (R - R_{plug})^{\frac{1}{n}} \quad (2.27)$$

$$\mu_w = \frac{\tau_w}{\dot{\gamma}_w} = K \left( \frac{\Delta P}{2LK} \right)^{1-\frac{1}{n}} \left( \frac{R}{(R - R_{plug})^{\frac{1}{n}}} \right). \quad (2.28)$$

The Herschel-Bulkley model also predicts an unrealistic infinite shear viscosity at the centre of the pipe for both shear-thinning and shear-thickening fluids. It also predicts a realistic finite viscosity at the pipe wall (Wiklund *et al.*, 2002).

The volumetric flow rate is given by:

$$Q = \pi v_{plug} R_{plug}^2 + \frac{\pi n R^2 (R - R_{plug})^{\frac{1}{n}}}{(n+1)} \left( \frac{\Delta P}{2LK} \right)^{\frac{1}{n}} \dots$$

$$\left[ 1 - \frac{2n}{(3n+1)} \left( 1 - \frac{R_{plug}}{R} \right)^2 - \frac{2n R_{plug}}{(2n+1)R} \left( 1 - \frac{R_{plug}}{R} \right) - \left( \frac{R_{plug}}{R} \right)^2 \right]. \quad (2.29)$$

Figure 2.10 shows laminar velocity profiles for Bingham plastic fluids. The constant  $c$  is defined in terms of the yield stress or the plug radius:  $c = \frac{\tau_y}{\tau_w} = \frac{R_{plug}}{R}$ . It can be seen that increasing the yield stress enlarges the radius of the plug flowing down the centre of the pipe. The curve for a Newtonian fluid is shown by the line with  $c = 0$  (Steffe, 1996).

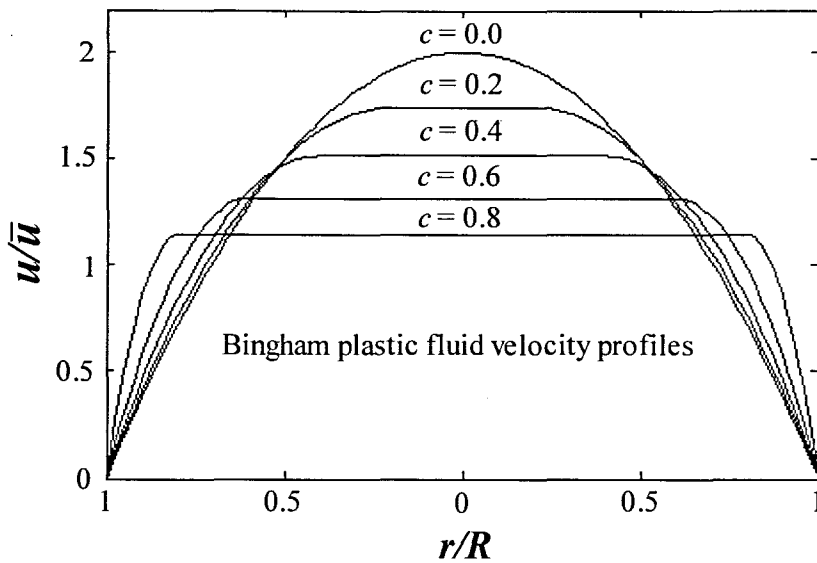


Figure 2.10: Laminar velocity profiles for Bingham plastic fluids (Steffe, 1996)

### 2.2.7 Conclusion

It is clear, from the literature, that rheology is a very complex subject, both experimentally and theoretically. The flow of non-Newtonian slurries in transportation pipes have significant applications in the field of mining where dense slurries have to be transported around plants and to tailing dams. As water becomes scarcer, limited by legislation and more expensive; higher concentrations need to be transported. Determining the rheological parameters of these highly concentrated slurries in the mining industry is a difficult challenge and is becoming even more complex with water becoming scarcer.

## 2.3 ULTRASOUND PHYSICS

This section is divided into three sub-sections. The first sub-section discusses basic ultrasound physics with regard to ultrasound propagation in fluids and the second explains ultrasound propagation through different materials. Parameters which influence ultrasound propagation in fluid suspensions are discussed in the last section. A brief introduction comprising the history and, lastly, a conclusion of ultrasound theory are also presented.

### 2.3.1 Introduction

The region of acoustical phenomena that are not accessible to human perception because of the high frequencies involved is characterised as ultrasound. Thus ultrasound can be thought of as analogous to ultraviolet light (Kuttruff, 1991). The history of ultrasound over a long period coincides with the history of general acoustics. However, two important discoveries which were of crucial importance for the future development of ultrasound technology took place in the 19<sup>th</sup> century: the discovery of magnetostriction by J. P. Joule in 1847, and that of piezoelectric effect by the brothers J. and P. Curie in 1880 (Kuttruff, 1991). Since then, ultrasound technology has improved significantly and today ultrasound is used in many applications. UVP is just one application from the vast majority of ultrasound applications ranging from medical to high-power industrial applications.

### 2.3.2 Ultrasound propagating in fluids

The attenuation of an ultrasound wave propagating in a fluid can be expressed if the function relating the wave amplitude to the propagating distance is known. The *spatial attenuation coefficient*  $\alpha_0$  characterises the damping of an ultrasound wave with distance in space (Shutilov, 1980). This coefficient is defined by:

$$\alpha_0 = \left( \frac{-1}{A_{MAX}} \right) \left( \frac{dA_{MAX}}{dx} \right). \quad (2.30)$$

$A_{MAX}$  is the wave amplitude of the transmitted ultrasound wave. Figure 2.11 shows how the amplitude of an ultrasound wave reduces with the distance  $\lambda$ , according to the exponential law given in Equation 2.31.

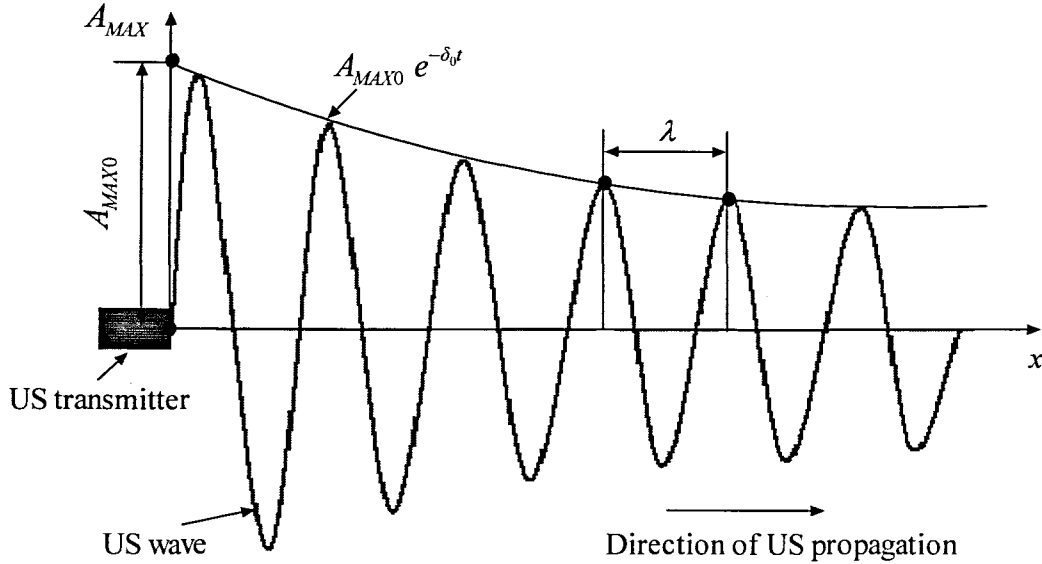


Figure 2.11: Attenuation of an ultrasound wave (Ouriev, 2000)

Within the time delay  $t$ , the sound wave propagates with a sound velocity across a distance  $x$ . Substituting the expression  $x = ct$  in Equation 2.30 gives a general law of ultrasound wave attenuation in a sample fluid, namely:

$$A_{MAX} = A_{MAX0} e^{-\alpha_0 c t}. \quad (2.31)$$

The *damping time constant*  $\tau_0$  is a time-related coefficient and can be expressed as

$$\tau_0 = (\alpha_0 c)^{-1}. \quad (2.32)$$

The inverse of  $\tau_0$  is known as the *temporal attenuation coefficient*  $\delta_0$ . By substituting Equation 2.32 in Equation 2.31, it can be seen that, with time  $t = \tau_0$ , the amplitude of the ultrasound wave has decreased by the factor of  $1/e$  (Ouriev, 2000).

$$A_{MAX} = A_{MAX0} e^{\frac{-t}{\tau_0}}. \quad (2.33)$$

The attenuation coefficient depends on the material, ultrasound frequency, temperature and other possible parameters. For measurements through a pipe wall, it is very important to optimise the choice of the wall material so that one does not use a wall material with a high attenuation coefficient.

### 2.3.3 Ultrasound propagating at the boundary between two materials

According to Shutilov (1980) and Kuttruff (1991), the following analysis is made for the description of ultrasound wave propagation at the boundary between two materials. Figure 2.12 shows that three material layers are taken into consideration.

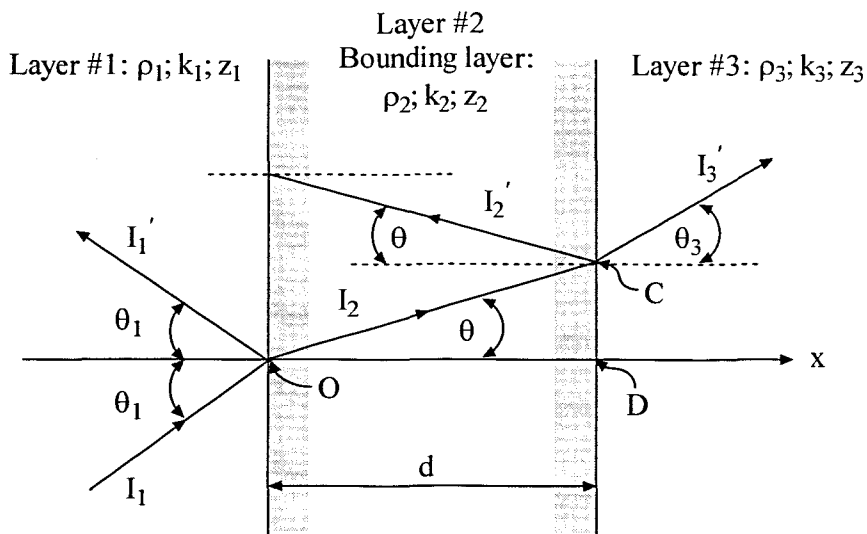


Figure 2.12: Ultrasound wave propagating between two materials (Ouriev, 2000)

The first material layer #1 has a specific acoustic impedance  $z_1 = \rho_1 c_1$ , where  $\rho_1$  is the material layer density and  $c_1$  is the sound velocity in the material (subscript 1 denotes parameters related to material layer #1). Equal definition can be used for material layer #2 and #3. Material layer #2 is defined as the bounding layer with specific acoustic impedance  $z_2 = \rho_2 c_2$ . As illustrated in Figure 2.12, the distance between interfacial locations O and D along the x-axis is the thickness of the bounding layer and is denoted as  $d$ . The ultrasound wave propagates in layer #1 with the inclination angle  $\theta_1$  to the x-axis. At each boundary surface or interface the ultrasound wave

will reflect and diffract. Thus, depending on the acoustic properties of the layer material, the direction of the ultrasound propagation will be changed from layer #1 to layer #2 and also from layer #2 to layer #3 (Ouriev, 2000). As shown in Figure 2.12, the angle  $\theta$  changes at the interface between two different materials. The following law holds for the angle  $\theta$  of refraction:

$$\frac{\sin \theta}{\sin \theta_1} = \frac{c_2}{c_1}. \quad (2.34)$$

Equation 2.34 is known in optics as ‘Snell’s law’ and  $\theta_1$  is the beam angle of the incident ultrasound wave. According to Snell’s law, the following conclusion can be drawn: the higher the sound velocity of material layer #2, the larger the beam angle  $\theta$  will be. If the Doppler method is used (see Section 2.4.2), the beam angle  $\theta$  is an important factor in interpreting the correct velocity information measured along the ultrasound beam (Ouriev, 2000).

When an ultrasound beam propagates through different boundaries or layers, the beam will experience some acoustic energy loss. The analysis that follows is performed to calculate the acoustic energy loss of an ultrasound beam. Consider the incident ultrasound wave perpendicular to the boundary layer #2. The intensity  $I_1$  of the initial ultrasound wave can be written as:

$$I_1 = I_1' + I_2, \quad (2.35)$$

where  $I_1'$  is the intensity of the reflected ultrasound wave and  $I_2$  is the intensity of the refracted ultrasound wave transmitted into the boundary layer #2.

The acoustic energy reflection coefficient can be written as:

$$r_1 = \frac{I_1'}{I_1}, \quad (2.36)$$

and the transmission coefficient can be written as:

$$\kappa_1 = \frac{I_2}{I_1}. \quad (2.37)$$

Thus, the balance of acoustic energy at the interface between two materials with different acoustic impedances is defined as:

$$r_1 + \kappa_1 = 1. \quad (2.38)$$

The energy reflection coefficient can also be written as:

$$r_1 = \left( \frac{z_1 - z_2}{z_1 + z_2} \right)^2 = \left( \frac{c_1 \rho_1 - c_2 \rho_2}{c_1 \rho_1 + c_2 \rho_2} \right)^2, \quad (2.39)$$

where  $z_1$ ,  $z_2$ ,  $\rho_1$ ,  $\rho_2$  and  $c_1$ ,  $c_2$  are the specific acoustic impedance, density and sound velocity of the material layer #1 and boundary layer #2, respectively.

Alternatively, according to Equation 2.37, the reflection coefficient can be written as:

$$r_1 = 1 - \kappa_1 = \frac{4z_1 z_2}{(z_1 + z_2)^2}. \quad (2.40)$$

At this point the phenomena of total reflection must be mentioned. If  $c_2 > c_1$ , then the refraction angle will be larger than the angle of incidence. Since the refraction angle can never exceed  $90^\circ$ , there is a maximum angle of incidence, or the limiting angle of total reflection (Kuttruff, 1991):

$$\theta_1 = \arcsin\left(\frac{c_1}{c_2}\right). \quad (2.41)$$

The maximum angle of incidence is also referred to as the critical angle. At steeper angles of incidence than the critical angle, the sound wave will be totally reflected from the boundary surface. It can be seen from Equation 2.40 and 2.39 that the reflection coefficient will be equal to zero when the material properties of two layers are equal, that is  $z_1 = z_2$ . In this case, the interface between the two layers is ‘transparent’ for the ultrasound wave and no energy loss due to wave reflection will be possible. However, an ultrasound wave reflection between layers #2 and #3 is still possible, provided that the acoustic impedances are not equal, that is  $z_2 \neq z_3$ . Thus



a reflection coefficient  $r_2$  between layers #2 and #3 can be calculated. It must be noted, again, that energy loss is still possible due to absorption of acoustic energy by the boundary layer or material (see Section 2.3.2).

Figure 2.13 shows two different ultrasound transducer installations (Ouriev, 2000).

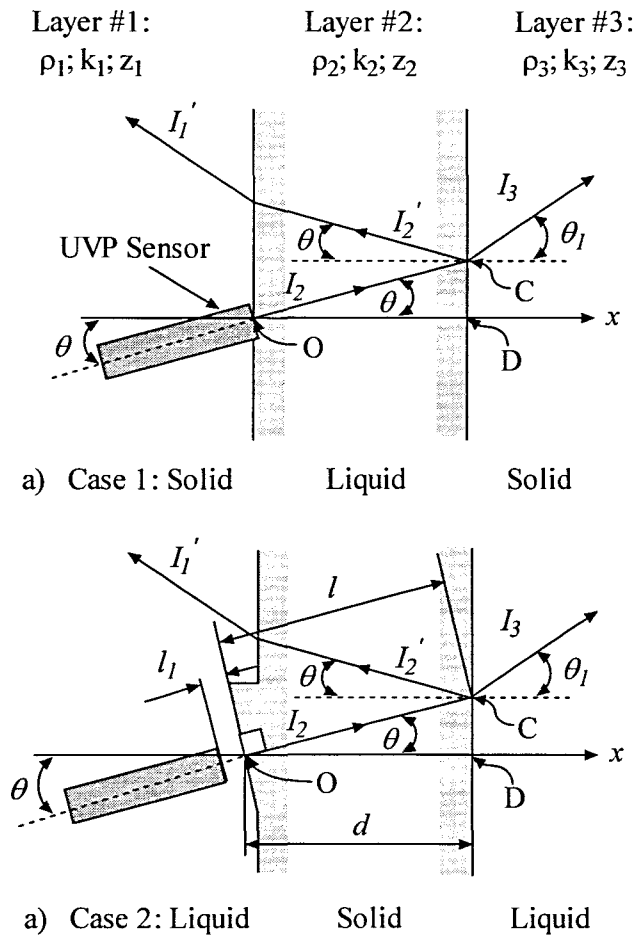


**Figure 2.13: Transducer installation setups and US wave propagation: a) which is in contact with the investigated fluid; b) without contact with the investigated fluid (Ouriev, 2000)**

In the first case it is assumed that layers #1 and #3 are made of solid material and the boundary layer is the investigated fluid sample. In the second case, boundary layer #2 is a solid material and the layers #1 and #3 are fluid samples. As shown in Figure 2.13a, the ultrasound transducer is in direct contact with the investigated fluid sample and is installed in the wall of the pipe or

tube. Under these conditions, no loss of acoustic energy entering the fluid sample occurs. In addition, no correction of the beam (analogous to the Doppler angle) angle  $\theta$  is required, because the beam angle is equal to the inclination angle of the installed ultrasound transducer (Ouriev, 2000).

In Figure 2.13b an ultrasound transducer is installed into an adapter wall and thus the US wave must propagate through the wall (layer #2) of known thickness  $d$ . In this case, layer #1, which is classified as a fluid, is a coupling medium for the ultrasound wave. Ultrasound gel can be used as a coupling medium. The following assumptions of the material layer ‘transparency’ can be made: As shown in Figure 2.13b, the ultrasound wave  $I_3$  propagates in the sample fluid, layer #3, and scatters from the particles which results in an echo signal containing the frequency shift information needed for velocity estimation. The intensity of the emitted ultrasound wave will define the maximum penetration depth (Ouriev, 2000). Assume that the acoustic impedances of layers #1 and #3 are equal, that is  $z_1 = z_3$  and  $r_2 = -r_1$ . The total transmission coefficient is then given by:

$$\kappa_t = \frac{1}{\cos(k_2 d) + i \frac{1+r_1^2}{1-r_1^2} \sin(k_2 d)}, \quad (2.42)$$

where  $k_2$  is the wave number of material layer #2. The wave number  $k$  relates the angular frequency  $\omega$  of the ultrasound wave to wave propagation velocity which is the sound velocity of the ultrasound wave (Ouriev, 2000). Thus, the wave number is a dimensionless parameter and is written as:

$$k = \frac{\omega}{c}. \quad (2.43)$$

According to Equation 2.42, the absolute value of the transmission coefficient becomes unity, corresponding to a completely transparent layer, if the sine function vanishes. For this to be true, the thickness  $d$  must be equal to one half of a wavelength or an integral multiple of it (Kuttruff, 1991). The thickness  $d$  is related to the length of the wave path as follows:

$$d = l \cdot \cos \theta = \frac{n\lambda}{2}, \quad (2.44)$$

where  $n = 0, 1, 2, \dots$ ,  $d = OD$  and  $\lambda$  is the acoustic wavelength. The wavelength  $\lambda$  is related to the sound velocity of the bounding layer #2, as:

$$\lambda = \frac{2\pi}{k} = \frac{c}{f}, \quad (2.45)$$

where  $c$  is the sound velocity and  $f$  is the ultrasound frequency. The frequency  $f$  is expressed in terms of angular frequency of the ultrasound wave according to the following expression:

$$f = \frac{\omega}{2\pi}, \quad (2.46)$$

where  $f = \frac{1}{T}$  and  $T = \frac{2\pi}{\omega}$  is a period of oscillation.

The ‘transparency’ of the bounding layer is characterised independently on its acoustic absorption, but is strongly related to the length  $l$  of the wave path inside the bounding layer #2 (see Figure 2.13b). If the length  $l$ , as well as  $l + l_1$ , are equal to an integer number of the half wavelength sum, then the bounding layer #2 will denote as ‘transparent’ (Ouriev, 2000). As shown in Figure 2.13b, the ultrasound transducer is recessed inside the layer #1, so that the distance between the sensor front and the boundary layer #2 is equal to  $l_1$ . According to these assumptions, the ‘transparency’ of bounding layer #2 can be maintained by adjustment of the distances  $l$  and  $l_1$ . The above analyses do not consider attenuation of the ultrasound beam within the material layer #2 and surrounding layers #1 and #3. Correct adjustment of the ultrasound transducer position is one of the most sensitive parts of the installation procedure and the following parameters must be optimised during the installation procedure (Ouriev, 2000):

- Length  $l$ , the optimisation of this parameter can be performed based on Equation 2.44.
- The distance  $l_1$  between the transducer front and the wall material (see Figure 2.13b) should be adjusted in order to maintain maximum ultrasound energy transfer through the boundary layer #2.

- Sound velocity of the adapter wall material (see Equations 2.44 and 2.45).
- Attenuation coefficient  $\alpha_0$  of the ultrasound wave within layers #1, #2 and #3 must be given consideration (see Section 2.3.2).

Polyvinyl chloride (PVC) was chosen for the adapter wall material, because of the reasonable acoustic properties and availability of the material. Table 2.2 shows ultrasound wave amplitude measurements, as well as sound velocity measurements, within the solid material. It can be observed that the amplitudes of the higher frequency (8 MHz) wave are lower than the amplitudes of the 4 MHz ultrasound wave (Ouriev, 2000).

**Table 2.2: Sound velocity and ultrasound wave amplitude measurements in PVC**

Sample	$T$ (°C)	$\rho$ (gr/cm <sup>3</sup> )	$f_0$ (MHz)	Distance (mm)	Amplitude (mVolt)	$c_L^*$ (m/s)	$c_M^*$ (m/s)
PVC	25	1.420	4	14	2.5	2300	2444
				25	0.65		
PVC	25	1.420	8	14	0.4	2300	2444
				25	0.2 (no response)		

\*  $c_L$  stands for sound velocity from literature and  $c_M$  for measured values.

### 2.3.4 Influences on ultrasound propagation

There are many parameters that influence ultrasound propagation in the fluids that are under investigation. The parameters that are discussed in this section are pressure, density, viscosity, solids concentration and temperature.

#### 2.3.4.1 Influence of absolute pressure and density on ultrasound

Figure 2.14 shows a small-volume element exposed to compression from all sides. The normal stresses acting on the surface of the cube are denoted as  $-\tau_{11} = -\tau_{22} = -\tau_{33} = P$  and are defined as parallel to axis directions  $x$ ,  $y$  and  $z$ . Equation 2.47 can be used to describe the absolute pressure  $P$  acting on a material element:

$$P = -\left(\lambda_{LM} + \frac{2}{3}\mu_{LM}\right) \cdot \Theta, \quad (2.47)$$

where  $\lambda_{LM}$  and  $\mu_{LM}$  are Lamé constants related to the linear elasticity modulus  $c_{nm}$  (Ouriev, 2000).

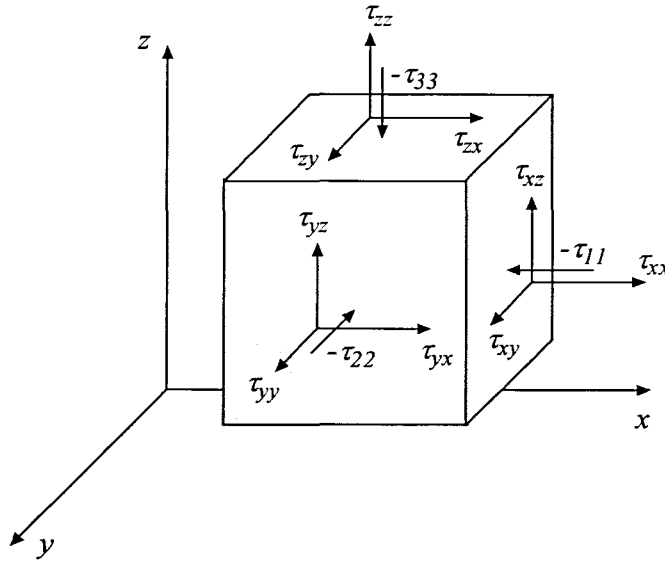


Figure 2.14: Normal stresses acting on a material element (Ouriev, 2000)

A term of volume compaction  $\Theta$  is used to express positive pressure and it can be resolved by summing the deformations acting in axial direction:

$$\Theta = \varepsilon_{11} + \varepsilon_{22} + \varepsilon_{33}. \quad (2.48)$$

The propagation of ultrasound is in general comparable to an adiabatic process of compaction and expansion and thus the definition of the elasticity modulus  $c_{nm}$  assumes an adiabatic deformation (Ouriev, 2000). Hook's law describes a more general form of volume contraction, namely

$$K = \lambda + \left(\frac{2}{3}\right) \cdot \mu, \quad (2.49)$$

where  $K$  is a volumetric elasticity modulus and  $\mu$  is resolved by Poisson's  $\nu_p$  and Young's modulus  $E$  as

$$\mu = E[2(1 + \nu_p)]^{-1}. \quad (2.50)$$

As discussed, the propagation of an ultrasound wave approaches an adiabatic process. Using general thermodynamics, the linear form of the adiabatic process can be described by the adiabatic linear modulus of bulk elasticity  $K_{AD}$  which is defined as

$$p_{\text{excess}} = K_{AD}^s, \quad (2.51)$$

where  $s = \Delta\rho / \rho_0$  and  $p_{\text{excess}} = P - P_0$  denote excess pressure (Ouriev, 2000). The subscript 0 describes the state of the medium at rest, thus  $P_0$  is the absolute atmospheric pressure.

From Equation 2.51 it can be seen that a change of absolute pressure is related to material density changes. The amplitude  $A_{MAX}$  of an ultrasound wave with ultrasound intensity  $I$  can be expressed as follows:

$$A_{MAX} = \sqrt{\frac{2I}{\rho \cdot c}}. \quad (2.52)$$

By changing the subject of the formula, the sound velocity  $c$  can be derived as

$$c = \frac{2I}{\rho \cdot A_{MAX}^2}. \quad (2.53)$$

The material density increases with the increase of absolute pressure and, according to Equation 2.53, an increase of material density causes a decrease of sound velocity (Ouriev, 2000).

#### 2.3.4.2 Influence of fluid viscosity on ultrasound

The attenuation of ultrasound is usually described by the spatial attenuation coefficient  $\alpha_0$  (see Section 2.3.2), which is related to the bulk viscosity of the fluid according to Stoke's equation:

$$\alpha_0 = \frac{2\pi^2 f^2 \mu}{(\rho_0 c_0^3)}, \quad (2.54)$$

where  $\rho_0$  is the material density,  $\mu$  is the bulk viscosity and  $f$  is the emitting frequency of the ultrasound wave. The attenuation of the ultrasound wave is described by the attenuation coefficient due to viscous losses. This means that the amplitude of the ultrasound wave will be reduced by a factor of  $e = 2.72$  if propagating for a distance  $x = \alpha_0^{-1}$  (Ouriev, 2000).

The attenuation coefficient  $\alpha_0$  is proportional to the square of the emitting frequency  $f^2$ . Therefore the scattering properties of the surrounding material are also related to frequency, namely:

$$\alpha_0 / f^2 = \frac{2\pi^2 \mu}{(\rho_0 c_0^3)} = \frac{8\pi^2 \mu_s}{(3\rho_0 c_0^3)}, \quad (2.55)$$

where  $\mu_s$  is a shear viscosity (Ouriev, 2000).

### 2.3.4.3 Influence of solids concentration on ultrasound in fluid suspensions

Newton's second law describes the propagation of sound very well, whereby a force acting on an element of the material accelerates the material. Therefore the mass and stiffness of the material through which the ultrasound passes, are the crucial factors determining the velocity of sound in the material (Povey, 1997).

Equation 2.56 describes the sound velocity as a function of adiabatic compressibility and density (Urlick, 1947):

$$c = (\rho K_{AD})^{-\frac{1}{2}}, \quad (2.56)$$

where  $c$  is the sound velocity,  $\rho$  is the fluid density and  $K$  is the adiabatic compressibility. This equation can only be applied for suspensions with infinitely small particles compared to the wavelength of the ultrasound wave (Ouriev, 2000). Another boundary condition is that the

density difference between the liquid matrix and the solid phase should be negligible. Taking these boundary conditions into consideration, the following equations can be derived:

$$K_{AD}^{-1} = (1 - C_V)K_{1AD} + C_V K_{2AD} \quad (2.57)$$

and

$$\rho = (1 - C_V)\rho_1 + C_V \rho_2, \quad (2.58)$$

where  $K_{1AD}$  and  $K_{2AD}$  are the adiabatic compressibility of the continuous and disperse phases, respectively, and  $C_V$  is the volume concentration of the suspension (Povey, 1997). Equation 2.57 and 2.58 can be used to modify the attenuation coefficient described in the previous section (Equation 2.55):

$$\alpha_0 / f^2 = 8\pi^2 \mu_s / (3c^3 ((1 - C_V)\rho_1 + C_V \rho_2)), \quad (2.59)$$

where  $f$  is the cyclic frequency of the ultrasound wave and  $\mu_s$  is the shear viscosity (Ouriev, 2000).

#### 2.3.4.4 Influence of temperature on ultrasound

It is very important to be aware of the temperature dependence of the propagation of ultrasound in water. The temperature coefficient of the velocity of sound in water is positive at temperatures up to 74 °C, unlike most other liquids. For instance, the sound velocity in water increases from  $c \approx 1482$  m/s at temperature 20 °C up to  $c \approx 1550$  m/s at 60 °C. This complicates the dependence of the velocity of sound in materials which contain water (Povey, 1997). According to the Stokes-Kirchoff equation, the attenuation coefficient  $\alpha_0$  can be written as:

$$\alpha_0 / f^2 = \frac{2\pi^2}{\rho_0 c_0^3} \left( \mu + \frac{\gamma - 1}{c_p} \lambda_0 \right), \quad (2.60)$$

where  $\mu$  is the bulk viscosity,  $\gamma = \frac{c_p}{c_v}$  is a ratio of heat capacities under constant pressure and



$\lambda_0$  denotes the thermal conductivity (Shutilov, 1980).

### 2.3.5 Conclusion

The physics of ultrasound is complicated and one should therefore always be aware of physical aspects such as beam divergence and attenuation when parameters are being measured. Theoretical knowledge of ultrasound physics should be applied in order to avoid negative aspects and to ensure accurate measurements.

## 2.4 ULTRASONIC DOPPLER VELOCIMETRY (UDV)

In this section, the theory and working principle of the pulse ultrasonic Doppler velocity profiling technique is discussed.

### 2.4.1 Introduction

Ultrasound can penetrate optically opaque materials and can provide high-quality information in a rapid and non-invasive manner. There are many benefits in the use of Ultrasonic Doppler Velocimetry for process monitoring: it can be fast, accurate, reliable and sometimes relatively low-cost. This method in some cases is also the only feasible way of determining process parameters (Povey, 1997).

Takeda (1986, 1995 & 1999) developed a new ultrasonic velocity profile method for fluid mechanical measurements in physics and engineering. This method makes use of pulsed ultrasonic echography together with the detection of the instantaneous Doppler shift frequency. This method was originally developed in medical engineering to measure blood flow by means of Doppler sonography during the 1960s (Kuttruff, 1991). The method gives an instantaneous velocity distribution or a ‘profile’ across a pipe vessel, but only along a single pulsed beam axis. This led to the development of the Ultrasonic Velocity Profile (UVP) Monitor. The UVP monitor has been marketed and further developed by Met-Flow, in Lausanne, Switzerland. There are several other instruments for use outside the medical field, such as the DOP ultrasonic

velocimeter marketed by Signal-Processing in Lausanne, Switzerland. In this research, however, the UVP monitor supplied by Met-Flow was used.

## 2.4.2 The Doppler effect

When an observer is in motion toward a stationary source of sound, the pitch (frequency) of the sound that is heard is higher than when the observer is at rest. If the observer is in motion away from the stationary source, a lower pitch is heard (Halliday & Resnick, 1962). This effect was proposed (although not fully worked out) by the Austrian physicist Johann Christian Doppler, who first noticed it in sound waves in 1842 (Halliday, Resnick & Walker, 1993).

Figure 2.15 shows a transducer which transmits a short ultrasound burst and then switches over to receiving mode. The basic frequency of the emitted ultrasonic wave is

$$f_e = \frac{c}{\lambda}, \quad (2.61)$$

where  $c$  is the sound velocity in the fluid sample and  $\lambda$  the wavelength of the emitted ultrasonic wave. When the US pulse hits a small target particle in the fluid, part of the US energy scatters from the particle and echoes back to the transducer. If the suspended particles or reflectors are moving with a non-zero velocity component into the acoustic beam and the transducer (source) is stationary with respect to a moving particle, the Doppler shift takes place, and the received signal frequency becomes ‘Doppler-shifted’ by the frequency  $f_d$ . The received signal frequency can be written as:

$$f_r = f_e \cdot \frac{c - V_{Tr}}{c + V_{Tr}}, \quad (2.62)$$

where  $V_{Tr}$  is the velocity of the target particle.

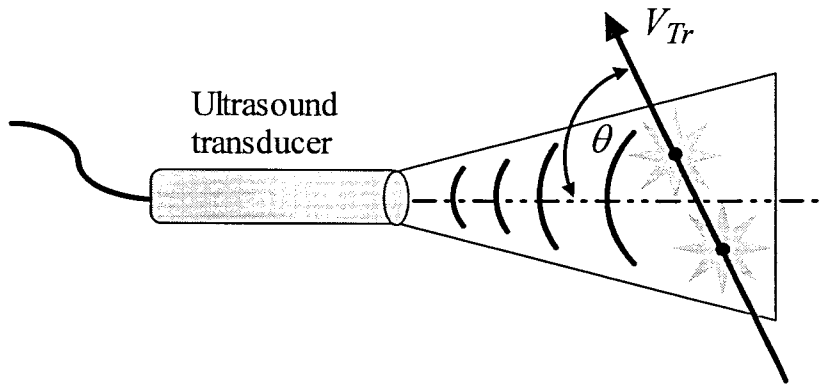


**Figure 2.15: Reflection from a moving particle**

The same transducer is used to receive the echo and a second Doppler shift of echoed frequency takes place, as the reflector now acts as a moving source. Thus, the received echo has been Doppler-shifted twice and by taking the Doppler angle  $\theta$  into consideration, the velocities of the moving reflectors in the fluid medium of interest can therefore be expressed as

$$v = \frac{c \cdot f_d}{2 \cdot f_e \cdot \cos \theta}, \quad (2.63)$$

where  $f_e$  is the emitting frequency and  $f_d = f_e - f_r$  is the difference between the emitted frequency and the received frequency, otherwise known as the Doppler shift frequency (DOP2000 user manual).

It must be emphasised that the Doppler effect is only an artefact in the UVP system. This is because it is not the Doppler shift frequency that is measured, but the time shift or time delay of the received signals. The time shift is then compared to the received proceeding and preceding signal frequencies, depending on the scatter motion. In other words, it is the shift of position of the signals between pulses that is employed, and thus the classical Doppler effect plays a minor role (Jensen, 1996).

### 2.4.3 Working principle of Ultrasonic Doppler Velocimetry

The working principle is described with much detail in Takeda (1986, 1995 & 1999) and in general medical books. Typical parameter values, limitations and practical measurement considerations regarding this type of instrument can also be found in Met-Flow SA (2002). In order to obtain spatial velocity information along the ultrasound beam, the US beam is divided into segments or channels, as depicted in Figure 2.16.

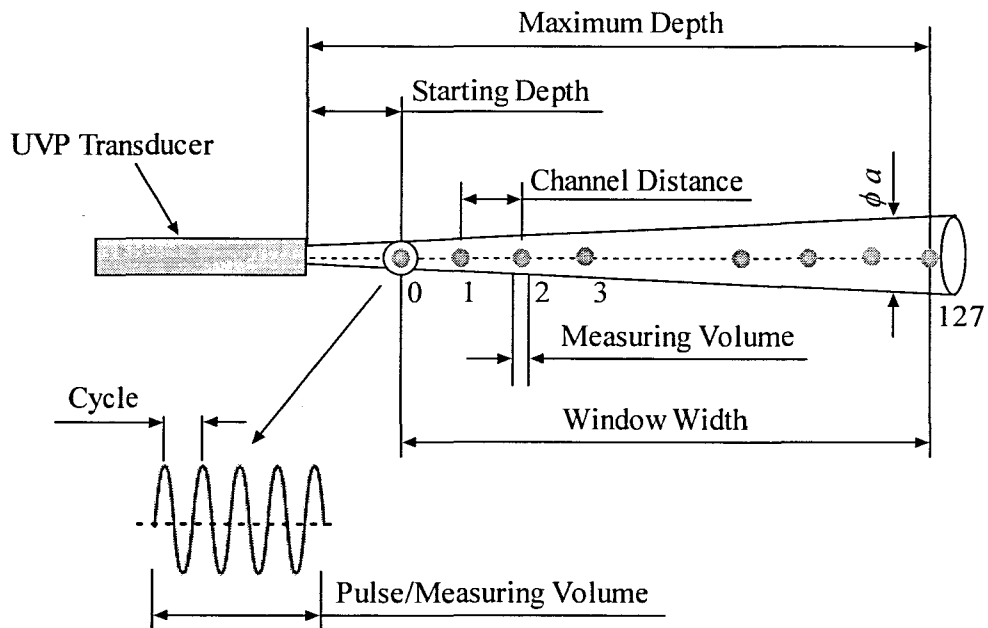


**Figure 2.16: Schematic of the ultrasound beam configuration where  $a$  is the active beam diameter (Ouriev, 2000)**

Each channel in fact is a measuring volume by which the velocity of the target particle is calculated. The UVP-DUO-MX from Met-Flow SA, Switzerland has up to 2048 channels, thus a maximum of 2048 points can be displayed on a velocity profile. However, a measurement does not usually occur over the maximum depth range and thus the highest amount of available channels within the measuring range must be selected in order to maximise the spatial resolution. The channel width is one of the parameters of the UVP monitor that can be exploited in order to increase the spatial resolution of a measurement. As seen in Figure 2.16, the channel width is dependent on the number of cycles per US pulse or emission. Also, no channels are present before the starting depth. This is because the starting depth distance from the transducer is in fact the near field distance, which is not suitable for taking measurements. These parameters are

explained in the next chapter. Figure 2.17 shows a measuring volume and a target particle that has moved a distance  $\Delta s$  in the flow direction and by  $\Delta d$  in the measuring direction.

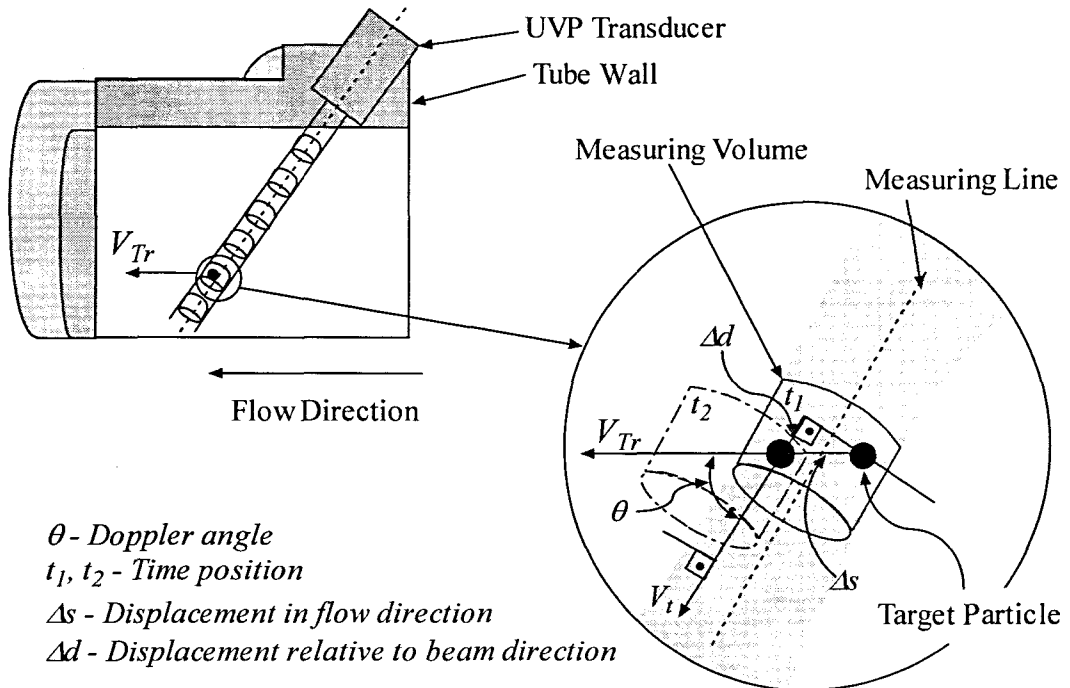


**Figure 2.17: Illustration of a moving target particle within a channel or measuring volume (Ouriev, 2000)**

Within the time delay  $\Delta t = t_2 - t_1$ , a particle suspended in a fluid has moved over the distance  $\Delta d$  along the US beam or measuring line. This distance is written as

$$\Delta d = \frac{(t_2 - t_1) \cdot c}{2}, \quad (2.64)$$

where  $c$  is the sound velocity in the fluid suspension (Ouriev, 2000).

In order to calculate the velocity in the flow direction, the velocity obtained along the ultrasonic beam is corrected with the Doppler angle  $\theta$  as:

$$\Delta s = \frac{\Delta d}{\cos \theta} = \frac{(t_2 - t_1) \cdot c}{2 \cdot \cos \theta}. \quad (2.65)$$

Finally, the velocity of the target particle is calculated according to the following expression:

$$V_{Tr} = \frac{\Delta d}{T_{prf}} = \frac{(t_2 - t_1) \cdot c}{2 \cdot T_{prf} \cdot \cos(90^\circ - \theta)} = \frac{V_t}{\cos(90^\circ - \theta)}, \quad (2.66)$$

where  $V_{Tr}$  is the velocity component in the direction of the mainstream and  $V_t$  is the velocity component in the direction of the measuring line (Ouriev, 2000).

In pulsed Doppler ultrasound, an emitter (US transducer) periodically emits a short ultrasonic burst and a receiver continuously collects echoes issued from targets or particles that may be present in the path of the ultrasonic beam. This echo signal also needs to be amplified to compensate for the attenuation of the ultrasound beam that takes place in most liquids. Furthermore, sophisticated analog and digital filtering techniques, as well as advanced signal processing methods, are used to detect the instantaneous Doppler shift frequencies and to eliminate unwanted frequency components that may be induced by environmental vibrations or noise (Wiklund, 2003). There are several methods for obtaining instantaneous Doppler shift frequencies, such as time domain and auto-correlation methods. Scientists are continuously trying to develop new signal processing algorithms in order to increase the time resolution of a velocity profile measurement, or, in other words, to decrease the amount of time needed to take a single measurement. Another aim is to find new algorithms that work well in a very noisy environment where the signal-to-noise ratio (SNR) is very bad.

#### 2.4.4 Doppler spectrum

In a practical environment with flow of a concentrated suspension, a single target equation of the Doppler shift frequency  $f_d$  (see Equation 2.66) can not be used directly for velocity estimation. Therefore, a group of moving targets or particles scattering ultrasound in a measuring volume must be taken into consideration (Ouriev, 2000). Let us assume that the particles are randomly distributed inside a pipe and the ultrasonic beam, as shown in Figure 2.18. The echoes returned by each particle are then combined in a random fashion, producing a random echo signal. This will result in a wide frequency spectrum being generated and a high number of pulse repetitions being needed. A high degree of correlation exists between US emissions and this is highlighted in all digital signal processing techniques used in UVP monitors in order to extract

information, such as the velocity (DOP2000 user manual). A more detailed explanation on velocity estimation and signal processing techniques can be found in Jensen (1996).

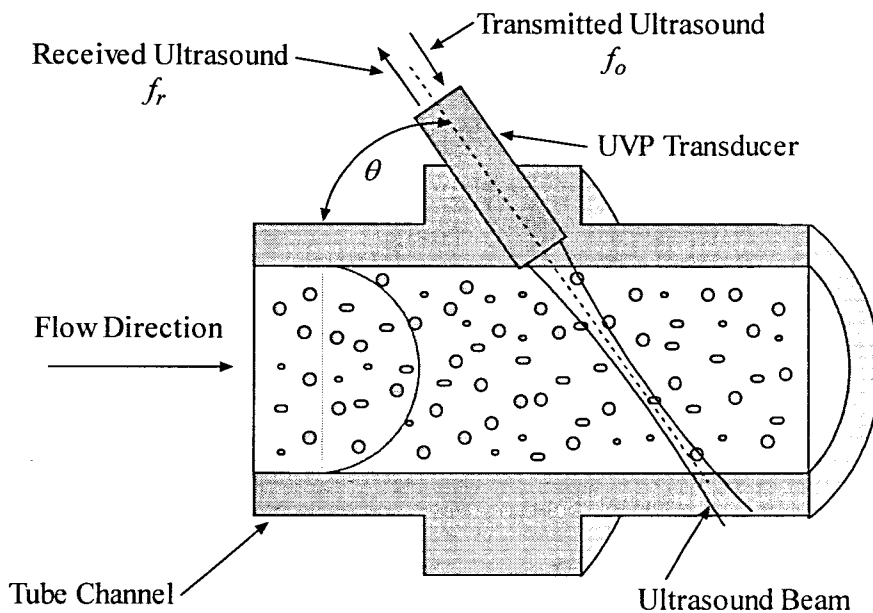


**Figure 2.18: Principle illustration of Doppler ultrasound flow velocity measurement.**

**The transducer positioned with Doppler angle  $\theta$  to the flow direction (Ouriev, 2000)**

Different suspensions within a wide range of concentrations were considered for flow velocity measurements in this research. It will be shown that the difference between low concentrated suspensions and highly concentrated suspensions causes changes in the penetration depth of the ultrasound beam, depending on the type of mineral suspension. The performance of this velocity measurement technique can be improved by optimising the ultrasonic pulse geometry and its intensity, as well as other parameters explained in Chapter 3.

## 2.4.5 Conclusion

It is clear that the pulse ultrasonic Doppler velocity profiling technique has many advantages and different types of applications in fundamental research as well as in industry. It is often quite difficult to put these applications into different categories since many different and interesting aspects of the measurement technique are often dealt with in each study. For readers who are interested, consulting the proceedings of the *International Symposium on Ultrasonic Doppler Methods for Fluid Mechanics and Fluid Engineering* (ISUD) is recommended. This international conference was instituted in 1996 and many different research studies as well as industrial applications in the UVP field are discussed. In this research, the UVP technique was used in combination with a pressure difference measurement to obtain rheological parameters of mineral suspensions. This is discussed in the following section.

## 2.5 THE UVP-PD RHEOMETRIC METHOD

The theory behind the UVP-PD measurement technique, as well as various research groups that have worked with the UVP-PD method from a rheological perspective and have contributed to the development of this concept, are briefly introduced in this section.

### 2.5.1 Introduction

Theoretically, anybody could simply buy a UVP monitor and some pressure transducers, together with peripherals such as a data acquisition board, etc., and set up their own system. However, quite a lot of knowledge about the pulsed Doppler velocity profile technique, transducer adaptor design, rheology, fluid mechanics or statistics, is required to be able to obtain useful and accurate data. This is probably the main reason why this method has so far been tested in a quite limited number of academic research studies, for which experiments have been carried out mainly in pilot-plants or laboratories (Wiklund, 2003).

The UVP-PD set-up and method was developed in Erlangen, Germany, by Steger (1994) and Muller (1997 & 1998). The concept is based on the Ultrasound Pulsed Echo Doppler Velocity



Profile technique (UVP), in combination with a pressure difference method (PD). Ouriev (2000) further developed the in-line ultrasound-based rheometer and this was further modified and optimised by Wiklund (2007) and Birkhofer (2007). For a much more detailed historical background to the development of the UVP-PD concept, please refer to Chapter 4 in Wiklund (2007).

The objective of this research was to use this particular method in order to obtain in-line measurements of concentrated mineral suspensions. Initial test work conducted at the Flow Process Research Centre in a pipe and open channel by Haldenwang, Kotzé, Slatter and Mariette (2006) has shown that ultrasound velocity profiling of these complex mineral suspensions is indeed possible.

### **2.5.2 UVP-PD data acquisition and processing procedures**

A system designed for in-line rheological measurements using the UVP-PD method consists of several components, starting with an instrument designed to measure velocity profiles by using the ultrasonic pulsed Doppler technique. A digital oscilloscope, highly accurate pressure transducers, flow adapters for mounting the ultrasound transducers, data acquisition devices and software development are also required for this method. Regardless of the actual set-up, the UVP-PD method requires several processing steps. A flowchart of the data acquisition and processing steps involved in an in-line rheometer based on the UVP-PD method is given in Figure 2.19 (Wiklund, 2003).

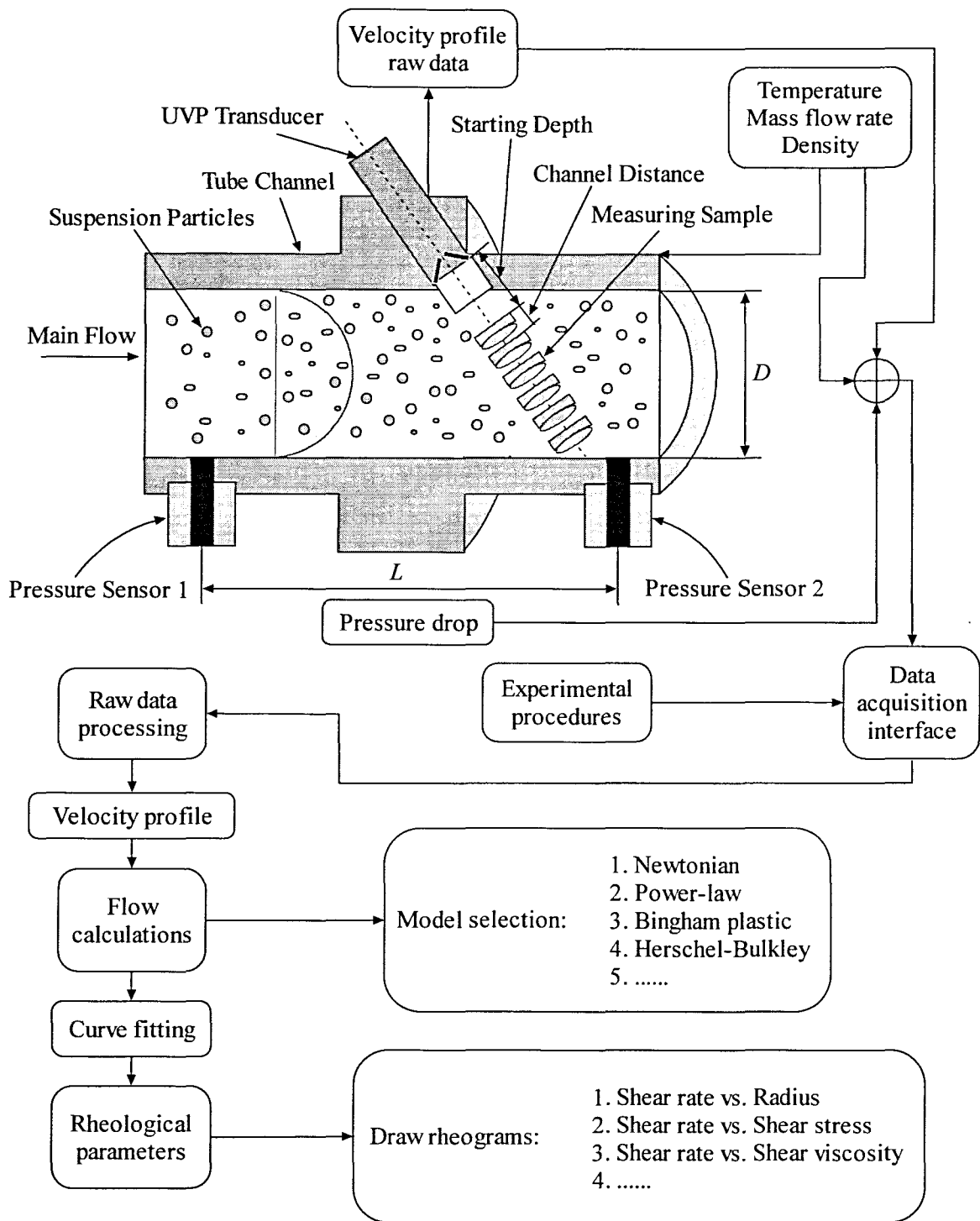


Figure 2.19: General flowchart of the UVP-PD rheometric method (Wiklund, 2003)

The number of steps may, of course, vary from one application to another, depending on what kind information the operator wants in each particular case.

### 2.5.3 Research studies based on UVP-PD

This section serves as background to the rather new UVP-PD rheometric concept. It is quite difficult to put the research studies into different categories since different fluids or model suspensions were used. Each published research study is discussed with a short description and a summary of the results that were obtained.

- Comparison between optical and acoustical rheometers

Brunn, Vorwerk and Steger (1993) introduced three different types of rheometers, two optical instruments and a new acoustical rheometer based on the UVP-PD method. Flow curves of aqueous hydroxylpropyl guar solutions and aqueous polyacrylamide solutions at different concentrations were obtained. The final results of this study showed that the UVP-PD method is the most versatile in-line/on-line rheological method. It can be used for non-invasive measurements of opaque materials and important parameters such as the yield point can also be determined with this method.

- Polyacrylamide and hydroxylpropyl Guar gum solutions

Müller, Brunn and Wunderlich (1997) carried out experiments using a modified DOP1000 instrument from Signal Processing SA. A 4 MHz transducer was mounted with an inclination angle of 5° outside a pipe with an inner diameter of 16.6 mm. A 4000-ppm aqueous Polyacrylamide (PAAm) solution with very strong non-Newtonian behaviour, as well as an 8000-ppm aqueous polymer solution based on Hydroxylpropyl guar gum (HPG), were studied. The results obtained from experiments using a conventional rotational rheometer and the UVP-PD method were in good agreement.

- Chocolate crystallisation process and pipe transport

Ouriev and Windhab (1999) performed direct in-line measurements conducted in a 32 mm straight transporting pipe section of a chocolate crystallisation process. A 4 MHz transducer was fitted to an in-line adapter and pressure sensors were mounted 990 mm apart. Velocity profiles were fitted to the power-law model in order to obtain the fluid consistency index  $K$ , and the fluid behaviour index  $n$ . Yield stress values were obtained from pressure drops and using the Herschel-Bulkley model in the fitting procedure. The in-line yield stress values were compared to values that were obtained using an off-line rheometer and it was found that they exceeded the off-line values slightly. Two major factors were found to influence the flow behaviour of the chocolate suspension: a temperature increase influenced an offset in the shear viscosity and the suspension was exposed to higher deformation rates with increasing flow velocity, which caused an increase in the power-law exponent. Detailed information about these experiments can be found in Ouriev (2000).

- Aqueous Xanthan gum solutions

Local viscosity was obtained at different flow rates of xanthan gum solutions with concentrations of 0.6 and 1.0 kg/m<sup>3</sup> at in a circulating flow system by Köseli, Zeybek and Uludag (2006). The flow system consisted of two tanks, a test section in the form of a rigid polypropylene pipe, connection hoses, a pump, a rotameter, and a control valve. The solutions exhibited shear-thinning behaviour under the experimental conditions and the viscosities obtained by the UVP-PD method as well as the conventional technique agreed well with each other. Dogan, McCarthy and Powell (2003) compared results from in-line measurements of 0.35 % xanthan gum solutions with a conventional off-line rotational rheometer and the difference in shear viscosity was less than 5 %. It has been shown that the viscosity of non-Newtonian fluids can be obtained in a wide range of shear rates and in a matter of a few minutes when using the UVP-PD method. Therefore, this technique shows promise for use as an on-line viscosity sensor for production processes.

- Cornstarch particles suspended in silicon oil

Ouriev and Windhab (2002 & 2003) performed in-line measurements of shear-thinning suspensions in an experimental flow loop, using the UVP-PD method. The suspensions consisted of cornstarch particles 10 – 40 % by weight (0.5 – 38  $\mu\text{m}$ ) suspended in two different silicon oils (AK10 and AK50 from Wacker-chemie GmbH). Rheological flow properties were derived from the simultaneous recording of the velocity profiles and the corresponding pressure drop within a 23 mm pipe. The parameters  $K$  and  $n$  were determined by the non-linear regression of the velocity profiles using a power-law or Herschel-Bulkley model. The yield stress could be determined by measuring the radius of the plug. The results are presented in more detail in a PhD thesis by Ouriev (2000).

- Cornstarch particles suspended in glucose syrup

In addition, Ouriev performed in-line measurements of concentrated shear-thickening suspensions in the same experimental flow loop. The investigated dilatant suspensions consisted of cornstarch particles 10 – 40 % by weight (0.5 – 38  $\mu\text{m}$ ) suspended in two different glucose syrup-water matrices (50- and 70 % by weight). The wall slip effect was investigated by Ouriev and Windhab (2002) and optimum wall slip velocities and power-law exponents were obtained using the UVP-PD method (according to the author).

Wiklund, Johansson, Shaik, Fischer, Windhab, Stading and Hermansson (2001) performed some experiments using the same experimental flow loop as Ouriev. The fluids consisted of cornstarch particles 10 – 30 % by weight suspended in a glucose syrup-water matrix (50 % by weight). The results were in good agreement with conventional rotational rheometers, Physica and Bohlin CS-50.

- Fat crystallisation process and pipe transport

Ouriev, Breitschuh and Windhab (2000) tested the UVP-PD method for in-line measurements in a pilot plant process. The measuring system was installed as part of a section of the transporting pipe in a fat crystallisation process. Measurements were performed in a small capillary slit-channel in a cylindrical pipe with an 8 MHz transducer. Fat crystal suspensions with crystal fractions of 1.6 % to 10.7 % were produced using a batch crystallisation process. A reduction in the power-law index  $n$  was observed at low velocities for the samples with high solid concentration in the fat suspensions over 6 %. This effect could not be seen for lower crystal concentrations. Birkhofer, Shaik, Ouriev and Windhab (2004 & 2006) investigated the response of a cocoa butter fat shear crystallisation process to a step change in flow rate and temperature by using the ultrasound Doppler method. New software was developed to integrate the simultaneous measurements of velocity profiles, pressure difference, temperature and velocity of sound. The cocoa butter suspension was found to be shear thinning depending on the solid fat content.

- Pulp suspensions

Wiklund, Pettersson, Rasmuson and Stading (2004 & 2005) did a comparative study between UVP and Laser Doppler Anemometry (LDA) techniques for highly concentrated pulp suspensions. The results obtained from the UVP technique and LDA were in good agreement. Wiklund and Stading (2004) carried out in-line rheological measurements in a highly concentrated pulp suspension of 7.8 % (w/w). Experimental results showed good agreement with off-line measurements obtained from conventional rotational rheometers.

- Shear-thinning viscoelastic surfactant solutions

Wiklund *et al.* (2001 & 2002) evaluated the UVP-PD method on non-transparent, shear thinning, viscoelastic, multiphase surfactant solutions (shampoo), over a wide range of flow rates. The flow loop and results are described in detail in the mentioned publications and will not be discussed here. Conventional rheometers, Bohlin CS-50, ARES and Physica MCR-300 were used as reference. The in-line results were found to be in very good agreement with the off-line measurements. Statistical data treatment of the recorded velocity profiles was necessary in order to reduce unwanted effects due to scattering air bubbles.

- Concentrated aqueous cellulose fibre suspensions

Wiklund *et al.* (2001 & 2002) performed numerous in-line measurements on highly concentrated aqueous cellulose fibre suspensions flowing through an experimental flow loop, using the UVP-PD method over a wide range of flow rates. Conventional rheometers could not be used for reference as the fibres and water were separated in the geometry due to compression and drainage of the sample occurred. Thus, the UVP-PD method was the only way of determining the viscosity of the fluid suspensions.

- Tomato suspensions

Choi, McCarthy K. L. and McCarthy M. J. (2002) examined the UVP-PD method by measuring the viscosity of tomato juice at different flow rates and comparing their readings with results obtained from Magnetic Resonance Imaging (MRI) measurements. The flow behaviour of the tomato juice was best described by the Bingham plastic model. The shear viscosities obtained using UVP agreed well with the MRI measurements.

Dogan *et al.* (2002 & 2006) performed in-line rheological measurements on diced tomato suspensions using the UVP-PD method. The diced tomato suspension was best described with the use of the Herchel-Bulkley model.

- Other food suspensions

Wiklund and Stading (2006) tested various industrial food suspensions with the use of the UVP-PD method. Food suspensions included rapeseed oil, tomato sauce, syrup and starch particles, strawberry yogurt, fruit jams, marmalades, pasta sauce, cheese sauce and vegetables sauces. Comparison with off-line rheometers showed that off-line measurements often produce unrealistic results since they are performed on rheologically different systems and under different flow conditions. Birkhofer, Wiklund, Stading, Jeelani and Windhab (2007) performed in-line tests on highly concentrated model suspensions which consisted of PA 12 particles in rapeseed oil. High speed rheological measurements including data processing in real time was performed for the first time by Wiklund, Stading and Trägårdh (2007) for a wide range of concentrated industrial and model suspensions. Very good agreement between off-line and in-

line viscometric measurements was found for each system in a comparison over a shear rate range and temperature that matched the conditions in the experimental flow loop.

#### **2.5.4 Conclusion**

The UVP-PD rheometric concept is still relatively unexplored and more research is required before it will be possible to fully utilise the great potential of the UVP-PD systems within the process industry. It can be concluded from the literature that the UVP-PD method has not yet been studied for highly concentrated model mining suspensions and this research therefore should be considered as an important contribution to both the development of this technique and its application in the mining industry.



# **CHAPTER THREE**

## **METHODS OF INVESTIGATION AND APPARATUS**

# CHAPTER THREE

## METHODS OF INVESTIGATION AND APPARATUS

### 3.1 INTRODUCTION

In this chapter, the apparatus used for gathering the data used in the evaluation of the UVP-PD rheometric method are described.

A pilot study was conducted at the Swiss Federal Institute of Technology (ETH) in Zurich, Switzerland during October 2006. The experimental flow loop and other equipment used during this pilot study are also described.

All of the apparatus and instruments were built specifically for this project in order to establish the following:

- Accurate in-line rheological characterisation of all the slurries, using the pipe viscometer (three pipes).
- Accurate in-line rheological characterisation of all the slurries, using the UVP-PD rheometric method (one pipe).
- Conventional off-line rheological characterisation of the slurries, using a rotary rheometer.

The design of the pipe rig was such that the same slurry could be tested in three pipe diameters to establish the *in-line rheology* by applying to two different methods.

Materials that were tested were water for calibration purposes, kaolin clay mineral suspensions, bentonite slurries and Carboxymethyl Cellulose (CMC) solutions, all of various concentrations.

## 3.2 APPARATUS

The different apparatus used for gathering the experimental data for the work presented in this thesis were the rheometer, the pipe rig and the ultrasound instrumentation

### 3.2.1 Rheometers

Two different Paar Physica rheometer models were used for off-line rheological characterisation of the mineral suspensions during the research. All the experiments were performed using the Couette geometry. Viscosity was measured over different shear rate ranges, depending on the type of material.

- Pilot study (ETH)

During the pilot study at ETH, a Paar Physica MCR300 rheometer was used. The MCR300 model is a rotational stress- or strain-controlled rheometer with a unique motor design concept, the permanent magnet synchronous drive. Flow curves were created for the bentonite suspensions and the results were compared with those obtained using the UVP-PD method.

- Research project (FPRC)

The conventional rheometer used at the Flow Process Research Centre (FPRC) was also a Paar Physica MCR300 instrument which was equipped with an air bearing. The configuration that was used to test the mineral suspensions was the cup and bob geometry. This measuring system was used for all off-line work and is depicted in Figure 3.1.

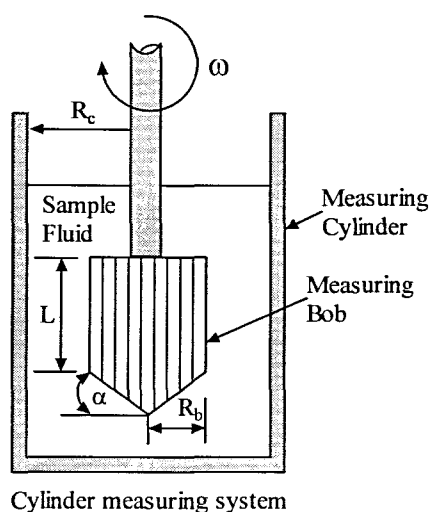


**Figure 3.1: Measuring systems used for off-line rheology**

Flow curves were created for all the mineral suspensions that were tested and the rheological parameters obtained were compared with those obtained from the pipe viscometer and the UVP-PD rheometric method.

### 3.2.2 Experimental flow loop (pilot study)

In this section, the experimental flow loop that was used during the pilot study at ETH, Zurich is briefly discussed.

A Waukesha rotary gear pump was used to feed the system, which consisted of a mixing tank with a capacity of 50 l. The bentonite suspensions were mixed by hand and pumped through the flow loop to assist the mixing process. A valve was fitted at the supply end of the pump in order to take mass flow rate measurements. The flow loop consisted of two pressure tappings with a tapping distance of 1.45 m lengthways. Pressure transducers with a range of 3.5 bar from Kulite were used for pressure difference measurements. A flow adapter for ultrasound transducers was installed between the two pressure tappings. The flow adapter design and sensor installation is explained in Section 3.2.6.3. Stainless steel pipes with a diameter of 22.9 mm were used to construct the experimental flow loop. A glass window installed after the second pressure sensor made it possible to observe the flow of the mineral suspensions inside the stainless steel pipe. For fluid temperature measurements, a thermocouple was submerged into the mixing tank. All the outputs of the pressure transducers and thermocouple were connected to a data acquisition unit linked to a personal computer (PC).

Figure 3.2 shows the schematic layout of the experimental flow loop.

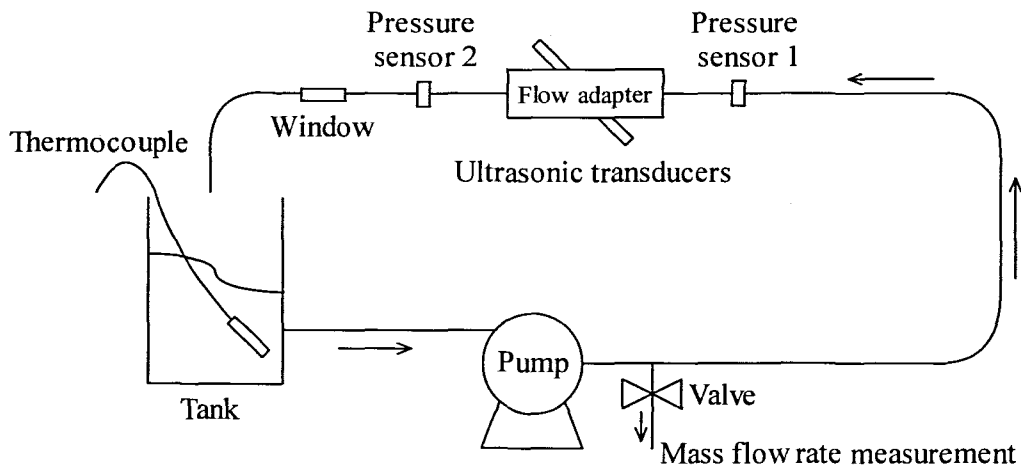


Figure 3.2: Experimental flow loop at ETH

### 3.2.3 The Pipe rig

A unique portable pipe rig was constructed at the Flow Process Research Centre. The pipe rig consisted of a progressive cavity positive displacement pump with variable speed drive which fed through a damper to three PVC tubes and one stainless steel pipe. Three PVC tubes were used as an in-line pipe viscometer. The stainless steel pipe, fitted with housing adapters for ultrasound transducers, was used to measure rheological parameters in-line by using the UVP-PD method. The PVC tubes were in parallel and had 16 mm, 9 mm and 13 mm inner diameters respectively. The stainless steel pipe had an inner diameter of 16 mm. All of the pipes were linked to one in-line mass-flow meter from Danfoss Instrumentation, which could also measure fluid temperature and density. The mixing tank had a capacity of 250 l and was fitted with an electrically driven mixer that ran continuously during the tests. All the outputs of the pressure transducers and the mass-flow meter were connected to a data acquisition unit linked to a personal computer (PC).

The schematic layout of the above is shown in Figure 3.3.

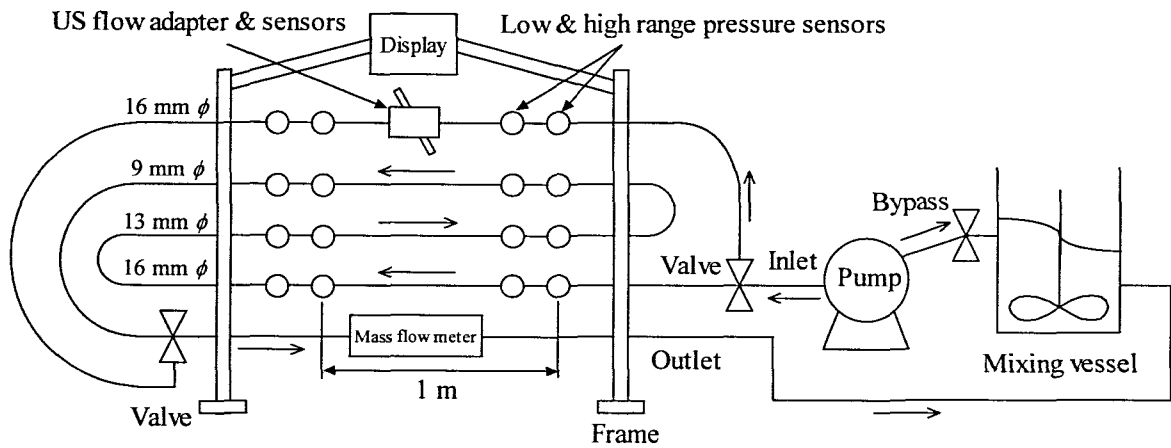


Figure 3.3: Pipe rig layout

### 3.2.3.1 Pressure tappings and transducers

Four pressure tappings that provided four static absolute pressure points, so that differential pressure could be measured, were included on each of the four lines. Two pressure points were reserved for the low-range pressure transducers and the other two points were connected to the high-range pressure transducers. Thus transducers were connected on each line to accurately measure low pressures as well as high pressures. The holes drilled into the pipe walls were 3 mm in diameter and the inside of the pipe was cleaned carefully so that no roughness was left at the tapping entry. Pressure adapters made from PVC, were specially designed and fitted to the pressure tappings. Each adapter contained a 3 mm hole at the side, which was fitted with a valve. This was used to flush any air or dirt out of the pressure configuration before measurements were taken. Figure 3.4 shows a schematic diagram of the pressure configuration. The adapters ensured that the point pressure transducers could easily be connected to the pipeline used for testing.

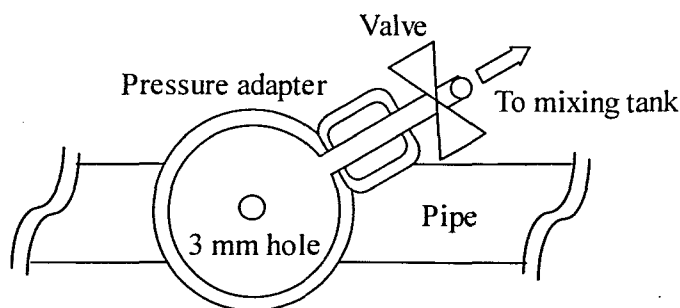


Figure 3.4: Pressure adapter and configuration

All the pressure transducers that were used were supplied by WIKA. The S-11 model with a pressure range of 0 – 10 bar, was selected for the high pressure measurements while the same model, but with a pressure range of 0 – 1 bar, was used for the low pressure readings.

According to Goldstein (1983), errors of less than 3 % of the measured wall shear stress,  $\tau_w$ , are encountered for

$$\left(\frac{D}{\nu}\right) \cdot \sqrt{\frac{\tau_w}{\rho}} \leq 400, \quad (3.1)$$

where  $\nu$  is the kinematic viscosity,  $\rho$  is the fluid density and  $D$  is the diameter of the hole. During testing the value for Equation 3.1 for each wall shear stress measurement was less than ten. Thus the error introduced due to the diameter of the tapping holes was less than 3 %.

### 3.2.3.2 Pump

A progressive cavity positive displacement pump, driven by a 2.2 kW motor regulated by a variable speed drive fed the closed system linking the stainless steel pipe used for ultrasound measurements and the pipe viscometer. The pump motor was also capable of changing direction and thus the flow direction inside the pipe rig could be reversed. This pump was able to deliver approximately 2.5 l/s of water through the pipe rig.

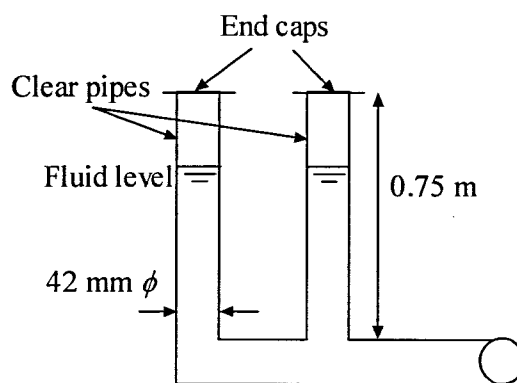


Figure 3.5: Pulsation damping unit

To minimise pump pulsations, a damper was fitted at the supply end of the pump. This is shown in Figure 3.5. The effectiveness of the damper could be observed by observing the large fluctuations of the pressure readings. The vertical pipes were 42-mm clear pipes with PVC caps fitted at the end of the pipes. The flow in the pipe rig was more regular after fitting the damping unit.

### 3.2.4 Ultrasound instrumentation

All of the equipment used to measure velocity profiles by means of the pulse ultrasonic Doppler velocity profiling technique is discussed in this section. The same UVP monitor and ultrasound transducers were used during the pilot study at ETH, Zurich.

#### 3.2.4.1 UVP monitor and parameters

The UVP monitor measures instantaneous velocity profiles including spatial information across the ultrasonic beam by utilising a pulsed Doppler velocity determination technique (Takeda, 1986, 1995 & 1999). The quality of the acoustic velocity profile measurements depends on correct interpretation and optimisation of the fundamental acoustic parameters of the UVP monitor. Therefore a detailed description of these parameters is necessary. A high-resolution ultrasound transducer which works in transmitting and receiving mode, as well as the UVP computer unit containing the signal and data acquisition system, form part of the UVP setup which contributes to the final quality of the measured velocity profile (Ouriev, 2000). The transducer emits ultrasound pulses along the measuring line at a preset rate. This rate is defined as the repetition time between the transmissions of two instantaneous pulses and is known as the Pulse Repetition Frequency (PRF). As mentioned in Section 2.4.3, there are up to 2048 selectable channels along the beam direction. If the sound velocity  $c$  is known, the delays between each channel are converted into absolute distance information during the measuring procedure (Ouriev, 2000). A detailed description and working principle of the UVP monitor can be found in Jensen (1996), Met-Flow SA (2002), Birkhofer (2007) and Wiklund (2007).

The UVP monitor has to compensate for the attenuation of the received echo signal which increases with increasing measuring depth. This is achieved by an amplification procedure which follows an exponential law. The received echo signals are amplified exponentially stronger with



increased measuring depth along the ultrasound beam. The amplification curve or law can be manually adjusted in the UVP monitor software by changing the start and end gain parameters. The following acoustic parameters can be adjusted for the optimisation of a pulsed ultrasonic velocity profile measurement (for more detail, refer to Figure 2.16 on page 2.38):

- *Channel width*: This is the length of the measuring or sample volume. The channel width directly influences the spatial resolution of velocity determination.
- *Number of cycles*: Number of wavelengths in the emitted burst. More cycles in a single ultrasonic burst will increase the signal-to-noise ratio, but will also increase the channel width, which decreases the spatial resolution.
- *Channel distance*: This is the distance between the centres of two adjacent channels or measuring volumes in the measuring window. The channel distance must be carefully selected, otherwise channel overlapping will occur.
- *Measurement window*: This is the distance between the first channel and the last one. When more channels are selected, the measurement window increases.
- *Maximum depth*: This parameter is the maximum measurable depth of the ultrasonic beam.
- *Maximum velocity*: This is the maximum measurable velocity and must be optimised in order to prevent aliasing.
- *Number of repetitions*: This is the number of pulses emitted for a single valid velocity profile measurement. More emitted pulses per profile measurement will increase the signal-to-noise ratio, but will also increase the time needed to measure one profile. Thus the time resolution between velocity profile measurements will decrease.
- *US voltage*: The peak-to-peak voltage applied to the transducer is controlled by this parameter setting. The voltage setting depends on the strength of the ultrasound attenuation and the concentration of particle reflectors in the fluid.
- *RF Gain (start, end)*: Compensation during amplification of the received echo according to an exponential law. Gain start is the gain setting at the beginning of the reception period and gain end is the gain setting at the end of the reception period.
- *Starting depth*: Distance between the first channel and the surface of the transducer. Useful in positioning the measuring window to avoid a wall or disturbed region.

The sound velocity is a fundamental parameter that must be measured accurately and be manually selected in the UVP monitor software. The method for sound velocity measurement is described further in Section 3.4.5.

There are quite a few parameters which have an influence on each other when the parameter setting is modified. This makes the optimisation of the UVP system for ultrasonic velocity profile measurements into quite a difficult challenge. For each unique application, time must be given to selecting the optimum UVP parameters to ensure accurate velocity profile measurements. Therefore a detailed description of the important parameters and limitations of the UVP system is necessary.

- Aliasing and the sampling frequency

In all pulsed Doppler-based instruments, the analog signal must be converted into a digital signal. This is done by sampling the analog signal at discrete points. In this case, the sampling rate or frequency is given by the Pulse Repetition Frequency,  $F_{prf}$  (Wiklund, 2003). The Nyquist Sampling Theorem states that the measured signal frequency must be equal or less than half of the sampling frequency, in order to have the measured signal uniquely reconstructed without distortion (Floyd, 2003). Under-sampling, i.e. to low  $F_{prf}$ , causes the measured frequency components that are higher than half of the sampling frequency,  $F_{prf}$ , to fold back into the low frequency region and overlap with the lower frequency components and, as a result, cause distortion of the measured signal. This type of signal distortion is known as aliasing and the effect of this phenomenon is that a single measured frequency (velocity) can correspond to several real-flow velocities (Wiklund, 2003).

- Maximum velocity and maximum depth

An estimate of the maximum measurable velocity must be calculated before velocity profiles are measured during the experiments. This calculation is necessary in order to choose the correct PRF value and to prevent aliasing during velocity profile monitoring. Due to the Nyquist Sampling Theorem, there is a limitation on the maximum velocity range and this is expressed as:

$$V_{max} = \frac{cF_{prf}}{4f_0}. \quad (3.2)$$

Since a single transducer is used for emitting and receiving, the ultrasonic pulse must have time to echo back before a new pulse is emitted. Thus the maximum measurable depth,  $P_{max}$ , of a velocity profile is determined by the PRF:

$$P_{max} = \frac{c}{2F_{prf}}. \quad (3.3)$$

This implies that the maximum measurable depth decreases with increasing PRF. From Equation 3.2 and 3.3 the following constraint exists for the pulse Doppler method:

$$P_{max} \times V_{max} = \frac{c^2}{8f_0}. \quad (3.4)$$

This means that, for a given transmitting frequency, a compromise must be made between the maximum measurable depth and velocity range. This is illustrated by Figure 3.6.

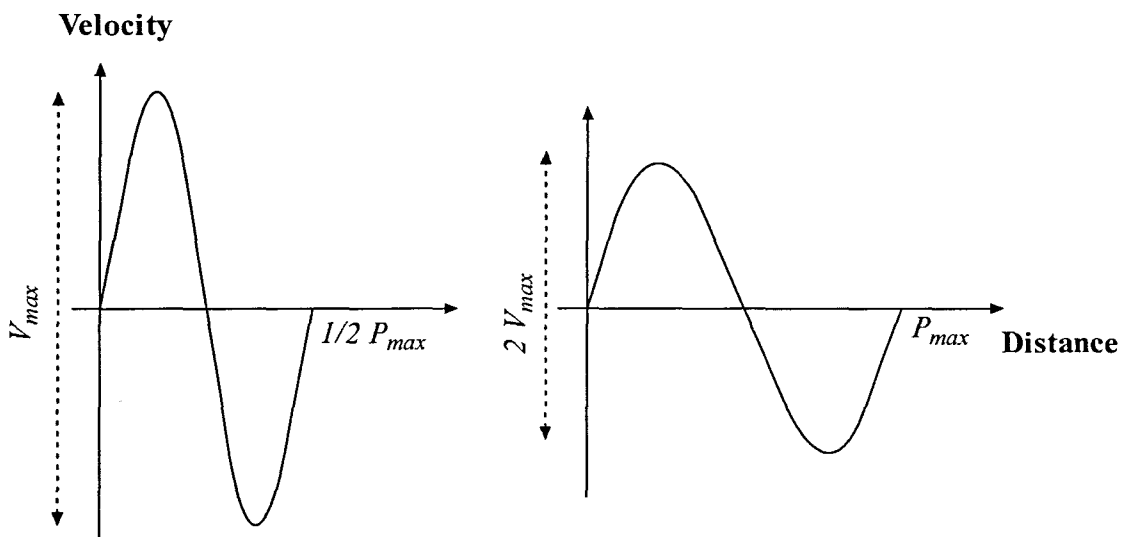


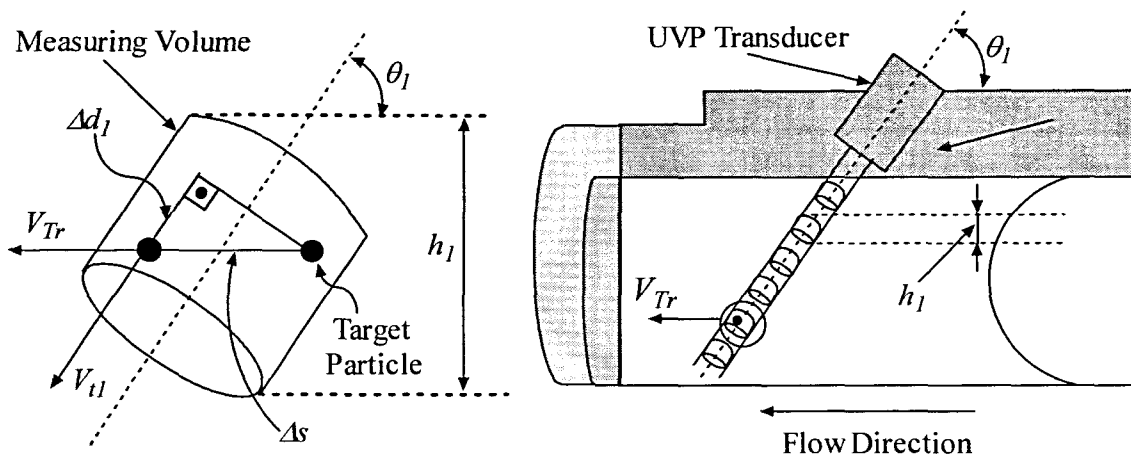
Figure 3.6: Comparison between maximum measurable depth and velocity

According to Equation 3.4, the emitting frequency,  $f_0$ , can be optimised in order to change the product value  $P_{max} \times V_{max}$ . The availability of more than one US working frequency makes it possible to further optimise measurement conditions. With lower emitting frequencies, higher velocities and more penetration depth can be achieved, but at a cost of decreasing spatial resolution due to increasing wavelength.

- Doppler angle

In order to increase the accuracy of velocity determination, the Doppler angle can be optimised. Consider two cases with two different Doppler angles shown in Figure 3.7. Subscript 1 denotes the first case of Doppler angle  $\theta_1$ , and subscript 2 denotes the second case with Doppler  $\theta_2$ , where  $\theta_1 < \theta_2$ . In both cases the moving target has the same velocity and thus covers the same distance,  $\Delta s$ . Due to the smaller selected Doppler angle, the perpendicular distance  $h_1$  in case a) is larger than the perpendicular distance  $h_2$  in case b). Such an increase of distance for all of the measuring volumes across the pipe diameter causes a large velocity spread or distribution. Such a velocity spread will generate a spectrum of Doppler shift frequencies. The accuracy of the velocity estimate is strongly related to the width of the measured Doppler shift spectrum and thus the velocity calculation will be more reliable if the received bandwidth of the shift frequency spectrum is narrower (Ouriev, 2000).

a)



b)

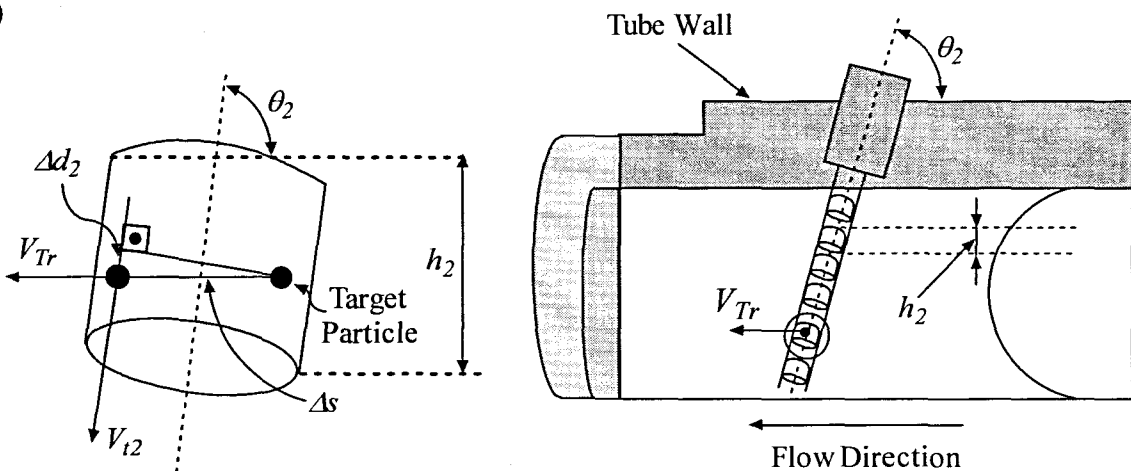


**Figure 3.7: Variation of the velocity spread distance along the pipe diameter by Doppler angle modification: a)  $\theta_1$  and b)  $\theta_2$**

It becomes even more complicated to determine the Doppler angle with high accuracy when the ultrasound transducer is mounted on the outside wall of the pipe, which is always the case for non-invasive measurements (Wiklund, 2003). When measuring through a pipe wall or material, the critical angle must be taken into consideration when selecting the Doppler angle. At steeper angles than the critical angle, the ultrasound wave will be totally reflected from the boundary surface (see Section 2.3.3). The ultrasound wave will also be refracted at the wall interface and thus the angle between the direction of scattering particles' main velocity vector and the ultrasound beam's direction will change, according to Snell's law. The accuracy of the velocity

determination is highly dependent on the accuracy of the Doppler angle (Wiklund, 2003). Based on experience and literature, a Doppler angle between 60 – 80 degrees is optimum for accurate velocity determination. Recall that the Doppler angle is the angle between the ultrasound beam direction and main flow direction or, in other words, the angle between the US transducer and the horizontal of the pipe.

- Spatial resolution, size of measuring volumes and channel overlapping

The size of the measurement volumes is called channel width,  $w$ , and is given by:

$$w = c \frac{N}{2f_0} = \frac{N\lambda_0}{2}. \quad (3.5)$$

From Equation 3.5 it can be seen that the channel width varies with sound velocity in the test medium,  $c$ , the number of cycles per pulse,  $N$ , and the basic emitting frequency of the US transducer,  $f_0$ . The channel width of the measuring volumes is only one half of the ultrasonic burst length because of the fact that the echo reception for a particular channel must stop before the burst reaches echoing particles beyond the far side of the measuring volume (Wiklund, 2003). In order to increase the spatial resolution, one could decrease the channel distance. However, the channel distance cannot be lower than the channel width, or channel overlapping will occur. The consequence of two adjacent channels overlapping is that a spatial averaging occurs, taking into account velocities of neighbouring channels, and a smoothing of velocity profiles will occur as a result (Wiklund, 2003). The spatial resolution is thus dependent on channel width and not the selected channel distance. This is described in detail in Met-Flow (2002) and the DOP2000 User Manual.

It is very important to note that the lateral dimensions of the sampling volumes are not constant. Their lateral dimensions increase with increasing measuring depth according to the ultrasonic beam produced by the transducer. Thus the measuring volumes are larger at the further end of the measuring window, which allows more echoing particles to pass and, as a result, more averaging effects occur. The ultrasonic beam geometry is described in the next section.

### 3.2.4.2 Ultrasound transducers

In this research, plain-wave type ultrasound transducers supplied by Met-Flow SA, which operate in transmitting and receiving mode, were used. A more detailed description, as well as technical information about ultrasound transducers, can be found in Met-Flow SA (1997 & 2002). In Table 3.1, the geometric dimensions and major acoustic parameters are given. The sensor housing diameter  $b$  is 8 mm and the length  $l$  of the transducer is 60 mm. Transducers with a central basic frequency ( $f_o$ ) of 4 MHz were chosen in order to obtain good spatial resolution, which is due to their short wavelength. The 4 MHz sensors have a fixed active beam diameter of 5 mm and for were used for velocity profile as well as sound velocity measurements.

**Table 3.1: Ultrasound transducer beam geometry**

Centre frequency (MHz)	Active diameter (mm)	Housing diameter (mm)	Overall length (mm)	Near-field distance (mm)	Divergence half-angle (deg)
4	5	8	60	16.9	2.2

In order to choose the correct ultrasonic transducer for a particular application, the physical ultrasound beam properties and characteristics have to be considered. The following equation expresses the relative acoustic pressure distribution along the transducer axis:

$$p = \frac{2\pi \cdot p_o}{k} \cdot \sqrt{2 - 2 \cdot \cos\left(k \cdot \sqrt{\frac{a^2}{2} + z^2} - k \cdot z\right)}, \quad (3.6)$$

where  $p$  is the acoustic pressure,  $p_o$  the reference acoustic pressure on the transducer and  $z$  the on-axis co-ordinate of the ultrasound beam (Wiklund, 2003). The generated ultrasound beam can be divided into two main regions called the “near-field” and the “far-field”. Figure 3.8 shows the sound field generated by an ultrasound transducer (Met-Flow, 2002).

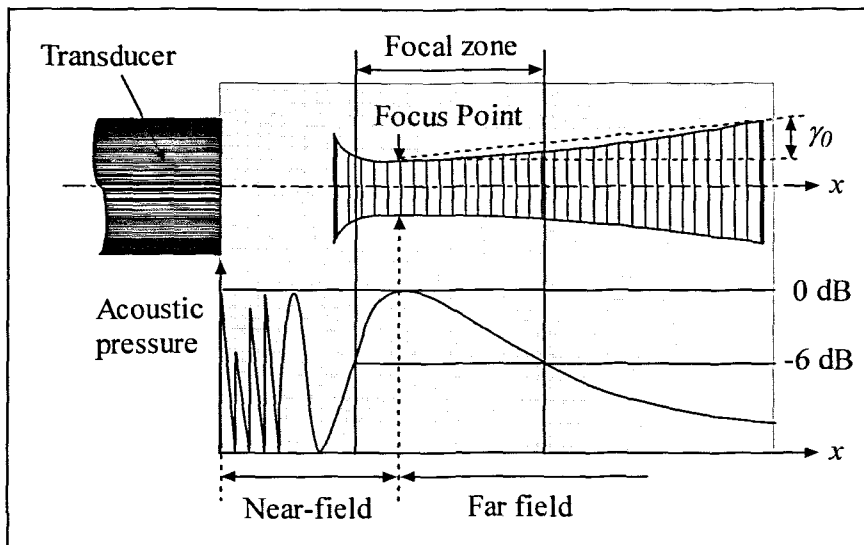


Figure 3.8: Sound field generated by an US transducer (Met-Flow, 2002)

In the near-field region, the intensity oscillates along the axis of the transducer and starts at the transducer's front surface. The distance  $N_f$  is called the "near-field distance" and can be estimated by the equation:

$$N_f = \frac{a^2 \cdot f_0}{4 \cdot c} \quad (3.7)$$

Practical velocity measurements were not conducted within the near-field zone. The unstable nature of the US beam in this region may cause weak echo problems and thus this region was avoided. The US adapters were specifically designed so that the transducers could be pulled back in order to have the far-field region of the ultrasound beam within the flow area of the pipe.

The far-field starts from the focus point  $N_f$  of the transducer and in this region the intensity of the acoustic field varies as the inverse square of the distance from the transducer,  $z$ . The sound beam also diverges at a constant angle for a given pressure amplitude drop. The beam divergence half-angle,  $\gamma_0$ , is defined as the half-width (-6 dB) of the sound pressure and can be expressed by (Metflow, 2002):

$$\gamma_0 = \sin^{-1} \left( 0.51 \frac{\lambda}{a} \right) \quad (3.8)$$



In Doppler echography, the axial dimension of the measured volumes is defined by the instrument that analyses the Doppler echoes and their lateral size by the amount of acoustic energy reflected by the particles. As mentioned before, the lateral dimensions of the measuring volumes depend on their position along the ultrasonic beam, as shown in Figure 3.9 below.

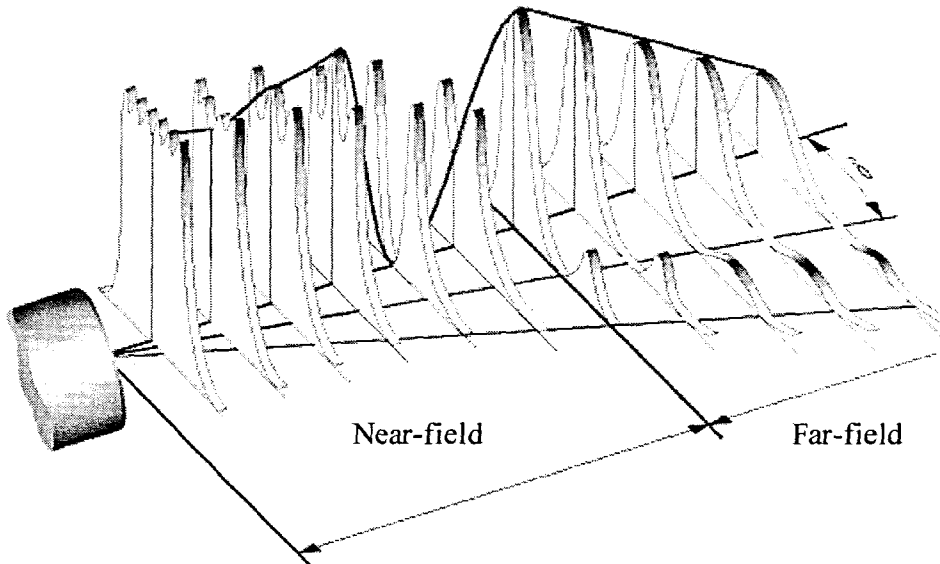


**Figure 3.9: Lateral dimensions of measuring volumes versus position along US beam (Signal Processing SA, 2007)**

The sample volumes increase according to the active beam diameter and the beam divergence half-angle. Thus the amount of target particles passing through the sample volumes increases. With increase of the number of target particles, the probability that some of the particles remain common within the measuring volumes of the consecutive ultrasound bursts decreases. Due to the larger number of moving particles, averaging effects occur and the accuracy of velocity determination within the measuring volumes consequently decreases (Birkhofer, 2007). As a result, distortion of the measured velocity profile occurs with increasing spatial depth, due to wider measuring volumes as well as attenuation of the ultrasonic beam.

The spectral characteristics of a 4 MHz transducer from Met-Flow are shown in Figure 3.10. The results were obtained from Imasonic, Switzerland. These transducer characteristics are important, especially when the shape quality of an emitted burst is considered. The transducer bandwidth is directly linked to the shape quality of an emitted ultrasound pulse. This is emphasised by the pulse length measurement at both the -6 dB reference (remaining oscillation

at half of the maximum signal amplitude) and the -20 dB reference (remaining oscillation at 10 % of the maximum amplitude). On this aspect the emitted burst will feature a more accurate pulse shape, tending more to the theoretical square-shaped emitted bursts and related measuring volumes, if there is better attenuation of the remaining ringing after the pulse emission. This is illustrated in Figure 3.11.

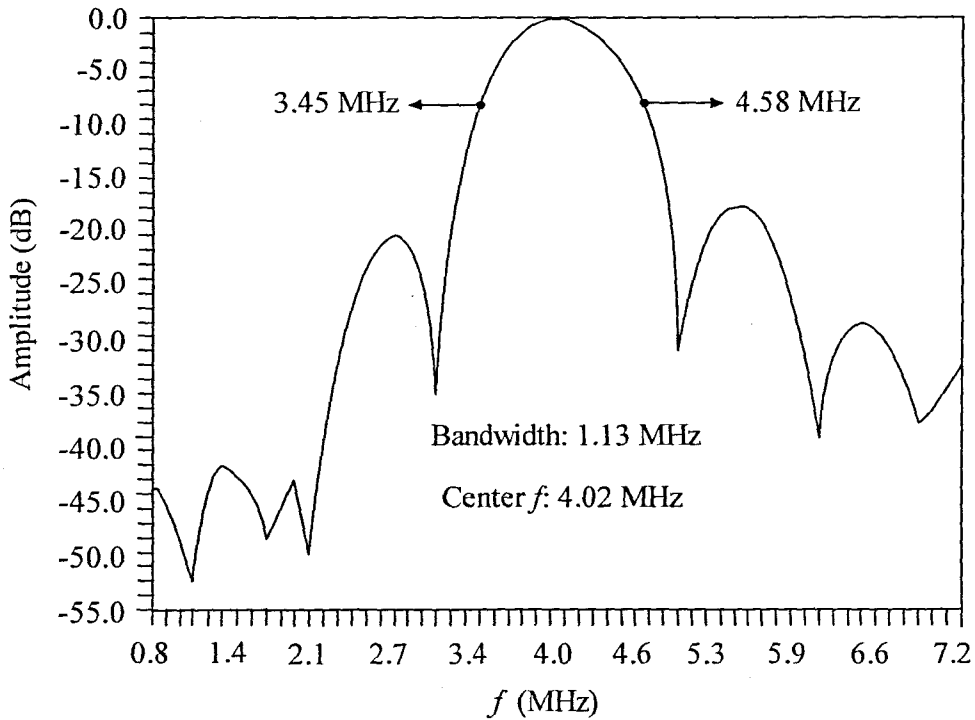


Figure 3.10: Spectral characteristics of 4 MHz Met-Flow SA transducer

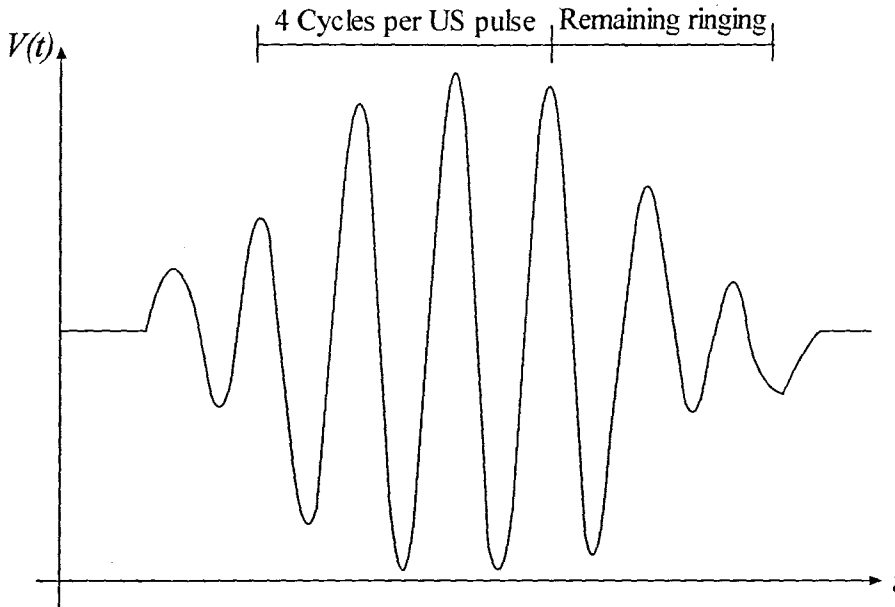


Figure 3.11: US pulse emission with remaining ringing

Birkhofer (2007) discusses the influence of different sizes of sample volumes as well as test setups in order to investigate the size of sample volumes.

### 3.2.4.3 Flow adapter geometry and sensor installation

Good and stable positioning of the ultrasound transducer is essential for the successful measurement of velocity profiles. As mentioned before, this especially concerns the angle of the transducer (Met-Flow SA, 2002). In this research, a special flow adapter was designed and manufactured for stable and repeatable positioning of the transducers. The flow adapter cell was made of PVC and designed for simultaneous measurements of velocity profiles and acoustic properties in-line. Transducers were mounted in flush with the pipe through cavities with diameters equal to the housing diameter of the transducer but installed at a distance equal to the near-field length from the actual pipe wall interface. This was done to avoid measurements in the near-field zone where the ultrasound field is highly irregular and not fully developed (Wiklund, 2007). The schematic layout of the flow adapter cell is shown in Figure 3.12.

As mentioned in Chapter 2 (Section 2.3.3), there are two main reasons for not mounting the transducers on the side walls of the pipe. The first is the loss of ultrasonic energy from absorption by the pipe material and reflection of the ultrasonic wave. The second reason is the

incorrect Doppler angle (angle between US beam and direction of main flow) resulting from the refraction of the ultrasonic wave according to Snell's law. Preliminary velocity profile measurements have been conducted by measuring through the pipe wall, but results indicated a decreased penetration depth due to energy loss as well as less accurate velocities due to the incorrect Doppler angle. It has been found that velocity profiles measured through a pipe wall are qualitatively and quantitatively, less accurate than when compared to profiles measured with transducers in direct contact with the fluid (Haldenwang *et al.* 2006).

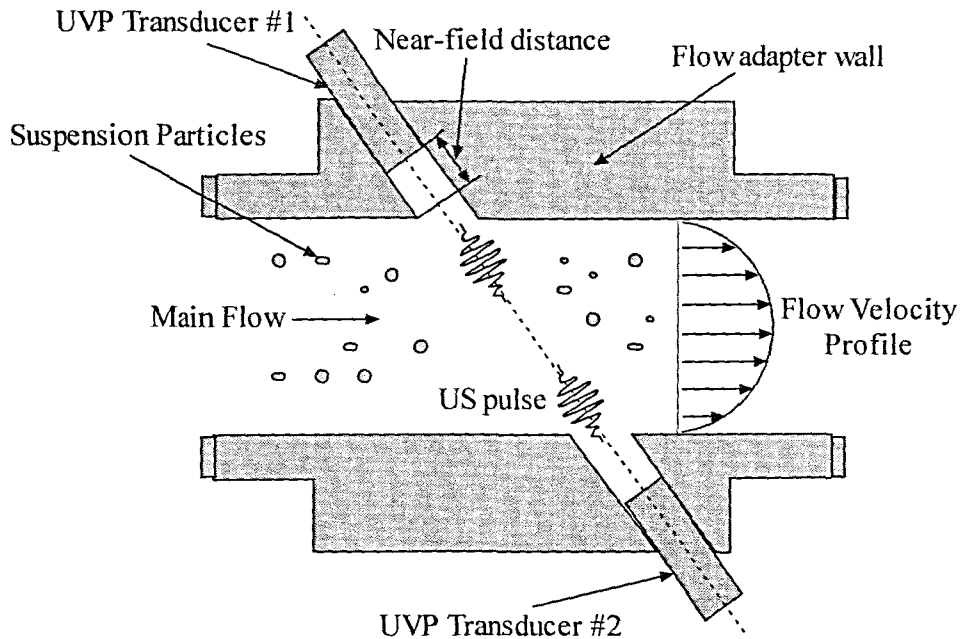


**Figure 3.12: Schematic illustration of the flow adapter fitted with two transducers**

Wiklund and Stading (2006) and Wiklund (2007) showed that this setup is generally the most favourable for simultaneous measurements of velocity profiles and acoustic properties such as in-line velocity of sound. The transducers were mounted in such a way so that the sensors could be removed with ease in order to flush the flow adapter before measurements were taken. This was done in order to remove initial air and to avoid problems with sedimentation and clogging of the cavities in front of the transducers.

The flow adapter used during the pilot study at ETHZ, Switzerland was based on the same design but was constructed from Tecapeek with 30 % glass fibres (given abbreviation Peek GF

30). More information on this particular design of flow adapter and transducer setup can be found in Shekarriz and Sheen (1998), Birkhofer *et al.* (2006), Birkhofer (2007) and Wiklund (2007).

### 3.3 CALIBRATION PROCEDURES

The calibration procedure for the electronic measuring systems is explained in the following section. Signal outputs from the instruments are standard 4-20 mA current output and are connected to a data acquisition unit with a 100 ohm resistance. A sixteen channel analog-to-digital converter (ADC) from Eagle Technologies was used to read the output voltages from the measuring instruments and to convert it to digital format for signal processing.

#### 3.3.1 Pressure transducers

High and low range pressure transducers were used during the tests. High-range pressure sensors ranged from 0 - 10 bar and low range pressure sensors ranged from 0 - 1 bar. The pressure sensors were calibrated with an air pump while pressure readings were taken with a digital manometer. The procedure was as follows:

- The pressure sensor is connected to the air pump.
- The digital manometer is then zeroed and a point pressure is applied to the pressure transducer.
- The voltage output from the pressure sensor and the applied pressure is recorded with the software.
- The pressure is then increased and the same procedure is followed. Several points over the range of the pressure transducer are recorded.
- The point pressures versus output voltages are then plotted and the least square linear regression gives the relationship between pressure and voltage as well as the error of the fit.

A typical test result for the calibration of a low-range (0 - 1 bar) pressure transducer is shown in Figure 3.13 below.

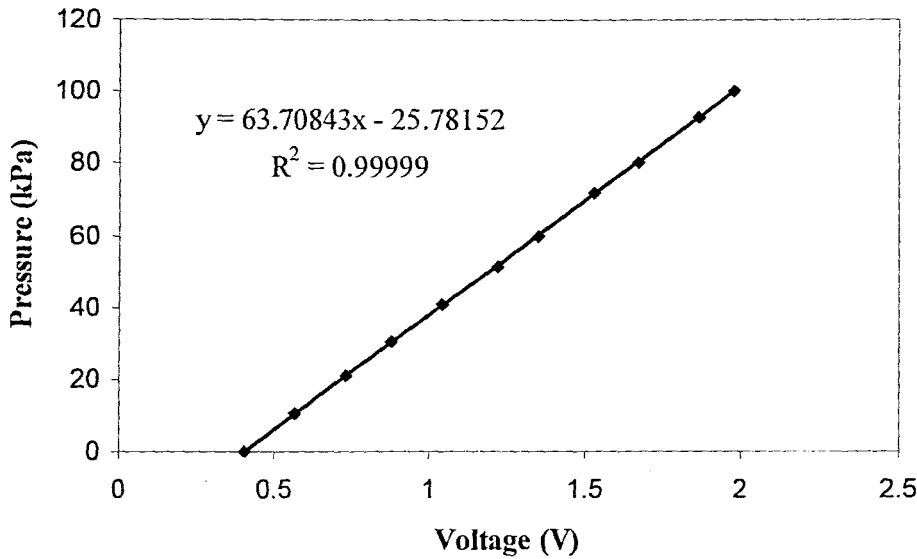


Figure 3.13: Low-range point pressure transducer calibration constants

According to the manufacturers, the accuracy of the pressure transducers is within 0.25 % of full scale. This means that, for the high-range (0-10 bar) pressure transducer the pressure error is +/- 2500 Pa and for the low-range pressure sensor the pressure error is +/- 250 Pa.

### 3.3.2 Mass-flow meter

As the materials varied in chemical composition and concentration, the mass-flow meter was calibrated for each material. The flow rates were measured by using the conventional bucket and stopwatch method.

The procedure was as follows:

- Firstly the density of the material was measured (see Section 3.4.2).
- A constant flow rate was applied to the system.
- This flow rate was measured by capturing the fluid in a bucket while monitoring the time with a stopwatch. An average of three readings was taken.
- The mass flow rate was calculated by using:

$$w = \frac{\text{Mass of slurry sample}}{\text{Time taken to fill sample}} \quad (3.9)$$

- In order to convert mass flow rate into volume flow rate the mass flow rate was divided by the material's density:

$$Q = \frac{w}{\rho} \quad (3.10)$$

- The flow rate was then increased and the same procedure was followed. Several points over the range of flow rates used for testing were recorded.
- The flow rates versus voltages were then plotted and the straight-line regression gave the relationship between volume flow rate and volts as well as the error of the fit.

A typical test result for the calibration of the mass-flow meter is shown in Figure 3.14 below. This calibration was done with CMC 7 % w/w.

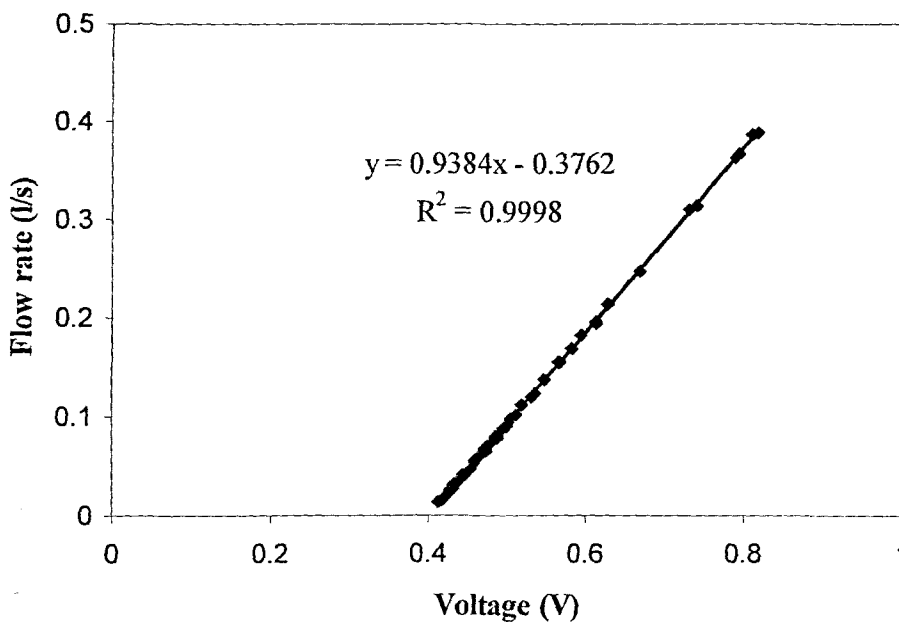


Figure 3.14: Mass-flow meter calibration for CMC 7 %

According to the manufacturers, the mass-flow meter is accurate for slurries. The flow rate error is within 0.1 % of the measured flow rate, the fluid density has an error of  $\pm 0.001 \text{ g/cm}^3$  and the temperature error is  $\pm 0.5 \text{ }^\circ\text{C}$ .

### 3.3.3 Clear water test in tube viscometer

After calibration of the mass-flow meter and pressure sensors, water tests were conducted in all three pipes of the tube viscometer.

The Colebrook-White equation for turbulent flow in pipes is given by:

$$\frac{1}{\sqrt{4f}} = -2 \log \left( \frac{k}{3.7D} + \frac{2.51}{Re \sqrt{4f}} \right). \quad (3.11)$$

This is used to calculate the friction factor  $f$ . The Darcy expression for friction head is as follows:

$$h_f = \frac{4fLV^2}{2gD}. \quad (3.12)$$

By substituting Equation 3.12 into  $\tau_w = \frac{D\Delta P}{4L} = \frac{D\rho gh_f}{4L}$  (Equation 2.14), one can deduce that:

$$\tau_w = \frac{f\rho V^2}{2}. \quad (3.13)$$

The procedure for clear water tests is as follows (Haldenwang, 2003):

- The mass-flow meter measures the flow in each pipe and the average velocity is calculated.
- The differential pressure ( $\Delta P$ ) is measured over a distance  $L$  that is 1 m for all three pipes.
- The average wall shear stress is calculated by using  $\tau_w = \frac{D\Delta P}{4L}$  (Equation 2.14).
- Theoretical values of  $\tau_w$  are calculated for a range of wall shear stresses by using the Colebrook-White formula. The theoretical range is the same as the experimental range covered in the pipe test.
- This is done by optimising the Colebrook-White equation, initially assuming a pipe roughness  $k$ , and by calculating the Reynolds number to obtain the friction factor ( $f$ ).



- The friction factor is then used to calculate the theoretical value for wall shear stress using Equation 3.12.

The theoretical and experimental data is then plotted on linear axes as shown in Figure 3.15, Figure 3.16 and Figure 3.17.

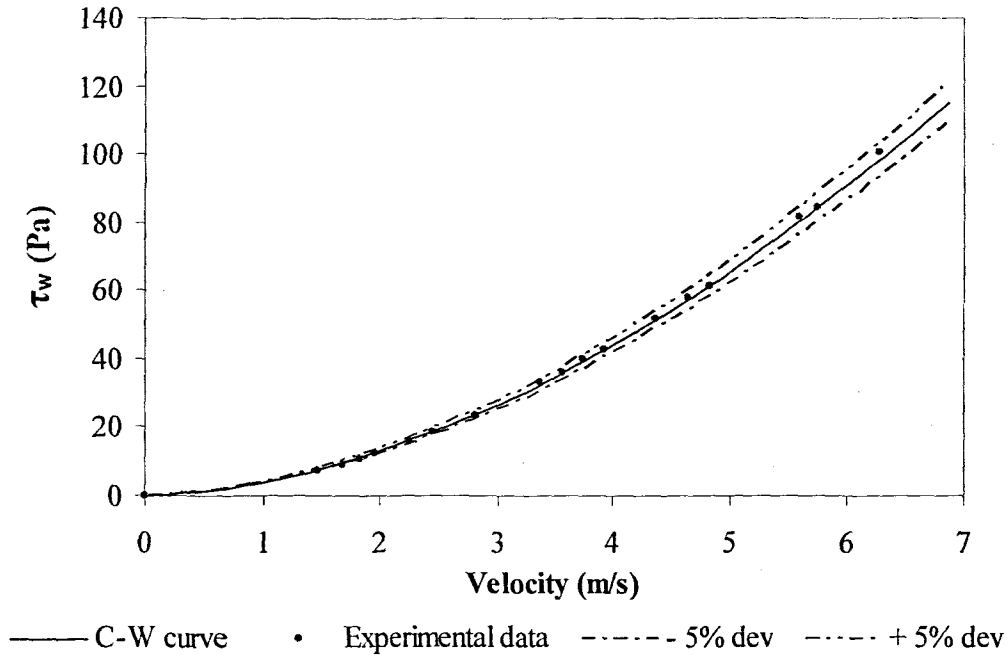


**Figure 3.15: Clear water test data against Colebrook-White equation in 9 mm pipe**

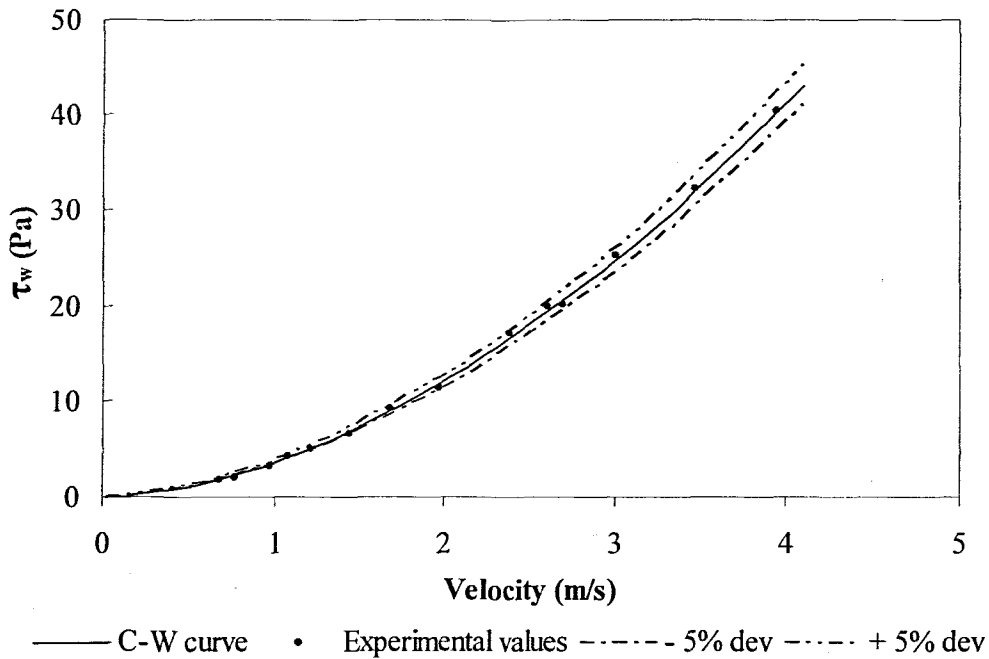


Figure 3.16: Clear water test data against Colebrook-White equation in 13 mm pipe

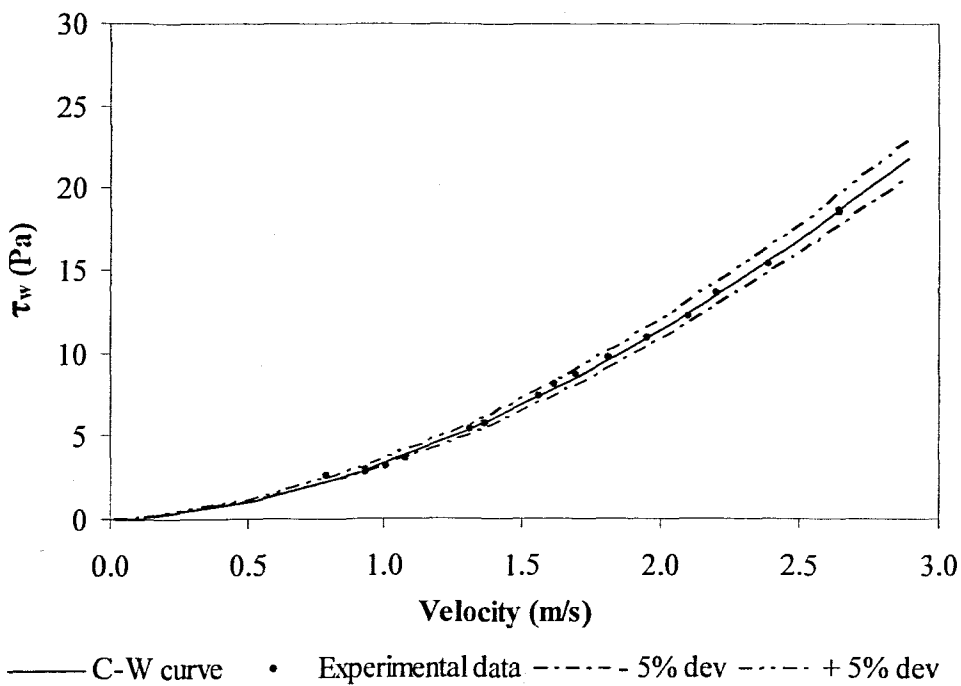


Figure 3.17: Clear water test data against Colebrook-White equation in 16 mm pipe

If the pipe is not smooth, the value for  $k$  can be optimised to find the actual pipe roughness (Slatter, 1994).

Table 3.2 shows the corresponding  $k$  values for each diameter pipe obtained.

**Table 3.2: Pipe roughness results for different pipe diameters**

Pipe diameter $D$	Pipe roughness $k$
9 mm	0 $\mu\text{m}$
13 mm	0 $\mu\text{m}$
16 mm	0 $\mu\text{m}$

During the clear water tests the mass-flow meter and the pressure transducers are tested together. If the Colebrook-White tests are successful, one can commence with the other tests. The clear water test results also indicate that the combined error from the mass-flow meter and the point pressure sensors is less than 5 % over the velocity range tested.

### 3.3.4 UVP monitor

The UVP monitor needs calibration of the internal clock to present accurate data. This is done by the manufacturer, Met-Flow SA in Switzerland. To verify the accuracy of the velocity profiles an integration method was performed. The flow rate was calculated by integrating the measured velocity profile using MATLAB® and then comparing it to the flow rate measured by the in-line mass flow meter. This is discussed in Section 3.6.2.2, page 3.42.

## 3.4 MEASURED VARIABLES

### 3.4.1 Measurement of pipe diameters

Before the pipes used in the test sections of the tube viscometer are linked to the pipe rig, the internal diameters of the pipes are checked. The pipe is placed in a vertical position and a valve is fitted at the bottom end of the tube. When this is complete, the pipe is filled with municipal tap water. The valve is opened and the water that flows out is captured in a container and weighed to obtain  $M_w$ . Note that  $M_w$  is the mass of the water and thus the weight of the container must be subtracted. The difference in head ( $L$ ) due to the decreased water level in the pipe is also measured and the internal pipe diameter is calculated by using Equation 3.14 (Slatter, 1994):

$$D = \sqrt{\frac{4M_w}{\pi\rho_w L}} \quad (3.14)$$

This process was repeated three times and the average of the three results was used. The actual internal diameters of the three pipes used in the tube viscometer are depicted in Table 3.3:

**Table 3.3 Actual pipe diameters of the tube viscometer**

Pipe diameter	Measured pipe diameter
9 mm	9.57 mm
13 mm	13.16 mm
16 mm (Stainless steel)	16.02 mm
16 mm (PVC)	16.64 mm

The difference in pipe diameters may not look significant, but errors are introduced when using the pipe diameters given by the manufacturers. Calculating the cross-sectional areas of the 9-, 13- and 16-mm pipes using the diameters given by the manufacturers introduces errors of 12, 3, 0.3 and 7.5 %, respectively.

### 3.4.2 Slurry density

The densities of the mineral suspensions were measured off-line as well as in-line by the mass-flow meter for comparison. The in-line monitoring of the fluid density was important as the density directly influences velocity of sound as well as ultrasonic velocity profile measurements. The relative density ( $S_m$ ) is defined as:

$$S_m = \frac{\rho}{\rho_w} \quad (3.15)$$

and can also be written as:

$$S_m = \frac{\text{Mass of slurry sample}}{\text{Mass of equal volume water}} \quad (3.16)$$

The mass of the slurry sample and equal volume of water are obtained by carrying out the following procedure (Haldenwang, 2003):

- A one-litre volumetric flask and a high-precision scale that can measure to a milligram are required.
- Dry the volumetric flask thoroughly and weigh the empty flask to obtain ( $M_1$ ).
- Fill the flask partially with a well-mixed slurry sample from the mixing tank and weigh ( $M_2$ ).
- Pour water into the remainder of the flask until the water/slurry level is at the graduated mark and weigh ( $M_3$ ).
- Empty the flask completely and clean it thoroughly. Fill the flask with water to the same graduated mark and weigh ( $M_4$ ).
- The procedure is repeated at least three times and the average density value is calculated.
- From Equation 3.16 the relative density can be calculated by:

$$S_m = \frac{M_2 - M_1}{(M_4 - M_1) - (M_3 - M_2)} \quad (3.17)$$

- The slurry density is calculated by manipulating Equation 3.15:

$$\rho_m = S_m \rho_w \quad (3.18)$$

### 3.4.3 Slurry temperature

The temperature of the mineral suspensions is measured by the mass-flow meter in-line, which is connected to a data acquisition unit that reads the temperature in degrees Celsius into an Excel spreadsheet. The temperature was monitored in order to try to stay within an acceptable temperature range during tests. This is especially important for velocity profile and sound speed measurements as temperature has an influence on ultrasound propagation. Slurry temperature varied from 17 – 25 degrees Celsius. During any test the temperature did not vary by more than 2 degrees Celsius. The temperature variation of 2 °C was mainly present during tube viscometer

tests, as these tests were considerably longer. Based on previous results obtained from tube viscometry and history of the model suspensions used at the Flow Process Research Centre (FPRC), the effect of temperature variation on fluid viscosity was deemed negligible (Haldenwang, 2003). During the ultrasound tests the temperature did not vary as the time of measurement is significantly faster than the previous method (process conditions are kept constant, i.e. flow rate and pressure). Therefore the effect of temperature on tube viscometer and ultrasound tests was deemed negligible. Also, during off-line tests the rotational rheometer kept the temperature constant, thus ruling out any errors due to temperature variation.

#### 3.4.4 Particle size distribution

Particle size distribution measurements were conducted at the Flow Process Research Centre. The Mastersizer2000 from Malvern Instruments was used to conduct the test. Figure 3.18 and Figure 3.19 show the particle size distribution for kaolin and bentonite.

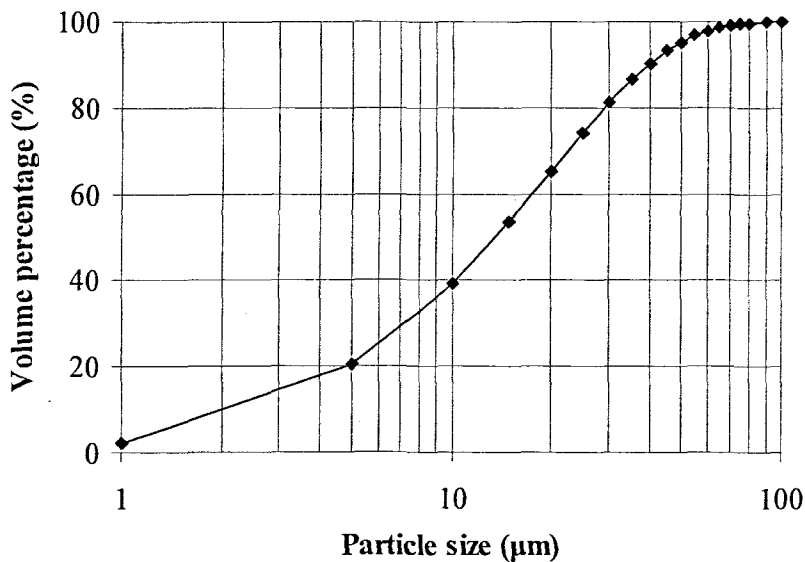


Figure 3.18: Particle size distribution of kaolin

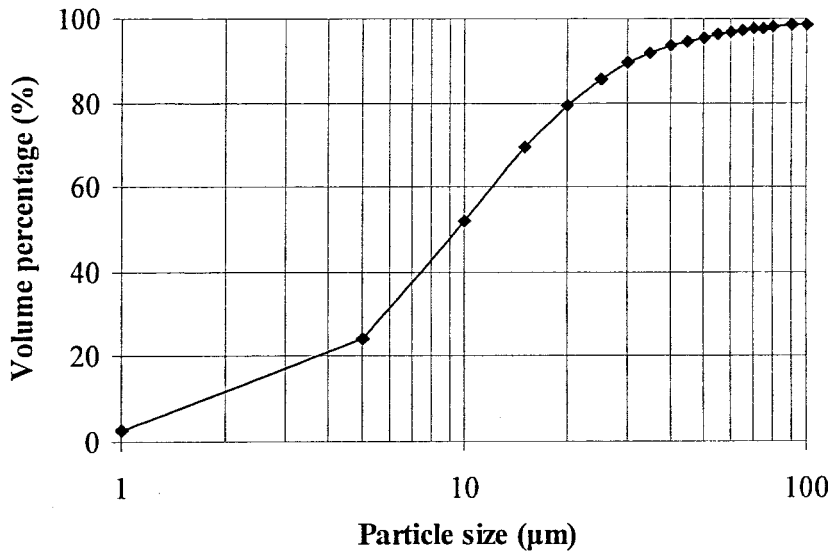


Figure 3.19: Particle size distribution of bentonite

According to Met-Flow (2002), particle sizes should be larger than a quarter of the emitted wavelength. Taking an average velocity of sound  $c = 1550$  m/s and a 4 MHz emitted signal frequency gives a wavelength of  $\lambda = 387.5$   $\mu\text{m}$ . Thus particle sizes should be larger than  $\approx 100$   $\mu\text{m}$ . However, this is only true for one type of scattering and several different types of scattering phenomena exist (Povey, 1997). Also, many scattering theories were mainly derived from blood and the fluid systems here are very different, with solid particles much denser than blood. According to Wiklund (2007), particle shapes play a role, as well, and affect the received echo. This might be the reason for the strong attenuating effects of kaolin. Further investigation needs to be done regarding this matter. It is definitely possible to get a good echo off particle sizes down to  $\approx 10$   $\mu\text{m}$ . More information on different types of scattering theories, backscattering in hydraulic engineering and backscattering measurement techniques can be found in Povey (1997) and Birkhofer (2007).

### 3.4.5 Velocity of sound

The velocity of sound in the mineral suspensions was measured in-line as well as off-line for comparison.

- Off-line measurement technique

The concept of sound velocity measurement is stipulated on time of flight measurement of emitted ultrasound pulse simultaneously with the measurement of the travelled distance. This technique is illustrated in Figure 3.20 and is variously known as “pulse-echo time of flight” or “Acoustic Time of Flight Measurement” (AToM).

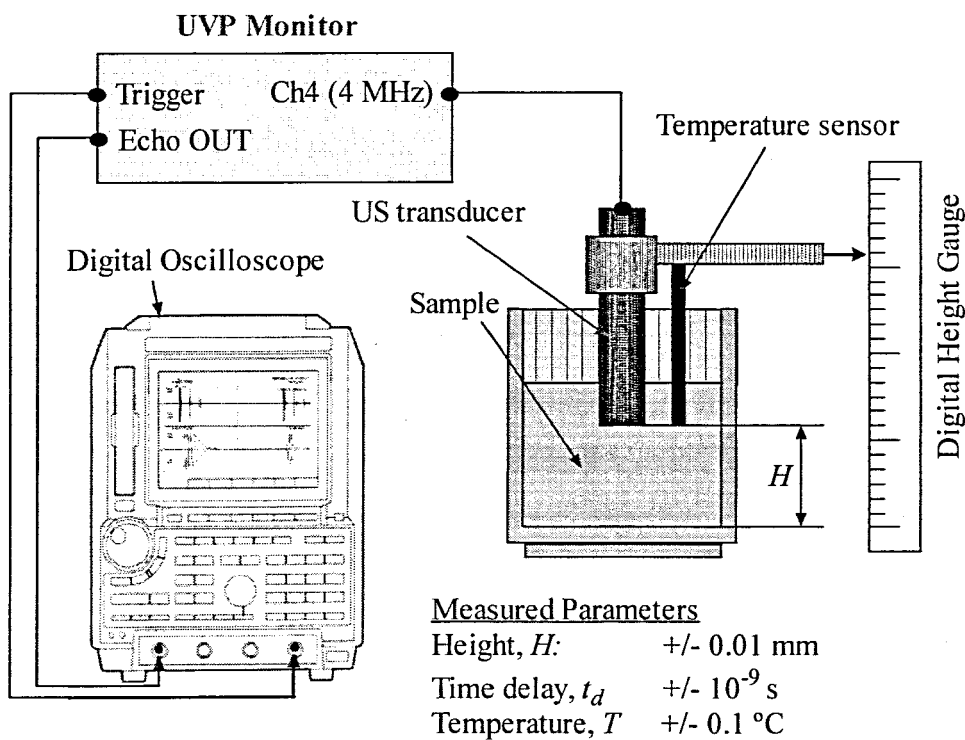


Figure 3.20: Principle scheme of off-line velocity of sound measurement (Ouriev, 2000)

An ultrasound pulse is generated using a UVP monitor (Met-Flow SA, Switzerland) and is emitted into the measuring sample. This pulse reflects from the opposite stainless steel wall back to the sensor front and is detected with the ultrasonic transducer. The reflected pulse and time delay is monitored using an Agilent 100 MHz Digital Oscilloscope (Model 54622A). While the



time delay is measured, the US transducer position  $H$  is recorded. The vertical position of the ultrasound sensor is measured by means of a digital height gauge from Mitutoyo, Japan (Model VDS20DC).

The sound velocity can be calculated using a simple equation:

$$c = \frac{2H}{t_d}, \quad (3.19)$$

where  $H$  is the distance between the front surface of the sensor and the reflecting surface, and  $t_d$  is the time of flight of the acoustic burst (Ouriev, 2000). Since the attenuation of ultrasound in water is very low, the ultrasound wave keeps going back and forth several times after the time delay,  $t_d$ . To eliminate the unwanted signals, a low PRF value and a low input voltage to the sensor, as well as two cycles per emitted ultrasound pulse, is selected. These parameters are optimised for sound velocity and not for Doppler velocity profile measurements.

In Figure 3.21, an example of an off-line sound velocity measurement is shown. This particular measurement was done for distilled water. The accuracy of sound velocity measurement depends on the accuracy of the measured distance  $H$ , the time of flight measurement  $t_d$ , and the temperature  $T$ . The tolerance of the displacement measurement (as shown in Figure 3.21) is +/- 0.01 mm and the time resolution of the digital oscilloscope is +/- 1 ns. According to Povey (1997), the monitoring of the temperature is important due to the possible variation of acoustic path length with temperature. Since the velocity of sound in water varies by approximately 3 m/s per °C at 20 °C, an error in temperature of 0.1 °C will produce an error of 0.3 m/s in the velocity of sound measurement. The main errors in off-line velocity of sound measurements arise from human observation of measuring instruments, especially the digital oscilloscope. A small error of 40 ns in the measured time delay results in a velocity of sound error of 2 m/s.

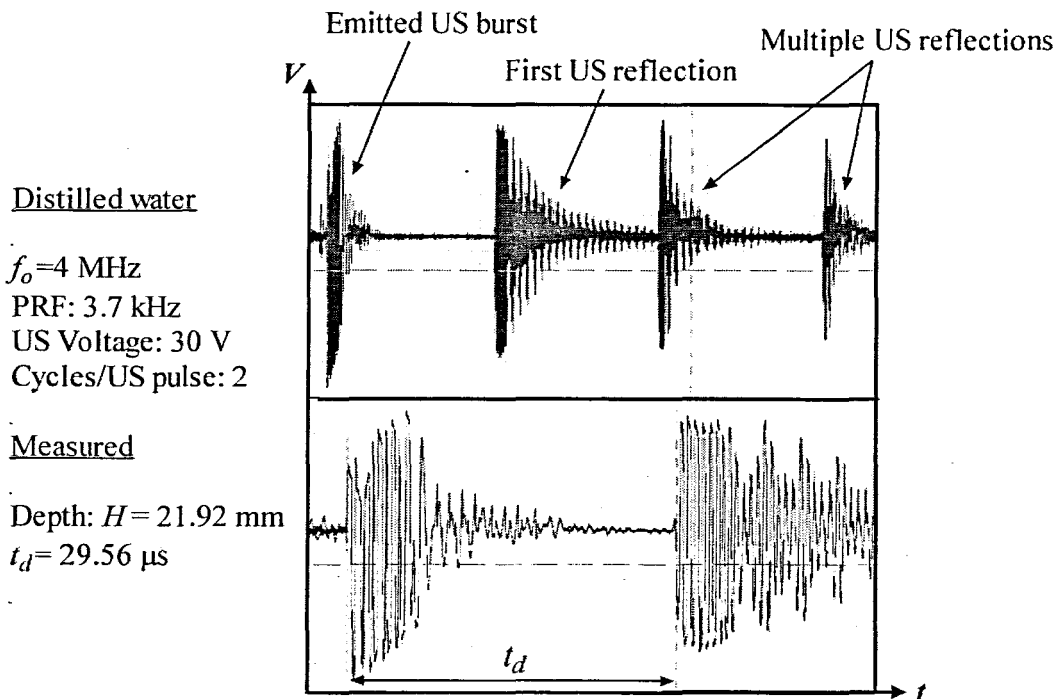


**Figure 3.21: Off-line sound velocity measurement in distilled water**

During this measurement, the US transducer was positioned at  $H = 21.92$  mm and the measured time delay consequently was  $t_d = 29.56$   $\mu$ s. Using Equation 3.18, the result of the reference sound velocity measurement was  $c = 1483.1$  m/s for distilled water at a temperature of 20 °C. This result agrees well with the reported value of  $c = 1481.3$  (Lubbers & Graaff, 1998).

- In-line measurement technique

Velocity of sound was measured in-line using the flow adapter discussed in Section 3.2.6.3. The sound velocity was determined by AToM and a known fixed transducer distance. This is illustrated in Figure 3.22.

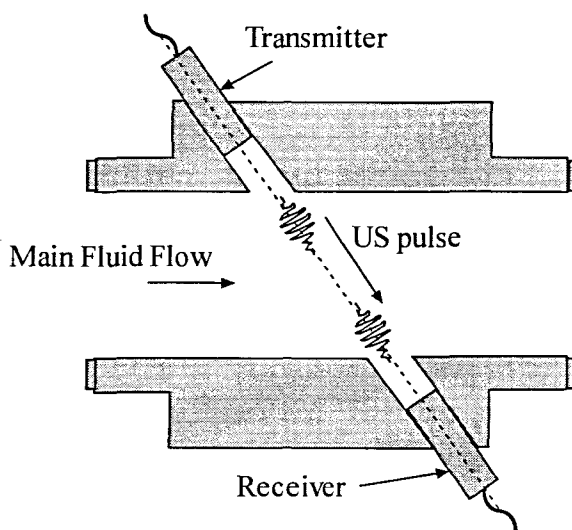


**Figure 3.22: Schematic illustration of method used for in-line velocity of sound measurement**

As mentioned before, the flow adapter construction allows the installation of two ultrasound transducers opposite each other. The transmitting transducer was connected to the UVP monitor and the receiving transducer was connected to the digital oscilloscope. In order to ensure accurate in-line velocity of sound measurements, the distance between the two transducers has to be accurate. The sound speed in water was measured off-line and also used to fill the flow adapter completely with both transducers installed. Using the digital oscilloscope, the acoustic time of flight was measured and the distance was calculated by manipulating Equation 3.19:

$$H = t_d \cdot c, \quad (3.20)$$

where  $H$  is the distance between the two opposite transducers. Such a calibration procedure was applied to the in-line flow adapter cell before velocity profiles of mineral suspensions were measured. Given the accuracy of off-line velocity of sound measurement  $c = \pm 2$  m/s and time resolution of the digital oscilloscope, the accuracy of in-line velocity of sound leads to  $c = \pm 2$  m/s.

### 3.5 COMBINED ERRORS

Certain derived quantities such as inner pipe diameter, shear stress and shear rate are dependent on more than one measurement. The same measurement is taken a number of times and the average value is extracted. This is done in order to overcome random errors due to electrical noise, for instance (Morris, 2001).

All of the measurements i.e. pressure, volumetric flow rate, temperature and density is converted into a digital signal by the data acquisition device. When converting from an analog signal to a digital signal, error is unavoidable. An ADC has several sources of errors such as quantisation error, which is intrinsic to any analog-to-digital conversion. The digital signal's accuracy depends on the quantisation resolution or number of bits of the ADC. The ADC used (uDAQ, Eagle Technologies) in this research was a 16-bit analog-to-digital converter with an accuracy of +/- 2 LSB (Least Significant Bit). This led to an accuracy of +/- 0.0031 % for a 16-bit ADC. Due to the high accuracy of the analog-to-digital conversion, the aggregation of the quantisation error is deemed negligible throughout this research.

Haldenwang (2003) and Slatter (1994) refer to Brinkworth (1968) for a procedure that quantifies the combined error using a root mean square approach.

The highest expected error  $\Delta X$ , if  $X$  is a function of  $N$  quantities is:

$$\left(\frac{\Delta X}{X}\right)^2 = \sum \left(\frac{\partial X}{\partial N}\right)^2 \left(\frac{N}{X}\right)^2 \left(\frac{\Delta N}{N}\right)^2 \quad (3.21)$$

This was used to calculate the following combined errors.

### 3.5.1 Pipe diameter

The internal pipe diameter ( $D$ ) was accurately calculated using Equation 3.14. By using Equation 3.21 and assuming the density of water to be accurate, the combined error for calculated pipe diameter was as follows:

$$\left(\frac{\Delta D}{D}\right)^2 = \left(\sqrt{\frac{1}{\pi\rho_w M_w L} \frac{M_w}{D} \frac{\Delta M_w}{M_w}}\right)^2 + \left(-\sqrt{\frac{M_w}{\pi\rho_w L^3} \frac{L}{D} \frac{\Delta L}{L}}\right)^2. \quad (3.22)$$

Table 3.4 shows a summary of the combined measurement errors for each calculated pipe diameter.

**Table 3.4: Summary of combined errors for different pipe diameters**

Pipe diameter (mm)	Measurement error $\frac{\Delta D}{D}$ (%)
9.57	0.248
13.16	0.231
16.64 (PVC)	0.101
16.02 (Stainless steel)	0.100

### 3.5.2 Wall shear stress

Two point pressure transducers were used and measurements were subtracted to calculate the differential pressure for a particular flow rate. The differential pressure measurement was then used to calculate the wall shear stress,  $\tau_w$ . Therefore the aggregation of errors from separate measurements had to be investigated. According to Morris (2001), the likely maximum error in terms of absolute errors is:

$$e = \sqrt{(ax^2 + by^2)}, \quad (3.23)$$

where  $\alpha x$  and  $\beta y$  are the absolute errors of the two pressure sensors in this particular case. Statistically, Equation. 3.23 takes account of the reasonable assumption that both absolute errors of the transducers are unlikely to be at their maximum or minimum value at the same time.

The highest expected error calculating the wall shear stress using Equation 2.14 and 3.21 was:

$$\left(\frac{\Delta\tau_w}{\tau_w}\right)^2 = \left(\frac{\Delta P}{4L} \frac{D}{\tau_w} \frac{\Delta D}{D}\right)^2 + \left(\frac{D}{4L} \frac{\Delta P}{\tau_w} \frac{\Delta(\Delta P)}{\Delta P}\right)^2 + \left(-\frac{D\Delta P}{4L^2} \frac{L}{\tau_w} \frac{\Delta L}{L}\right)^2. \quad (3.24)$$

The results are graphically depicted in Figure 3.23.

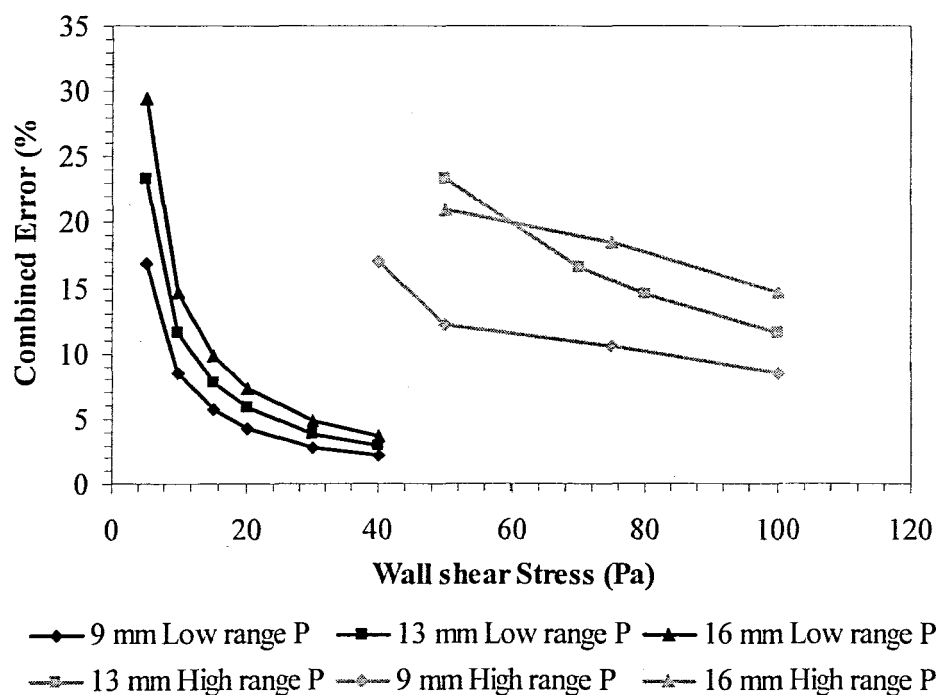


Figure 3.23: Pipe wall shear stress combined errors

There is a steep increase in error percentage at the very low range, which was expected due to the very low differential pressures at this range. The low-range (0-1 bar) pressure sensors yielded a lower error when compared to the high-range (0-10) pressure transducers, which was also expected. The high-range pressure transducers can be replaced with a lower range (e.g. 3-bar) in order to reduce the combined error percentage at the high wall shear stress range. This is discussed in Chapter 5.

### 3.5.3 Pseudo shear rate

The highest expected error calculating the pseudo shear rate using Equation 3.21 was expressed as:

$$\left(\frac{\Delta 8V/D}{8V/D}\right)^2 = \left(\frac{\Delta G}{G}\right)^2 = \left(-\frac{32Q}{\pi D^3} \frac{Q}{G} \frac{\Delta Q}{Q}\right)^2 + \left(-\frac{96Q}{\pi D^4} \frac{D}{G} \frac{\Delta D}{D}\right)^2. \quad (3.25)$$

The results are graphically displayed in Figure 3.24.

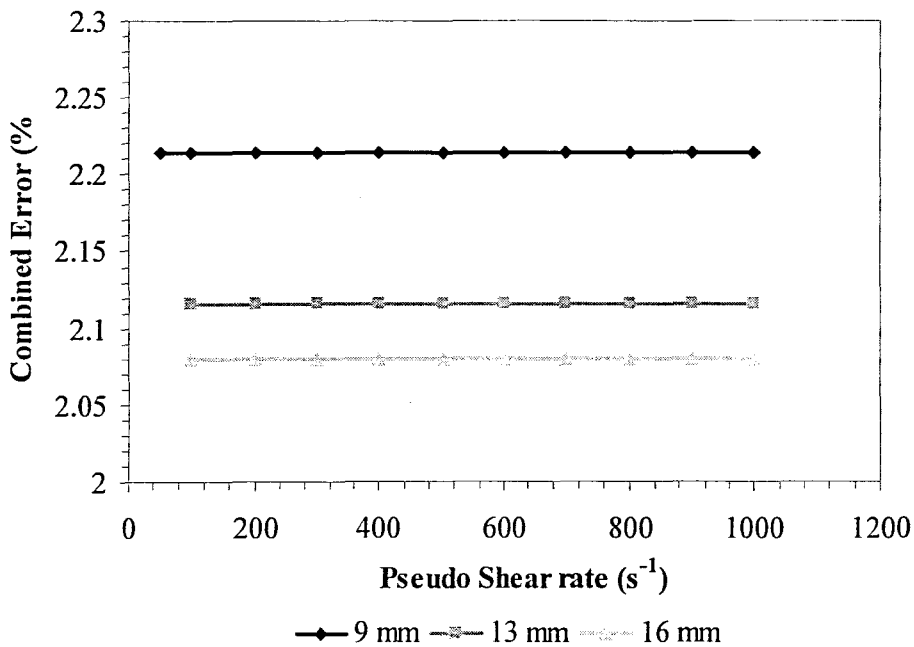


Figure 3.24: Highest combined errors for calculating pseudo shear rate

The combined errors for pseudo shear rate are low when compared to the wall shear stress because shear rate was only related to the volumetric flow measurement and the inner diameter of the pipes.

## 3.6 EXPERIMENTAL PROCEDURES AND INVESTIGATION

In this section the experimental procedures pertaining to the tube viscometer and the in-line rheometer (UVP-PD method) are presented. Methods of investigation and analysis of velocity profiles are also discussed.

### 3.6.1 Tube viscometer rig

The following procedure is followed in order to establish a range of differential pressure and velocity values. The procedure is the same for all three pipe diameters (Haldenwang, 2003).

- Before any mineral suspension is tested, the point pressure transducers and mass-flow meter are calibrated.
- The tube viscometer rig is calibrated by conducting water tests in all three tubes and the results are compared with the Colebrook-White equation.
- About 200 litres of slurry are mixed in the main mixing tank until the mineral suspension is properly hydrated and well mixed.
- An off-line relative density test is done for a representative sample. This is also compared with the in-line density value obtained from the mass-flow meter. If the required concentration is not achieved, more solids or water are added and mixed, depending on whether a higher or lower concentration is required.
- During the mixing process, the mineral suspension is circulated through all three pipes so that initial water in the system is mixed in the slurry. All the valves from the pressure adapters are also opened to flush out water in the system. The in-line density is monitored until it has stabilised, showing that the slurry concentration will be constant throughout the tests.
- The flow rate is regulated by controlling a valve which diverts excess flow through a bypass line back into the mixing tank. This also helps to ensure that the slurry is well mixed during pipe tests.
- The specially written visual basic programme for the tube viscometer test on the PC is opened and the data is exported to an Excel spreadsheet.



- When the desired flow rate is set and constant, the data acquisition device is triggered and the program samples flow rates and point pressures over a preset time interval.
- The average flow rate and pressure is calculated and exported to the Excel spreadsheet. These values are visually displayed on a graph plotting wall shear stress against pseudo shear rate. By visually looking at results obtained during tests, one can quickly spot errors related to flow rate or differential pressure.
- This process is repeated with a range of flow rates until sufficient data points are recorded over the desired pseudo shear rate range.
- All three sets of data points are plotted on the same graph, which enables one to see whether any errors, such as wall slip, are present. The overlapping of laminar flow data of all three tubes indicates that no obvious errors are present and that the plotted curve is the flow curve of the material on a pseudo shear diagram.

As the three tubes are linked to one another to form one flow line, the tube viscometer test takes about an hour to complete, provided that no errors occur during the test.

### **3.6.2 In-line rheometer**

The UVP-PD method requires two important measurements, the differential pressure and ultrasonic velocity profile measurement. Differential pressure measurements were done by using the Pipe rig software while velocity profiles were recorded. In this section the procedure for the optimisation of a velocity profile is given. The analysis of velocity profile measurements, as well as post data analysis for the calculation of rheological parameters, is discussed.

#### **3.6.2.1 Velocity profile measurement optimisation**

It is very important to monitor the raw echo amplitude while measuring velocity profiles. This can be done by selecting the echo amplitude option in the Met-Flow UVP software and by connecting the Echo Output from the UVP monitor to the oscilloscope. The digital oscilloscope has a much better time resolution than the UVP software. The echo signal from the transducer is the best indicator of SNR, and it reliably monitors unwanted reflections from walls (Met-Flow SA, 2002).

The following steps should be carried out in order to measure an accurate velocity profile (Met-Flow SA, 2002):

- As mentioned before, the UVP monitor does not require any calibration.
- Before measurements are taken, the mineral suspension is circulated through the stainless steel pipe so that initial water in the system is mixed in the slurry. All the valves from the pressure adapters are also opened to flush out water and air in the pressure configurations. The US sensors are also removed from the flow adapter to remove any air and dirt inside the cavities.
- The PRF is set to a lower value to observe any strong reflections from walls and other interfaces. Unwanted reflections can be recognised easily since they are stationary, while reflections from moving particles have a transient nature.
- After identifying and possibly removing unwanted reflections, the PRF is optimised to adjust the velocity range to the flow. Afterwards, the channel distance and number of channels are adjusted to set a window width to cover the measured region.
- Depending on the SNR at each particular case, the number of US repetitions is increased for computer averaging. Remember that by increasing the number of US bursts per velocity profile decreases the time resolution of the overall measurement.
- If the channel distance is large enough, the number of cycles per US pulse can be increased to improve the SNR, as long as the decreased spatial resolution does not affect the quality of the measured velocity profile.
- In case of too high attenuation of the US energy, the emission voltage is increased. If this does not help, the gain parameter is increased. Use gain control with prudence, as too high amplification also amplifies electronic noise.

If the attenuation is too high and the above procedure does not help for a particular application, a different US frequency can be selected. Lower US frequencies are less susceptible to attenuation and absorption.

### 3.6.2.2 Velocity profile analysis

This section describes how velocity profiles are analysed in order to determine parameters such as the distance between US transducer and wall interface, as well as the yield stress from measured plug flow velocity profiles.

- Volumetric flow rate calculation and estimation of wall position

A common problem for ultrasound pulsed Doppler methods is the need to locate the precise positions of the first and last measuring volumes (channels) along the ultrasound beam axis corresponding to a position within a vessel or pipe. As described below, the wall positions and radial coordinates are used to obtain the volumetric flow rates but, even more important, are required as input parameters when the data are fitted to constitutive rheological models (Wiklund, 2007). In order to perform the volumetric flow rate calculation, the velocity profile has to be integrated. Only half of the velocity profile is required for the calculation of the volumetric flow rate. Figure 3.25 shows a measured velocity profile for bentonite 7 % w/w.

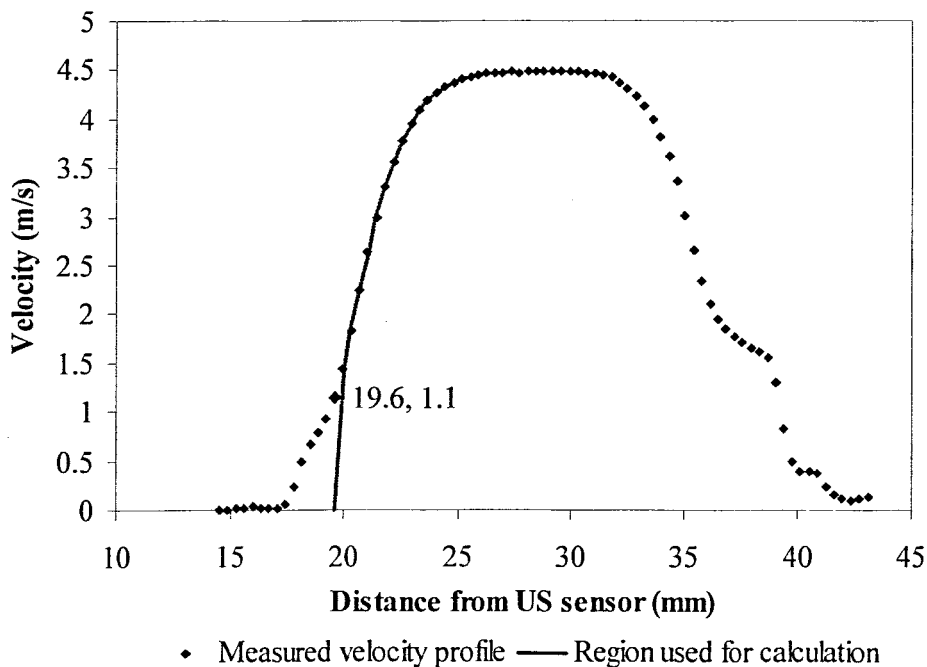


Figure 3.25: Region used for volume flow rate calculation

The symbols represent measuring volumes or channels and are at a certain distance from the front surface of the ultrasound transducer. Note that there is an increase in velocity before the actual wall interface. This is due to the flow inside the cavity in front of the ultrasound transducer. According to Figure 3.24, the channel at distance equal to 19.6 mm is chosen as the wall position corresponding to the pipe diameter. With the wall position set, the pipe radius is added (8 mm) and this region is then used for the calculation of the volumetric flow rate. The flow rate is calculated by using equation 3.26:

$$Q = \frac{\pi}{2} \cdot \sum_{i=1}^{N_c} (r_{i+1}^2 - r_i^2) (v_{i+1} + v_i), \quad (3.26)$$

where  $N_c$  is the number of channels across the pipe radius,  $v$  the point velocity at a specific channel number and  $r$  equals the distance from the centre of the pipe towards a specific channel along the pipe radius. The accuracy of volumetric flow rate calculations depends on the accuracy of the velocity profile measurement as well as the position of the wall interface. The channels or, in actual fact, wall positions are varied and volume flow rates are calculated. The channel that yields the most accurate flow rate compared to the measured volume flow rate is chosen as the estimated wall position. Table 3.5 shows results of volumetric flow rate calculations from different channels or wall positions, as well as the corresponding error percentage when compared to the measured volumetric flow rate. The measured volume flow rate was 0.63 l/s.

**Table 3.5: Volumetric flow rate calculations for different wall positions**

Channel number	Distance from sensor (mm)	Calculated flow rate (l/s)	Error percentage (%)
12	18.87	0.527	15.4
13	19.24	0.582	8.11
14	19.61	0.626	0.72
15	19.97	0.668	5.89
16	20.34	0.711	11.9

Table 3.5 shows that the flow rate calculation for channel 14 has the minimum error when compared to the measured flow rate. In this particular case the corresponding distance is

chosen as the estimated wall position namely 19.61 mm (see Figure 3.24). Theoretically, the velocity at the pipe wall should be zero. Here the velocity measurement is 1.1 m/s at the wall interface due to the increase of flow inside the cavity. When the volumetric flow rate is calculated, the velocity at the wall position is forced to zero. However, when not forced to zero the difference between the results is small. Two volumetric flow rate calculations with pipe wall velocity forced to zero and with original pipe wall velocity are shown in Table 3.6. The results are compared to the measured flow rate (0.63 l/s) and the error percentage is calculated.

**Table 3.6: Comparison between volumetric flow rate calculations for the same wall positions at two different velocities**

Wall position (mm)	Velocity (m/s)	Calculated flow rate (l/s)	Error percentage (%)
19.61	0	0.626	0.72
19.61	1.135	0.636	0.87

The calculation of rheological parameters is very sensitive to the estimated pipe wall position, measured from the front of the ultrasound transducer. This is illustrated in Section 3.6.2.3.

- Determination of yield stress from plug flow profiles

Some non-Newtonian fluids do not flow until a critical shear stress is exceeded. This shear stress is known as the yield stress. The application of a stress greater than the yield stress results in the formation of a moving plug in the centre of the pipe (see Figure 3.26). The radius of the plug and the pressure difference is related to the yield stress of the particular material:

$$\tau_y = \frac{\Delta P \cdot R_{plug}}{2L} \quad (3.27)$$

The principle of the calculation procedure is shown in Figure 3.25 and displays a velocity profile measurement for kaolin 12 % v/v at a flow rate of 0.44 l/s. It consists of a plug radius combined with a pressure difference measurement. First a theoretical profile is fitted to the measured velocity profile and then the plug radius is measured. In this case the measured velocity profile distorts at the further end of the pipe diameter due to attenuation of the ultrasound signal.

However, only half of the velocity profile is required for the fitting procedure and this is illustrated in Figure 3.25. The plug was determined by evaluating each channel from the experimental time-averaged velocity profile. When the velocity of each channel reached above 90 % of the plug velocity it was considered as part of the plug radius. In this method the plug radius would also be dependent on the spatial resolution of the velocity profile measurement (Wiklund *et al.* 2004 & 2005). Another method was to vary the plug radius during the fitting procedure and then analyse the rheological parameters obtained from the particular plug radius value. The plug radius value which yielded the most accurate rheological result, when compared to other conventional methods, was used to calculate the yield stress. Also, after the fitting procedure the theoretical profile would then be compared to the experimental profile to see whether the assumed plug radius obtained from fitting represents a reasonably accurate and realistic value.

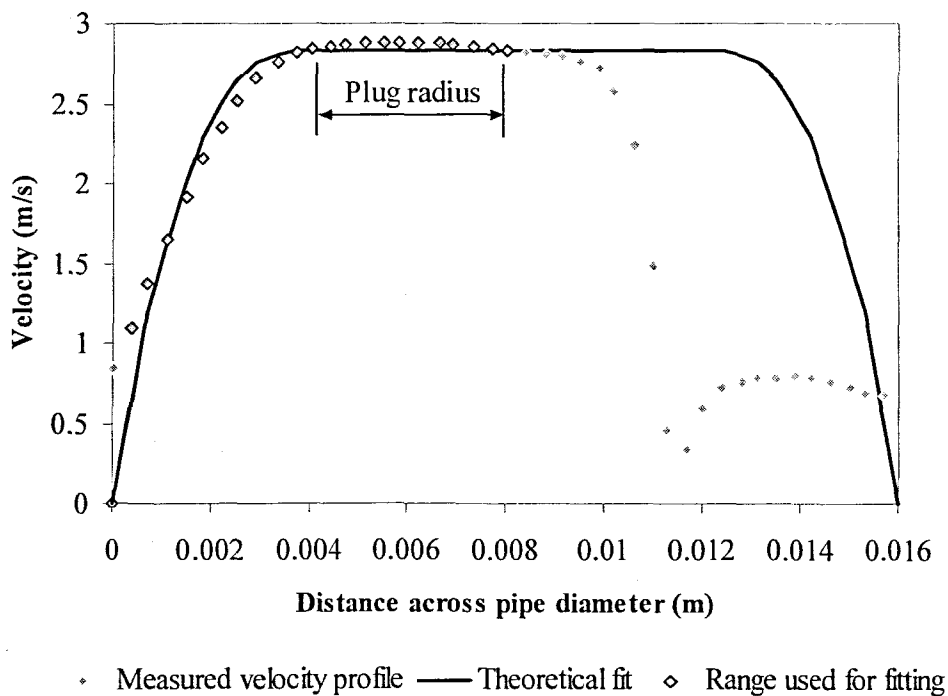


**Figure 3.26: Yield stress estimation using the plug radius**

If the plug radius and the pressure difference are known, the value of the yield stress can be derived according to Equation 3.27. The measured plug radius was  $R_{plug} = 4$  mm and consequently the pressure difference was  $\Delta P = 22197$  Pa. Using Equation 3.27, the calculated

yield stress was  $\tau_y = 44.4$  Pa. This is in good agreement when compared to offline rotational rheometry and in-line tube viscometry. The results are displayed in Table 3.7.

**Table 3.7: Yield stress measurements obtained from three different methods**

Method used	Yield stress (Pa)
Tube viscometry	40.1
Rotational rheometry	46.2
UVP-PD	44.4

In this research, yield stress values were derived from theoretical velocity profiles which were fitted to Bingham plastic and Herschel-Bulkley rheological models.

### 3.6.2.3 Calculation of rheological parameters

In order to select reliable raw data for computation of rheological parameters the following methods were used:

- The accuracy of velocity profile measurements are influenced by the presence of pulsating flow. The standard deviation of each instantaneous velocity (channels) across the pipe diameter was monitored. According to Ouriev (2000) a limit between 4 % and 6 % of the ratio between standard deviation and the average velocity is acceptable for computation of rheological parameters. Velocity profiles with standard deviations larger than the limit are defined as profiles of pulsating flow. During the tests, the maximum standard deviation from average velocity ratio was not more than 6 % for measuring volumes across the pipe diameter.
- The volumetric flow rate  $Q$ , which is integrated from the measured velocity profile, was compared with the reference volume flow rate obtained from the in-line mass-flow meter. This gave an indication of whether the overall accuracy, quantitatively and qualitatively, of the measured velocity profile was acceptable for further computation.

- Pressure fluctuations were analysed by monitoring the standard deviation of absolute pressure signals. The ratio of standard deviation to the average pressure signal within the measurement time was analysed. During measurements, the maximum standard deviation from the average pressure was not more than 2 %. The accuracy of the pressure measurement is important as the calculation of the fluid consistency index is very sensitive to the pressure difference measurement. Also, constant pressure readings showed that pulsating flow was not present during velocity profile measurements.

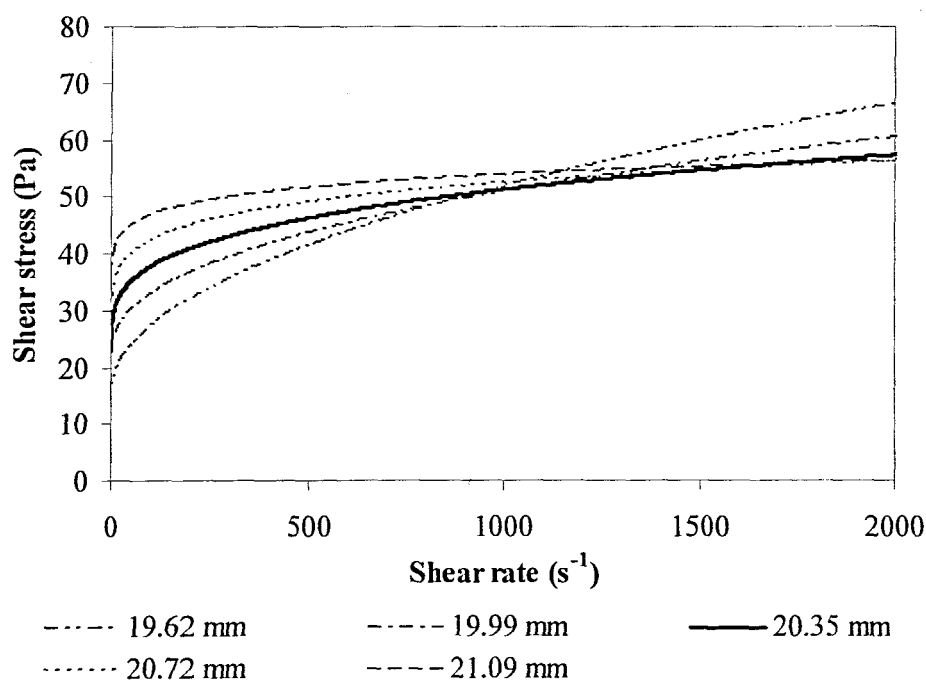
Computation of rheological parameters from measured velocity profiles comprises of two steps. The first step concerns the validation of the measured velocity profile. This is done by integrating the first half of the profile, as explained in the previous section. If the volumetric flow rate obtained from integration agrees well with the measured flow rate, the measured velocity profile is accurate and accepted for computation of rheological parameters. The next step involves the fitting of a theoretical velocity profile to the measured profile. Special software was developed in MATLAB® to fit theoretical velocity profiles to the experimental data. The software implements a minimisation algorithm and varies corresponding rheological parameters (depending on which rheological model is used) to try and calculate the best possible theoretical fit. The results are plotted on a rheogram for further comparison.

It was shown by Wiklund (2007) that the power-law parameters,  $n$ ,  $K$ , volumetric flow rate and apparent shear viscosities obtained from the UVP-PD method are sensitive to the estimated pipe wall position. This was also found for the rheological characterisation of mineral suspensions. Table 3.8 shows results for different wall positions obtained from the UVP-PD method for kaolin 10 % v/v. The results are graphically displayed in Figure 3.27. Kaolin is classified as a yield pseudoplastic fluid and thus the Herschel-Bulkley rheological model was used.



**Table 3.8: Rheological parameters for different estimated wall positions**

Wall position (mm)	$\tau_y$	$K$	$n$
19.62	15.15	1.33	0.48
19.99	21.22	1.84	0.40
20.35	22.72	4.21	0.28
20.72	18.94	11.48	0.16
21.09	17.42	21.05	0.09

**Figure 3.27: Flow curves obtained from different estimated wall positions**

In this particular case the correct estimated wall position is 20.35 mm and the result is shown by the solid line in Figure 3.27. Recall that the estimated wall position is the distance between the front surface of the transducer and pipe wall interface. Note that the difference between adjacent wall positions is equal to 0.37 mm. This in actual fact is the channel distance between measuring volumes. It is thus important to estimate the wall position as accurately as possible and also to be certain that the ultrasound transducer is mounted in a fixed position, as even a small movement or error can lead to significantly different results.

The fluid consistency index and flow behaviour index values determined from the empirical fit to experimental data depend on the shear rate range over which the data was measured, but also on the distribution of the experimental data over this range. Wiklund *et al.* (2002) and Wiklund (2007) showed that velocity profile fits to experimental data at different flow rates yield significantly different rheological parameters. The experimental (symbols) velocity profiles along the pipe diameter for CMC (density  $\rho = 1034 \text{ kg/m}^3$ , velocity of sound  $c = 1568 \text{ m/s}$ ) at different flow rates measured by the in-line UVP-PD method is shown in Figure 3.28. These are well represented by the theoretical profiles (curves) obtained by fitting the experimental data and pressure drop using the power-law model with the values of  $K$  and  $n$  listed in Table 3.9. The flow is laminar since the maximum value of the Reynolds number is less than 310, validating the use of the theoretical velocity profile equations.

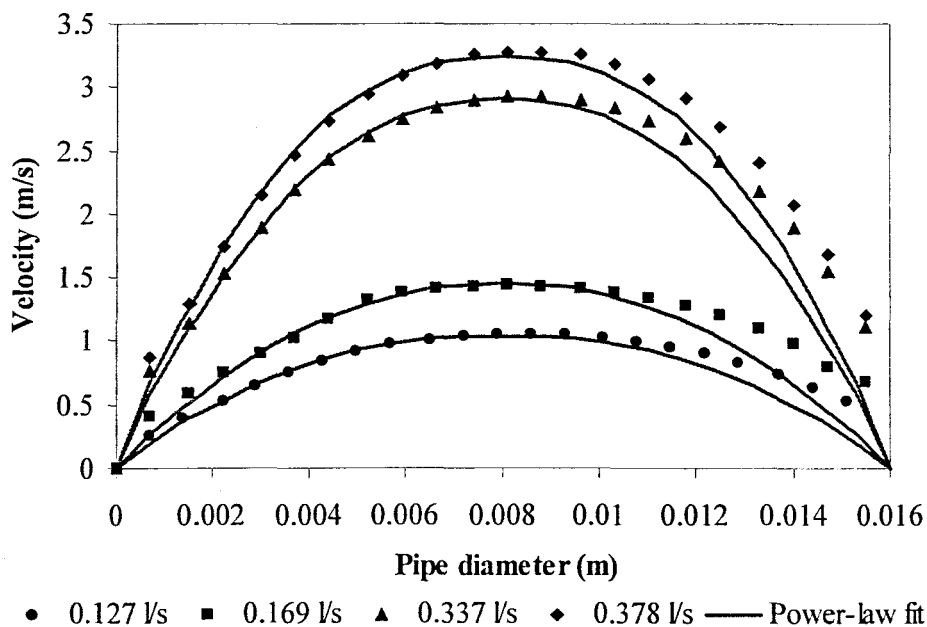


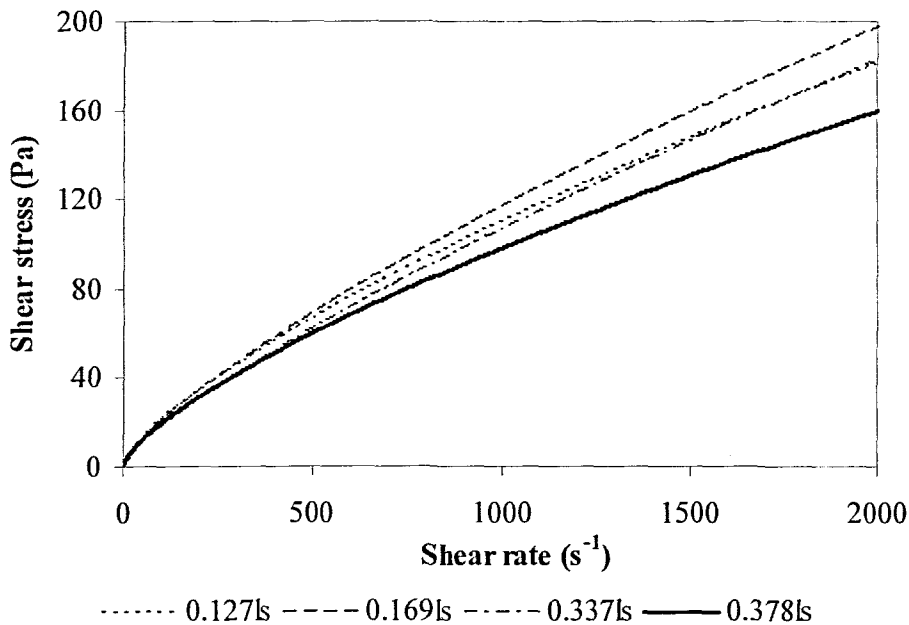
Figure 3.28: Experimental and power-law fitted velocity profiles for CMC 6% w/w

The reason for the bad fit at the further end of the pipe diameter is related to the increase in velocity inside the cavities in front of the ultrasound transducer. This resulted in a wider velocity profile across the diameter of the pipe. Only the radius of the pipe (8 mm) was used for the fitting procedure and calculation of rheological parameters.

**Table 3.9: Power-law model parameters obtained from experimental velocity profiles**

Flow rate (l/s)	Pressure drop (Pa)	$n$	$K$
0.127	12244	0.81	0.49
0.169	14963	0.76	0.64
0.337	23178	0.77	0.51
0.378	24554	0.70	0.78

The results obtained from the measured velocity profile at the highest flow rate (0.378 l/s) agrees well with off-line results measured by the Paar Physica MCR-300 rheometer ( $n = 0.68$ ,  $K = 0.89$ ) and in-line results measured by the tube viscometer ( $n = 0.69$ ,  $K = 0.86$ ). Figure 3.29 shows the comparison between the results obtained from different flow rates when plotted on a rheogram.

**Figure 3.29: Flow curves obtained from different flow rates for CMC 6% w/w**

Thus, in order to make the most accurate comparison between the three different methods, the range of shear rates as well as the distribution of the data over this range ideally should be equal. However, this situation is rarely achieved practically due to common experimental problems and limitations (Wiklund, 2007). The influence of estimated wall position as well as the effect of

shear rate range and distribution of experimental data was true for all the mineral suspensions tested during this research.

### **3.7 MINERAL SUSPENSIONS TESTED**

The materials used in this research were selected to represent a wide range of rheological properties. Water was selected for calibration purposes. Carboxymethyl Cellulose (CMC) was selected for the power-law fluid and is generally regarded as an ideal solution for experimental work (Haldenwang, 2003). Bentonite was selected as the Bingham plastic mineral suspension. The yield pseudoplastic or shear-thinning mineral suspension selected was kaolin clay. This material has been used at the Flow Process Research Centre (FPRC) over a very long period of time and is reasonably stable (Haldenwang, 2003).

#### **3.7.1 Water**

Municipal tap water was used as a basis or reference for the other slurries as water is a chemically reasonably stable fluid. As large volumes of water were used for testing and mixing the mineral suspensions, municipal tap water was the only option.

#### **3.7.2 Carboxymethyl Cellulose (CMC)**

CMC is a polymer solution and is used in the industry as a thickening agent. The polymer was mixed with water in order to produce a pseudoplastic solution. Concentrations varied from 5.3 – 6.5 % per weight. All of the concentrations were tested in the pipe viscometer and in-line rheometer (UVP-PD method) to obtain rheological parameters. The same concentrations were tested in a rheometer to obtain off-line rheological parameters which were then compared with the in-line results obtained from the pipe viscometer and ultrasound method.

### 3.7.3 Bentonite

Bentonite powder was mixed with water to obtain different concentrations of bentonite:water suspensions. The concentrations varied from 6 - 7.5 % per weight. During the pilot study bentonite powder was supplied from S&B Industrial Minerals, Switzerland. The bentonite powder chosen for testing has almost similar apparent viscosities when compared to the bentonite used at the FPRC. All of the concentrations were rheologically tested in-line by using the pipe viscometer and UVP-PD method as well as off-line by using a conventional rheometer.

### 3.7.4 Kaolin

Dry kaolin powder was used to prepare the kaolin:water suspensions. The kaolin was obtained from one source and supplied by the Flow Process Research Centre (FPRC). Different concentrations were prepared ranging from 8 to 12 % per volume. The kaolin suspensions were mixed in a mixing tank and left overnight for mixing to ensure that the suspensions were properly mixed. All of the kaolin concentrations were rheologically characterised by using the pipe viscometer and the UVP-PD method. Rheological results were obtained off-line from all of the concentrations by using the conventional off-line rheometer.

## 3.8 GENERAL OBSERVATIONS

This section describes observations made during the testing and experimental phase of this research project.

### 3.8.1 Pressure fluctuations in pulsating flow

Pulsating flow was caused by the vibration and pumping action of the positive displacement pump. Figure 3.30 shows pressure fluctuations observed in the presence of pulsating flow in water. The absolute pressure was monitored with a point pressure sensor (range 0-1 bar) by taking consecutive measurements at time intervals of 10 ms. Al-Zaharnah, Yilbas and Hashmi (2001) as well as Ray, Ünsal, Durst, Ertunc and Bayoumi (2005) showed similar pressure

variations in fully developed pulsating flow.

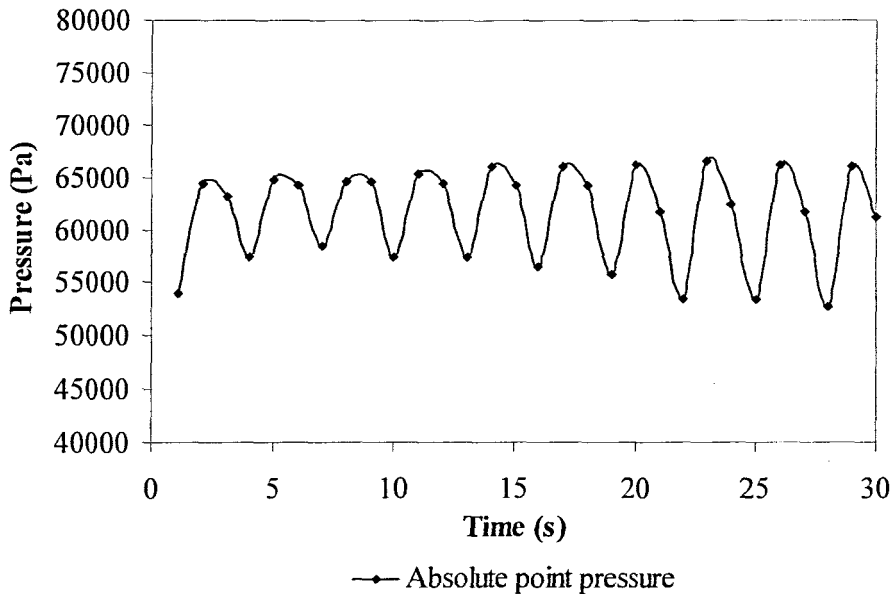


**Figure 3.30: Pressure fluctuations in pulsating flow**

The average pressure of the readings was  $\pm 61000$  Pa and pressure measurements deviated between approximately 66000 Pa and 56000 Pa. This means that there were pressure fluctuations of  $\pm 5000$  Pa while pulsating flow was present. As a result, pressure difference measurements were inaccurate under these conditions. A dampener was fitted in the flow loop (as discussed in Section 3.2.3.2) and results showed a significant improvement. The maximum standard deviation between the mean pressure values was determined to be less than  $\pm 150$  Pa in laminar flow.

### 3.8.2 Off-line vs in-line velocity of sound measurements

Velocity of sound measurements were conducted off-line as well as in-line for all of the mineral suspensions and results were compared. Table 3.10 shows off-line and in-line velocity of sound results for CMC at different concentrations.

**Table 3.10: In-line and off-line velocity of sound results for different concentrations of CMC**

Slurry concentrations (w/w)	CMC 5.3 %	Temp (°C)	CMC 6 %	Temp (°C)	CMC 6.5 %	Temp (°C)
In-line sound speed (m/s)	1520	17.9	1533	17.7	1548	25.2
Off-line sound speed (m/s)	1412	18.3	1308	17.4	1404	25.1

Although temperatures were not exactly similar for both methods, sound speed results from the off-line method were found to be significantly different when compared to results obtained using the in-line method. Tables 3.11 and 3.12 show velocity of sound results for different concentrations of kaolin and bentonite suspensions.

**Table 3.11: In-line and off-line velocity of sound results for different concentrations of kaolin**

Slurry concentrations (v/v)	Kaolin 8 %	Temp (°C)	Kaolin 10 %	Temp (°C)	Kaolin 12 %	Temp (°C)
In-line sound speed (m/s)	1540	17.2	1540	18.1	1555	18.5
Off-line sound speed (m/s)	1457	17.7	1437	17.5	1448	18.2

**Table 3.12: In-line and off-line velocity of sound results for different concentrations of bentonite**

Slurry concentrations (w/w)	Bentonite 7 %	Temp (°C)	Bentonite 6.5 %	Temp (°C)	Bentonite 5.7 %	Temp (°C)
In-line sound speed (m/s)	1565	17.9	1550	16.7	1560	19.7
Off-line sound speed (m/s)	1485	17.2	1480	17.2	1479	20.6

Off-line velocity of sound results did not correlate with results obtained using the in-line method for bentonite as well as kaolin for all of the investigated concentrations. The in-line results were generally found to be larger than the off-line results. Here one must assume that the in-line results were correct due to the fact that the velocity of sound in these mineral suspensions must be larger when compared to water (1481.3 at 20°C). The velocity of sound in a flowing fluid depends on the local density and temperature fluctuations of the material across the pipe diameter. With the in-line measurement technique discussed in Section 3.4.5, the time of flight will decrease at higher flow rates and consequently the sound speed will increase. Further investigation is required for higher sound speeds in fluids flowing at higher flow rates. The lower values of sound speeds obtained using the off-line method could also be due to suspended air bubbles in the samples. Povey (1997) showed that very small amounts of undissolved air can have a dramatic effect on the velocity of sound in pure water. Figure 3.31 shows the impact of suspended air bubbles on acoustic propagation in water.

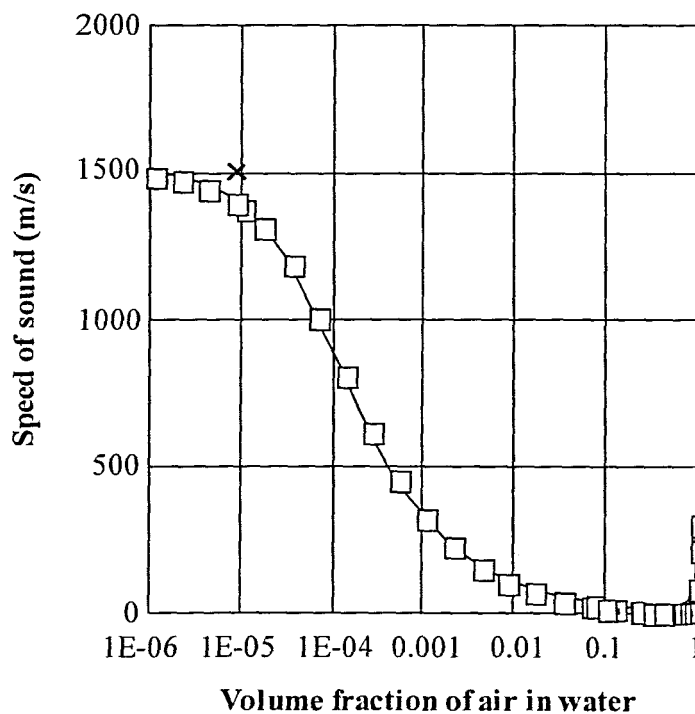


Figure 3.31: The velocity of sound in air/water mixtures at 20°C (Povey, 1997)

The cross indicates the velocity of sound in the absence of air. The velocity reaches a minimum of 22.27 m/s at 53 % undissolved air. This is far smaller than the velocity of sound either in water (1505.76 m/s) or in air (322.16 m/s) at 20 °C. The features exhibited by the concentration



dependence of sound velocity presented in the air/water mixture, are present in all mixtures to a greater or lesser extent (Povey, 1997).

### 3.8.3 Temporal behaviour of sound velocity in mineral suspensions

To gain knowledge of the temporal behaviour of the sound velocity in the model mining mineral suspensions, a number of acoustic characterisation experiments were conducted. The sound velocity was measured for each model fluid at a certain concentration while the fluid temperature was increased over time due to the mechanical heating of the slurry flowing through the positive displacement pump. Figure 3.32 shows the sound velocity plotted as a function of temperature for a number of fluids.

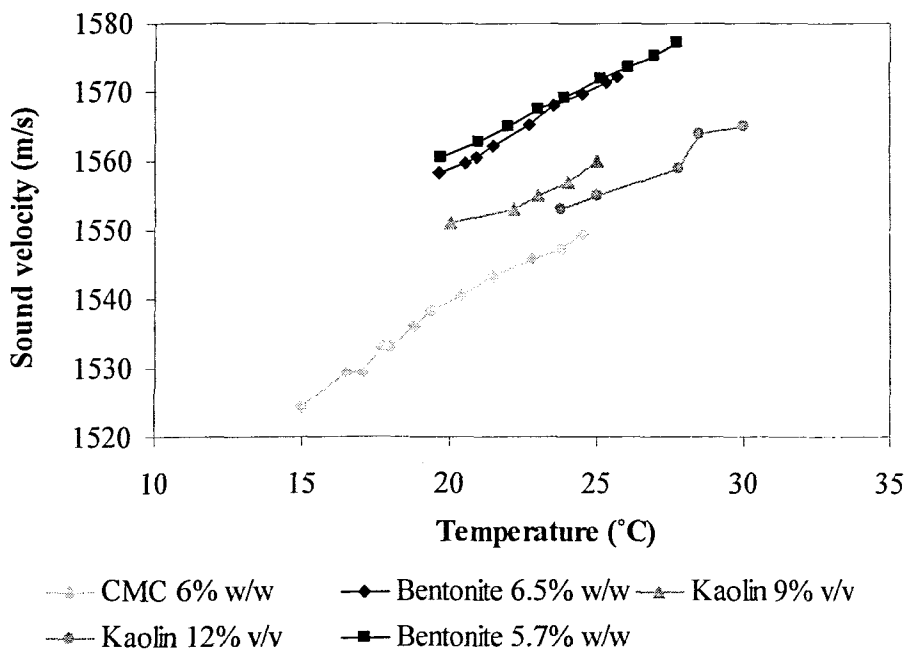


Figure 3.32: Sound velocity as function of temperature for some investigated fluids

The sound velocity was generally found to be a linear function of increasing temperature. In CMC 6 %, the sound velocity increased by approximately 25 m/s over the temperature range of 15-25 °C. For bentonite 6.5 %, there was an increase of +/- 14 m/s over a temperature range of 20-25 °C. The two concentrations of kaolin 9 and 12 % showed a velocity of sound increase of

approximately 10 m/s over a temperature range of 20-25 °C and 25-30 °C, respectively. The present method for measuring the temporal behaviour of fluids has to be modified in order to cover a wide range of temperatures. This can be done by driving a temperature ramp from ambient to the maximum working temperature of the transducers (up to 60 °C), as discussed by Wiklund (2007). It is thus shown here that the present UVP-PD system with a method for measuring sound velocity in-line has a significant advantage as erroneous velocity of sound values due to temperature changes may result in inaccurate velocity profiles.

### 3.8.4 Time frame aliasing

Time frame aliasing occurs when emitted energy from the previous ultrasonic emission reflects back to the transducer and interferes with reflections from the following emitted burst. This usually occurs when a large stationary echo signal is present. In this case a large stationary echo is present due to the reflection of US energy from the opposite transducer's stainless steel front surface, which has a large difference in acoustic impedance compared to the fluid under test. Figure 3.33 illustrates this effect. In the first case a lower PRF value is chosen and reflections are observed (when looking at an oscilloscope) after the first emitted ultrasound burst. Multiple echoes occur (2A and 3A) due to energy travelling back and forth between the two transducers, but with lower amplitudes as a result of attenuation and absorption. After the second emission (B) the third reflection is still observed, but in this hypothetical case its small amplitude causes no interference.

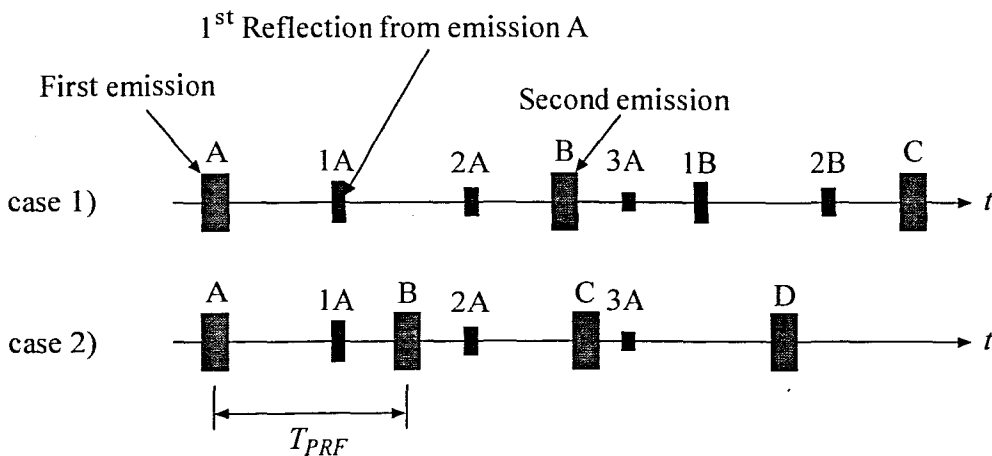


Figure 3.33: Schematic illustration of time frame aliasing

When the PRF is increased the consecutive ultrasonic emissions occur in shorter time intervals, as shown in case 2. Now the second stationary echo from emission A is observed after the following emitted burst (B). In this case the larger amplitude interferes with reflections coming from suspended particles in the investigated fluid, which causes distortion and loss of data. Figure 3.34 shows an example of time frame aliasing when observed on a digital oscilloscope. The unwanted echo is present approximately in the middle of the pipe diameter. This interference results in a loss of data in the centre of the measured velocity profile, as shown in Figure 3.35.

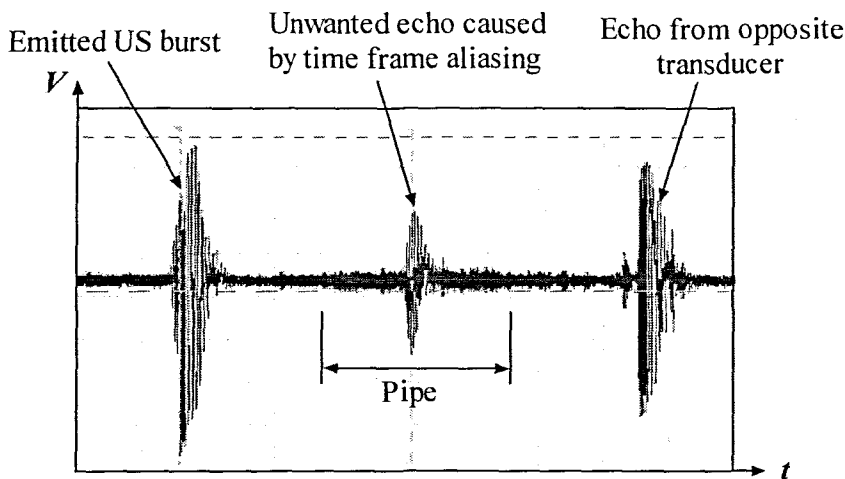


Figure 3.34: Time frame aliasing example on oscilloscope

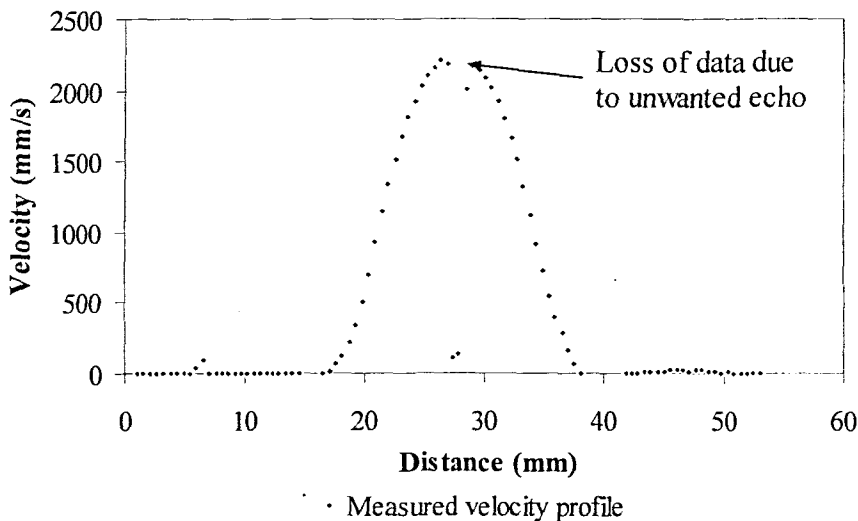


Figure 3.35: Loss of data due to interference from stationary echo

From Figure 3.33 it can be seen that time frame aliasing can be overcome easily by optimising the PRF value. It is thus very important to monitor the raw echo amplitude while measuring velocity profiles in order to identify possible unwanted reflections and interference, such as time frame aliasing.

### 3.8.5 Reflected wave effect

The reflected wave effect is generated by multiple reflections of the ultrasonic wave. The time duration of this effect is strongly dependent on the attenuation of the ultrasound in the medium, on Doppler angle, tube diameter and acoustic properties of the pipe wall material. The energy of the reflected ultrasonic signal can be sufficient to generate an additional echo signal. The additional echo signal will contribute to an additional portion of the visualised velocities that are received by the UVP monitor and are shown on a depth distance that overshoots the pipe diameter (Ouriev, 2000). Therefore, it is very common to obtain non-zero velocities and apparent constant plug behaviour toward the far pipe wall, as shown in Figure 3.36, with fluid systems containing a large amount of scattering particles (Wang, Wang, Ren & Jin, 2003; Wiklund, 2007).

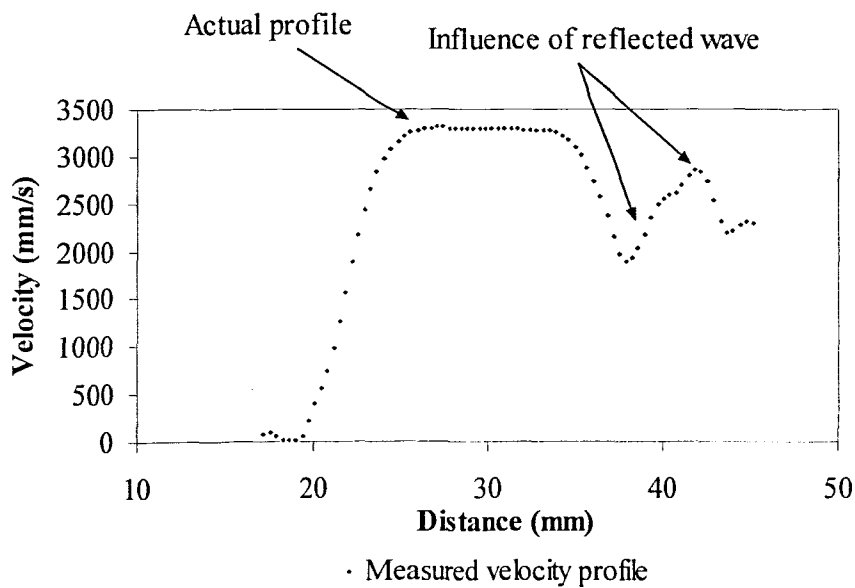


Figure 3.36: Influence of multiple reflections on measured profile for kaolin 8.7 % v/v

The first velocity profile reflects the actual flow situation in the pipe diameter. The second profile is estimated from the delayed echo signals which occur due to multiple reflections of the ultrasound wave.

## 3.9 CONCLUSION

### 3.9.1 Empirical behaviour

The difference between pressure fluctuations in pulsating flow and non-pulsating flow was very noticeable. The flow was more regular after a pulsation dampener was installed in the pipe rig system.

Off-line and in-line velocity of sound results did not correlate. In-line sound speed results are assumed to be correct as the values obtained seemed to be more realistic when compared to water.

The temporal behaviour of mineral suspensions was investigated. The present UVP-PD system with a method for measuring sound velocity in-line has a significant advantage as erroneous velocity of sound values due to temperature changes may result in inaccurate velocity profiles.

The effect of time frame aliasing was very noticeable throughout tests. Time frame aliasing was removed by adjusting the PRF. However, this effect can only be spotted by monitoring the received echo from ultrasound emissions.

Reflected wave effect was recognised in most of the measured velocity profiles. This effect did not influence the calculation of rheological parameters as only the first half (radius of the pipe) was used for post data analysis.

### 3.9.2 Experimental equipment and procedures

The equipment was equipped with all the necessary instrumentation to measure flow rates, point pressures, temperature, velocity profiles and speed of sound in the investigated fluid.

Software was developed for the tube viscometer to sample the data and log it in spreadsheets where the results were displayed in graphical format for a user-friendly interface between operator and test rig.

Post data analysis was an important part of the ultrasound measurements. Software was developed for velocity profile curve fitting in order to obtain the desired rheological parameters of the investigated mineral suspensions.

The equipment was commissioned with clear water tests.

Calibration and test procedures were developed to accurately produce pipe flow data in order to establish relevant rheological parameters of all the mineral suspensions tested. The ultrasound equipment (UVP monitor and transducers) did not need any calibration.

The experimental errors pertaining to the pipe viscometer and UVP-PD method have been analysed and discussed and are deemed to be within acceptable limits.

Several concentrations of bentonite and kaolin suspensions, as well as CMC solutions, were used for the tests. This yielded a wide range of rheological properties.

The results obtained were used to compare and evaluate the UVP-PD method with rheological parameters obtained from in-line tube viscometry and conventional off-line rotary rheometry.

# **CHAPTER FOUR**

**ANALYSIS**

**OF**

**RESULTS**

# **CHAPTER FOUR**

## **ANALYSIS OF RESULTS**

### **4.1 INTRODUCTION**

In this chapter, the rheological parameters for each investigated mineral suspension are presented on a rheogram for comparison and results are discussed. Highly concentrated mineral suspensions were rheologically characterised using three different methods:

- Tube viscometry.
- UVP-PD rheometric method.
- Conventional off-line rotational rheometry.

The fluids that were investigated yielded a wide range of rheological properties. Results of Carboxymethyl Cellulose (CMC) solutions, as well as bentonite and kaolin clay mineral suspensions of various concentrations are presented. Tube viscometer (pipe) data, off-line rotational rheometric data, theoretical fits of experimental velocity profiles, as well as parameter settings and test conditions, are depicted in Appendix A.

### **4.2 CARBOXYMETHYL CELLULOSE (CMC)**

Three different concentrations of CMC were rheologically characterised. The CMC solutions tested were 5.3 %, 6 % and 6.5 % w/w. CMC is classified as a pseudoplastic (shear-thinning) fluid and thus the power-law model is used to rheologically characterise the CMC solutions.



### 4.2.1 Carboxymethyl Cellulose 5.3 % w/w

Figure 4.1 compares experimental data (symbols) measured using the UVP monitor with a theoretical velocity profile determined from the power-law model. As explained before in Section 3.6.2.3, the cavity influences the quality of the measured velocity profile and thus it becomes difficult to fit theoretical velocity profiles (Equation 2.18, page 2.18) with experimental data without error. However, these are well represented by the theoretical profile (curve) obtained by fitting the experimental data and pressure drop using the power-law model with the values of  $K$  and  $n$  listed in Table 4.3. The volumetric flow rate obtained from integration of the measured velocity profile equals 0.397 l/s and has an error difference of 4.6 % when compared to the flow rate obtained from the mass-flow meter (0.416 l/s).

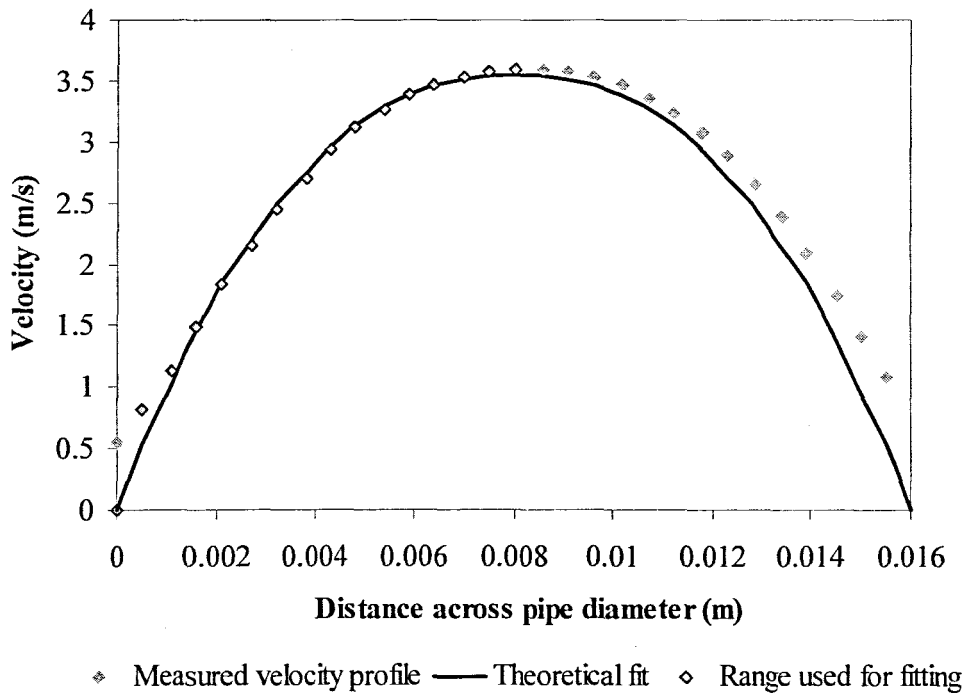


**Figure 4.1: Experimental and theoretical velocity profile for CMC 5.3 % w/w**

The test conditions and UVP parameter settings for the velocity profile measurement is depicted in Tables 4.1 and 4.2. For CMC the ultrasonic energy could penetrate across the whole pipe diameter and generally good echo was obtained for all concentrations. As a result, UVP parameters, such as the number of US repetitions and number of cycles per US pulse, could be set to lower values in order to increase the spatial and time resolution for a velocity profile measurement. Also, the total measurement time decreases as an average of 256 consecutive

measured velocity profiles was needed for a good and accurate measurement. Measurement times of velocity profiles should be kept as low as possible due to the possibility of small variations in flow rate over time.

**Table 4.1: UVP parameter settings for CMC 5.3 % w/w**

PRF (kHz)	US Voltage (V)	Number of cycles/pulse	Number of US repetitions	Sound speed (m/s)
13.69	90	2	256	1520

The Doppler angle was fixed at  $70^\circ$  and the emitting frequency was equal to 4 MHz for all velocity profile measurements in this research. The calculated Reynolds number,  $Re_2$ , (Equation 2.2, page 2.2) shows that the velocity profile in Figure 4.1 was measured in laminar flow, validating the use of theoretical power-law models.

**Table 4.2: Test conditions for CMC 5.3 % w/w**

Reynolds number	Pressure drop (Pa)	Volume flow rate (l/s)	Slurry density (kg/m <sup>3</sup> )	Temperature (°C)
600	14823	0.416	1030	15.5

Flow curves could be measured at a low shear rate range (from 0.1 to 300 s<sup>-1</sup>) for all CMC concentrations, using the off-line rotational rheometer. The reason for the lower shear rate range when using the rheometer is that the fluid consistency index ( $K$ ) is accurately determined from the curve at the low shear rate range. The flow behaviour index ( $n$ ) is determined over the higher shear rate range. At this range, the power-law model starts to tend towards a straight line. For this reason it is not necessary to move into very high shear rates, as the flow curve starts to lose its curvature from approximately 50 s<sup>-1</sup>. One could argue that the rest of the experiments should be carried out over the same shear rate range, but it is very difficult and even impossible to achieve such low shear rates with pipe flow experiments (UVP-PD method and tube viscometry). Thus the rheological characterisation of all the suspensions in this research was

compared over a shear rate range from 0 to  $1000 \text{ s}^{-1}$  to compensate for the two in-line methods as well as the different mineral suspensions. It is very important to compare rheological results over the same range of shear rates, especially when viscosities are obtained from different methods, as described in this research (Wiklund, 2007). The experimental data obtained from the off-line rotational rheometer is schematically illustrated in Figure 4.2 on a rheogram.

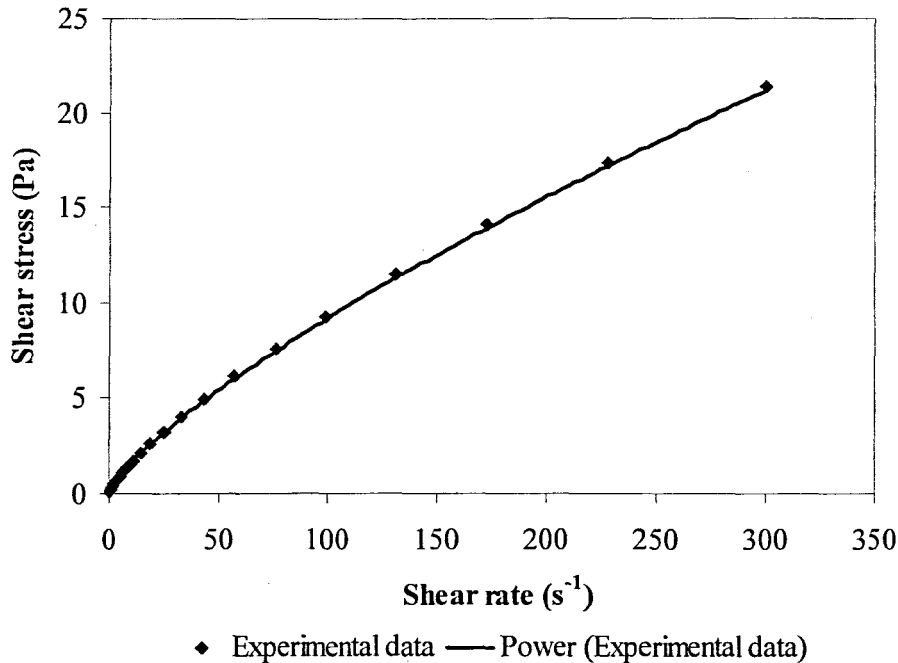


Figure 4.2: Flow curve measured by off-line rheometer for CMC 5.3 % w/w

Figure 4.3 shows experimental data from three different pipe diameters measured by the tube viscometer. Based on these results, it can be observed that no wall slip was present during the tests. The bulk shear rate values ( $8V/D$ ) are not the true shear rate values and still need to be converted by using the Rabinowitsch-Mooney (Equation 2.11) procedure for reducing pipe viscometer data. The result is illustrated on a rheogram in Figure 4.4.

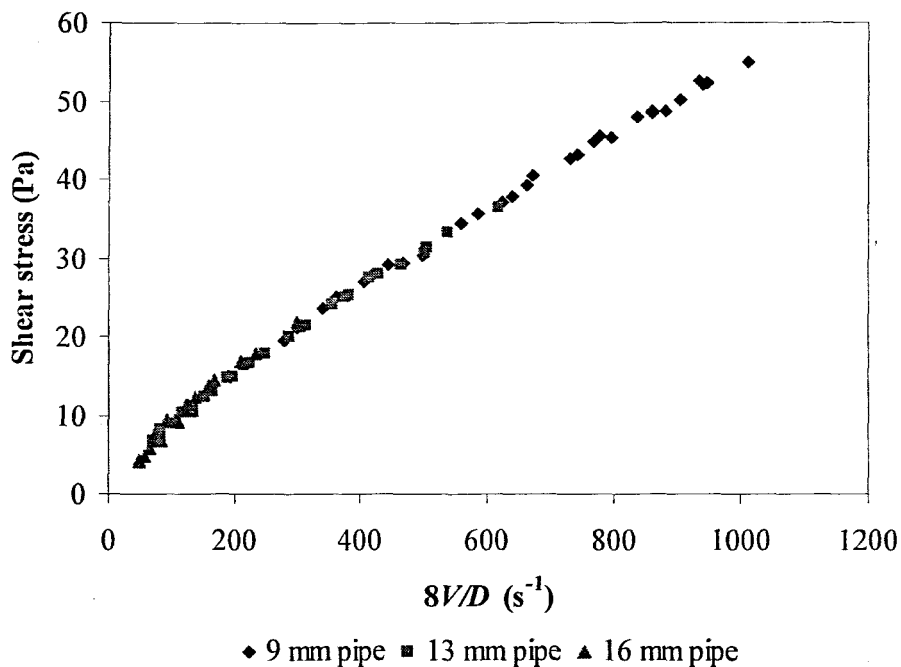


Figure 4.3: Pipe data measured by the tube viscometer for CMC 5.3 % w/w

As expected, low shear rate ranges could not be obtained with the tube viscometer due to pressure drop and volumetric flow rate limitations. This is explained in the next chapter.

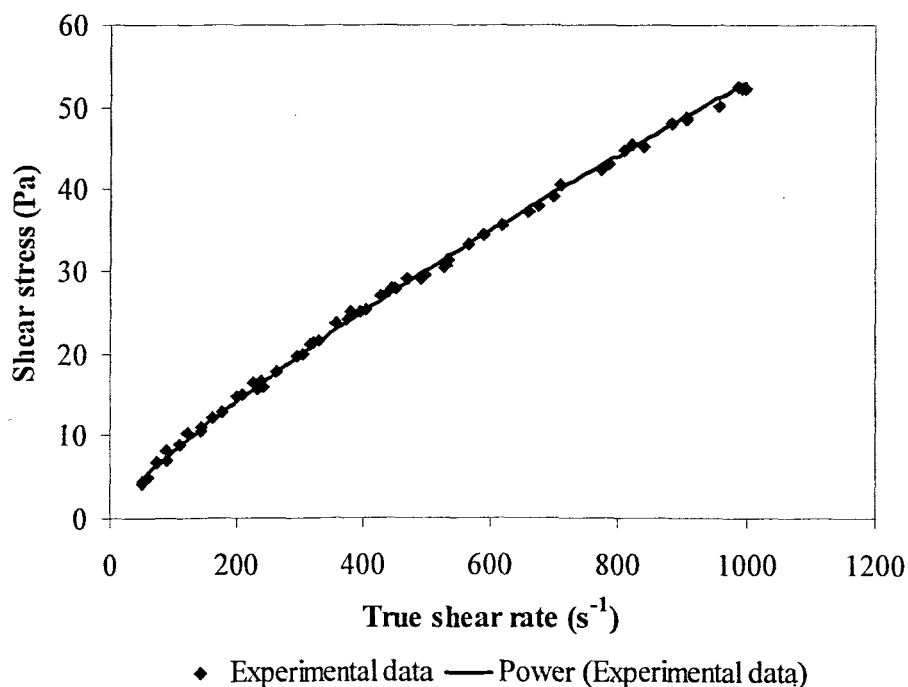


Figure 4.4: Flow curve measured by the tube viscometer for CMC 5.3 % w/w

Figures 4.5 and 4.6 present summaries of the rheological results obtained from off-line rheometry, tube viscometry and the use of the UVP-PD rheometric method. Results are plotted on a rheogram in Figure 4.5 for comparison. The variation with shear rate in the viscosity of the CMC solution is also shown in Figure 4.6. The flow curve obtained from the UVP-PD rheometric method is determined from mathematical curve fitting in order to obtain rheological parameters. This is the reason why flow curves determined by the UVP-PD method are presented as a solid line over the total shear rate range, and not as experimental data points.

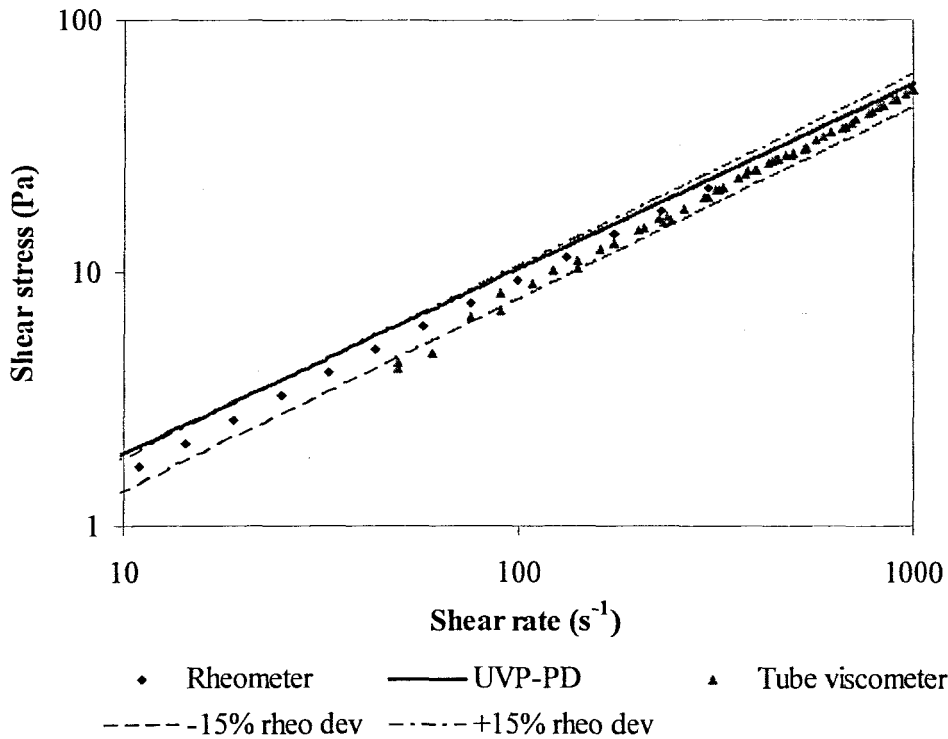
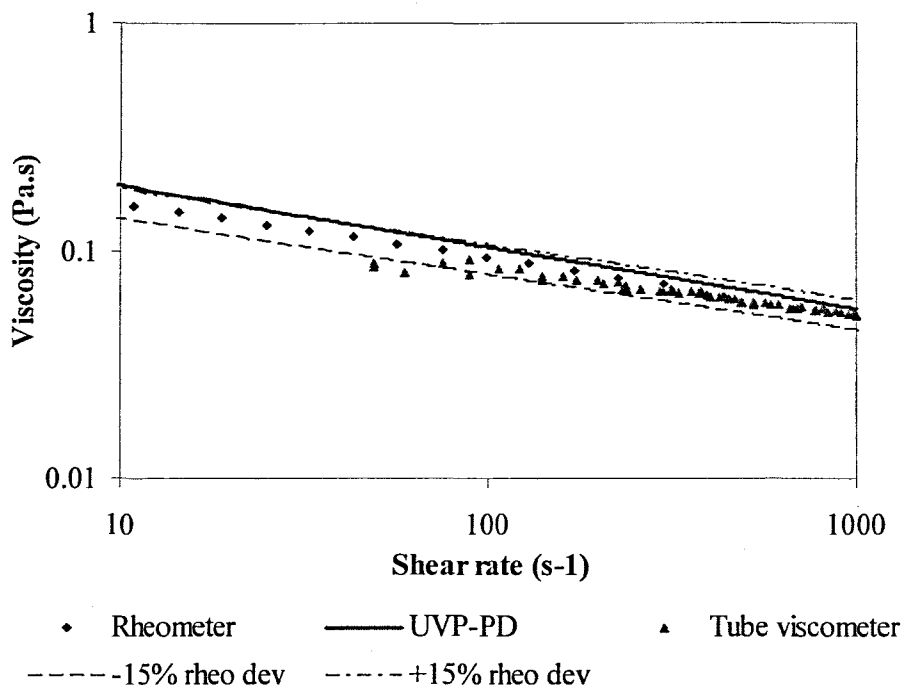


Figure 4.5: CMC 5.3 % w/w rheogram

Experimental data obtained from the tube viscometer and off-line rheometer agrees well with that determined by the in-line UVP-PD rheometric technique. The error curves illustrate a deviation of  $\pm 15\%$  from the flow curve measured by the off-line rheometer. Based on this it can be seen that flow curves obtained from the two in-line methods agree within  $15\%$  with the flow curve measured by the off-line rheometer. It may be expected that results obtained from the two in-line methods (i.e. UVP-PD method and tube viscometry) would show excellent agreement when compared with each other. However, it must be stressed that the in-line methods comprise two separate large-scale experiments and thus error is unavoidable.



**Figure 4.6: Variation with shear rate in viscosity for CMC 5.3 % w/w**

The tube viscometer results show apparent viscosities with magnitudes lower than 15 % between shear rate ranges of 50 – 100 s<sup>-1</sup>, when compared to the apparent viscosities obtained from the off-line rheometer. This is expected as the combined errors for the tube viscometer are larger at low shear rates, due to system limitations. At higher shear rate ranges (from 100 to 1000 s<sup>-1</sup>), the variation with shear rate in viscosity for all three methods agree within 15 % with each other. From Figure 4.6 it can be seen that the apparent viscosity decreases by less than one order of magnitude for a shear rate increase of two orders of magnitude, indicating shear thinning behaviour.

Table 4.3 shows fluid consistency coefficients ( $K$ ) and flow behaviour index ( $n$ ) values obtained with the use of mathematical curve fitting using the power-law model for results obtained from three different methods.

**Table 4.3: Rheological parameters obtained from three different methods for CMC 5.3 % w/w**

Parameters	UVP-PD	Tube viscometry	Rotational rheometry
$K$ (Pa.s <sup><math>n</math></sup> )	0.36	0.19	0.28
$n$	0.73	0.82	0.76

Table 4.3 shows that the rheological parameters do not agree well with each other, especially when observing fluid consistency coefficients for the three independent methods. However, when the parameters ( $K$  and  $n$ ) are compared as flow curves on a rheogram using the power-law model, results agree within 15 % with each other, as depicted in Figures 4.5 and 4.6. Here it must be noted that these values or rheological parameters are mathematically determined from curve fitting or minimisation algorithms and can change significantly when determined over different shear rate ranges or when initial parameters are varied. When a more manual approach for determining rheological parameters is taken, initial parameters are sometimes set as a fixed value. This is even more acute for the three parameter models, such as for Herschel-Bulkley fluids. For these reasons, results obtained from the three different rheological methods are compared graphically as flow curves.

#### 4.2.2 Carboxymethyl Cellulose 6 % w/w

Figure 4.7 compares flow curves for CMC 6 % w/w (density  $\rho = 1034 \text{ kg/m}^3$ ) measured by the in-line tube viscometer and off-line rheometer, as well as the UVP-PD method. The experimental and theoretical velocity profile, test conditions and UVP parameter settings are depicted in Appendix A. In this case the results measured by the off-line rheometer are in excellent agreement (less than 5 %) with the flow curve determined by the UVP-PD method. The result measured by the tube viscometer is within 15% when compared to the flow curves obtained from the UVP-PD method and off-line rheometer.

Figure 4.8 shows the variation with shear rate in viscosity for the CMC 6 % solution. In this particular case, the viscosities obtained from all rheometric methods are in good agreement over the total shear rate range. Once again the apparent viscosity decreases by approximately one order of magnitude for a shear rate increase of three orders of magnitude, also indicating shear thinning behaviour.

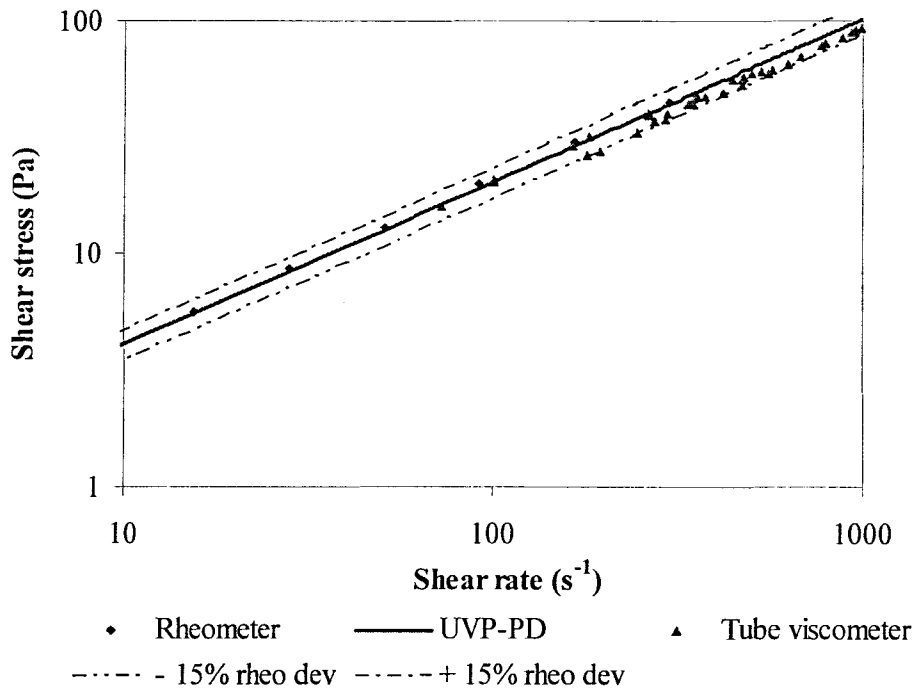


Figure 4.7: CMC 6 % w/w rheogram

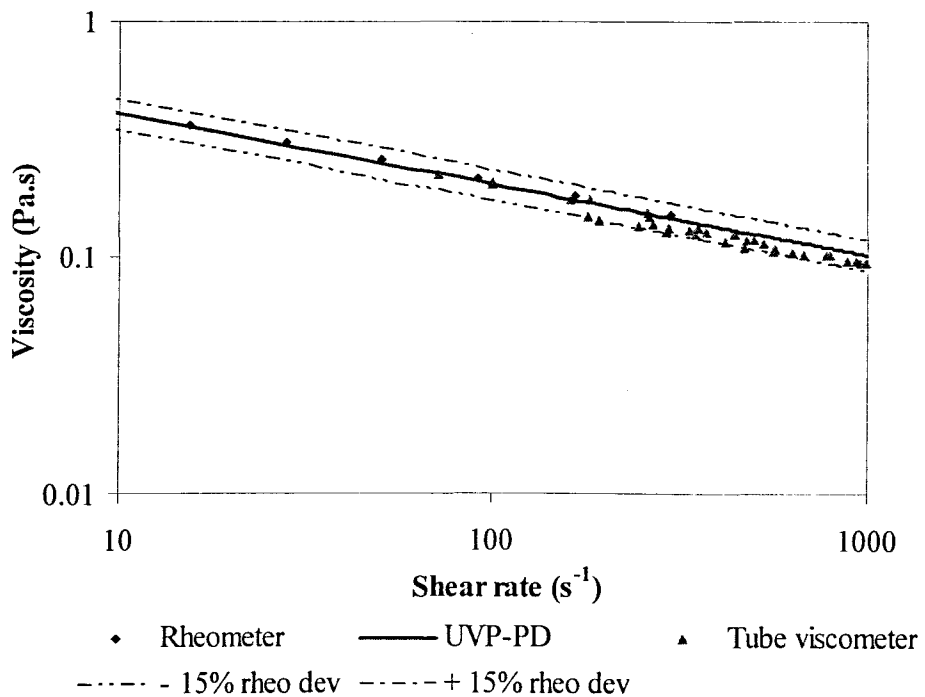


Figure 4.8: Variation with shear rate in viscosity for CMC 6 % w/w



Rheological parameters obtained from two in-line methods and one off-line method are shown in Table 4.4. Here, based on numerical values, the fluid consistency indices and flow behaviour index values are in good agreement with each other.

**Table 4.4: Rheological parameters obtained from three different methods for CMC 6 % w/w**

Parameters	UVP-PD	Tube viscometry	Rotational rheometry
$K$ (Pa.s <sup>n</sup> )	0.81	0.86	0.86
$n$	0.7	0.68	0.69

### 4.2.3 Carboxymethyl Cellulose 6.5 % w/w

Rheological results for CMC 6.5 % w/w (density  $\rho = 1040 \text{ kg/m}^3$ ) are schematically illustrated in Figures 4.9 and 4.10. From Figure 4.9 it can be observed that results are in good agreement (within 15 %) with each other across the whole shear rate region (10 to  $1000 \text{ s}^{-1}$ ).

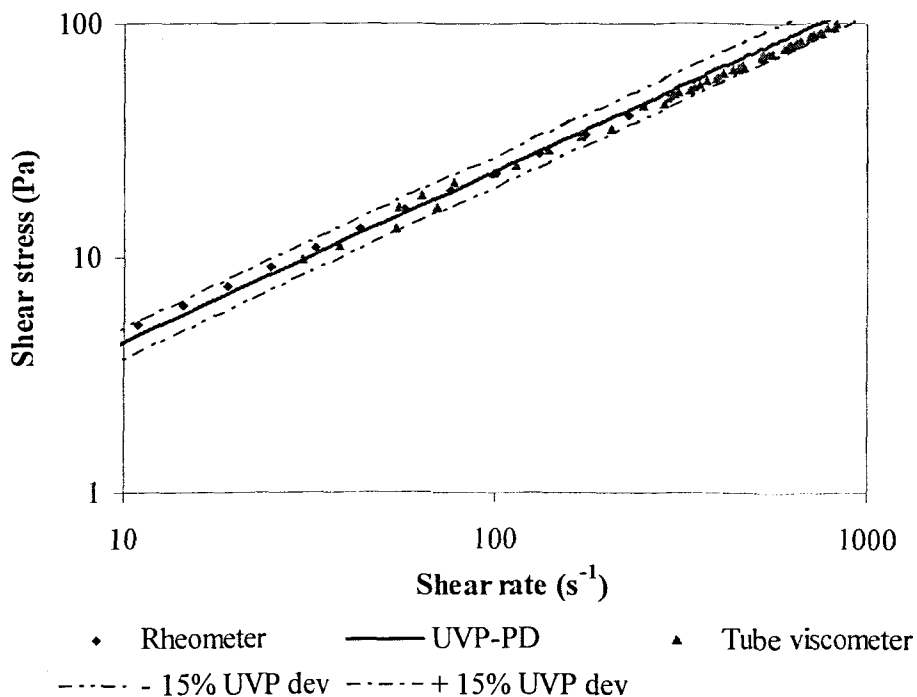


**Figure 4.9: CMC 6.5 % w/w rheogram**

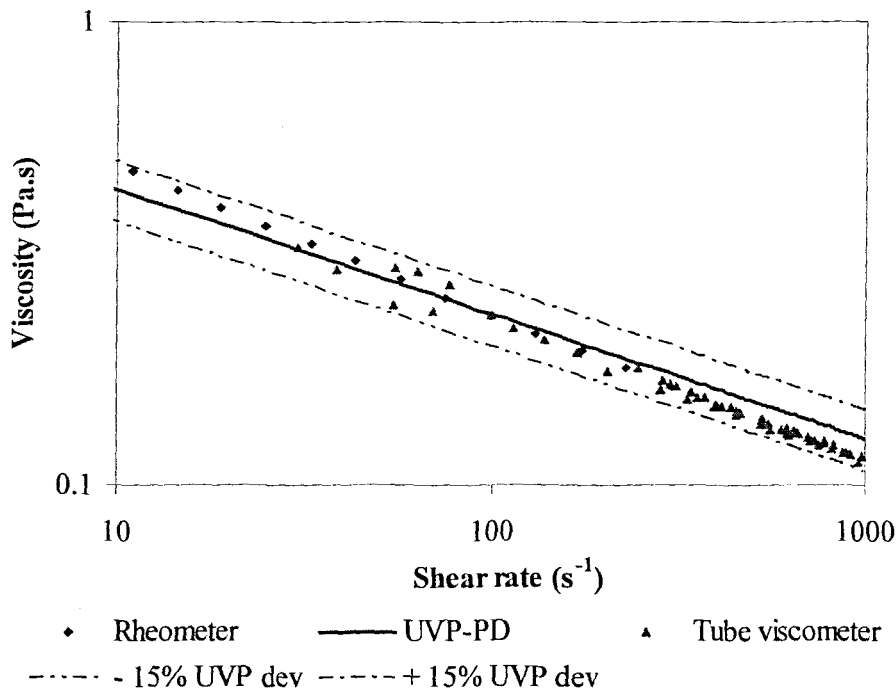


**Figure 4.10: Variation with shear rate in viscosity for CMC 6.5 % w/w**

The apparent viscosities obtained by off-line rheometry, tube viscometry and by the in-line UVP-PD method show a good agreement of 15 % when compared over the total shear rate range. The apparent viscosities measured by the tube viscometer show some fluctuations at the lower shear rate range. This could be due to flow limitations of a highly concentrated solution in the pipe rig. At the higher shear rate range, the apparent viscosities show good consistency and agreement between results obtained from the other two rheological methods. The results shown in Figure 4.10 show a decrease in viscosity with increasing shear rate, indicating shear thinning behaviour.

The rheological parameters ( $K$  and  $n$ ) for CMC 6.5 % are depicted in Table 4.5. The  $K$  and  $n$  values determined by the UVP-PD method are different from the tube viscometer and off-line rheometer, which have almost similar rheological parameters.

**Table 4.5: Rheological parameters obtained from three different methods for CMC 6.5 % w/w**

Parameters	UVP-PD	Tube viscometry	Rotational rheometry
$K$ (Pa.s <sup><math>n</math></sup> )	0.81	0.93	1.05
$n$	0.73	0.69	0.67

### 4.3 BENTONITE

Four different concentrations of bentonite were rheologically characterised. The concentrations that were tested were 5.7, 6.5, 7 and 7.5 % w/w. Bentonite is classified as a Bingham plastic fluid and this model (Equation 2.4) is used to rheologically characterise the bentonite mineral suspensions.

#### 4.3.1 Bentonite 5.7 % w/w

An experimental (symbols) velocity profile along the pipe diameter for bentonite 5.7 % (density  $\rho = 1035 \text{ kg/m}^3$ , velocity of sound  $c = 1560 \text{ m/s}$ ) measured by the in-line UVP-PD method is shown in Figure 4.11. These are represented by the theoretical profile (curve) obtained by fitting the experimental data and pressure drop using the Bingham plastic model (Equation 2.24, page 2.19) with the values of  $K$  and  $\tau_y$  listed in Table 4.8. Recall that the flow behaviour index ( $n$ ) for a Bingham plastic fluid is equal to one. The flow is laminar, since the value of the Reynolds number ( $Re_2$ ) is equal to 280, validating the use of the theoretical point velocity distribution equations.

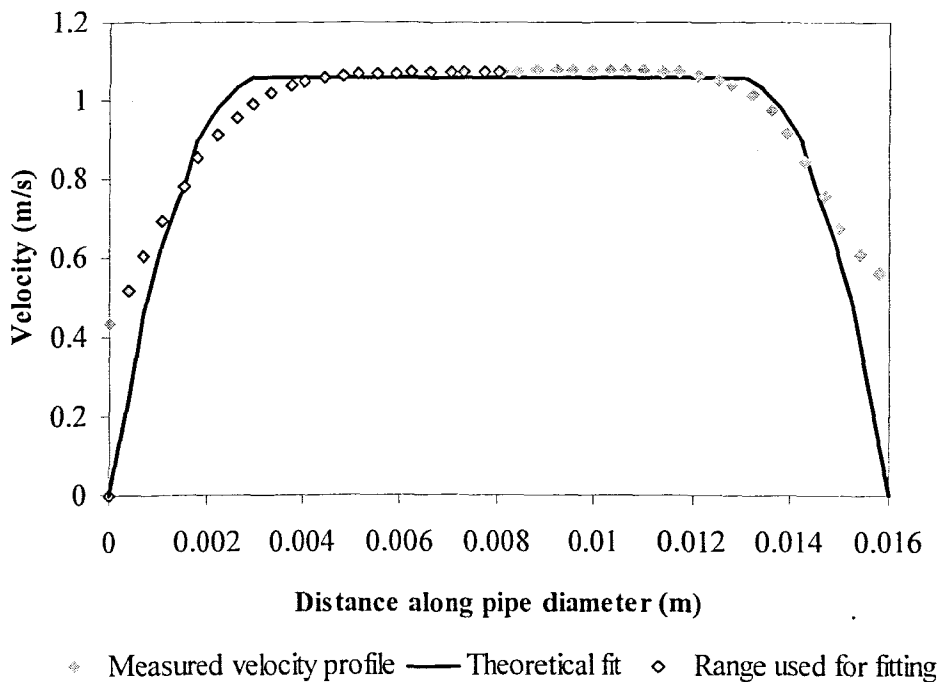


Figure 4.11: Experimental and theoretical velocity profile for bentonite 5.7 % w/w

The volumetric flow rate obtained from integration of the measured velocity profile equals 0.173 l/s and differs by 7.3 % when compared to the flow rate obtained from the mass-flow meter (0.160 l/s). UVP parameter settings and test conditions for the velocity profile measurement displayed in Figure 4.8 are shown in Tables 4.6 and 4.7.

**Table 4.6: UVP parameter settings for bentonite 5.7 % w/w**

PRF (kHz)	US Voltage (V)	Number of cycles/pulse	Number of US repetitions	Sound speed (m/s)
5.13	60	2	256	1560

**Table 4.7: Test conditions for bentonite 5.7 % w/w**

Reynolds number	Pressure drop (Pa)	Volume flow rate (l/s)	Slurry density (kg/m <sup>3</sup> )	Temperature (°C)
275	5712	0.160	1035	20.5

Bentonite suspensions showed little attenuation and absorption of ultrasonic energy and thus the acoustic energy could penetrate across the whole pipe diameter. Generally a good echo signal was obtained for all concentrations of bentonite. The spatial and time resolution could be optimised for accurate velocity profile measurements in concentrated bentonite suspensions. An average velocity profile was calculated from 512 profiles to minimise the standard deviation of the measurement and the total sampling time was approximately 36 ms.

Flow curves could not be measured at low shear rate ranges with the off-line rotational rheometer. The reason for this was the highly viscous structure of the bentonite mineral suspensions, as well as the influence of the high apparent yield stresses at low shear rates. Bentonite was tested off-line over a shear rate range of +/- 100 to 1000 s<sup>-1</sup>, using the rotational rheometer. Figure 4.12 shows a flow curve measured with the use of the off-line rheometer for bentonite 5.7 % w/w.

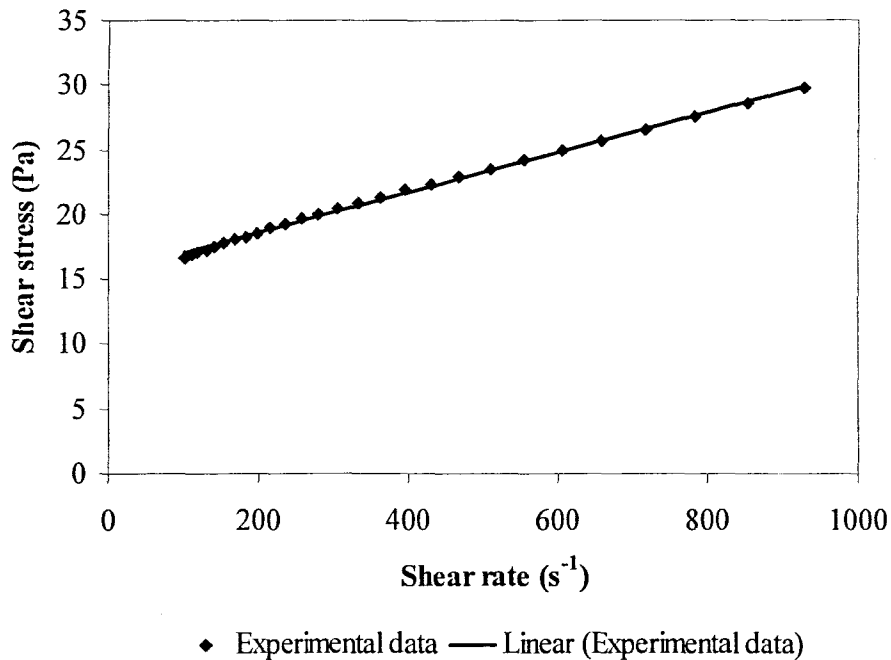


Figure 4.12: Flow curve measured by off-line rheometer for bentonite 5.7 % w/w

Experimental data of three different diameter pipes (9, 13 and 16 mm) measured by the pipe rig are shown in Figure 4.13. The raw pipe data indicate that no wall slip was present during the pipe tests. The final result after the Rabinowitsch-Mooney transformation is shown in Figure 4.14.

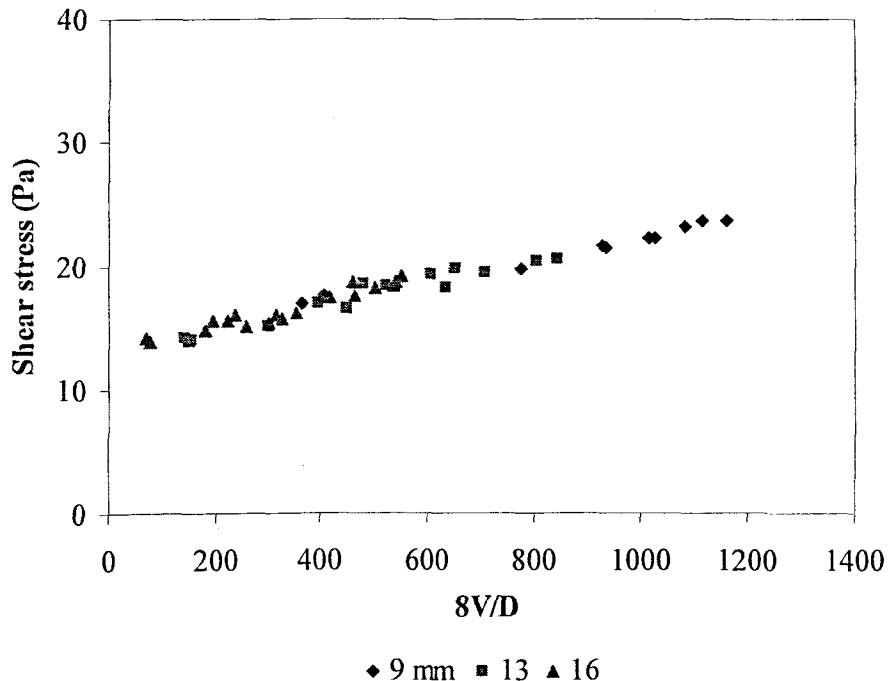


Figure 4.13: Pipe data measured by the tube viscometer for bentonite 5.7 % w/w

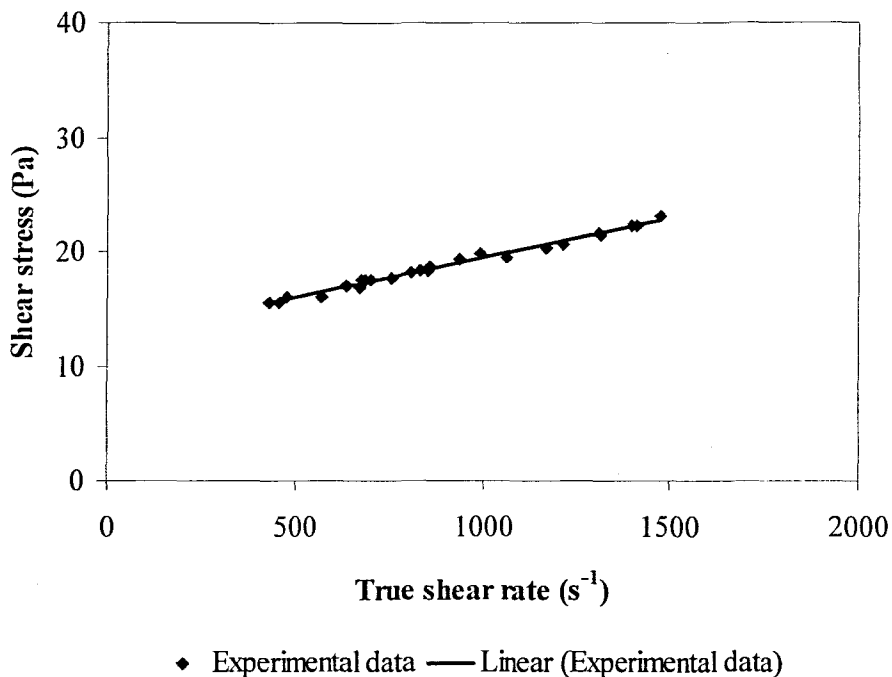


Figure 4.14: Flow curve measured by the tube viscometer for bentonite 5.7 % w/w

The end results or flow curves obtained from off-line conventional rheometry and in-line tube viscometry, as well as determined by the in-line UVP-PD rheometric method, are displayed in Figure 4.15. The error curves are  $\pm 15\%$  error deviations from the UVP-PD flow curve. Based on these error curves, results measured by the tube viscometer and off-line rheometer show a 15% agreement with the flow curve determined by the UVP-PD method. However, when the variation with shear rate in viscosity is observed for all measured flow curves (Figure 4.16), results show that apparent viscosities measured by the tube viscometer are  $\pm 20\%$  lower than apparent viscosities determined by the UVP-PD method. Also, when apparent viscosities measured with the tube viscometer are compared with results obtained by means of the off-line rheometer, results indicate a difference of approximately 30%. Here it must be noted that the structure of concentrated bentonite mineral suspensions change with the time of shearing. As mentioned before (see Section 2.2.3.2), the fluids under investigation in this work are classified as time-independent fluids to a certain degree. It is thus difficult to get the rheological structure of the bentonite suspensions to a steady state. For this reason, the off-line rheological characterisation does not correlate well with the in-line methods, due to the large differences in shearing times and shear rates between the pipe rig (pump) and conventional rheometer. In order to compensate for this problem, the bentonite samples were pre-sheared in the rheometer at the highest shear rate ( $1000\ s^{-1}$ ) for one minute, before a flow curve was measured.

The samples were pre-sheared in order to break down time dependent structures and to closely simulate the conditions of the in-line tests.

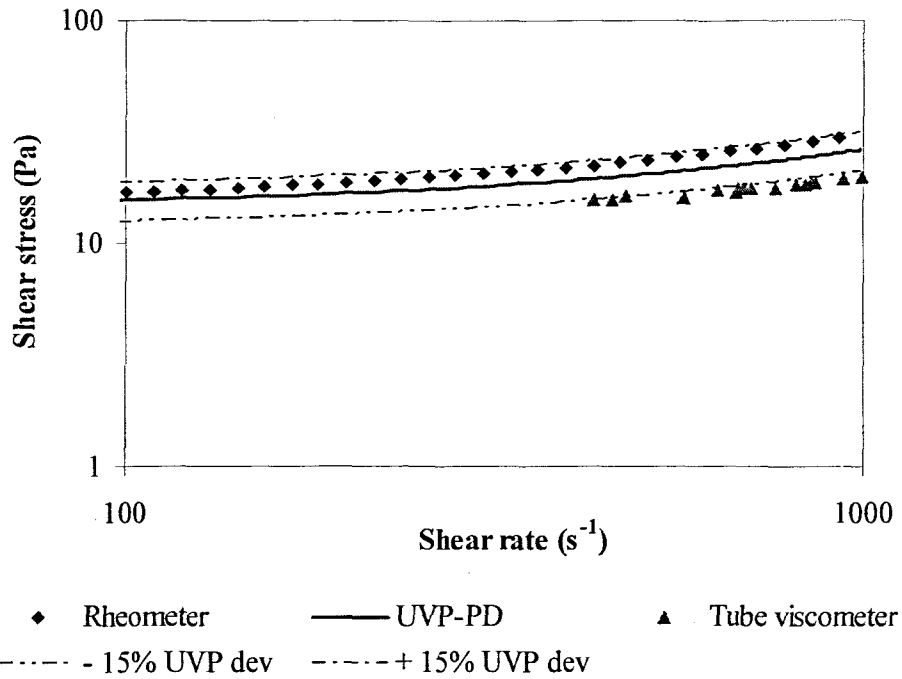


Figure 4.15: Bentonite 5.7 % w/w rheogram

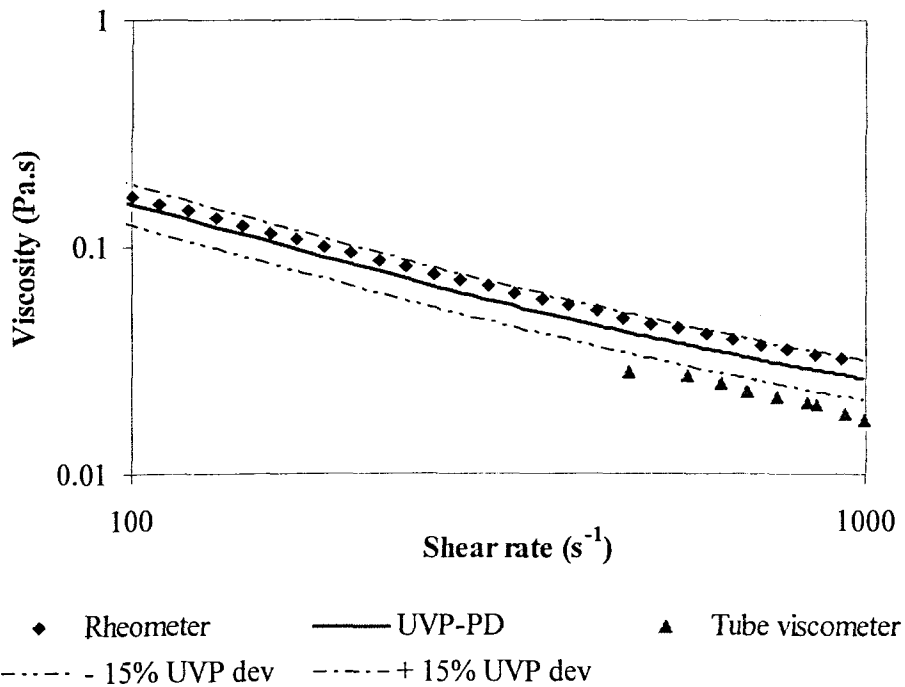


Figure 4.16: Variation with shear rate in viscosity for bentonite 5.7 % w/w

The rheological parameters ( $K$ ,  $n$  and  $\tau_y$ ) determined by two in-line and one off-line method are depicted in Table 4.8. When observing the fluid consistency coefficients, one can see that the rheometer yields a considerably higher value compared to results determined by the UVP-PD method and tube viscometer.

**Table 4.8: Rheological parameters obtained from three different methods for bentonite 5.7 % w/w**

Parameters	UVP-PD	Tube viscometry	Rotational rheometry
$K$ (Pa.s <sup><math>n</math></sup> )	0.012	0.0069	0.0156
$n$	1	1	1
$\tau_y$ (Pa)	14.28	12.52	15.45

Fluid behaviour index values were assumed to equal unity. The yield stress values obtained from all three methods were found to be in good agreement (+/- 20 %) when compared with each other.

### 4.3.2 Bentonite 6.5 % w/w

Figure 4.17 compares flow curves for bentonite 6.5 % w/w (density  $\rho = 1040 \text{ kg/m}^3$ ) measured by means of the in-line tube viscometer and off-line rheometer, as well as the UVP-PD method. The experimental and theoretical velocity profiles, test conditions, UVP parameter settings, off-line rheometric data and in-line pipe data are depicted in Appendix A. In this case the results measured by the in-line tube viscometer are in excellent agreement with the flow curve determined by the UVP-PD method. The results measured by the off-line conventional rheometer are within 15 % when compared to the flow curves obtained from the in-line UVP-PD method and tube viscometer.



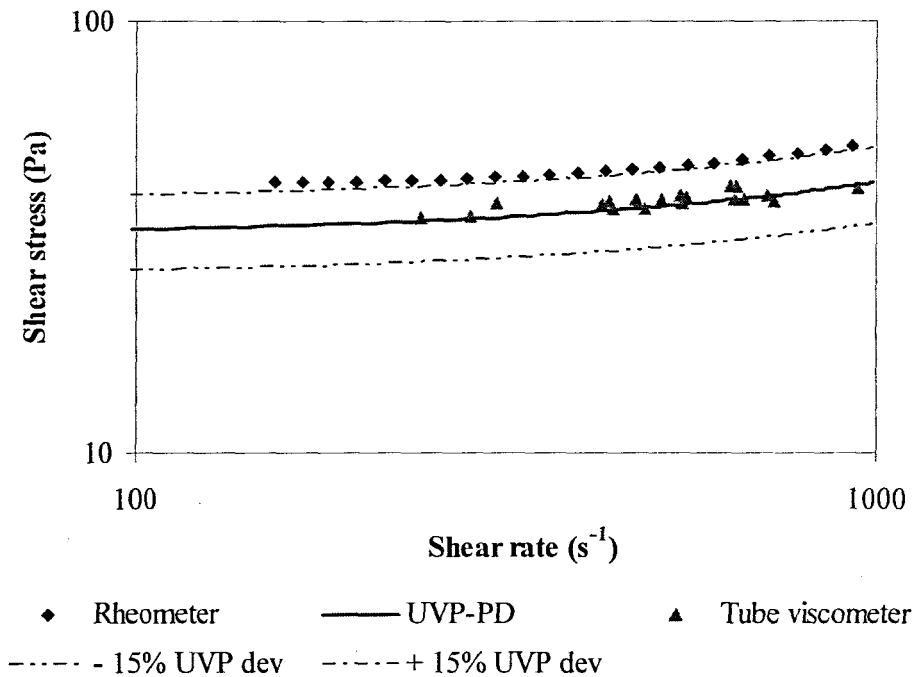


**Figure 4.17: Bentonite 6.5 % w/w rheogram**

As the concentration of the bentonite mineral suspensions increases it becomes increasingly difficult to obtain experimental data at low shear rates due to the increased viscosity and yield stress. As a result, accurate data could only be obtained from shear rates above  $153 \text{ s}^{-1}$  by using the conventional rheometer. Pipe data were measured from shear rates above  $242 \text{ s}^{-1}$ , due to pipe flow limitations.

Figure 4.18 shows the variation with shear rate in viscosity for the bentonite 6.5 % suspension. In this particular case, the viscosities obtained from all rheometric methods are in good agreement (within 15 %) over the total shear rate range.

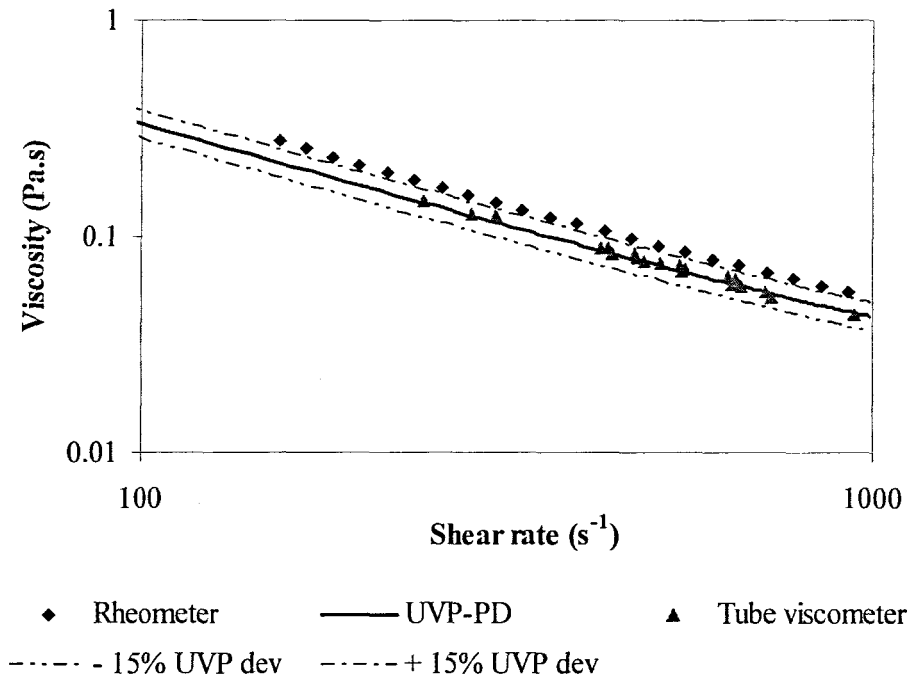


**Figure 4.18: Variation with shear rate in viscosity for bentonite 6.5 % w/w**

From Table 4.9 it can be observed that, once again, the fluid consistency index determined by the off-line rheometer is 30% higher than the value obtained by the tube viscometer.

**Table 4.9: Rheological parameters obtained from three different methods for bentonite 6.5 % w/w**

Parameters	UVP-PD	Tube viscometry	Rotational rheometry
$K$ (Pa.s <sup>n</sup> )	0.0105	0.0083	0.0121
$n$	1	1	1
$\tau_y$ (Pa)	31.91	34.09	39.87

Yield stress values were found to be in good agreement between the results obtained from the tube viscometer and the UVP-PD method. The rheometer measured a yield stress which was considerably higher than the values obtained from the previous two methods.

### 4.3.3 Bentonite 7 % w/w

Rheological results for bentonite 7 % w/w (density  $\rho = 1044 \text{ kg/m}^3$ ) are depicted in Figures 4.19 and 4.20. From Figure 4.19 it can be observed that results are in good agreement (within 15 %) with each other across the whole shear rate region (100 to 1000  $\text{s}^{-1}$ ). As previously mentioned, in Section 4.3.2, the increase in solids concentration and hence viscosity, makes it more difficult to measure apparent viscosities at low shear rates due to system limitations. The off-line rheometer measured flow curves from a minimum shear rate value of 167  $\text{s}^{-1}$ , which is higher than the minimum shear rate value (153  $\text{s}^{-1}$ ) for the bentonite 6.5% suspension, which indicates a more viscous mineral suspension.

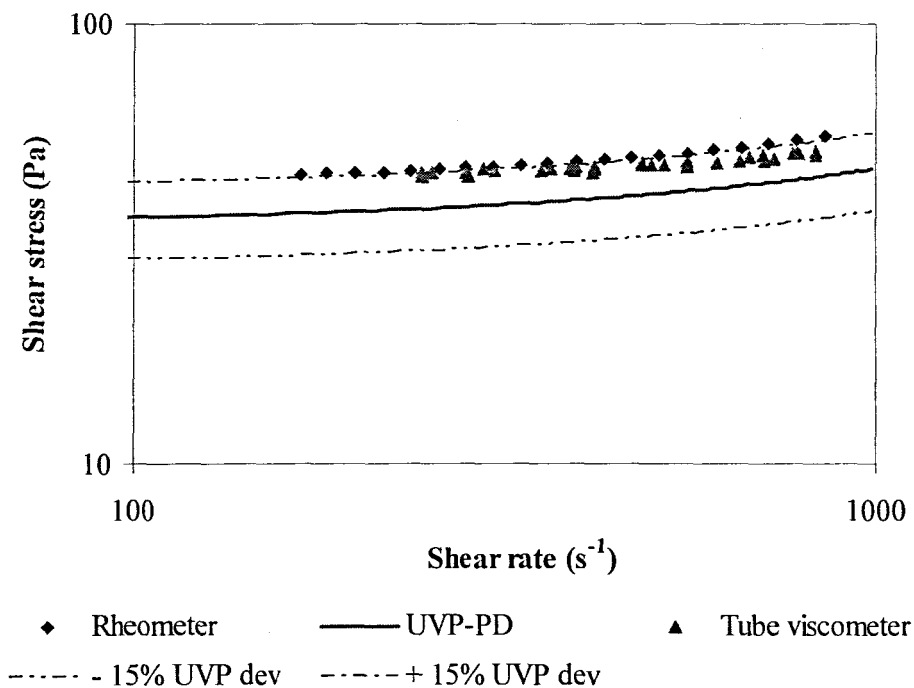
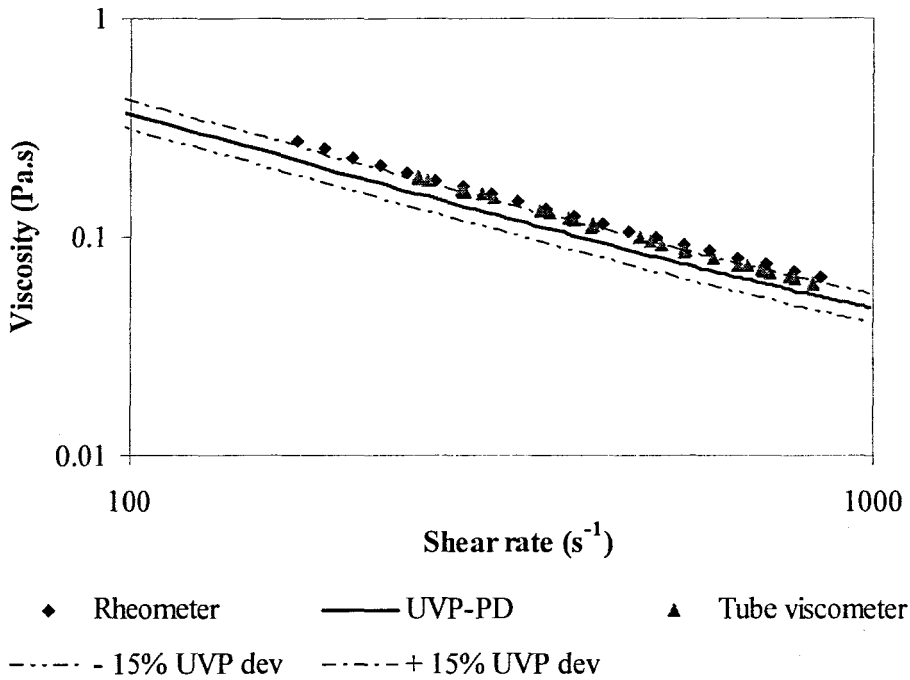


Figure 4.19: Bentonite 7 % w/w rheogram

The variation with shear rate in viscosity for the highly concentrated bentonite 7 % w/w mineral suspensions is shown in Figure 4.17.



**Figure 4.20: Variation with shear rate in viscosity for bentonite 7 % w/w**

In contrast to the previous results obtained from the tube viscometer and conventional rheometer, the apparent viscosities show good agreement when compared with each other over the shear rate range. The UVP-PD method shows lower apparent viscosities when compared to those determined from the other two rheological methods. However, results show a 15 % agreement when apparent viscosities obtained from all three methods, are compared.

The rheological parameters ( $K$ ,  $n$  and  $\tau_y$ ) determined by the three different rheological methods are shown in Table 4.10. When observing the fluid consistency coefficients one can see that the rheometer yields a considerably higher value compared to results determined by the tube viscometer. Although the consistency index determined by the UVP-PD method is closer to that of the rheometer, the calculated yield stress is 20 % lower than that determined by the rheometer and tube viscometer.

**Table 4.10: Rheological parameters obtained from three different methods for bentonite 7 % w/w**

Parameters	UVP-PD	Tube viscometry	Rotational rheometry
$K$ (Pa.s <sup>n</sup> )	0.0116	0.0089	0.0145
$n$	1	1	1
$\tau_y$ (Pa)	35.15	43.14	42.86

#### 4.3.4 Bentonite 7.5 % w/w (Pilot study)

Figure 4.21 shows flow curves measured by means of the off-line Paar Physica MCR300 rheometer as well as that determined by using the UVP-PD method. Tube viscometry was not available during the pilot study, thus only two methods are compared.

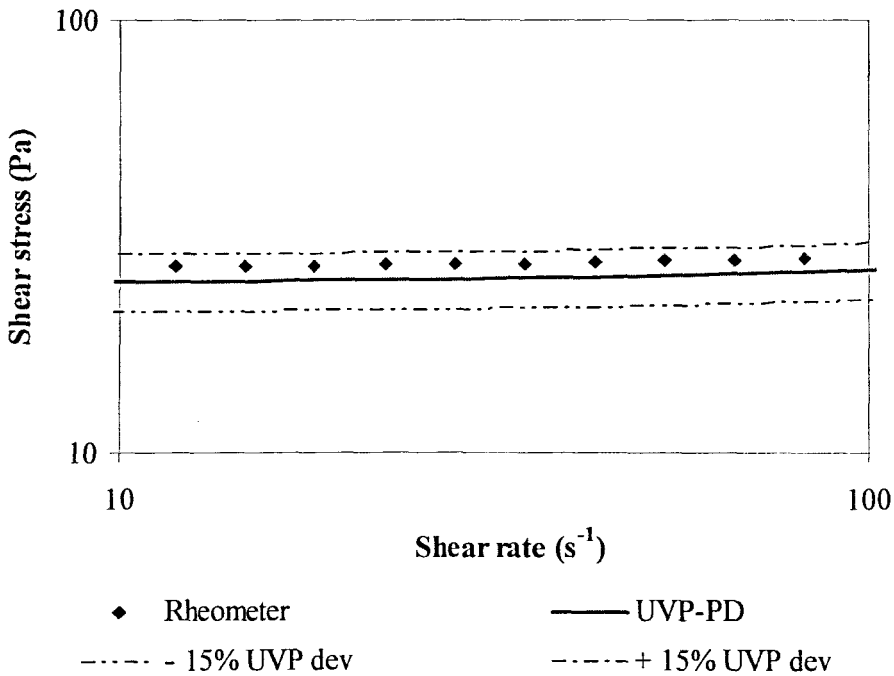
**Figure 4.21: Bentonite 7.5 % w/w rheogram**

Figure 4.22 shows the variation with shear rate in viscosity for the bentonite 7.5 % mineral suspension. It is clear, from observing the apparent viscosities determined by both methods, that the results show excellent agreement of less than 15 % compared with one another.

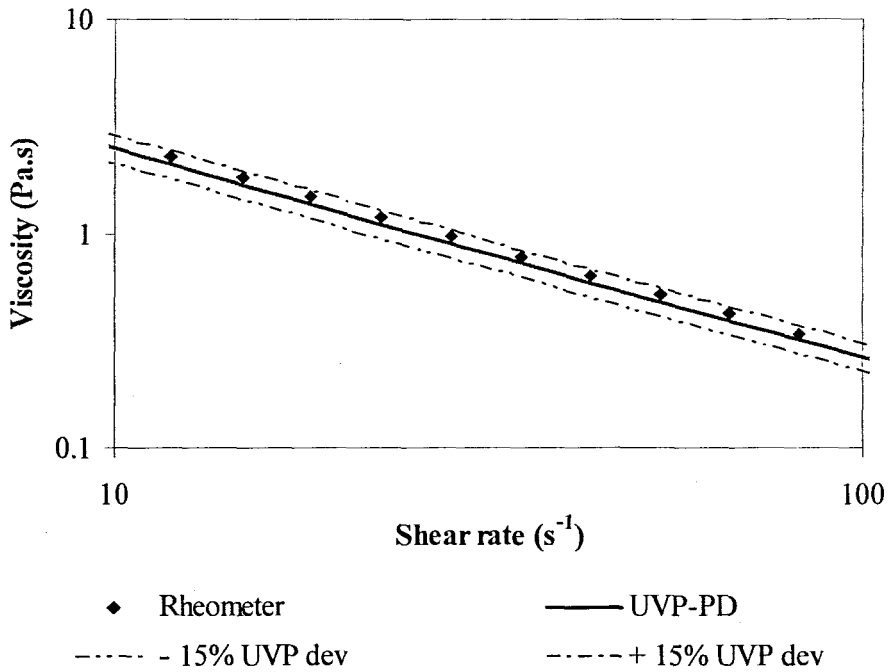


Figure 4.22: Variation with shear rate in viscosity for bentonite 7.5 % w/w

The mathematically determined rheological parameters are depicted in Table 4.11. The fluid consistency coefficients and estimated yield stress values are in good agreement with one another. In addition, the estimated yield stress values are significantly lower than the yield stress values of the previous bentonite concentration (6.5 %). The reason for this is that the bentonite powder used in ETH, Zurich is not the same as the bentonite used at the FPRC, and has different rheological properties for different amounts of solids in concentrations.

Table 4.11: Rheological parameters obtained from three different methods for bentonite 7.5 % w/w

Parameters	UVP-PD	Tube viscometry	Rotational rheometry
$K$ (Pa.s <sup>n</sup> )	0.167	n/a	0.0169
$n$	1	n/a	1
$\tau_y$ (Pa)	24.6	n/a	26.66

## 4.4 KAOLIN

Three different concentrations of highly concentrated kaolin suspensions were rheologically characterised. The kaolin mineral suspensions that were tested were 8.7 %, 10 % and 12 % v/v. Kaolin is a fluid that exhibits yield stress and is classified as a yield pseudoplastic (shear-thinning) fluid and thus the Herschel-Bulkley model (see Section 2.2.6.2) is used to rheologically characterise the kaolin mineral suspensions.

### 4.4.1 Kaolin 8.7 % v/v

An experimental (symbols) velocity profile along the pipe diameter for kaolin 8.7 % (density  $\rho = 1143 \text{ kg/m}^3$ , velocity of sound  $c = 1551 \text{ m/s}$ ) measured by the in-line UVP-PD method is shown in Figure 4.23. These are represented by the theoretical profile (curve) obtained by fitting the experimental data and pressure drop using the Herschel-Bulkley model (Equation 2.24) with the values of  $K$ ,  $n$  and  $\tau_y$  listed in Table 4.14. The flow is laminar since the value of the Reynolds number is equal to 1458 validating the use of theoretical Herschel-Bulkley models.

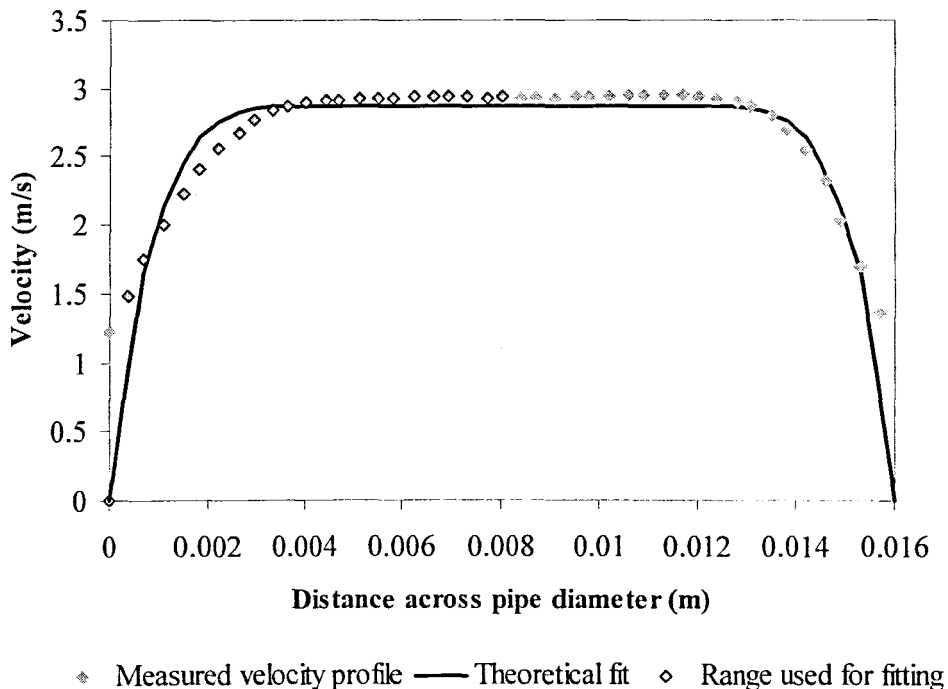


Figure 4.23: Experimental and theoretical velocity profile for kaolin 8.7 % v/v

The volumetric flow rate determined by the integration of the profile is equal to 0.455 l/s and differs by 8.2 % when compared to the flow rate measured by the mass-flow meter (0.421 l/s). Table 4.12 shows the UVP parameters selected for the velocity profile measurement in Figure 4.23. The test conditions are shown in Table 4.13.

**Table 4.12: UVP parameter settings for kaolin 8.7 % v/v**

PRF (kHz)	US Voltage (V)	Number of cycles/pulse	Number of US repetitions	Sound speed (m/s)
12.91	150	2	512	1551

Kaolin mineral suspensions attenuated the ultrasonic energy significantly more than when compared to bentonite suspensions and CMC solutions. The attenuation and absorption of US energy increased as the solids concentrations of the kaolin mineral suspensions increased. For this reason a compromise between spatial and time resolution had to be made. In this case it was decided to optimise the spatial resolution but at a loss of time resolution.

**Table 4.13: Test conditions for kaolin 8.7 % v/v**

Reynolds number	Pressure drop (Pa)	Volume flow rate (l/s)	Slurry density (kg/m <sup>3</sup> )	Temperature (°C)
1458	8080	0.421	1143	20.5

From Table 4.12 it is seen that the number of US repetitions was increased to 512 repetitions which increased the times between consecutive measured profiles, but due to increased signal strength the number of US cycles per emitted pulse could be kept to two cycles per pulse, thus keeping the spatial resolution at a maximum. The US input voltage for all kaolin suspensions was also set to the maximum value of 150 V in order to increase the signal strength and to minimise the effect of ultrasound attenuation and absorption.



The experimental data measured by the off-line conventional rheometer is displayed in Figure 4.24. Lower shear rates for measuring flow curves could be obtained by using the rheometer. Shear rate ranges of approximately 30 to 900  $\text{s}^{-1}$  were used for the off-line rheological characterisation.

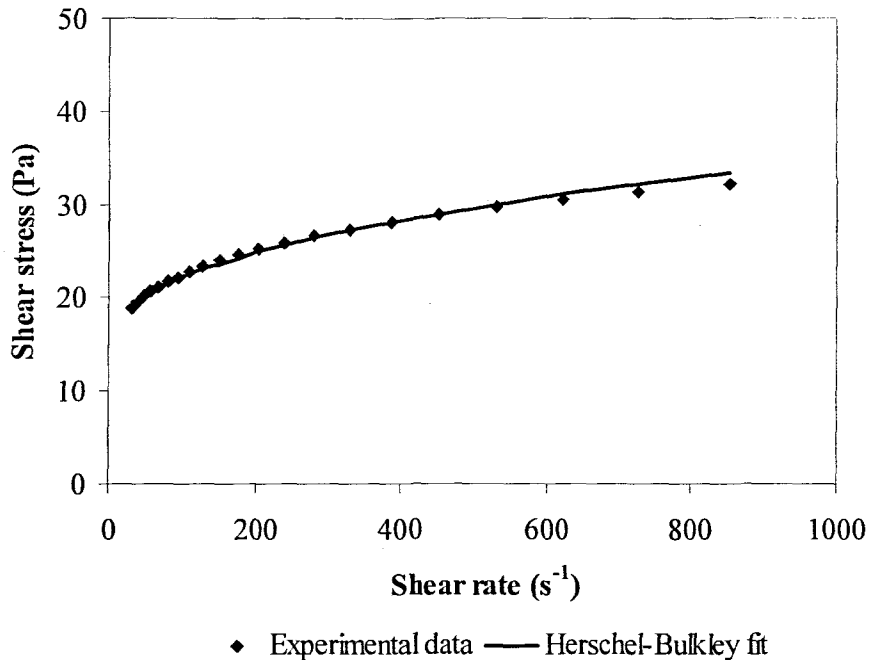


Figure 4.24: Flow curve measured by off-line rheometer for kaolin 8.7 % v/v

Pipe data for each different diameter pipe are shown in Figure 4.25. The pipe data were derived from pressure drop and volumetric flow rate measurements by the tube viscometer. Based on the results displayed in Figure 4.25, one can observe that no wall slip was present during in-line tube viscometer tests.

The calculated shear rate values ( $8V/D$ ) were not the true shear rate values and still needed to be converted by using the Rabinowitsch-Mooney transformation (Equation 2.11) procedure for pipe viscometer data. The result is illustrated on a rheogram in Figure 4.26.

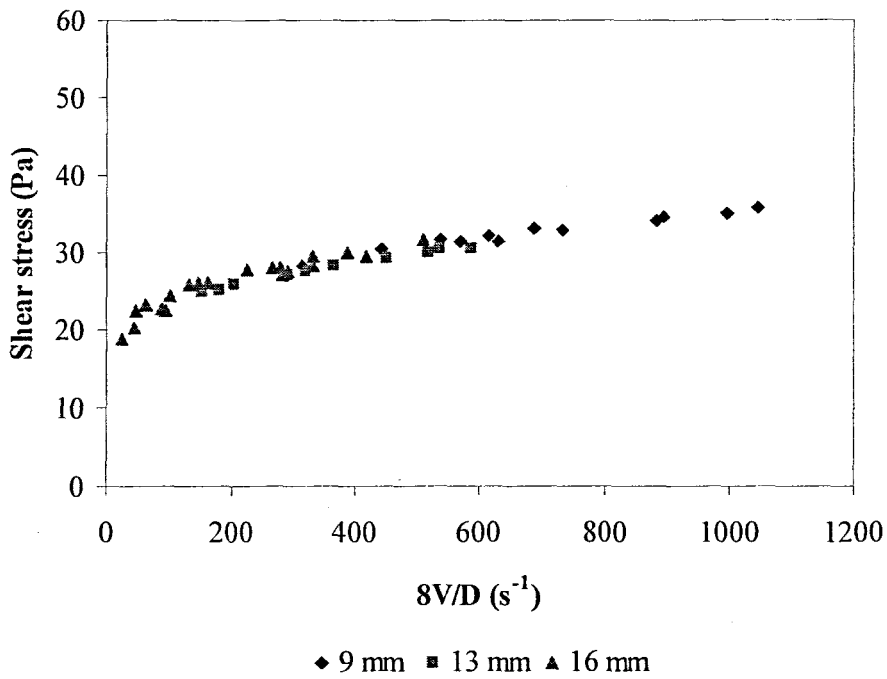


Figure 4.25: Pipe data measured by the tube viscometer for kaolin 8.7 % v/v

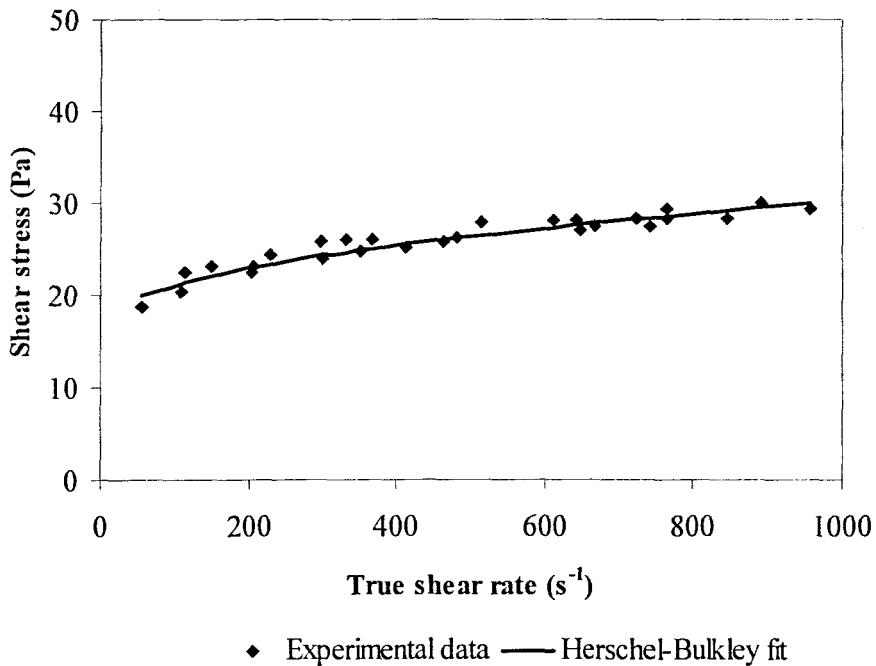


Figure 4.26: Flow curve measured by the tube viscometer for kaolin 8.7 % v/v

Figures 4.27 and 4.28 show the summary of rheological results obtained from off-line rheometry, tube viscometry and the UVP-PD rheometric method. Results are plotted on a rheogram in Figure 4.27 for comparison and the variation with shear rate in viscosity is shown in Figure 4.28. Experimental data obtained from the tube viscometer and off-line rheometer agree well with that determined by the in-line UVP-PD rheometric technique. The error curves illustrate a deviation of +/- 15 % from the flow curve determined by the in-line UVP-PD method. Based on this, it can be seen that flow curves obtained from the two in-line methods (UVP-PD method and tube viscometry) show excellent agreement (less than 10 %) when compared with one another.

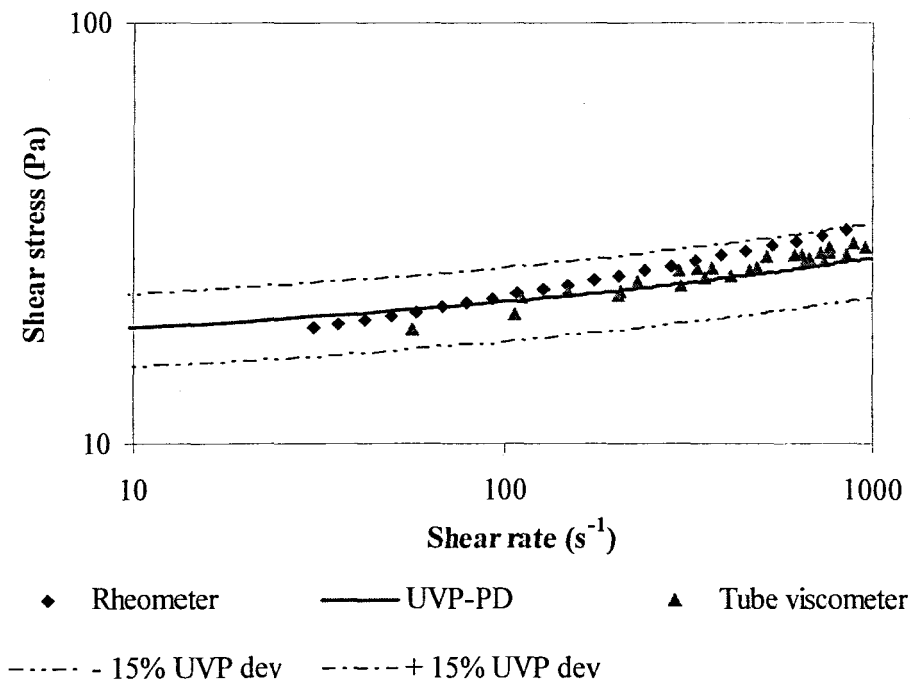
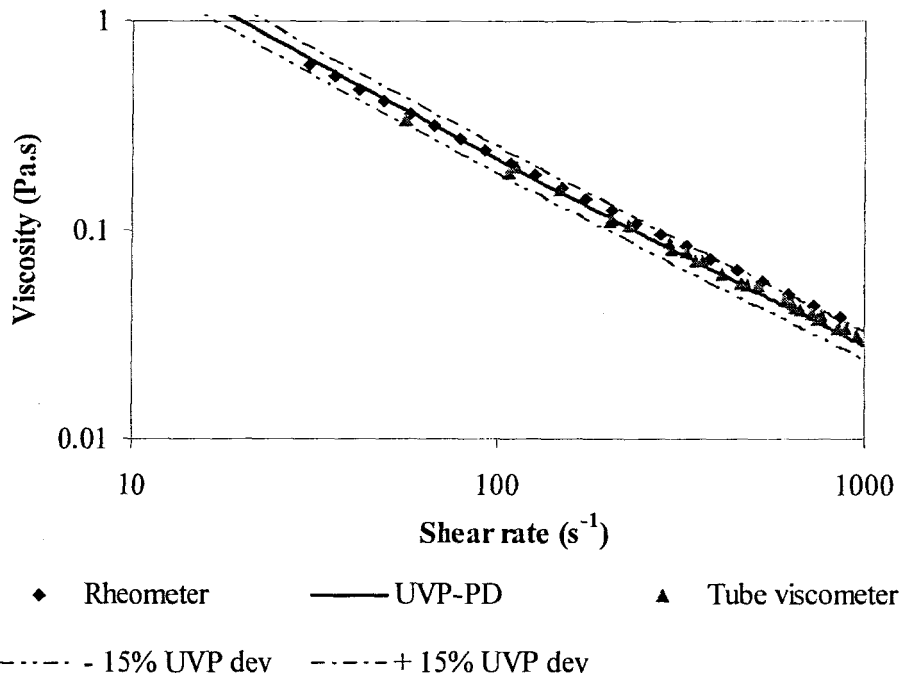


Figure 4.27: Kaolin 8.7 % v/v rheogram

The apparent viscosities obtained from all three rheological methods agree within 15% when compared with one another. The apparent viscosity decreases with increasing shear rate, indicating shear thinning behaviour.



**Figure 4.28: Variation with shear rate in viscosity for kaolin 8.7 % v/v**

Table 4.14 depicts the rheological parameters used to fit the Herschel-Bulkley model with experimental data. The estimated yield stress values show good agreement when results from all three methods are compared.

**Table 4.14: Rheological parameters obtained from three different methods for kaolin 8.7 % v/v**

Parameters	UVP-PD	Tube viscometry	Rotational rheometry
$K$ (Pa.s <sup>n</sup> )	1.36	0.57	0.93
$n$	0.31	0.46	0.44
$\tau_y$ (Pa)	16.16	16.41	15.21

#### 4.4.2 Kaolin 10 % v/v

Figure 4.29 compares flow curves for kaolin 10 % v/v (density  $\rho = 1166 \text{ kg/m}^3$ ) measured by the in-line tube viscometer and off-line rheometer, as well as by the UVP-PD method. The experimental and theoretical velocity profiles, test conditions, UVP parameter settings, off-line rheometric data and in-line pipe data are depicted in Appendix A. In this case the results measured by the in-line tube viscometer are in excellent agreement with the flow curve determined by the UVP-PD method, especially at the higher shear rates. The results measured by the off-line conventional rheometer are also within 10 % across the whole shear rate range when compared to the flow curves obtained from the in-line UVP-PD method and tube viscometer. At the lower shear rate region, the off-line results show very good agreement with results obtained from the in-line UVP-PD method.

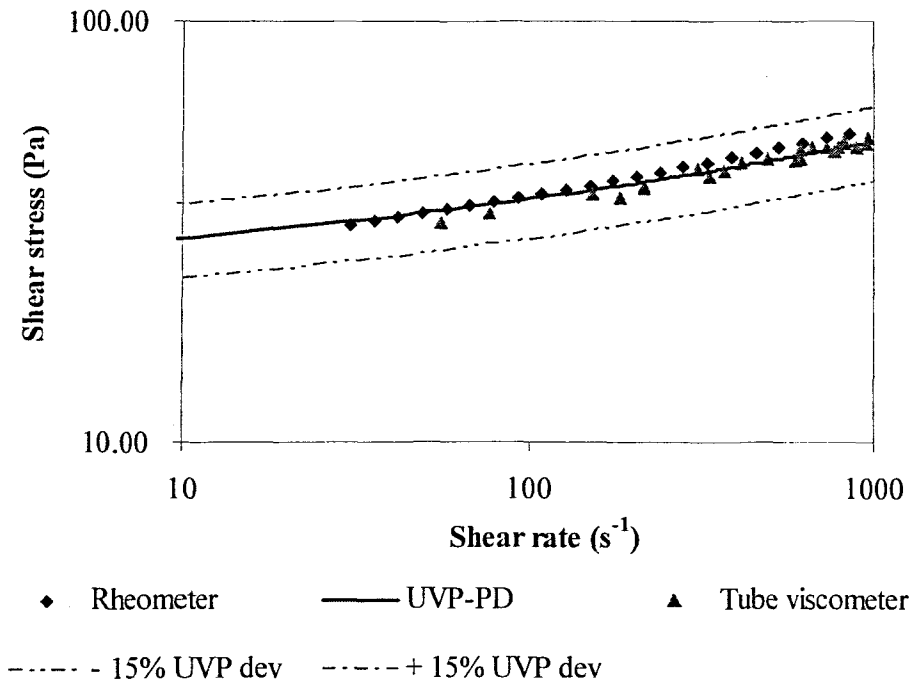
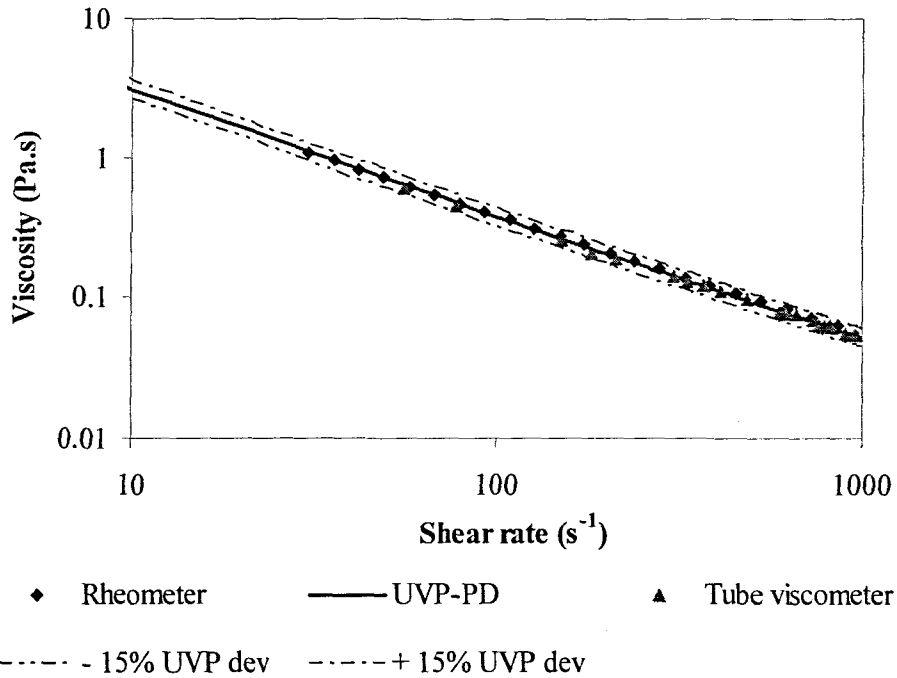


Figure 4.29: Kaolin 10 % v/v rheogram

Figure 4.30 shows the variation with shear rate in apparent viscosity for the kaolin 10 % v/v mineral suspension. Here it must be mentioned again that viscosities at low shear rates are obtained with difficulty with the use of the tube viscometer, due to system limitations.

The apparent viscosities determined by all three methods show good agreement over the total shear rate range. There is a decrease of less than one in order of magnitude in apparent viscosity for an increase of one order of magnitude in shear rate, illustrating shear thinning behaviour.



**Figure 4.30: Variation with shear rate in viscosity for kaolin 10 % v/v**

The rheological parameters determined by the Herschel-Bulkley model are shown in Table 4.15. According to these results, the estimated yield stress values determined by the conventional rheometer and tube viscometer are in good agreement, whereas the yield stress determined by the plug flow and pressure drop (UVP-PD method) is 20 % less than that of the previous two methods.

**Table 4.15: Rheological parameters obtained from three different methods for kaolin 10 % v/v**

Parameters	UVP-PD	Tube viscometry	Rotational rheometry
$K$ (Pa.s <sup>n</sup> )	4.21	0.90	1.32
$n$	0.28	0.48	0.46
$\tau_y$ (Pa)	22.73	28.57	27.54

### 4.4.3 Kaolin 12 % v/v

Rheological results for kaolin 12 % v/v (density  $\rho = 1198 \text{ kg/m}^3$ ) are schematically illustrated in Figures 4.31 and 4.32. From Figure 4.31 it can be observed that results are in good agreement (within 15 %) with each other across the whole shear rate region (100 to 1000  $\text{s}^{-1}$ ). As mentioned in the previous section, the increase in solids concentration and hence viscosity, makes it more difficult to measure apparent viscosities across low shear rates due to system limitations. Even at this high concentration, the off-line rheometer measured flow curves from a minimum shear rate value of 35  $\text{s}^{-1}$ . However, as the solids concentration of the kaolin mineral suspensions increases, it becomes more difficult to measure apparent viscosities at lower shear rates. Apparent viscosities were measured from a shear rate range of 128  $\text{s}^{-1}$ , using the in-line tube viscometer.

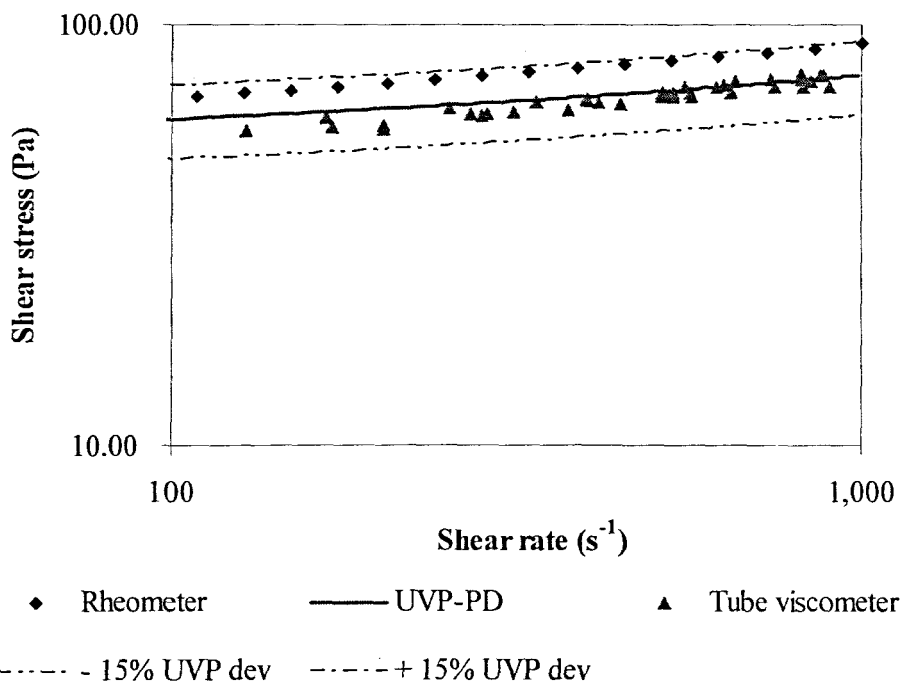
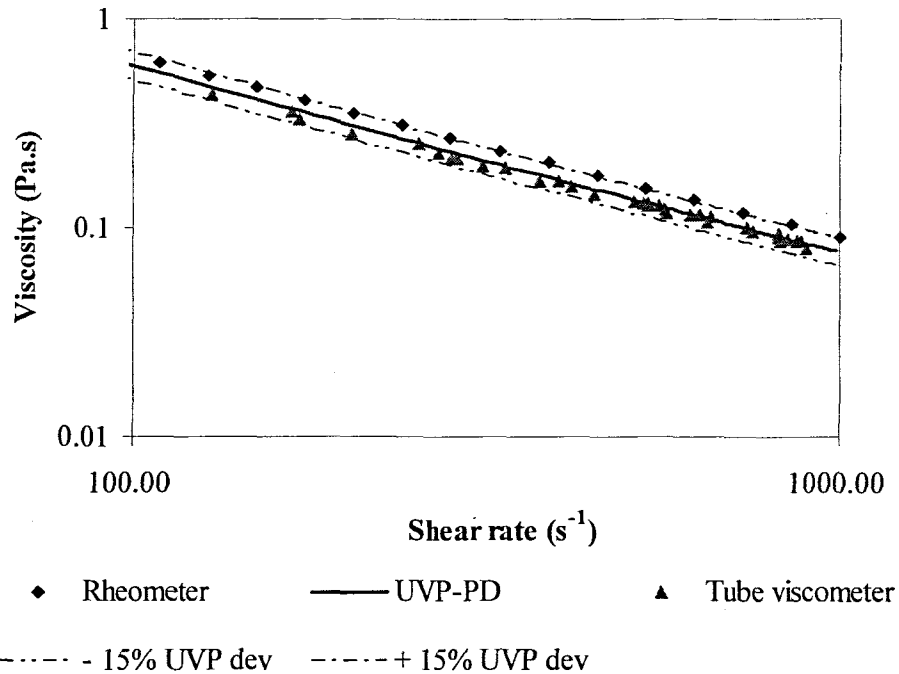


Figure 4.31: Kaolin 12 % v/v rheogram

From Figure 4.32 it can be seen that the apparent viscosities measured by the tube viscometer agree very well across the whole shear rate range with those determined by the in-line UVP-PD rheometric method.



**Figure 4.32: Variation with shear rate in viscosity for kaolin 12 % v/v**

The rheological parameters ( $K$ ,  $n$  and  $\tau_y$ ) determined by two in-line and one off-line method are depicted in Table 4.16. When observing the estimated yield stress values, one can see that the results obtained from all three rheological methods are in good agreement when compared to one another. Also, the high estimated yield stress value of the investigated fluid is an indication of the highly viscous structure of this highly concentrated mineral suspension.

**Table 4.16: Rheological parameters obtained from three different methods for kaolin 12 % v/v**

Parameters	UVP-PD	Tube viscometry	Rotational rheometry
$K$ (Pa.s <sup><math>n</math></sup> )	1.32	0.62	3.52
$n$	0.43	0.57	0.36
$\tau_y$ (Pa)	49.94	46.15	47.30



## 4.5 CONCLUSION

Highly concentrated non-Newtonian mineral suspensions were rheologically characterised using three distinct rheometrical methods, namely tube viscometry, off-line conventional rheometry and in-line UVP-PD rheometric method.

The capabilities of the UVP-PD technique for the rheological characterisation of different concentrations of non-Newtonian slurries have been evaluated. Results were compared with those obtained by off-line rheometry and in-line tube viscometry.

Concentrated Carboxymethyl Cellulose (CMC) solutions have been tested and rheological results determined by the UVP-PD method agreed well within 15 % with results measured by the tube viscometer and conventional rheometer.

Various concentrations of bentonite mineral suspensions have been rheologically characterised, using two in-line methods and one off-line method. Results obtained from all three methods showed a 15 % agreement when compared over the total shear rate range. Bentonite concentrations tended to be very viscous, especially when rheologically characterised using the tube viscometer. The degree of time dependence of the concentrated bentonite mineral suspensions influenced the off-line rheometric results.

Rheological results obtained from all three methods for kaolin mineral suspensions agreed well over the shear rate range. In comparison ultrasonic energy was seen to have attenuated significantly more than the attenuation in bentonite suspensions and CMC solutions. However, velocity profiles required for calculation of rheological parameters could still be measured in the highest concentration of kaolin (12 % v/v).

The limitations of the UVP-PD rheometric system, conventional rheometer and tube viscometer are discussed in the next chapter.

This method, if used in combination with a pressure difference technique (PD), has been found to have significant potential for the development of new in-line rheometers for process control within the mining and minerals industry.

# **CHAPTER FIVE**

**SUMMARY,  
CONTRIBUTIONS,  
RECOMMENDATIONS  
AND  
CONCLUSIONS**

## CHAPTER FIVE

# SUMMARY, CONTRIBUTIONS, RECOMMENDATIONS AND CONCLUSIONS

### 5.1 INTRODUCTION

This thesis reports on an investigation into the rheological characterisation of highly concentrated mineral suspensions using a Pulsed Echo Doppler Velocity Profile technique (UVP) in combination with a differential pressure (PD).

Rheological parameters were determined by the UVP-PD method for all non-Newtonian slurries that included pseudoplastic, yield pseudoplastic and Bingham fluids.

Results obtained with the use of the UVP-PD method were compared to results determined by one in-line method, tube viscometry, and one off-line method, conventional rotary rheometry.

It was found that the apparent viscosities obtained with the use of the three methods showed 15% agreement when compared over the measured shear rate range.

The capabilities and limitations of the UVP-PD technique for rheological characterisation of different concentrations of non-transparent, non-Newtonian slurries were evaluated.

### 5.2 SUMMARY

The rheological behaviour of non-Newtonian, highly concentrated and non-transparent fluids used in industry have so far been analysed using commercially available instruments, such as conventional rotational rheometers and tube viscometers. When dealing with the prediction of non-Newtonian flows in pipes, pipe fittings and open channels, most of the models that are used are empirical in nature (Haldenwang *et al.*, 2006).

Knowledge of the rheological parameters of the slurries is essential for mines and tailing facilities to control processes. If a change in the rheology of the slurries being transported could be observed instantaneously, pipe blockages and other problematic situations could be prevented. However, obtaining the rheology of these mining tailings is complex and in-line rheometers would therefore be of great assistance to the mining industry.

The aim of this research was to evaluate the capabilities of the UVP-PD technique for rheological characterisation of different concentrations of non-transparent, highly concentrated non-Newtonian slurries.

Takeda (1986, 1995 & 1999) developed a new ultrasonic velocity profile method for mechanical measurements of fluids in physics and engineering. It uses pulsed ultrasonic echography together with the detection of the instantaneous Doppler shift frequency. This method was originally developed in medical engineering to measure blood flow by means of Doppler sonography during the 1960s (Kuttruff, 1991).

The UVP-PD set-up and method was developed in Erlangen, Germany by Steger (1994) and Muller (1997 & 1998). This concept is based on the Ultrasound Pulsed Echo Doppler Velocity Profile technique (UVP), in combination with a pressure difference method (PD). Ouriev (2000) further developed the in-line ultrasound-based rheometer, which was further modified and optimised by Wiklund (2007) and Birkhofer (2007).

Brunn *et al.* (1993) had already introduced three different types of rheometers, two optical instruments and a new acoustical rheometer based on the UVP-PD method. Flow curves of aqueous hydroxylpropyl guar solutions and aqueous polyacrylamide solutions at different concentrations were obtained.

Müller *et al.* (1997) subsequently carried out experiments using a modified DOP1000 instrument from Signal Processing SA. A 4000-ppm aqueous Polyacrylamide (PAAm) solution with very strong non-Newtonian behaviour, as well as an 8000-ppm aqueous polymer solution based on Hydroxylpropyl guar gum (HPG), was studied.

Ouriev *et al.* (1999 & 2000) tested the UVP-PD method for in-line measurements in a pilot plant process. The measuring system was installed as part of a section of the transporting pipe in a fat crystallisation process.

Local viscosity was obtained at different flow rates of xanthan gum solutions with concentrations of 0.6 and 1.0 kg/m<sup>3</sup> at in a circulating flow system by Köseli *et al.* (2006). Earlier, Dogan *et al.* (2003) had compared results from in-line measurements of 0.35 % xanthan gum solutions with a conventional off-line rotational rheometer.

Ouriev and Windhab (2002 & 2003) meanwhile performed in-line measurements of shear-thinning suspensions in an experimental flow loop using the UVP-PD method. In addition, Ouriev performed in-line measurements of concentrated shear-thickening suspensions in the same experimental flow loop. The investigated dilatant suspensions consisted of cornstarch particles 10 – 40 % by weight, suspended in two different glucose syrup-water matrices.

Wiklund *et al.* (2001) performed experiments using the same experimental flow loop as Ouriev. The fluids consisted of cornstarch particles 10 – 30 % by weight suspended in a glucose syrup-water matrix (50 % by weight).

Birkhofer *et al.* (2004 & 2006) investigated the response of a cocoa butter fat shear crystallisation process to a step change in flow rate and temperature, by using the ultrasound Doppler method.

Wiklund *et al.* (2001 & 2002) evaluated the UVP-PD method on non-transparent, shear thinning, viscoelastic, multiphase surfactant solutions (shampoo), over a wide range of flow rates. Numerous in-line measurements of highly concentrated aqueous cellulose fibre suspensions flowing through an experimental flow loop using the UVP-PD method over a wide range of flow rates were also performed by Wiklund *et al.* (2001 & 2002).

In another project, Wiklund *et al.* (2004 & 2005) undertook a comparative study with UVP and Laser Doppler Anemometry (LDA) techniques for highly concentrated pulp suspensions. Wiklund and Stading (2004) carried out in-line rheological measurements in a highly concentrated pulp suspension of 7.8 % (w/w).

Choi *et al.* (2002) examined the UVP-PD method by measuring the viscosity of tomato juice at different flow rates and comparing these with results obtained from Magnetic Resonance Imaging (MRI) measurements.

In-line rheological measurements on diced tomato suspensions using the UVP-PD method were performed by Dogan *et al.* (2002 & 2006).

Wiklund and Stading (2006) tested various industrial food suspensions using the UVP-PD method. Food suspensions included rapeseed oil, tomato sauce, syrup and starch particles, strawberry yogurt, fruit jams, marmalades, pasta sauce, cheese sauce and vegetables sauces.

As far as can be ascertained, the Ultrasonic Velocity Profile with Pressure Difference (UVP-PD) method has not been used to measure velocity profiles and rheological parameters of mineral suspensions such as mining tailings.

For this research work a unique pipe viscometer was designed and constructed. It consisted of four pipes, one of stainless steel and three of PVC, linked to an in-line mass-flow meter and equipped with two different ranges of pressure transducers on each pipe. The stainless steel pipe, with an inner diameter of 16 mm, was equipped with a specially designed flow adapter for in-line rheological characterisation using the UVP-PD method. The three PVC pipes with different diameters of 9 mm, 13 mm and 16 mm served as a tube viscometer for in-line rheological characterisation of mineral suspensions. Test procedures were developed to determine rheological parameters and flow data for three different fluids with concentrations from 5 % - 12 %, slurry relative densities of 1.03 - 1.198, and flows from 0.07 to 0.50 l/s.

The test facility was used to evaluate the UVP-PD method by comparing results with those obtained from tube viscometry and off-line rotational rheometry.

It was found that some fluids influenced velocity profile measurements due to ultrasound attenuation and absorption, while other fluids influenced tube viscometer and off-line rheometric measurements due to high viscosities and flow limitations in the system.

The results obtained in using all three rheometric methods showed good agreement when compared over the shear rate range used for measuring rheological parameters.

### 5.3 CONTRIBUTIONS

Although the UVP-PD method has already been developed and heavily optimised by previous authors, the following contributions towards the research goals of the FPRC and mining industry can be made:

- A new method for rheological characterisation of highly concentrated mineral suspensions has been tested and evaluated. The UVP-PD rheometric method was found to be a viable method to accomplish in-line rheometry of complex non-Newtonian fluids.
- Important acoustic information such as in-line and off-line velocity of sound measurements, acoustic penetration depths and temporal behaviours of different concentrations of mineral suspensions were compiled into a database for future research.
- Software was developed for post data analysis (interpolation of data, volumetric flow rate calculation by integration, etc.) and calculation of rheological parameters from velocity profile measurements.

### 5.4 LIMITATIONS

The main limitations found in this work were due to ultrasound attenuation and high apparent fluid viscosities.

- Velocity profile and sound speed measurements

Ultrasound energy could penetrate across the entire pipe diameter (16 mm) in highly concentrated bentonite suspensions as well as CMC solutions. Kaolin mineral suspensions attenuated the ultrasound energy significantly more than CMC and bentonite. It was found that, for a 4 MHz transducer, the ultrasonic beam could penetrate 8 mm in kaolin 12 % v/v, excluding the near-field distance. In larger diameter pipes this would cause velocity distribution problems and thus affect rheological characterisation of suspensions. In such a case, a lower emitting frequency (e.g. 2 MHz), which is less susceptible to attenuation, should be selected. If spatial resolution is important it might be possible to extrapolate data, such as plug flows in profiles, in order to determine rheological parameters. Further investigation is required for such methods. The attenuation of the ultrasound increases with solids concentration and higher concentrations of more than 12 % v/v would therefore definitely require ultrasound transducers with lower emission frequencies. Velocity of sound measurements are also influenced due to the larger distance across which the ultrasonic signal has to travel in order to reach the opposite transducer. However, in the case of the kaolin suspensions, there was still enough signal quality and parameters such as amplification gain and input voltage could also be optimised to increase signal strength.

- Pipe flow

The main limitations of the tube viscometer involved the flow rate and absolute pressure measurements. For CMC solutions, low flow rates were possible (0.05 l/s) but pressure readings at these low flow rates unfortunately were inaccurate due to the low pressures. However, due to the high yield stress and apparent viscosity, high pressures were present for bentonite and kaolin suspensions, but it was impossible to maintain constant low flow rates in pipes with small diameters such as the 9 -16 mm pipes. The lowest true shear rates obtained for measuring flow curves in the tube viscometer were therefore in the order of  $50 \text{ s}^{-1}$  (CMC),  $240 \text{ s}^{-1}$  (bentonite) and  $70 \text{ s}^{-1}$  (kaolin).



- Off-line rheometry

As mentioned in Chapter 4, apparent viscosities of concentrated CMC solutions could be measured using the off-line rheometer at low shear rates. This was not the case for the bentonite and kaolin suspensions. The reason for this involved the particular degree of time-dependence and the large yield stresses of the concentrated mineral suspensions. Accurate flow curves for bentonite suspensions could be measured from shear rates of approximately  $100 \text{ s}^{-1}$ , whereas lower shear rates of  $\pm 30 \text{ s}^{-1}$  could be obtained for kaolin suspensions.

## 5.5 RECOMMENDATIONS FOR FUTURE RESEARCH

The following aspects should be investigated for future research.

- Flow adapter and ultrasound transducer design

As mentioned in Chapter 4, the cavity in front of the transducer influences the measurement of the velocity profile due to the increase of velocity before the actual pipe wall interface. A stainless steel pipe with inner diameter of 16 mm was used in this project. On the basis of the ratio of diameters between the cavity and pipe, it is recommended that a pipe with a larger diameter (such as 23 mm) be used to minimise the effect of the cavity ahead of the ultrasound transducer.

This problem could also be reduced by the introduction of new ultrasound transducers incorporating a delay line. The delay line is a material optimised for beam forming that contains the near field distance. This delay line should be fixed ahead of the transducer and in flush with the pipe wall, thus making it possible to have the focal point of the ultrasound beam at the wall interface. This technology will minimise the divergence angle and the precision of velocity profile and wall shear rate measurements would be increased. A transducer of this kind is currently under development (Birkhofer *et al.* 2006 & 2007, Wiklund, 2007). In addition, the experimental problem of sedimentation and clogging of the cavities ahead of the transducers, as found by Birkhofer *et al.* (2007) and Wiklund (2007), would be solved.

- Demodulated Echo Amplitude (DMEA) monitoring

As explained by Birkhofer (2007) and Wiklund (2007), the direct access to demodulated echo amplitude (DMEA) data or ‘raw data’ allows for several advantages during velocity profile measurements. Direct access to DMEA data moreover provides the option of implementing alternative algorithms for velocity estimation. Several advantages were found, such as increased control of signal quality and gain amplification levels, detection of signal artifacts and DC-offset correction, detection and correction of aliasing phenomena and monitoring the influence of a stationary noise signal on the velocity spectrum. The Active X library driver and custom firmware provided by Met-Flow SA could be used to implement the DMEA data with MATLAB® software.

- Pipe wall detection

As shown by Birkhofer *et al.* (2007) and Wiklund *et al.* (2007), and also in Chapter 3, the power-law fitted rheological parameters are sensitive to the estimated pipe wall position measured from the front of the ultrasound transducer. Methods for wall detection based on cross-correlation and singular value decomposition (SVD) were successfully developed and implemented by Wiklund *et al.* (2007). Accuracy in determining the position of the pipe wall interface is within one measurement volume, i.e. with a resolution approaching the wavelength of the ultrasound beam. The methods and results are presented in detail in Wiklund *et al.* (2007). This problem can also be reduced by the introduction of new ultrasound transducers, as described earlier (Wiklund, 2007).

- Data enhancement and analysis

Smoothing filters and methods for data enhancement were implemented in order to reduce the effects of correlated and uncorrelated noise. Sources of noise may include the electronic filters in the UPV hardware, measurement geometry used, noise due to fluid characteristics and electromagnetic noise from apparatus used in the laboratory. Results reported by Wiklund *et al.* (2007) show that UVP data can be significantly improved by the implementation of different kinds of filters. However, one must be prudent when applying filters as they can introduce artifacts and modify the original data (Wiklund, 2007).

- Wall shear stress measurements

It was found that the pressure difference measurement is very important due to the sensitivity of this parameter when calculating the fluid consistency index of mineral suspensions. Thus highly accurate pressure transducers must be used for absolute pressure measurements. During this research two different pressure sensors with ranges 0 - 1 bar and 0 - 10 bar were used. It is recommended to use pressure sensors with lower ranges at the low flow rates (e.g. 0 - 0.5 bar), especially when dealing with yield stress measurements in tube viscometry. For the higher flow rates it was found that pressures did not exceed more than 2.5 bar and thus transducers with a range of 0 - 3 bar should be installed. These modifications should reduce the combined error in wall shear stress measurements. Another option would be to introduce a pipe with a larger diameter (e.g. 28 mm) to the pipe viscometer. This would allow larger point pressures, thus more accurate and lower flow rates could be possible for higher concentrations of mineral suspensions, and the limitations of the pipe rig could be reduced.

## 5.6 CONCLUSIONS

The following final conclusions can be made:

- Validation

The agreement between the UVP-PD method, tube viscometry and conventional rheometry was good for all the highly concentrated mineral suspensions investigated over a given range of shear rates. The quality of the agreement between flow curves measured in-line and off-line was highly sensitive to the estimated position of the pipe wall interface. As described earlier, a new type of transducer which is currently under development is required to overcome this problem (Birkhofer, 2007; Wiklund, 2007). The accuracy of the pressure measurement is important as the calculation of the fluid consistency index is very sensitive to the differential pressure parameter. In order to make the most accurate comparison between the three different rheometric methods, the range of shear rates as well as the distribution of the data over this range ideally should be equal. It was shown that the present UVP-PD system with a method for measuring sound velocity in-line has a significant advantage as erroneous velocity of sound values may result in inaccurate velocity profiles and, thus, in incorrect rheological parameters.

- Application

The UVP-PD rheometric method can be used effectively for in-line rheological characterisation of highly concentrated mineral suspensions. The velocity distribution could generally be determined across the entire pipe diameter in concentrations up to 12 % v/v. Measurements of instantaneous velocity profiles and rheological parameters, such as the yield stress, can be made in concentrated kaolin suspensions of up to 12 % v/v inside a pipe with inner diameter 16 mm, due to ultrasonic attenuation and absorption. The main advantage of the in-line UVP-PD rheometric method is its applicability for flow behaviour characterisation of non-transparent and highly concentrated suspensions, while the process conditions (i.e. volumetric flow rate, absolute pressure and temperature) are kept constant. This technique is expected to find several applications in many different branches of the mining industry.

The work presented in this thesis, as previously mentioned, is new within the mineral industry and more work is needed in order to improve the in-line rheometric method for future industrial applications.

## 5.7 FUTURE OUTLOOK

Ultrasonic velocity profiling (UVP) techniques have significant advantages over conventional techniques, such as application to opaque liquids, instantaneous spatiotemporal information, i.e. a velocity field as function of time and space, the possibility to perform flow-mapping and non-invasive measurements.

New avenues of research have opened, namely:

- In-line measurement of rheology.
- Flow profiles in flumes of different cross-sectional shapes.
- Flow profiles of developing flow through fittings (currently under investigation).
- Flow over weirs and notches.
- Flow profiles of transitional and turbulent flow in above configurations.

The in-line velocity of sound measurement and attenuation of transmitted ultrasound can be used as an important parameter to measure the concentration of solids in-line. The results of such measurements in-line can also be further maximised by correlating it to particle sizes and particle distributions. Based on previous literature and work, the UVP-PD method has proved to be a highly versatile system and can be used in several industrial applications.

---

## REFERENCES

- Al-Zaharah, I., Yilbas, B.S. & Hashmi, M.S.J. 2001. Pulsating flow in circular pipes – the analysis of thermal stresses. *International Journal of Pressure Vessels and Piping*, Dhahran, Saudi Arabia. 78:567-579.
- Barr, G. 1931. *A Monograph of Viscometry*. Oxford, Great Britain: Oxford University Press.
- Bechtold, J. 2006. *Jill Bechtold's home page: Department of Astronomy, University of Arizona*. [http://boojum.as.arizona.edu/~jill/NS102\\_2006/Lectures/Lecture12/turbulent.html](http://boojum.as.arizona.edu/~jill/NS102_2006/Lectures/Lecture12/turbulent.html) [14 November 2006].
- Birkhofer, B., Shaik, J.A.K., Ouriev, B. & Windhab, E.J. 2004. In-Line Characterization and Rheometry of concentrated suspensions using ultrasound. *Proceedings of the 4<sup>th</sup> International Symposium on Ultrasonic Doppler Methods for Fluid Mech and Fluid Eng*, Sapporo, Japan, 6-8 September 2004. ISUD4:65-68.
- Birkhofer, B. H., Shaik, J. A. K., Ouriev, B. & Windhab, E. J. 2006. Monitoring of fat crystallization process using UVP-PD technique. *Proceedings of the 5<sup>th</sup> International Symposium on Ultrasonic Doppler Methods for Fluid Mech and Fluid Eng*, Zurich, Switzerland, 12-14 September 2006. ISUD5:149-153.
- Birkhofer, B. H. 2007. *Ultrasonic In-Line Characterization of Suspensions*. Laboratory of Food Process Engineering, Institute of Food Science and Nutrition, Swiss Federal Institute of Technology (ETH), Zurich, Switzerland. ISBN 978-3-905609-34-7.
- Birkhofer, B.H., Wiklund, J.A., Stading, M.T., Jeelani, S.A.K. & Windhab, E. 2007. Ultrasound Doppler based in-line rheometry of particulate suspensions. *Experiments in Fluids* (Submitted).
- Brinkworth, B.J. 1968. *An Introduction to experimentation*. London: English University Press.
- Brunn, P.O., Vorwerk, J. & Steger, R. 1993. Optical and acoustic rheometers: three examples. *Rheology*, 3:20-27.
- Chhabra, R.P. & Richardson, J.F. 1999. *Non-Newtonian Flow in the Process Industries*. Oxford, Great Britain: Butterworth-Heinemann.
- Choi, Y.J., McCarthy, K.L. & McCarthy, M.J. 2002. Tomographic techniques for measuring fluid flow properties. *Journal of Food Science*, 67(7):2718-2724.
- Dogan, N., McCarthy, M.J. & Powell, R.L. 2002. In-line measurement of rheological parameters and modeling of apparent wall slip in diced tomato suspensions using ultrasonics. *Journal of Food Science*, 67(2):2235-2240.

- Dogan, N., McCarthy, M.J. & Powell, R.L. 2002. Comparison of in-line consistency measurement of tomato concentrates using ultrasonics and capillary. *Journal of Food Process Engineering*, 25(6):571-585.
- Dogan, N., McCarthy, M.J. & Powell, R.L. 2003. In-line flow and rheology measurement of complex, opaque fluids with velocimeter based rheometry using ultrasonics. In P. Fischer, I. Marti & E.J. Windhab, *Proceedings of the 3<sup>rd</sup> International Symposium on Food Rheology and Structure*, Zurich, Switzerland, 9-13 February 2003. EuroRheo 2003-01:453-454.
- DOP2000 User's Manual. Model 2125/2032. Software version: 4.03. Revision: 1. Signal Processing S.A., Lausanne, Switzerland.
- Floyd, T.L. 2003. *Digital Fundamentals*. 8<sup>th</sup> ed. USA: Von Hoffman Press. ISBN 0-13-046411-2.
- Goldstein, R.J. 1983. *Fluid Mechanics Measurements*. Washington, New York, London: Hemisphere Publishing Corporation.
- Haldenwang, R. 2003. Flow of Non-Newtonian fluids in Open Channels. Unpublished D. Tech Thesis. Cape Technikon.
- Haldenwang, R., Kotzé, R., Slatter, P.T. & Mariette, O. 2006. An Investigation in Using UVP for assisting in Rheological characterisation of Mineral Suspensions. *Proceedings of the 5<sup>th</sup> International Symposium on Ultrasonic Doppler Methods for Fluid Mechanics and Fluid Engineering*, Zurich, Switzerland, 12-14 September 2006. ISUD5:77-79.
- Haldenwang, R., Slatter, P., Alderman, N., Kotzé, R., Sery, G. & George, N. 2006. Balanced Beam Tube Viscometry vs Rotary Viscometry: A Comparison. *12<sup>th</sup> International Conference on Transport and Sedimentation of Solid Particles*, Tbilisi, Georgia. 12:145-156.
- Halliday, D. & Resnick, R. 1962. *Physics for students of science and engineering*. Combined Edition. John Wiley.
- Halliday, D., Resnick R. & Walker, J. 1993. *Fundamentals of Physics*. 4<sup>th</sup> Edition (Extended). John Wiley.
- Hardy, S. . 2002. Commissioning of a New Instrument for Non-Newtonian Flow Characterisation. Unpublished M.Tech. thesis. Cape Peninsula University of Technology. Cape Town. South Africa.
- Jensen, J.A. 1996. *Estimation of Blood Velocities Using Ultrasound: A Signal Processing Approach*. Great Britain: Cambridge University Press. ISBN 0-521-46484-6.
- Köseli, V., Zeybek, S. & Uludag, Y. 2006. Online Viscosity Measurement of Complex Solutions Using Ultrasound Doppler Velocimetry. *Turk J Chem.*, 30:297-305.
- Kuttruff, H. 1991. *Ultrasonics: Fundamentals and Applications*. London and New York: Elsevier Applied Science.

- Lazarus, J.H. & Sive, A.W. 1984. A novel balanced beam tube viscometer and the rheological characterisation of high concentration fly ash slurries. *9<sup>th</sup> Int. Conf. on the hydraulic transport of solids in pipes*. Hydrotransport 9. Paper E1.
- Lazarus, J.H. & Slatter, P.T. 1986. Comparative rheological characterisation using a balanced beam tube viscometer and rotary viscometer. *British Hydromechanics Research Association 10<sup>th</sup> Int. Conf. On the hydraulic transport of solids in pipes*. Hydrotransport 10. Paper J2. ISBN 1 – 85166 – 064 –x. pp 291-232.
- Lazarus, J.H. & Slatter, P.T. 1988. A method for the rheological characterisation of tube viscometer data. *Journal of pipelines*, V7:165-176.
- Lubbers, J. & Graaff, R. 1998. A simple and accurate formula for the sound velocity in water. *Ultrasound Med. Biol.* 24(7):1065-1068.
- Met-Flow SA. 1997. Technical Note – Ultrasonic Beam and Beam optics, Met-Flow SA, Lausanne, Switzerland.
- Met-Flow SA. 2002. UVP Monitor – Model UVP-DUO User’s Guide. Software version 3. Met-Flow SA, Lausanne, Switzerland.
- Metzger, T. 1998. A little course in rheology Part 1. Physica, Messtechnik GmbH, Stuttgart, Germany: 49-53.
- Mezger, T.G. 2002. *The Rheology Handbook: For users of rotational & oscillation rheometers*. Hannover: Curt R. Vincentz Verlag.
- Mobley, R.K. 2000. *Fluid Power Dynamics*. Woburn, MA: Butterworth-Heinemann. ISBN 0-7506-7174-2.
- Morris, A. 2001. *Measurements & Instrumentation Principles*. Butterworth-Heinemann.
- Mott, R. L. 2006. *Applied Fluid Mechanics*. 6<sup>th</sup> ed. USA: Banta Book Group. ISBN 0-13-114680-7.
- Müller, M., Brunn, P.O. & Wunderlich, T. 1997. New Rheometric Technique: the Gradient-Ultrasound Pulse Doppler Method. *Applied Rheology*, 7:204-210.
- Muller, M. 1998. Neue Methoden Der Prozessviskosimetrie: Kugelschüttungsströmung Und Gradienten – Ultraschall – Puls – Doppler – Verfahren Vol. Doctoral thesis, University of Erlangen, Germany.
- Neill, R.I.G. 1988. The rheology and flow behaviour of high concentration mineral slurries. Unpublished M.Sc. thesis. University of Cape Town. South Africa.



- Ouriev, B. & Windhab, E.J. 1999. Study of flow processes of concentrated suspensions using in-line non-invasive rheological technique. In Y. Takeda, *Selected Papers of the 2<sup>nd</sup> International Symposium on Ultrasonic Doppler Methods for Fluid Mechanics and Fluid Engineering, held at PSI. PSI Proceedings 99*, Villigen, Switzerland, 20-22 September 1999. ISUD2:31-35.
- Ouriev, B. 2000. *Ultrasound Doppler Based In-Line Rheometry of Highly Concentrated Suspensions*. ETH dissertation No. 13523, ISBN 3-905609-11-8. Zurich. Switzerland.
- Ouriev, B., Breitschuh, B. & Windhab, E. J. 2000. Rheological investigation of concentrated suspensions using a novel In-line Doppler ultrasound method. *Kolloidnyi Zhurnal*, 62(2):268-271.
- Ouriev, B. & Windhab, E.J. 2002. Investigation of the wall slip effect in highly concentrated disperse systems by means of non-invasive UVP-PD method in the pressure driven shear flow. *Kolloidnyi Zhurnal*, 64(6):740-745.
- Ouriev, B. & Windhab, E.J. 2002. Rheological study of concentrated suspensions in pressure-driven shear flow using a novel in-line ultrasound Doppler method. *Experiments in fluids*, 32:204-211.
- Ouriev, B. & Windhab, E.J. 2003. Transient flow of highly concentrated suspensions investigated using the ultrasound velocity profiler-pressure difference method. *Measurement Science and Technology*, 14:1963-1972.
- Povey, M.J.W. 1997. *Ultrasound Techniques For Fluids Characterization*. Academic Press. San Diego, California, USA: Harcourt Brace & Company (Publishers). ISBN 0-12-563730-6.
- Powell, R.L., Dogan, N. & McCarthy, M.J. 2006. In-line ultrasonic device for flow and rheology measurements of complex fluids. *Proceedings of the 5<sup>th</sup> International Symposium on Ultrasonic Doppler Methods for Fluid Mech and Fluid Eng*, Zurich, Switzerland, 12-14 September 2006. ISUD5:155-158.
- Ray, S., Ünsal, B., Durst, F., Ertunc, Ö. & Bayoumi, O.A. 2005. Mass Flow Rate Controlled Fully Developed Laminar Pulsating Pipe Flows. *Journal of Fluid Engineering*, 127:405-418.
- Shekarriz A. & Sheen D.M. 1998. Slurry Pipe Flow Measurements using Tomographic Ultrasonic Velocimetry and Densitometry. *Proceedings of FEDSM, ASME Fluids Engineering Division Summer Meeting*, Washington, D.C., USA, 21-25 June 1998, FEDSM98-5076.
- Shutilov, V.A. 1980. *Fundamental Physics of Ultrasound – English Translation by Michael E. Alferieff, 1988*. Amsterdam, Netherlands: Gordon and Breach Science Publishers.
- Signal Processing SA. 2007. *Transducers ultrasonic field*.  
[http://www.signal-processing.com/transducers/transducers\\_theory\\_frame.htm](http://www.signal-processing.com/transducers/transducers_theory_frame.htm)  
[11 May 2007].

- Slatter, P.T. & Lazarus, J.H. 1993. Critical flow in slurry pipelines. British Hydromechanics Research Group, *12th International Conference on Slurry Handling and Pipeline Transport, HYDROTRANSPORT 12*; Brugge, Belgium: 28-30 September 1993. ISBN 0 85298 874 5. pp 639-654.
- Slatter, P.T. 1994. Transitional and Turbulent flow of non-Newtonian slurries in pipes. Unpublished PhD thesis. Cape Town: University of Cape Town.
- Slatter, P.T. 1997. The Rheological Characterisation of Sludges. *Wat. Sci. Tech.*, 36(11):9-18.
- Steffe, J.F. 1996. *Rheological Methods in Food Process Engineering*. 2<sup>nd</sup> ed. USA: Freeman Press.
- Steger, R. 1994. Optisch Und Akustische Methoden in Der Rheometrie. Erlangen: University of Erlangen: 1-100.
- Takeda, Y. 1986. Velocity Profile Measurement by Ultrasound Doppler Shift Method. *Int. J. Heat Fluid Flow*, 7(4):313-318.
- Takeda, Y. 1995. Velocity Profile Measurement by Ultrasonic Doppler Method. *Experimental Thermal and Fluid Science*, 10:444-453.
- Takeda, Y. 1999. Ultrasonic Doppler Method for Velocity Profile Measurement in Fluid Dynamics and Fluid Engineering. *Experiments in Fluids*, 26:177-178.
- Thorvaldsen, G.S. 1996. *The Effect of the Particle Size Distribution on non-Newtonian Turbulent Slurry Flow in Pipes*. Unpublished M.Tech. Thesis. Cape Town: Cape Technikon.
- Urick, R.J. 1947. A Sound Velocity Method for Determining the Compressibility of Finely Divided Substances. *Journal of Applied Physics*, 18:983-987.
- Wang T., Wang, J., Ren, F. & Jin, Y. 2003. Application of Doppler ultrasound velocimetry in multiphase flow. *Chem Eng J.*, 92:111-122.
- Wiklund, J. & Johansson, M. 2001. Rheological In-Line Measurements of Complex Model Fluids using an Ultrasound UVP-PD Based Method. Unpublished M.Sc. thesis. Chalmers University of Technology (Gothenburg), ETH – Swiss Federal Institute of Technology (Zurich), SIK – The Swedish Institute for Food and Biotechnology (Gothenburg), Sweden.
- Wiklund, J., Johansson, M., Shaik, J., Fischer, P., Windhab, E., Stading, M. & Hermansson, A. M. 2001. In-Line Rheological measurements of Complex Model Fluids using an Ultrasound UVP-PD based method. *Annual Transactions – The Nordic Rheology Society, 10<sup>th</sup> Anniversary conference*, Trondheim, Norway 2001. 8/9:128-130.
- Wiklund, J., Johansson, M., Shaik, J., Fischer P., Windhab, E., Stading, M. & Hermansson, A. 2002. In-line ultrasound based rheometry of industrial and model suspensions flowing through pipes. *Proceedings of the 3<sup>rd</sup> International Symposium on Ultrasonic Doppler Methods for Fluid Mech and Fluid Eng*, Lausanne, Switzerland, Sep 9-11. ISUD3:69-76.

- 
- Wiklund, J. 2003. *Rheological in-line techniques based on ultrasound Doppler methods for the food industry: A literature survey*. LUND University & The Swedish Institute for Food and Biotechnology. SIK-Report SR-710, ISBN 91-7290-225-X. Sweden.
- Wiklund, J. & Stading, M. 2004. In-line ultrasonic rheometry of complex suspensions. *Proc. XIVth Int. Congr. on Rheology*, Seoul, Korea, 22-27 August 2004.
- Wiklund, J., Pettersson, J., Rasmuson, A. & Stading, M. 2004. A comparative study between UVP and LDA techniques for highly concentrated pulp suspensions in pipe flow. *Proceedings of the 4<sup>th</sup> International Symposium on Ultrasonic Doppler Methods for Fluid Mech and Fluid Eng*, Sapporo, Japan. ISUD4:69-75.
- Wiklund, J.A., Stading, M., Petterson, A.J. & Rasmuson, A. 2005. A comparative study of UVP and LDA techniques for pulp suspensions in pipe flow. *AIChE Journal*. 52:484-495.
- Wiklund, J. & Stading, M. 2006. Application of in-line ultrasound Doppler based UVP-PD method to concentrated model and industrial suspensions. *Proceedings of the 5<sup>th</sup> International Symposium on Ultrasonic Doppler Methods for Fluid Mech and Fluid Eng*, Zurich, Switzerland, 12-14 September 2006. ISUD5:145-148.
- Wiklund, J. 2007. *Ultrasound Doppler Based In-Line Rheometry: Development, Validation and Application*. SIK – The Swedish Institute for Food and Biotechnology, Lund University, Sweden. ISBN 978-91-628-7025-6.
- Wiklund, J., Shahram, I. & Stading, M. 2007. Methodology for in-line rheology by ultrasound Doppler velocity profiling and pressure difference techniques. *Chemical Engineering Science*, 62(16), August 2007:4159-4500.
- Wiklund, J., Stading, M. & Trägårdh, C. 2007. Monitoring liquid displacement of model and industrial fluids in pipes using in-line ultrasound Doppler velocimetry. *Journal of Food Engineering* (2007), Accepted for publication.

# APPENDIX

# APPENDIX A

## EXPERIMENTAL RESULTS

The following is depicted in this appendix:

- The experimental velocity profiles and theoretical fits as well as UVP parameter settings and test conditions are given in Section A.1.
- The flow curves that were measured using the off-line Paar Physica MCR300 rheometer are depicted in the form of rheograms in Section A.2.
- Experimental pipe data (three pipes) and flow curves that were measured using the pipe viscometer are presented in Section A.3.

The following materials were used:

CMC 5.3 – 6.5 % by weight

Bentonite 5.7 – 7.5 % by weight

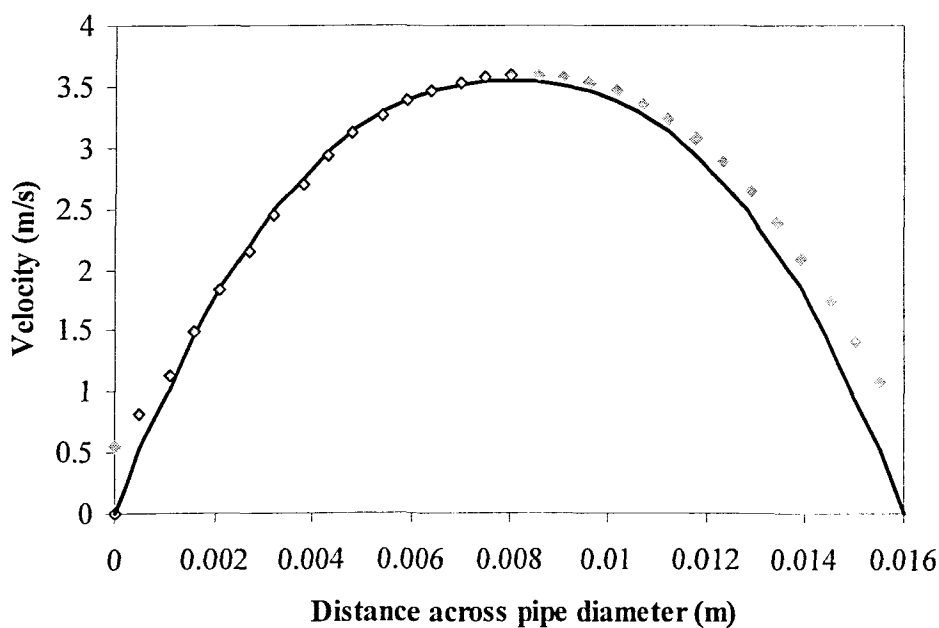
Kaolin 8.7 – 12 % by volume

## A.1 EXPERIMENTAL AND THEORETICAL PROFILES

### CMC 5.3 %

#### UVP PARAMETER SETTINGS AND TEST CONDITIONS

PRF (kHz)	US Voltage (V)	Number of cycles/pulse	Number of US repetitions	Sound speed (m/s)
13.69	90	2	256	1520
Reynolds number	Pressure drop (Pa)	Volume flow rate (l/s)	Slurry density (kg/m <sup>3</sup> )	Temperature (°C)
600	14823	0.416	1030	15.5

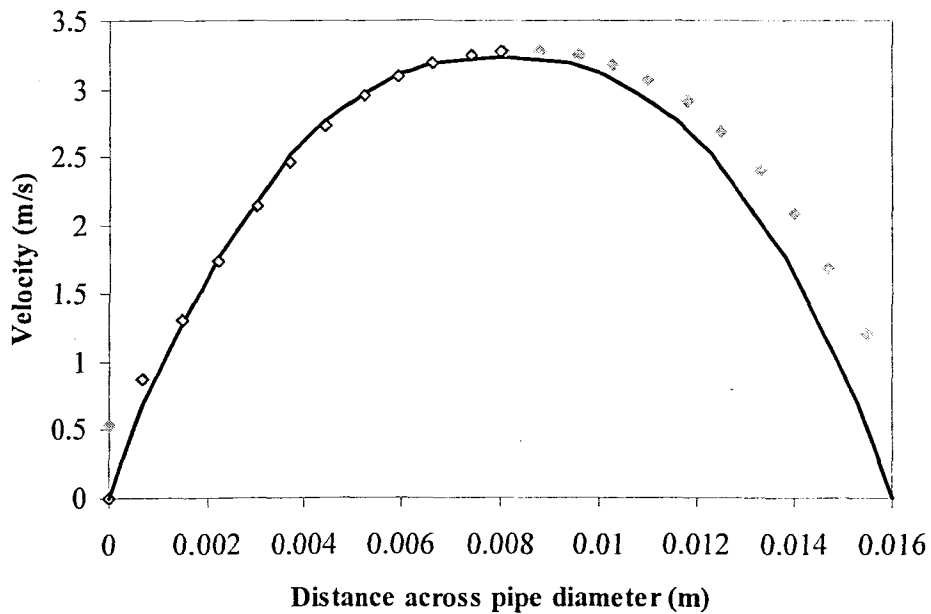


◆ Measured velocity profile — Theoretical fit ◇ Range used for fitting

### CMC 6 %

#### UVP PARAMETER SETTINGS AND TEST CONDITIONS

PRF (kHz)	US Voltage (V)	Number of cycles/pulse	Number of US repetitions	Sound speed (m/s)
15.26	90	4	256	1568
Reynolds number	Pressure drop (Pa)	Volume flow rate (l/s)	Slurry density (kg/m <sup>3</sup> )	Temperature (°C)
306	24554	0.378	1034	20.1

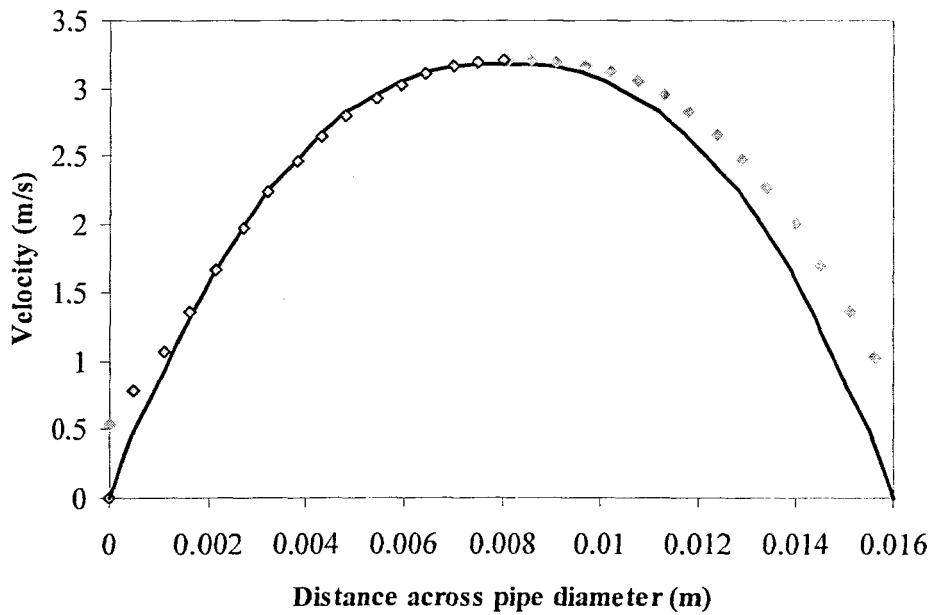


◆ Measured velocity profile — Theoretical fit ◇ Range used for fitting

## CMC 6.5 %

## UVP PARAMETER SETTINGS AND TEST CONDITIONS

PRF (kHz)	US Voltage (V)	Number of cycles/pulse	Number of US repetitions	Sound speed (m/s)
13.16	90	2	256	1525
Reynolds number	Pressure drop (Pa)	Volume flow rate (l/s)	Slurry density (kg/m <sup>3</sup> )	Temperature (°C)
229	31832	0.38	1040	17.5

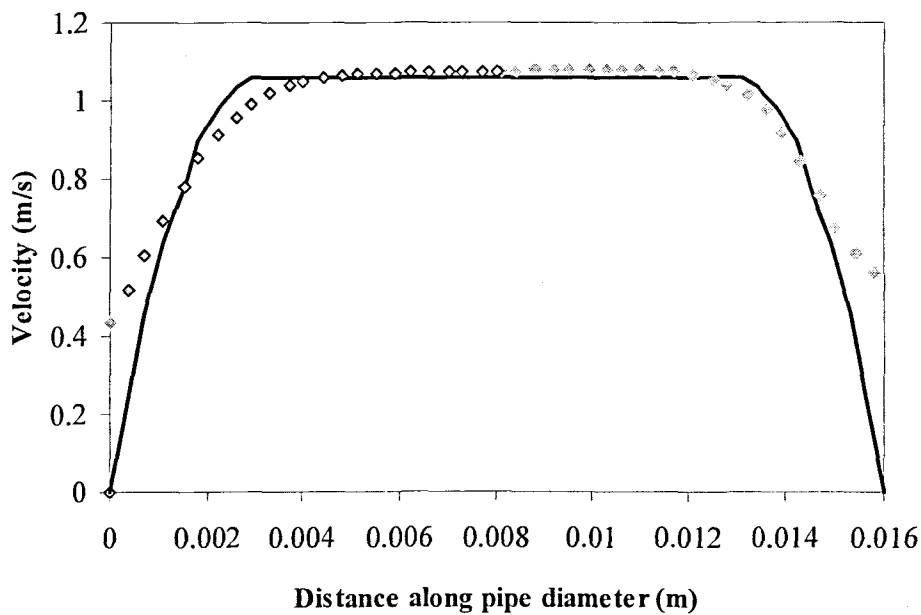


◆ Measured velocity profile — Theoretical fit ◇ Range used for fitting



**BENTONITE 5.7 %****UVP PARAMETER SETTINGS AND TEST CONDITIONS**

PRF (kHz)	US Voltage (V)	Number of cycles/pulse	Number of US repetitions	Sound speed (m/s)
5.13	60	2	256	1560
Reynolds number	Pressure drop (Pa)	Volume flow rate (l/s)	Slurry density (kg/m <sup>3</sup> )	Temperature (°C)
275	5712	0.160	1035	20.5



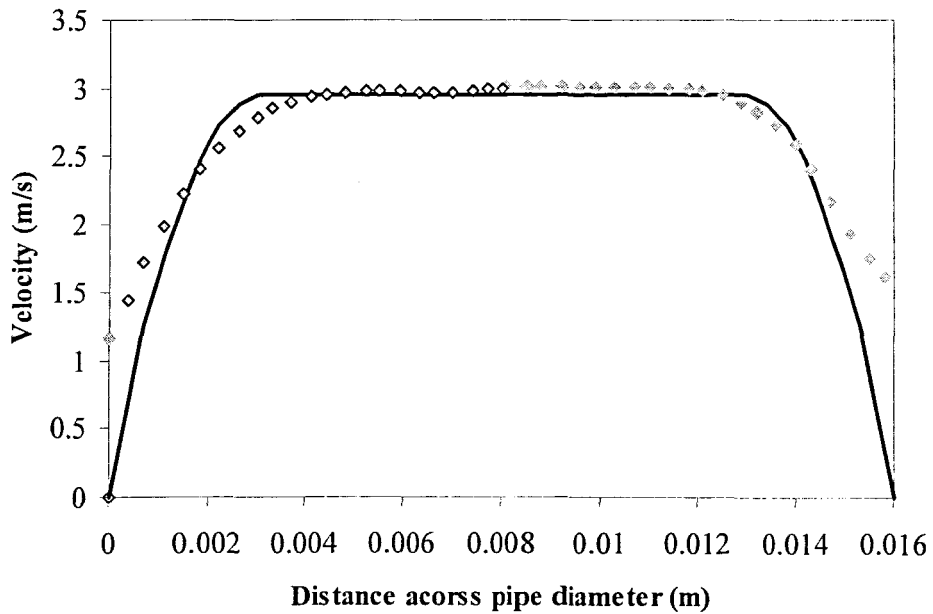
## BENTONITE 6.5 %

### UVP PARAMETER SETTINGS AND TEST CONDITIONS

PRF (kHz)	US Voltage (V)	Number of cycles/pulse	Number of US repetitions	Sound speed (m/s)
12.27	60	2	256	1565

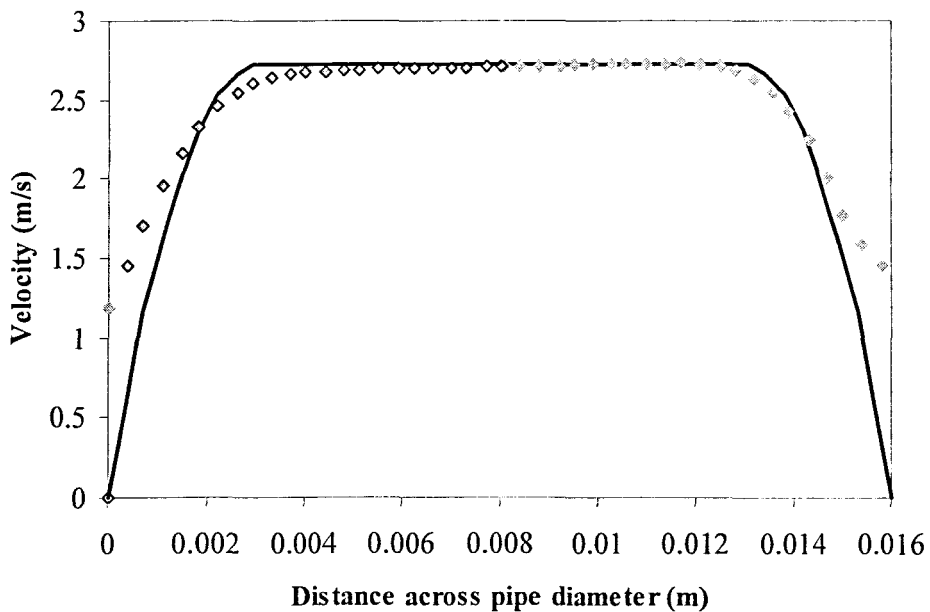
Reynolds number	Pressure drop (Pa)	Volume flow rate (l/s)	Slurry density (kg/m <sup>3</sup> )	Temperature (°C)
977	12953	0.455	1040	25.3



◆ Measured velocity profile — Theoretical fit ◇ Range used for fitting

**BENTONITE 7 %****UVP PARAMETER SETTINGS AND TEST CONDITIONS**

PRF (kHz)	US Voltage (V)	Number of cycles/pulse	Number of US repetitions	Sound speed (m/s)
11.29	60	2	256	1560
Reynolds number	Pressure drop (Pa)	Volume flow rate (l/s)	Slurry density (kg/m <sup>3</sup> )	Temperature (°C)
742	14060	0.411	1044	20.2

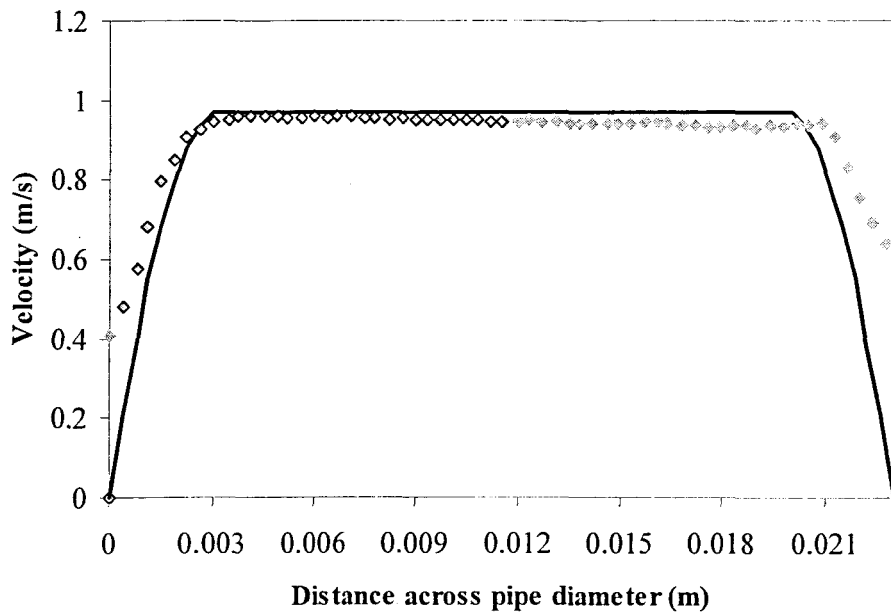


◆ Measured velocity profile — Theoretical fit ◇ Range used for fitting

## BENTONITE 7.5 % (PILOT STUDY)

### UVP PARAMETER SETTINGS AND TEST CONDITIONS

PRF (kHz)	US Voltage (V)	Number of cycles/pulse	Number of US repetitions	Sound speed (m/s)
5.44	90	2	512	1566
Reynolds number	Pressure drop (Pa)	Volume flow rate (l/s)	Slurry density (kg/m <sup>3</sup> )	Temperature (°C)
292	6002	0.45	1049	24.1

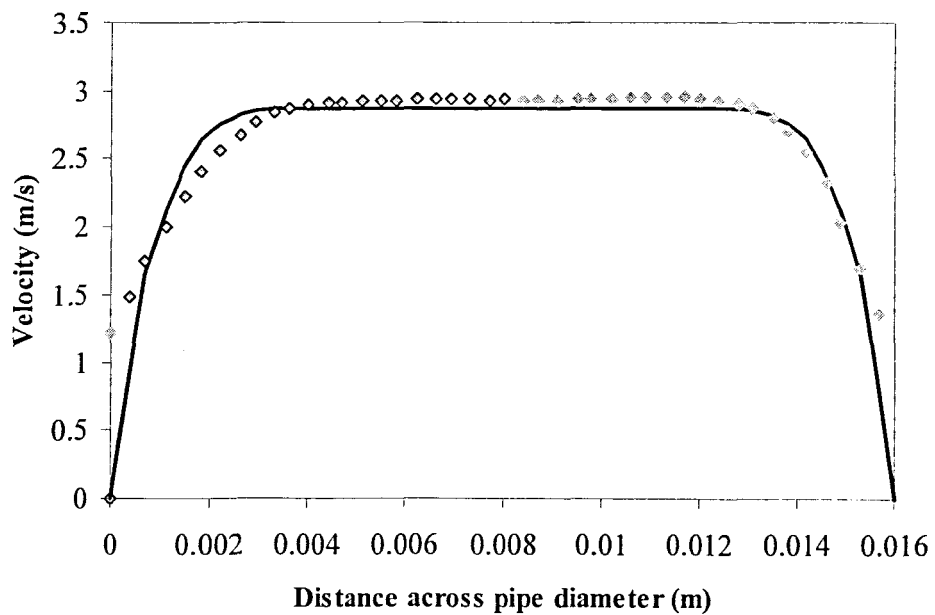


◆ Measured velocity profile — Theoretical fit ◇ Range used for fitting

## KAOLIN 8.7 %

### UVP PARAMETER SETTINGS AND TEST CONDITIONS

PRF (kHz)	US Voltage (V)	Number of cycles/pulse	Number of US repetitions	Sound speed (m/s)
12.91	150	2	512	1551
Reynolds number	Pressure drop (Pa)	Volume flow rate (l/s)	Slurry density (kg/m <sup>3</sup> )	Temperature (°C)
1458	8080	0.421	1143	20.5



◆ Measured velocity profile — Theoretical fit ◇ Range used for fitting

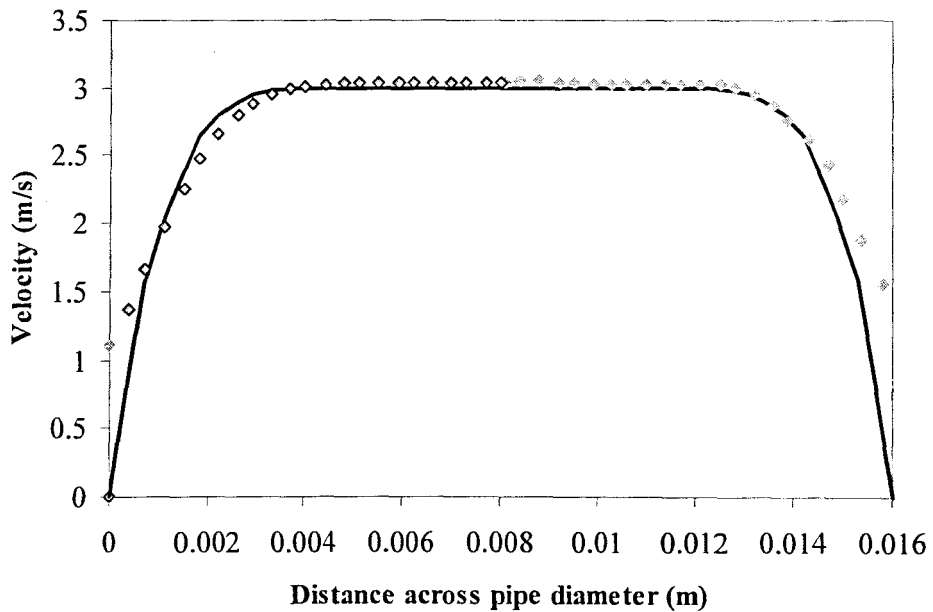
## KAOLIN 10 %

### UVP PARAMETER SETTINGS AND TEST CONDITIONS

PRF (kHz)	US Voltage (V)	Number of cycles/pulse	Number of US repetitions	Sound speed (m/s)
13.33	150	2	512	1561

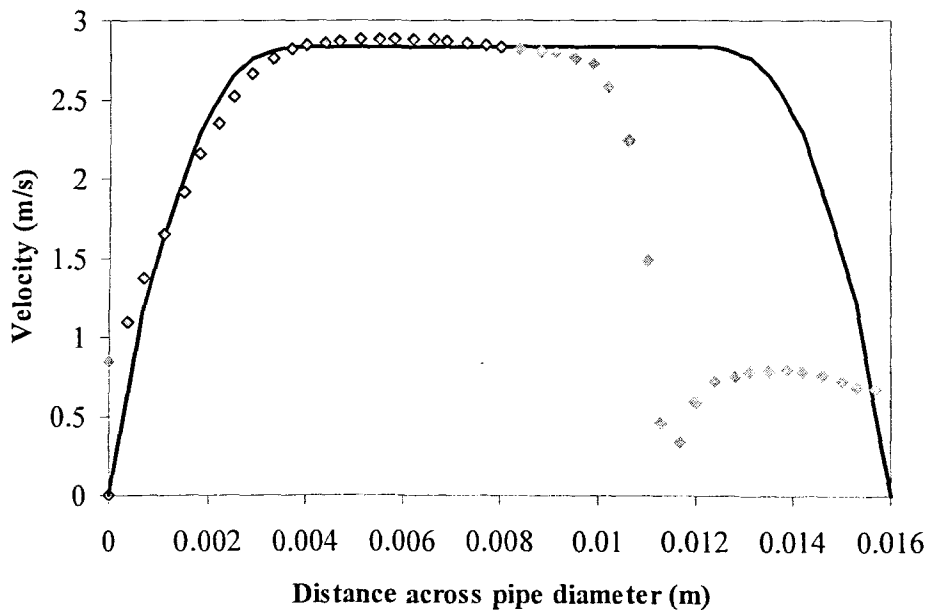
Reynolds number	Pressure drop (Pa)	Volume flow rate (l/s)	Slurry density (kg/m <sup>3</sup> )	Temperature (°C)
912	15150	0.455	1166	24.5



## KAOLIN 12 %

### UVP PARAMETER SETTINGS AND TEST CONDITIONS

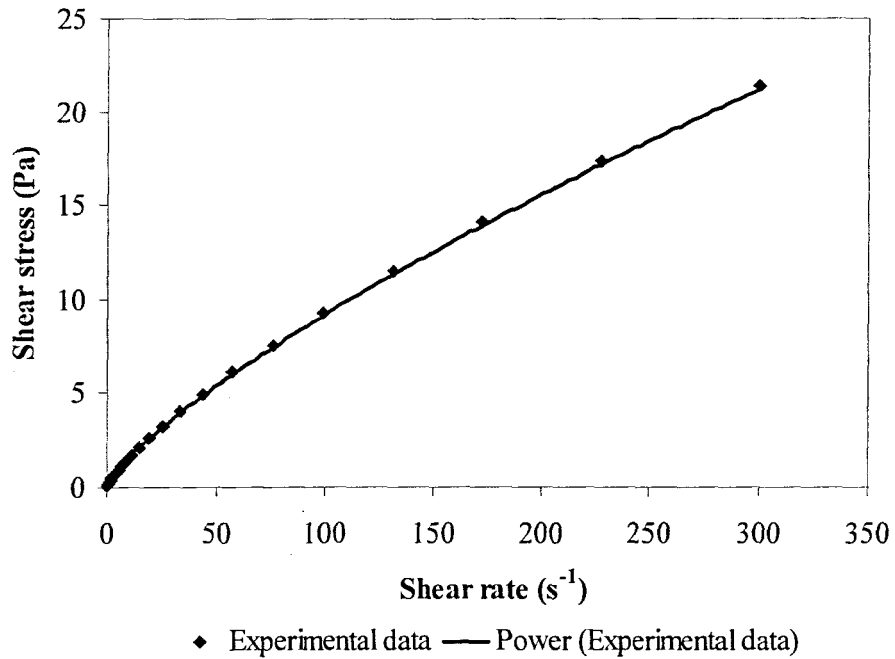
PRF (kHz)	US Voltage (V)	Number of cycles/pulse	Number of US repetitions	Sound speed (m/s)
13.16	150	2	512	1555
Reynolds number	Pressure drop (Pa)	Volume flow rate (l/s)	Slurry density (kg/m <sup>3</sup> )	Temperature (°C)
601	22197	0.44	1199	21.3



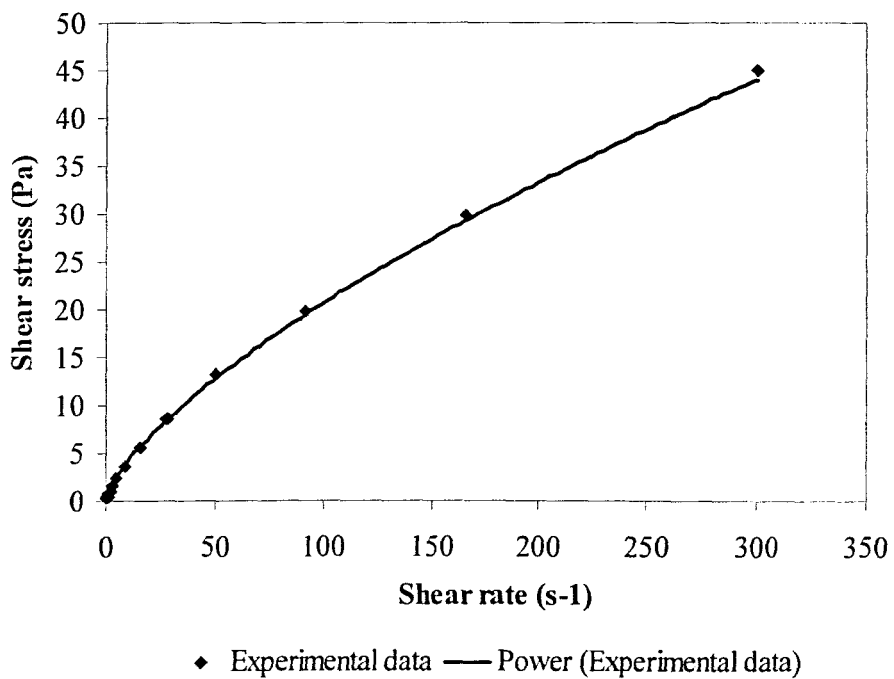
◆ Measured velocity profile — Theoretical fit ◆ Range used for fitting

## A.2 OFF-LINE FLOW CURVES

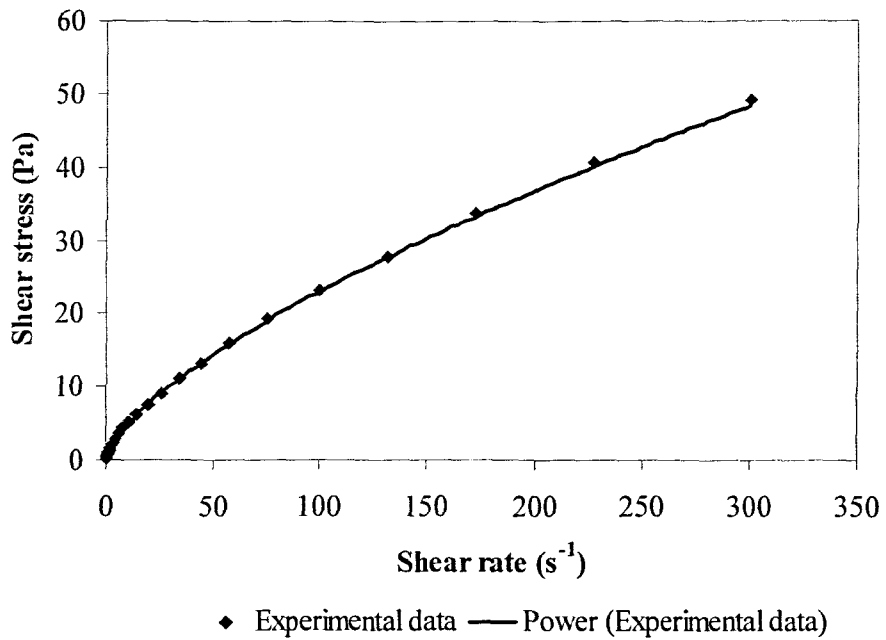
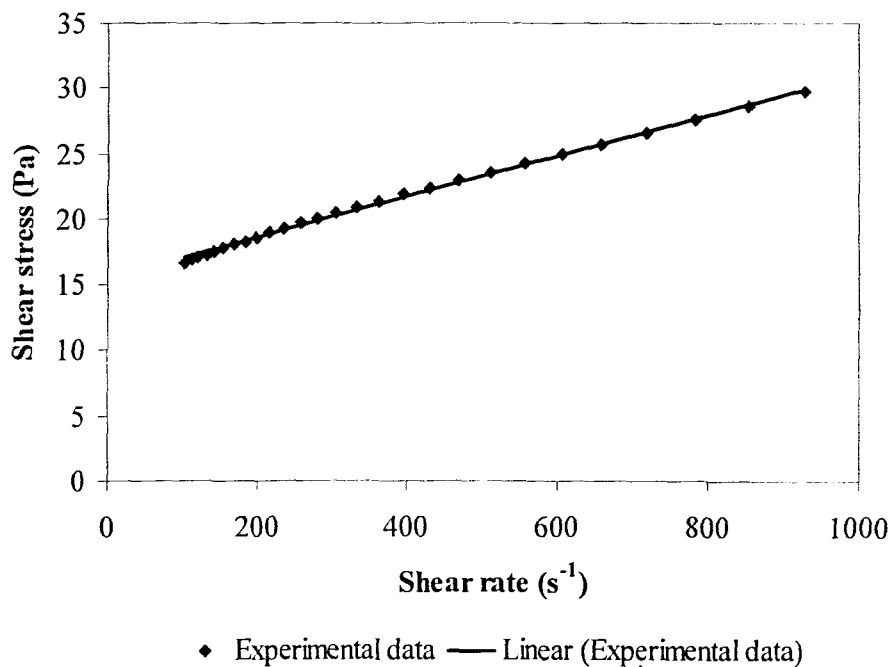
### CMC 5.3 %

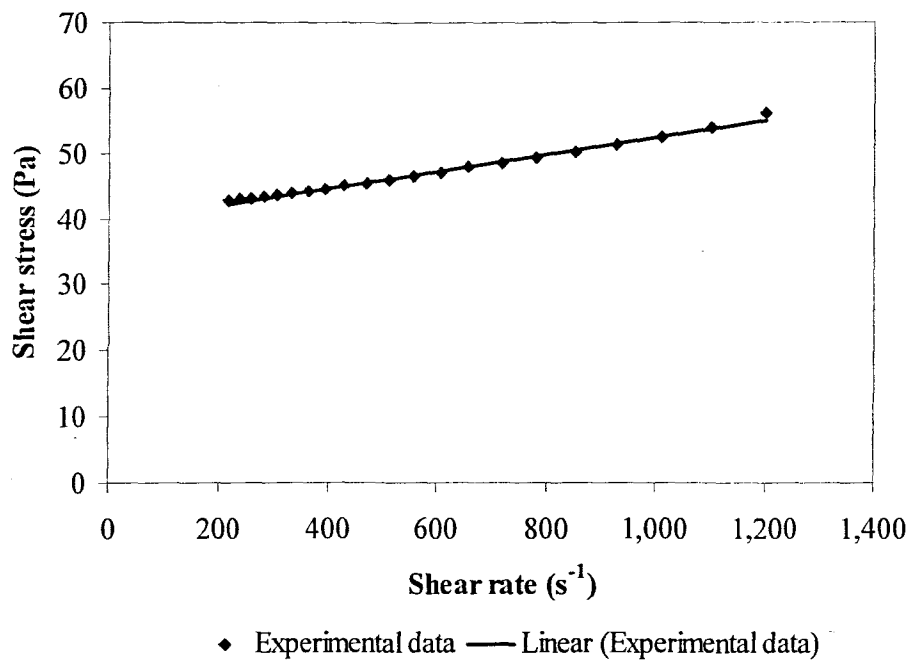
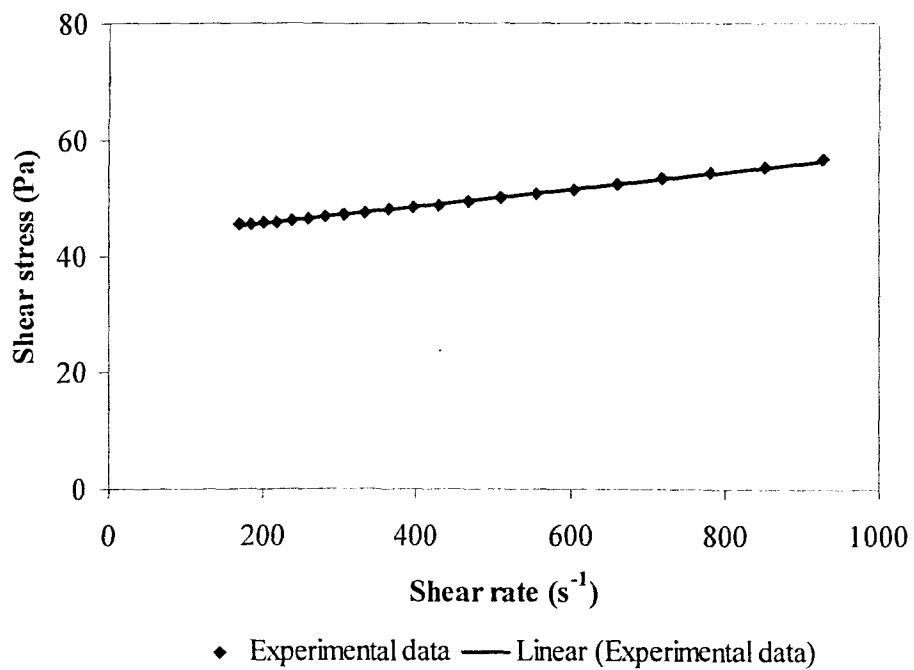


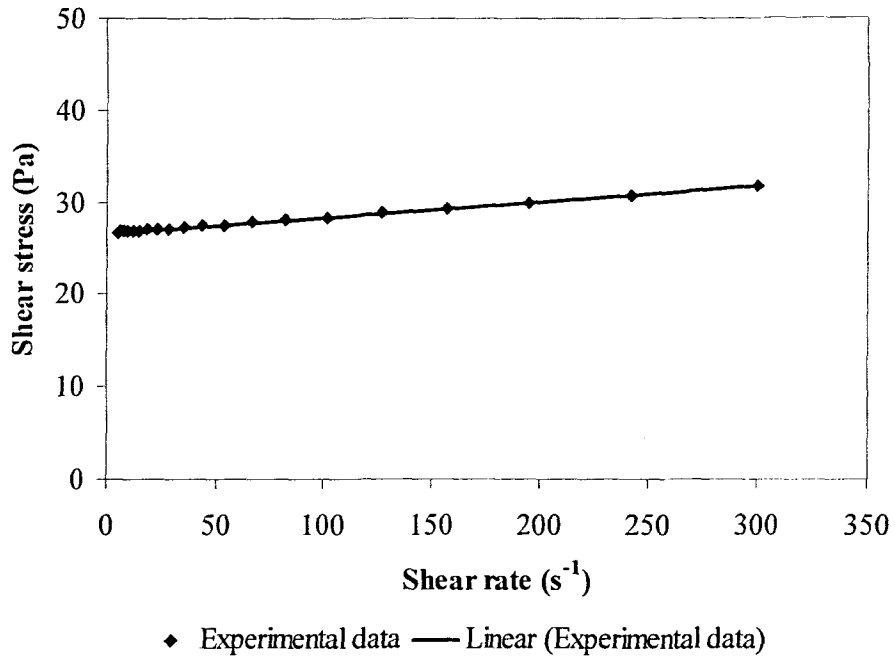
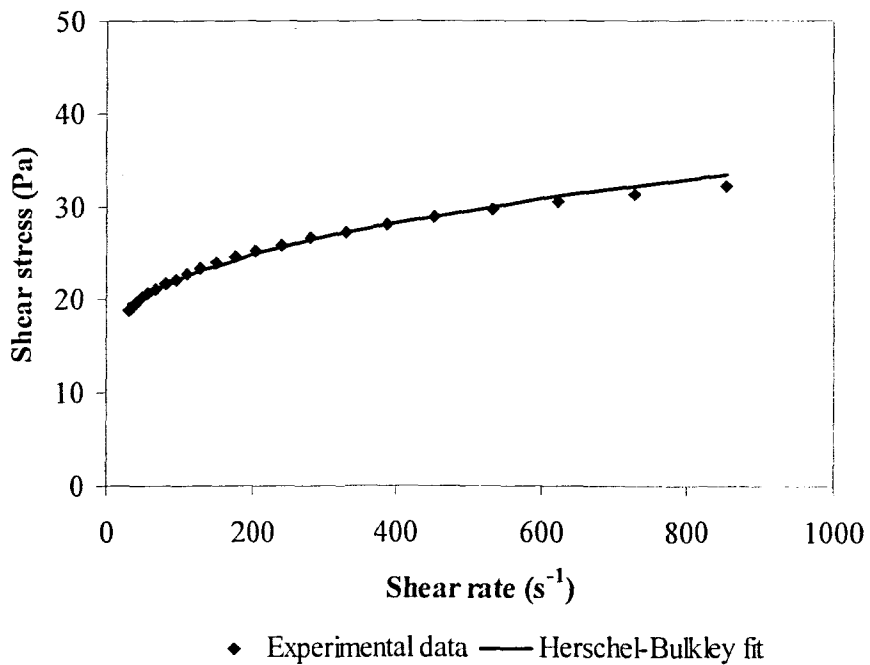
### CMC 6 %

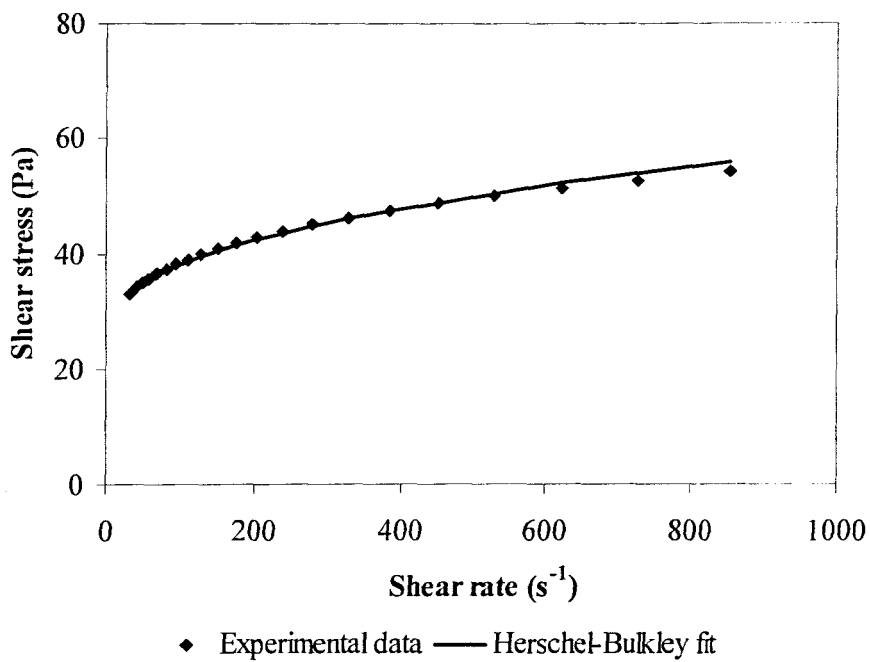
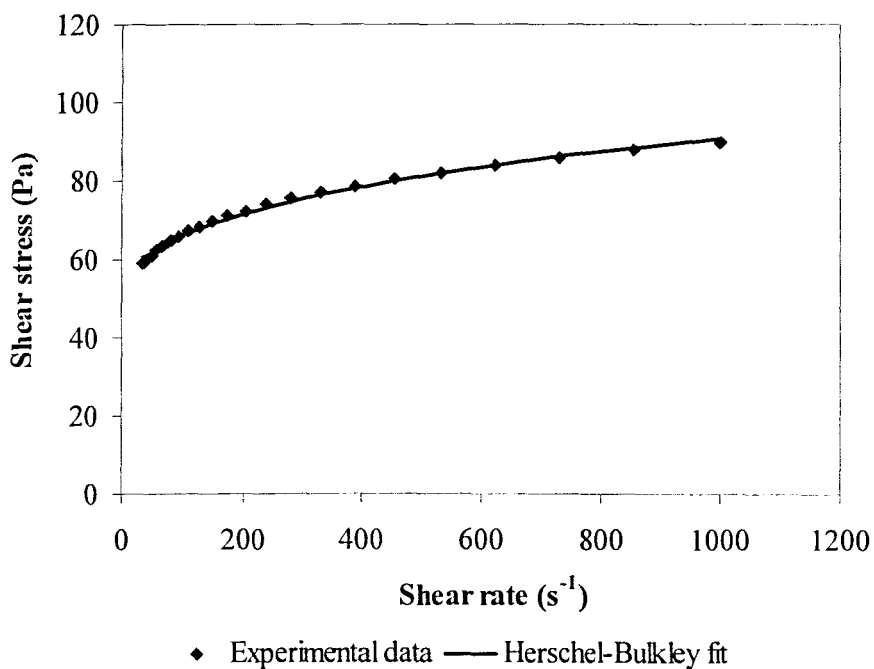




**CMC 6.5 %****BENTONITE 5.7 %**

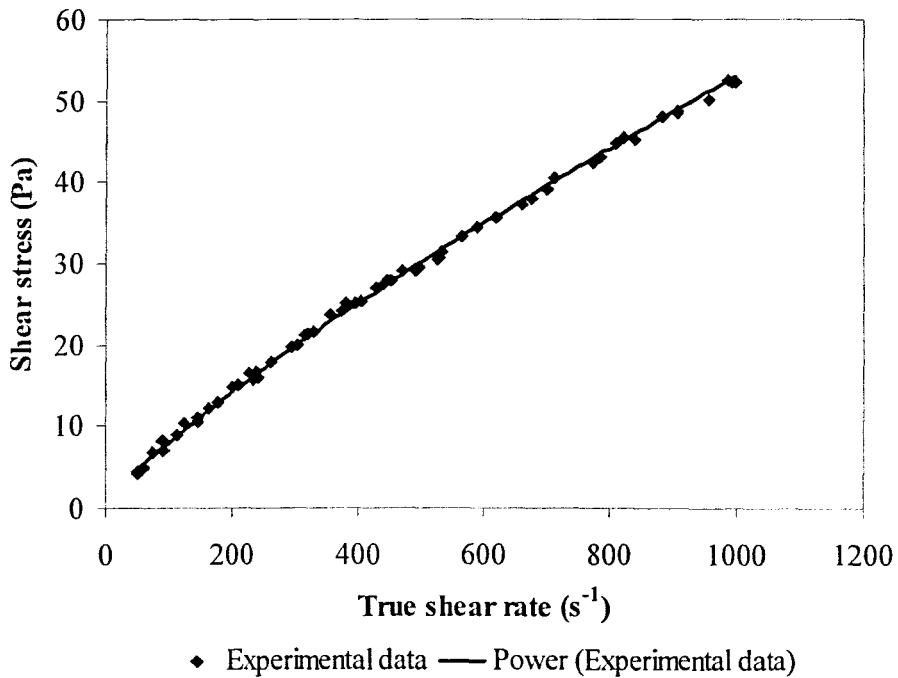
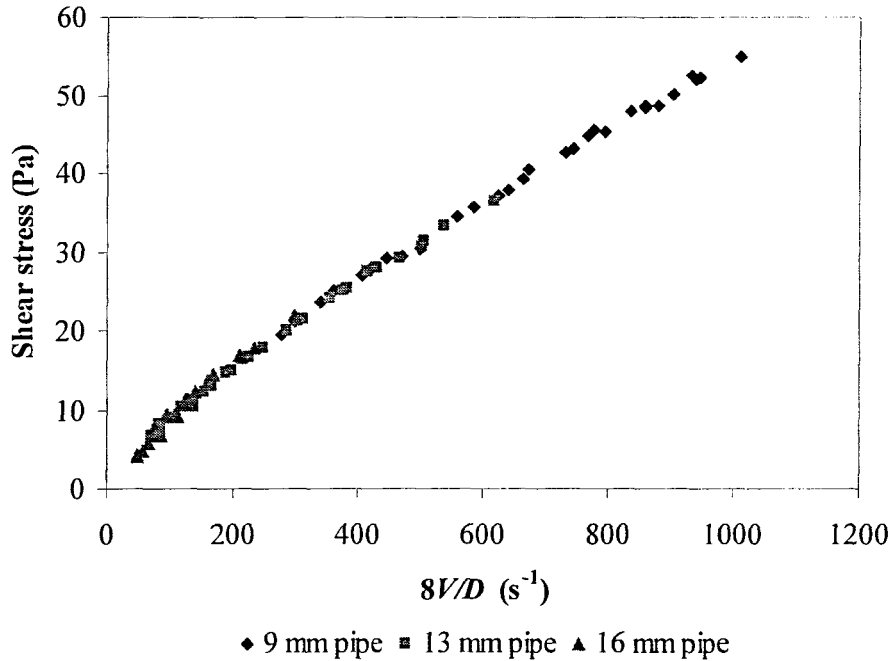
**BENTONITE 6.5 %****BENTONITE 7 %**

**BENTONITE 7.5 % (PILOT STUDY)****KAOLIN 8.7 %**

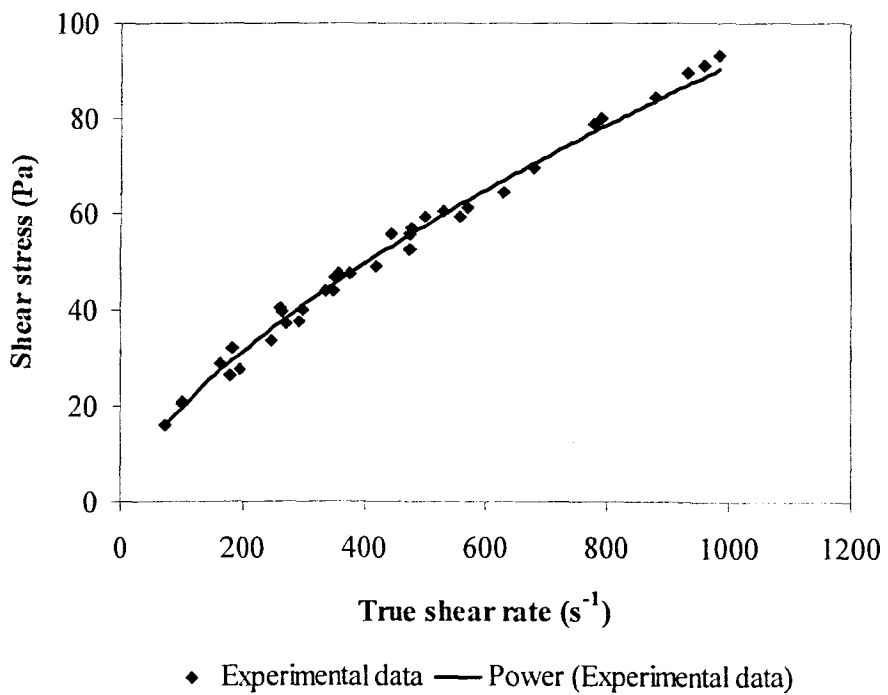
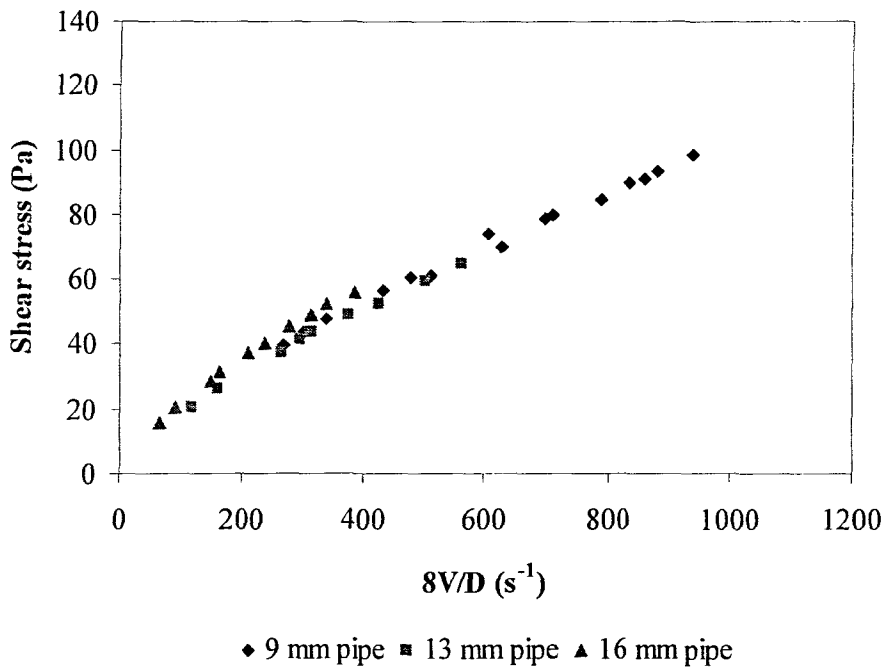
**KAOLIN 10 %****KAOLIN 12 %**

### A.3 PIPE VISCOMETER DATA

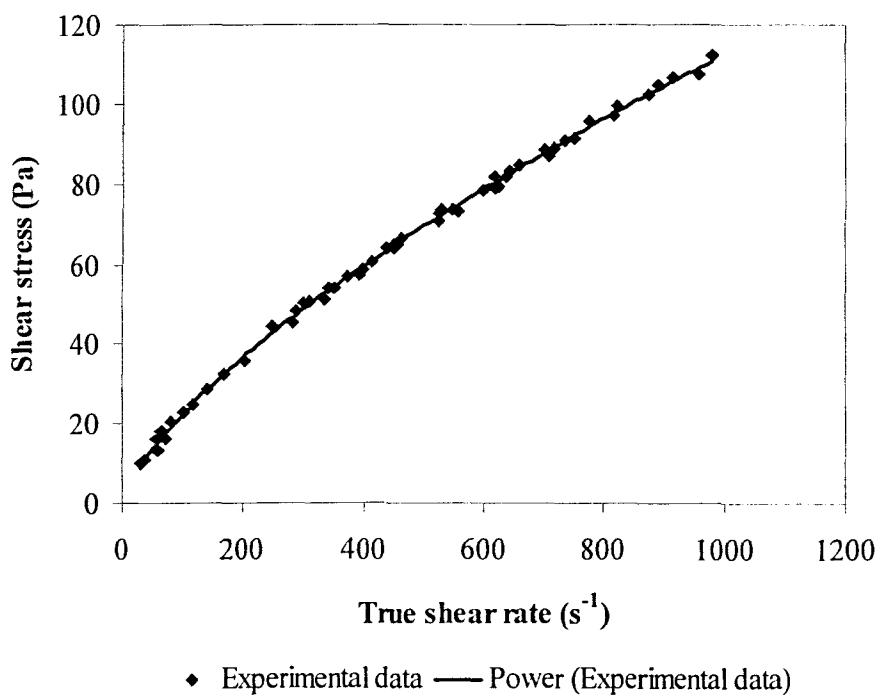
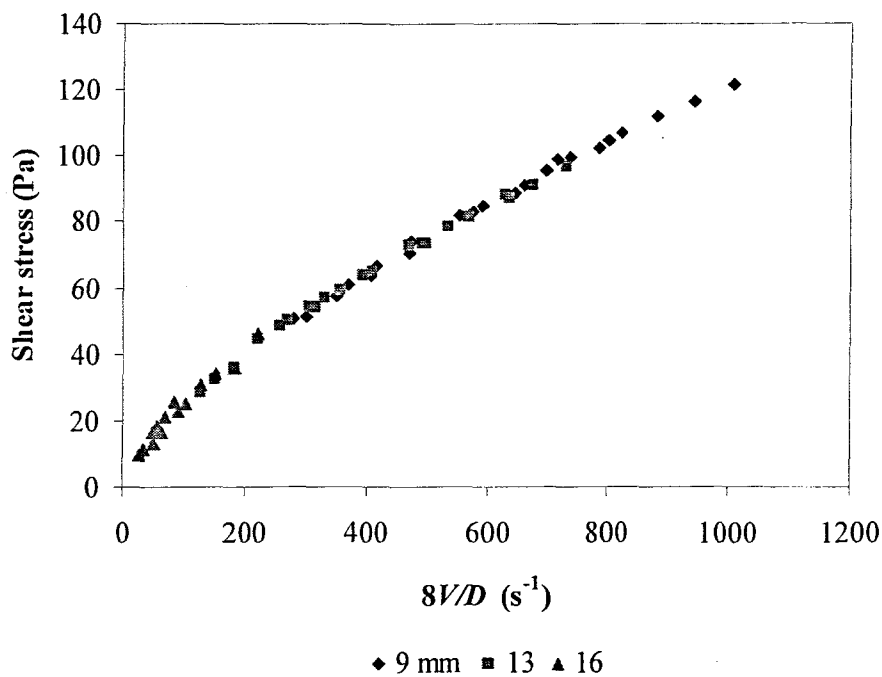
CMC 5.3 %



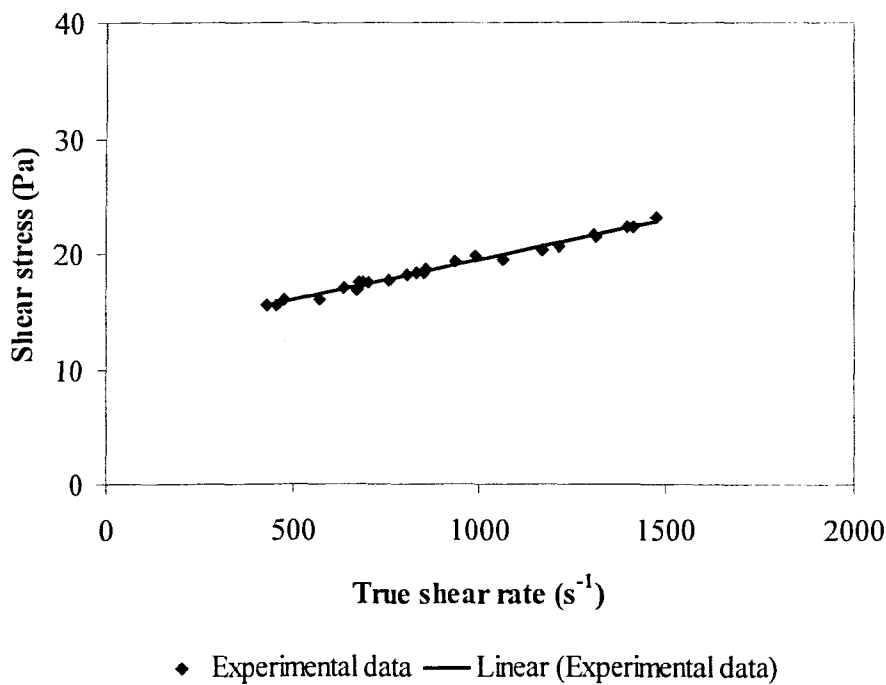
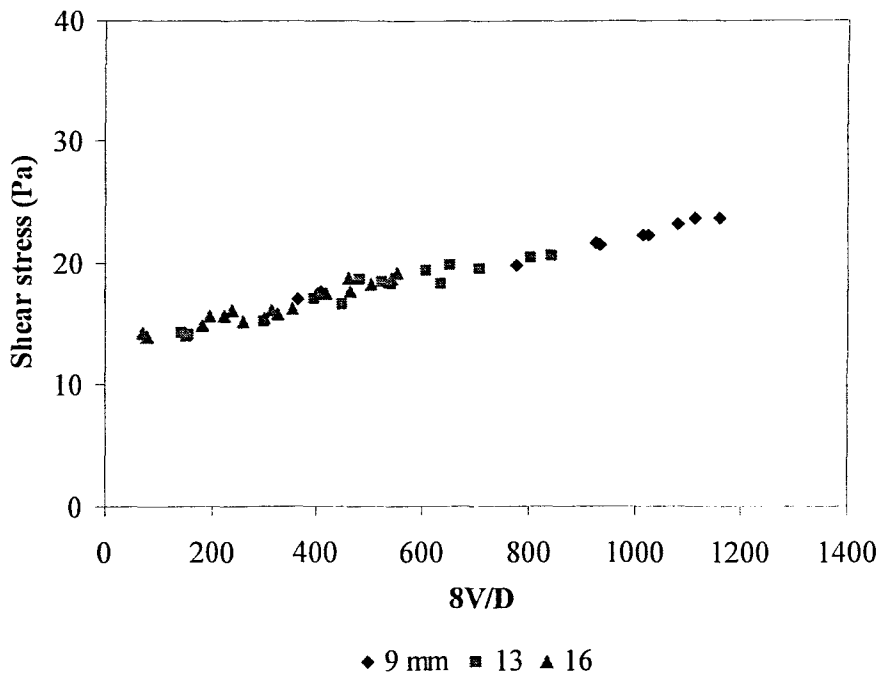
CMC 6 %



## CMC 6.5 %

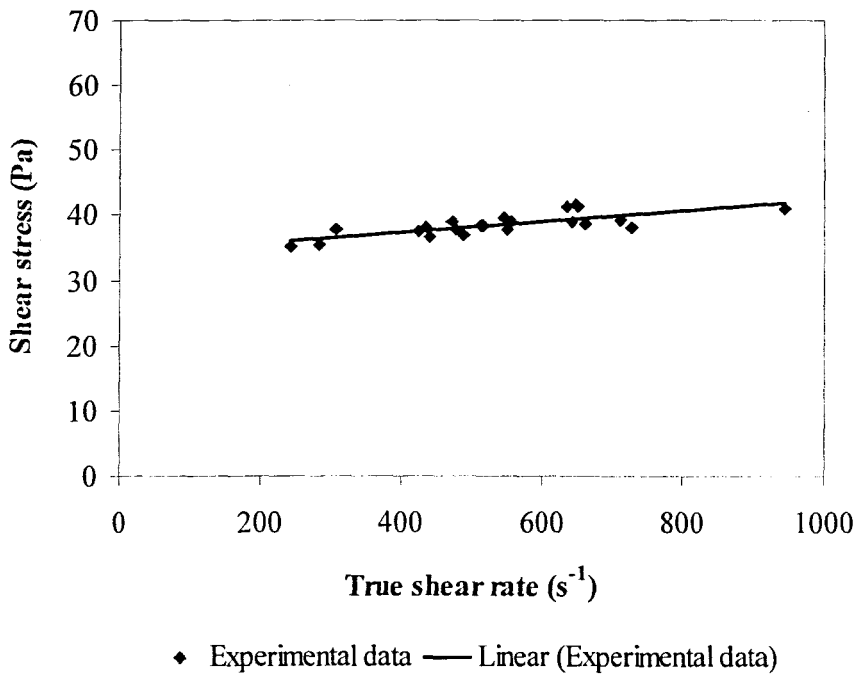
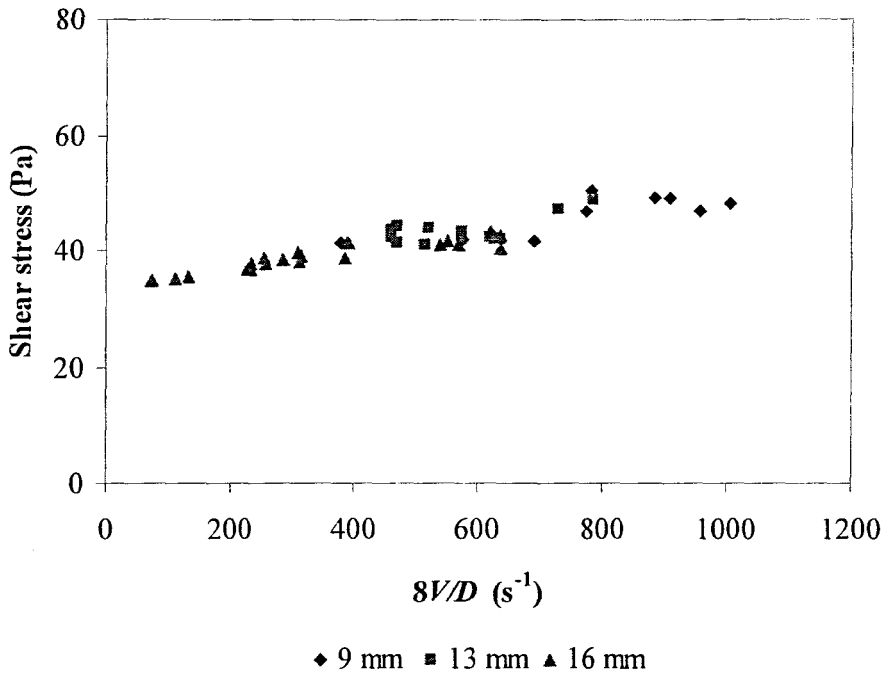


**BENTONITE 5.7 %**

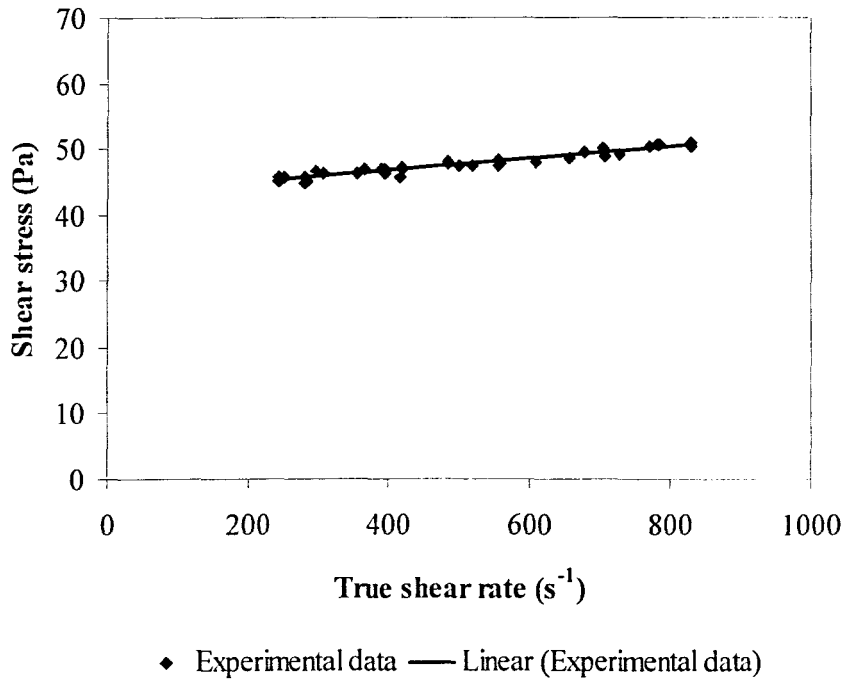
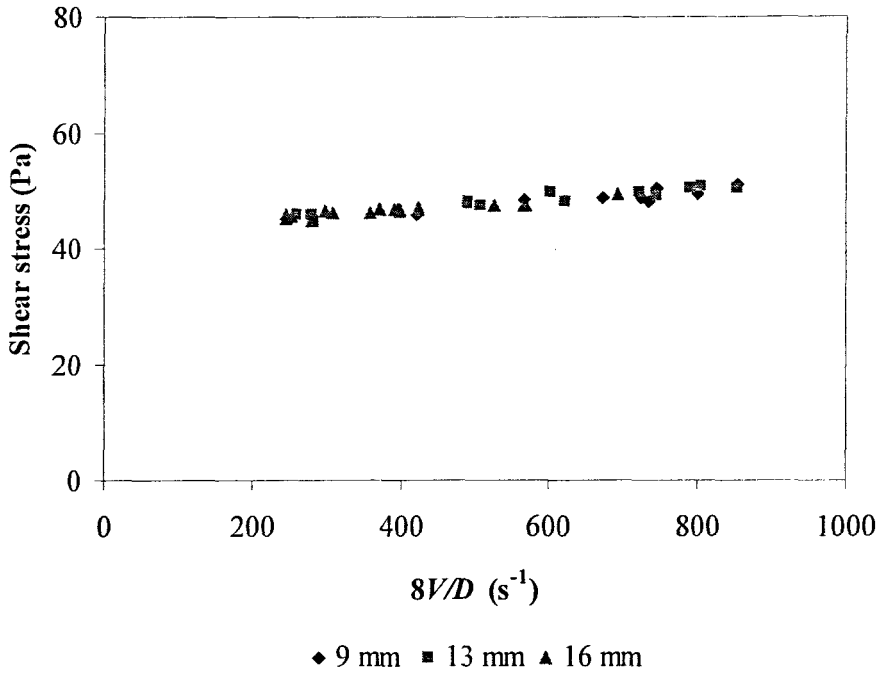




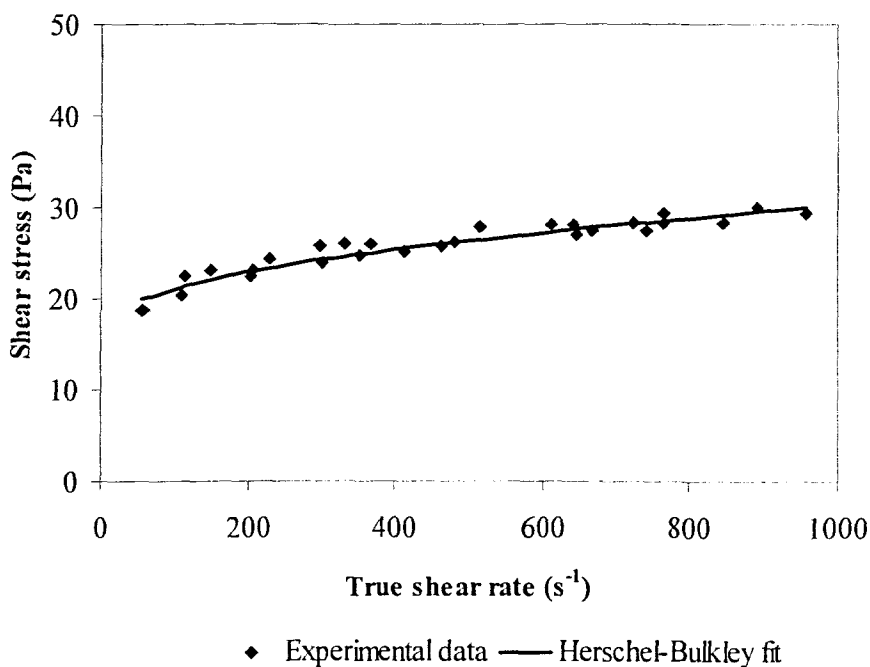
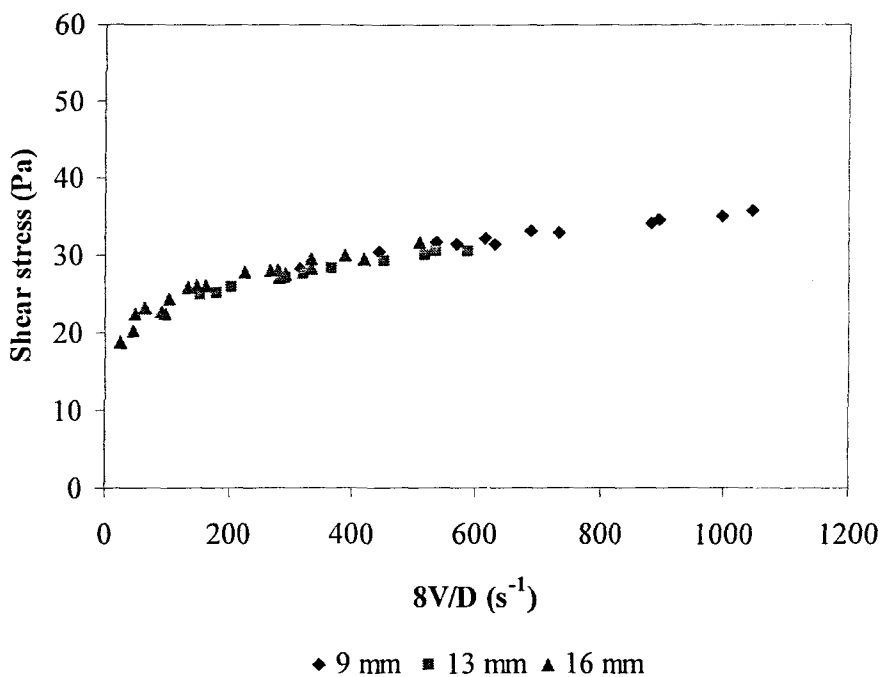
**BENTONITE 6.5 %**



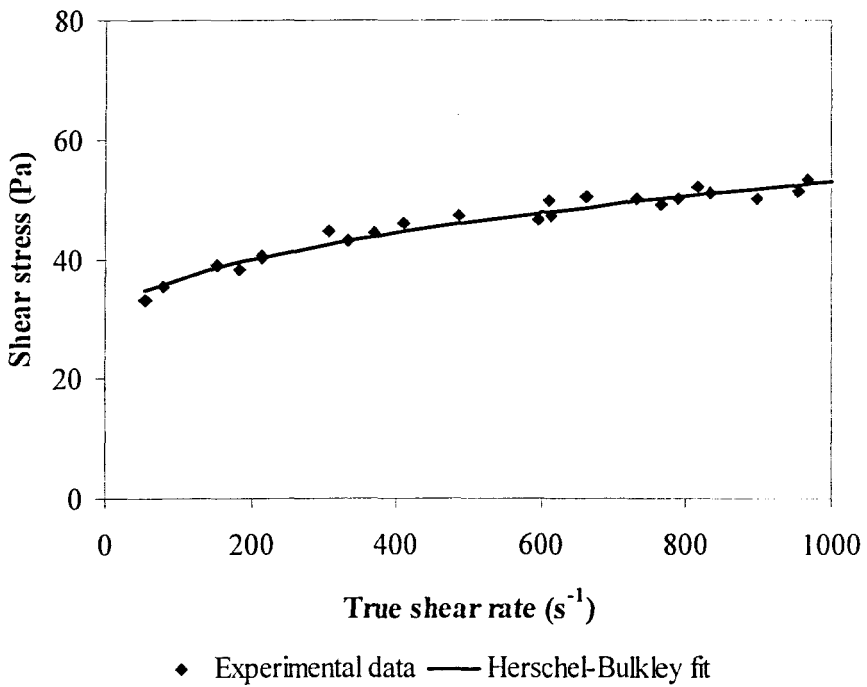
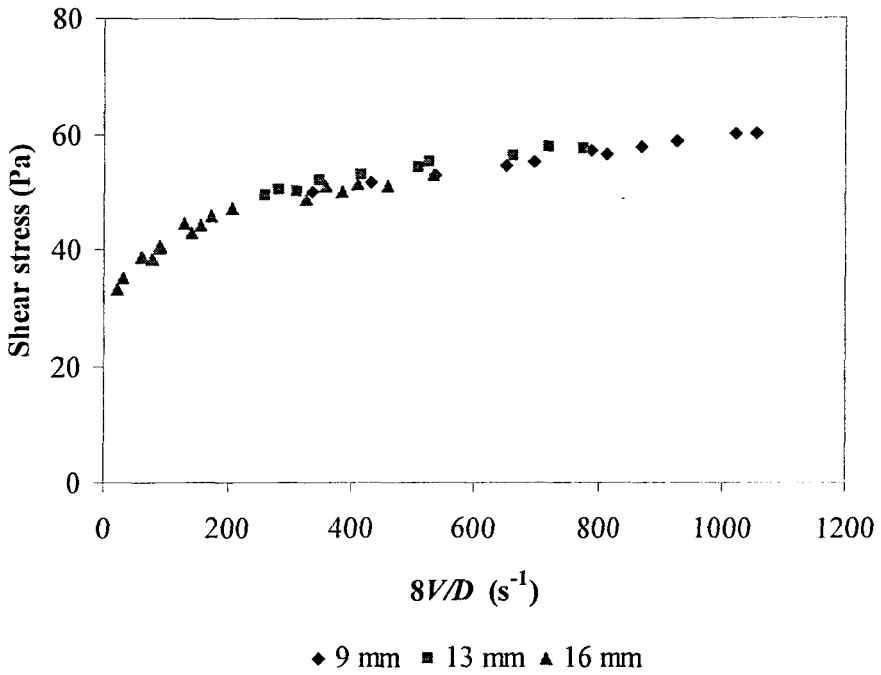
**BENTONITE 7 %**



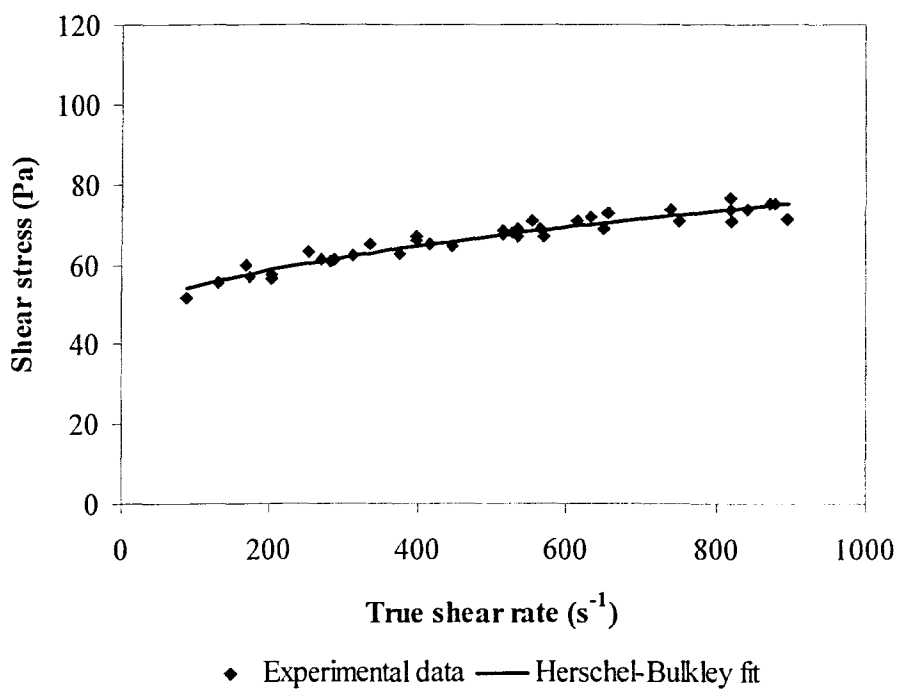
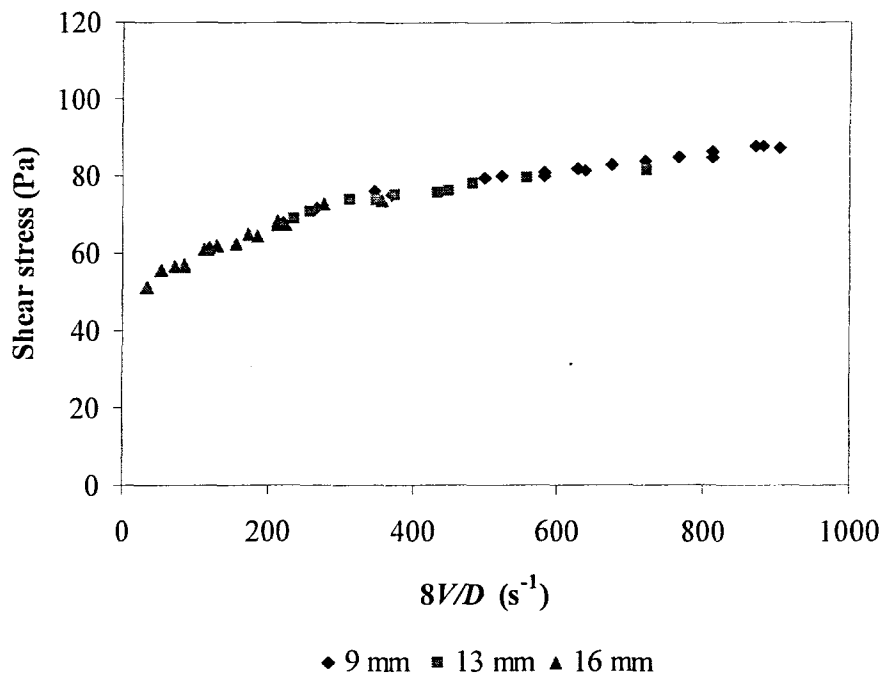
**KAOLIN 8.7 %**



**KAOLIN 10 %**



## KAOLIN 12 %



# APPENDIX B

## DRAWING OF THE PIPE VISCOMETER RIG

